

Vol. 17

2024

No. 03

GEOGRAPHY  
ENVIRONMENT  
SUSTAINABILITY

«The journal GEOGRAPHY, ENVIRONMENT, SUSTAINABILITY was founded in 2008 by Russian Geographical Society, the Lomonosov Moscow State University Geography Department, and the Russian Academy of Sciences Institute of Geography. Since that time the journal publishes **4 issues per year**, containing original research papers and reviews. The journal issues are open source and distributed through subscriptions, library exchanges of leading universities, and via the website through the world»

**FOUNDERS OF THE JOURNAL:** Russian Geographical Society, Faculty of Geography, Lomonosov Moscow State University and Institute of Geography of the Russian Academy of Sciences

The journal is published with financial support of the Russian Geographical Society.

The journal is registered in Federal service on supervision of observance of the legislation in sphere of mass communications and protection of a cultural heritage. The certificate of registration: ПИ № ФС77-67752, 2016, December 21.

#### **PUBLISHER**

Russian Geographical Society  
Moscow, 109012 Russia  
Novaya ploshchad, 10, korp. 2  
Phone 8-800-700-18-45  
E-mail: [press@rgo.ru](mailto:press@rgo.ru)  
[www.rgo.ru/en](http://www.rgo.ru/en)

#### **EDITORIAL OFFICE**

Lomonosov Moscow State University  
Moscow 119991 Russia  
Leninskie Gory, 1,  
Faculty of Geography, 1806a  
Phone 7-495-9391552  
Fax 7-495-9391552  
E-mail: [ges-journal@geogr.msu.ru](mailto:ges-journal@geogr.msu.ru)  
[www.ges.rgo.ru](http://www.ges.rgo.ru)

#### **DESIGN**

Layout designer: Tereshkin Anton  
Moscow, 115088,  
26 Simonovsky Val str., bldg. One  
Phone: +7 (903) 108-04-44  
E-mail: [smile.tai@gmail.com](mailto:smile.tai@gmail.com)

DOI prefix: 10.24057

Format A4 (210x297mm)

“GEOGRAPHY, ENVIRONMENT, SUSTAINABILITY” is the only original English-language journal in the field of geography and environmental sciences published in Russia. It is supposed to be an outlet from the Russian-speaking countries to Europe and an inlet from Europe to the Russian-speaking countries regarding environmental and Earth sciences, geography and sustainability. The main sections of the journal are the theory of geography and ecology, the theory of sustainable development, use of natural resources, natural resources assessment, global and regional changes of environment and climate, social-economical geography, ecological regional planning, sustainable regional development, applied aspects of geography and ecology, geoinformatics and ecological cartography, ecological problems of oil and gas sector, nature conservations, health and environment, and education for sustainable development.

OPEN ACCESS POLICY. “GEOGRAPHY, ENVIRONMENT, SUSTAINABILITY” is an open access journal. All articles are made freely available to readers immediately upon publication. Our open access policy is in accordance with the Budapest Open Access Initiative (BOAI) definition - it means that articles have free availability on the public internet, permitting any users to read, download, copy, distribute, print, search, or link to the full texts of these articles, crawl them for indexing, pass them as data to software, or use them for any other lawful purpose, without financial, legal, or technical barriers other than those inseparable from gaining access to the internet itself.

Date of publication: October 1<sup>st</sup>, 2024.



# EDITORIAL BOARD

## EDITORS-IN-CHIEF:

**Kasimov Nikolay S.**

Lomonosov Moscow State University,  
Faculty of Geography, Russia

**Kotlyakov Vladimir M.**

Russian Academy of Sciences  
Institute of Geography, Russia

## DEPUTY EDITORS-IN-CHIEF:

**Solomina Olga N.** - Russian Academy of Sciences,  
Institute of Geography, Russia

**Tikunov Vladimir S.** - Lomonosov Moscow State  
University, Faculty of Geography, Russia

**Vandermotten Christian** - Université Libre de Bruxelles  
Belgium

**Chalov Sergei R.** - (Secretary-General) Lomonosov  
Moscow State University, Faculty of Geography, Russia

**Alexeeva Nina N.** - Lomonosov Moscow State University,  
Faculty of Geography, Russia

**Baklanov Alexander** - World Meteorological Organization,  
Switzerland

**Baklanov Petr Ya.** - Russian Academy of Sciences, Pacific  
Institute of Geography, Russia

**Chubarova Natalya E.** - Lomonosov Moscow State  
University, Faculty of Geography, Russia

**De Maeyer Philippe** - Ghent University, Department of  
Geography, Belgium

**Dobrolubov Sergey A.** - Lomonosov Moscow State  
University, Faculty of Geography, Russia

**Ferjan J. Ormeling** - University of Amsterdam, Amsterdam,  
Netherlands

**Sven Fuchs** - University of Natural Resources and Life  
Sciences

**Haigh Martin** - Oxford Brookes University, Department of  
Social Sciences, UK

**Golosov Valentin N.** - Lomonosov Moscow State  
University, Faculty of Geography, Russia

**Golubeva Elena I.** - Lomonosov Moscow State University,  
Faculty of Geography, Russia.

**Gulev Sergey K.** - Russian Academy of Sciences, Institute  
of Oceanology, Russia

**Guo Huadong** - Chinese Academy of Sciences, Institute of  
Remote Sensing and Digital Earth, China

**Jarsjö Jerker** - Stockholm University, Department of  
Physical Geography and Quaternary Geography, Sweden

**Jeffrey A. Nittrouer** - Rice University, Houston, USA

**Ivanov Vladimir V.** - Arctic and Antarctic Research  
Institute, Russia

**Karthe Daniel** - German-Mongolian Institute for Resources  
and Technology, Germany

**Kolosov Vladimir A.** - Russian Academy of Sciences,  
Institute of Geography, Russia

**Kosheleva Natalia E.** - Lomonosov Moscow State  
University, Faculty of Geography, Russia

**Konečný Milan** - Masaryk University, Faculty of Science,  
Czech Republic

**Kroonenberg Salomon** - Delft University of Technology,  
Department of Applied Earth Sciences, The Netherlands

**Kulmala Markku** - University of Helsinki, Division of  
Atmospheric Sciences, Finland

**Olchev Alexander V.** - Lomonosov Moscow State  
University, Faculty of Geography, Russia

**Malkhazova Svetlana M.** - Lomonosov Moscow State  
University, Faculty of Geography, Russia

**Meadows Michael E.** - University of Cape Town,  
Department of Environmental and Geographical Sciences  
South Africa

**O'Loughlin John** - University of Colorado at Boulder,  
Institute of Behavioral Sciences, USA

**Paula Santana** - University of Coimbra, Portugal

**Pedroli Bas** - Wageningen University, The Netherlands

**Pilyasov Alexander N.** - Institute of Regional Consulting,  
Moscow, Russia

**Radovanovic Milan** - Serbian Academy of Sciences and  
Arts, Geographical Institute "Jovan Cvijić", Serbia

**Sokratov Sergei A.** - Lomonosov Moscow State University,  
Faculty of Geography, Russia

**Tishkov Arkady A.** - Russian Academy of Sciences,  
Institute of Geography, Russia

**Wuyi Wang** - Chinese Academy of Sciences, Institute of  
Geographical Sciences and Natural Resources Research,  
China

**Zilitinkevich Sergey S.** - Finnish Meteorological Institute,  
Finland

# EDITORIAL OFFICE

## ASSOCIATE EDITOR

**Maslakov Alexey A.**

Lomonosov Moscow State University,  
Faculty of Geography, Russia

## ASSISTANT EDITOR

**Mozolevskaya Irina V.**

Lomonosov Moscow State University,  
Faculty of Geography, Russia

## ASSISTANT EDITOR

**Komova Nina N.**

Lomonosov Moscow State University,  
Faculty of Geography, Russia

## PROOF-READER

**Denisova Irina S.**

Lomonosov Moscow State University,  
Faculty of Geography, Russia

# CONTENTS

**Mokhamad Y. N. Khakim, Pradanto Poerwono, Azhar K. Affandi,  
Muhamad F. Anhar, Febri Indrawan, Tomi Ardiansyah, Takeshi Tsuji**

LAND COVER AND BURN SEVERITY DYNAMICS OF THE OGAN KOMERING  
ILIR PEATLANDS FROM 2015 TO 2023 USING SAR AND OPTICAL DATASETS .....6

**Gleb G. Alexandrov, Alexander S. Ginzburg**

STATISTICAL MODELING OF THE EFFECTS OF WIND SPEED, AIR TEMPERATURE  
AND RELATIVE HUMIDITY ON THE CONCENTRATION OF CARBON MONOXIDE  
IN THE URBAN ATMOSPHERE ..... 19

**Bayimkhanim A. Huseynova**

CONTEMPORARY PROBLEMS OF SETTLEMENT IN THE ETHNIC PLAIN VILLAGES  
OF THE NORTHWESTERN REGIONS OF AZERBAIJAN (ON THE EXAMPLE OF  
THE BALAKAN ADMINISTRATIVE DISTRICT) .....35

**Nikolai A. Grudtsyn**

THE IMPACT OF GLOBAL AND REGIONAL CHALLENGES ON  
THE DECREASE IN TOURIST FLOWS .....47

**Vladimir A. Myazin**

PETROLEUM HYDROCARBONS IN ARCTIC URBAN LAKE  
SEDIMENTS (MURMANSK, RUSSIA).....64

**Dmitrii Vlasov, Irina D. Eremina, Natalia E. Kosheleva, Galina Shinkareva,  
Natalia E. Chubarova, Nikolay S. Kasimov**

POTENTIALLY HAZARDOUS ELEMENTS IN ATMOSPHERIC PRECIPITATION DURING  
THE WARM SEASON (MAY-SEPTEMBER 2019) IN MOSCOW.....70

**Rafael Brugnolli Medeiros, Charlei Aparecido da Silva**

CAPACITY AND CURRENT USE OF THE FORMOSO RIVER WATERSHED, BONITO MUNICIPALITY,  
MATO GROSSO DO SUL, BRAZIL: CONFLICTS AND LAND USE RECOMMENDATIONS.....85

**Nadezhda V. Chugunova, Fedor N. Lisetskii, Anastasiya G. Narozhnyaya,  
Tatjana A. Polyakova, Darja N. Morkovskaya**

METROPOLIZATION PROCESS IN THE RURAL SETTLEMENT SYSTEM OF THE CENTRAL  
CHERNOZEM REGION OF RUSSIA .....98

**Arpana Handique, Pradyut Dey, Santanu Kumar Patnaik**

INTEGRATION OF GEOSPATIAL TECHNIQUES AND ANALYTICAL HIERARCHY  
PROCESS (AHP) IN DEMARCATING GROUNDWATER POTENTIAL  
ZONES IN LAKHIMPUR DISTRICT, ASSAM, INDIA ..... 109

**Disclaimer:**

*The information and opinions presented in the Journal reflect the views of the authors and not of the Journal or its Editorial Board or the Publisher. The GES Journal has used its best endeavors to ensure that the information is correct and current at the time of publication.*

# LAND COVER AND BURN SEVERITY DYNAMICS OF THE OGAN KOMERING ILIR PEATLANDS FROM 2015 TO 2023 USING SAR AND OPTICAL DATASETS

**Mokhamad Y. N. Khakim<sup>1\*</sup>, Pradanto Poerwono<sup>1</sup>, Azhar K. Affandi<sup>1</sup>, Muhamad F. Anhar<sup>1</sup>, Febri Indrawan<sup>1</sup>, Tomi Ardiansyah<sup>1</sup>, Takeshi Tsuji<sup>2</sup>**

<sup>1</sup> Universitas Sriwijaya, Jl. Palembang-Prabumulih Km. 32, Indralaya, Ogan Ilir, South Sumatra, 30662, Indonesia

<sup>2</sup> University of Tokyo, 113-8654, 7-3-1 Hongo, Bunkyo-ku, Japan

\*Corresponding author: myusup\_nkh@mipa.unsri.ac.id

Received: January 20<sup>th</sup> 2024 / Accepted: July 25<sup>th</sup> 2024 / Published: October 1<sup>st</sup> 2024

<https://doi.org/10.24057/2071-9388-2024-3217>

**ABSTRACT.** Land cover changes and wildfires have had an increasing impact on the Ogan Komering Ilir Peatland ecosystems in South Sumatra, Indonesia. This study aims to understand the peatland land cover and burn severity dynamics from 2015 to 2023. The random forest method was applied to classify land cover, while the differenced Normalized Burn Ratio (dNBR) was used for mapping fire severity. We combined various satellite data to classify land cover, consisting of Landsat-8, Sentinel-1, and Sentinel-2. Landsat-8 or Sentinel-2 images were also used for the dNBR calculation. We revealed complex climate, human, and restoration interactions in land cover and burn severity fluctuations over 273,799 hectares of the study area from 2015 to 2023. The 2015 El Niño-induced drought led to 21,754 fire hotspots and 2.01% of the area in high-severity burns. In 2016, it reduced tree cover by 10.18% and increased bare/sparse vegetation by 6.11%. The 2019 El Niño event led to 7,893 fire hotspots, lessening unburned areas and worsening burns. Due to the extreme effects of the 2015 drought, restoration efforts between 2016 and 2020 significantly decreased fire hotspots in 2016. Tree cover stabilized, reaching 48.46% by 2020, whereas unburned areas rose to 69.46% in 2018, showing good recovery and lower fire severity. In 2021-2023, fire hotspots were modest relative to El Niño years but increased in 2023. After 2020, tree cover decreased, but other land cover classes fluctuated. Therefore, continual monitoring and adaptive management are critical for reducing negative consequences and increasing ecosystem resilience.

**KEYWORDS:** peatlands, land cover change, burn severity, remote sensing, restoration

**CITATION:** Khakim M. Y. N., Poerwono P., Affandi A. K., Anhar M. F., Indrawan F., Ardiansyah T., Tsuji T. (2024). Land Cover And Burn Severity Dynamics Of The Ogan Komering Ilir Peatlands From 2015 To 2023 Using Sar and Optical Datasets. *Geography, Environment, Sustainability*, 3(17), 6-18

<https://doi.org/10.24057/2071-9388-2024-3217>

**ACKNOWLEDGEMENT:** We would like to acknowledge Universitas Sriwijaya for financial support through «Penelitian Hibah Kompetitif», Contract Number: 0096.105/UN9/SB3.LP2M.PT/2023, dated on May 8<sup>th</sup> 2023. We also thank the European Space Agency (ESA) for providing Sentinel-1 data, anonymous reviewers, and the academic editor for their valuable comments and suggestions.

**Conflict of interests:** The authors reported no potential conflict of interest.

## INTRODUCTION

Peat is an organic material created from incompletely decomposed plant residues that accumulate in wetlands and have a thickness of 50 cm or more (Osaki and Tsuji 2015; Osman 2018). Peat ecosystems play an essential ecological role in sustaining human life, living organisms, and maintaining natural balance. Using peatlands without regard for the environment has harmed the peat ecosystem, resulting in disasters. Due to the 'El Niño phenomenon's prolonged dry seasons, peatland drainage increases fire risk (Khakim et al. 2022; Khakim et al. 2020; Usup et al. 2004). In its natural state, peat is saturated with water. When peat is damaged due to forest removal and drying, water from the peat flows easily, causing the peat area to dry out. As a result, the peat volume will decrease, decreasing the peat surface (Khakim et al. 2020).

Peatland fires are a global concern that must be addressed seriously. Fires caused by 'El Niño 2015 had a significant influence on the hydrological and vegetative conditions (Khakim et al. 2022). The restoration target for the 2016-2020 period is 2.4 million hectares, with Pulang Pisau Regency in Central Kalimantan Province, Musi Banyuasin Regency in South Sumatra Province, Ogan Komering Ilir Regency in South Sumatra Province, and Meranti Islands Regency in Riau Province being prioritized (Dohong 2019). The government accelerated area recovery to mitigate the impact of the 2015 forest and land fires. It restored the hydrological function of peat due to forest and land fires in a systematic, targeted, integrated, and comprehensive manner by establishing BRG by Presidential Regulation Number 1 of 2016 (Peat Restoration Agency 2016).

In the specific case of South Sumatra, the restoration objective encompassed 30 peat hydrological units (PHUs), corresponding to an area of approximately 711,479.55 hectares (Badan Restorasi Gambut 2017). This target represents a significant portion of the overall peat acreage in South Sumatra, estimated to be around 1.2 million hectares. Restoration is achieved by implementing water retention structures, filling open canals, and constructing drilled wells. In rehabilitation, revegetation involves deliberately planting native and adaptable seeds in open peatlands and enhancing plantings in areas of degraded peat forests (Peat Restoration Agency 2016). Nevertheless, El Niño in 2019 resulted in the combustion of the peatland in South Sumatra. In 2019, the Ogan Komering Ilir (OKI) regency in the South Sumatra province had the most significant area burned, which amounted to 194,824 hectares. Musi Banyu Asin and Banyu Asin regencies also had substantial amounts of burning, with 63,091 and 27,705 hectares affected, respectively<sup>1</sup>. Therefore, monitoring restoration efforts to evaluate the impacts on peatlands and detect any resultant alterations is crucial.

Assessment and comprehension of land cover changes and fire intensity in the peatland of South Sumatra are critical for several reasons. First and foremost, this technology facilitates the evaluation of the influence of human activities on these vulnerable ecosystems, hence aiding in the formulation of environmentally conscious land-use strategies (Biancalani and Avagyan 2014; Goldstein et al. 2020; Hapsari et al. 2018; Miettinen and Liew 2010). Additionally, monitoring fire severity is essential in anticipating and preventing peatland wildfire's ecological and public health consequences (Harrison et al. 2020; Picotte et al. 2021; Sirin and Medvedeva 2022). Finally, the observation of these parameters contributes to the conservation of environmental diversity and the preservation of a healthy environment within the region.

Satellite-based remote sensing data, such as radar and optical data, plays an important role in addressing these challenges. ENVISAT ASAR is less developed for C-band SAR data because of its low spatial and temporal coverage in tropical regions. However, on April 3, 2014, the Sentinel-1 C-band satellite was launched, becoming the first to guarantee open data access with a 12-day return acquisition period at the equator and systematic global coverage (Panetti et al. 2014). The JAXA ALOS-2 L-band mission launched on May 24, 2014, to continue the ALOS-1 global forest data-collecting policy (Kankaku et al. 2015). However, JAXA's unacceptably high price strategy may prevent this data from being used as part of a worldwide tropical forest monitoring system.

However, the concurrent accessibility of L- and C-band data presents promising prospects for monitoring and administrating tropical forests. The LiDAR technique is a remote sensing technology that offers the distinct advantage of providing high-resolution Fields (Pu 2021; Zhen et al. 2016). Nevertheless, LiDAR technology incurs significant costs and entails extended processing times (Novero et al. 2019). The European Space Agency's Copernicus program offers a valuable chance to enhance monitoring by providing access to new optical and Synthetic Aperture Radar satellite data that exhibit excellent temporal and spatial resolution (Gomarasca et al. 2019; Shirvani et al. 2019).

The readily available data provides notable benefits in facilitating monitoring endeavors. The European Space Agency's mission includes a diverse array of sensors designed specifically for ground monitoring. The satellites encompass Sentinel-1, equipped with a synthetic aperture radar operating in the C-band frequency, and Sentinel-2, an

optical satellite. Landsat 8 can capture images exhibiting diverse levels of spatial resolution. Spatial resolution can vary between 15 and 100 meters, and these variations are accompanied by 11 channels with different spectral resolution levels (Loveland and Irons 2016). The primary benefit of Landsat 8 is its provision of unrestricted access to data.

This study aims to assess the restoration of peatlands in the OKI regency, South Sumatra, Indonesia, by analyzing the alterations in land cover and fire severity from 2018 to 2023. Sentinel-1's radar imaging capabilities guarantee all-weather monitoring, supplemented by high-resolution optical imagery from Sentinel-2 and Landsat-8. This integrated technique allows for a more complete analysis and in-depth evaluation of both land cover changes and burn severity. This synergistic use of satellite data results in a more robust understanding of ecosystem dynamics, allowing for timely and informed decision-making for sustainable land management, fire prediction, and environmental conservation activities.

## MATERIALS AND METHODS

### Study Area

The OKI Regency experienced the most extensive peat fires in South Sumatra, Indonesia, in 2015 and 2019. The fire hotspots of 2015 and 2019 are presented in Figs. 1a and 1b, respectively. In this study, we selected four peat hydrology units (PHUs), namely PHU S. Burnai – S. Sibumbung, PHU S. Sibumbung – S. Talangrimba, PHU S. Talangrimba – S. Ulakedondong, and PHU S. Ulakedondong – S. Lumpur, within this regency, as seen in Fig. 1. The area encompasses a total area of 273,799 hectares. The peat ecosystem in this region covers a cultivation area of 123,800 hectares and a protected area spanning 149,201 hectares. The peat thickness reaches 500 cm over this region.

Consequently, it has been identified as a priority location for restoration efforts, particularly for the PHU S. Burnai – S. Sibumbung. Nevertheless, a notable alteration in land utilization occurred at this specific site, wherein an area designated for conservation purposes was instead utilized to cultivate oil palm plantations. Hence, mapping land cover becomes of significant importance.

### Data

The current study employed a combination of remote sensing data from several sources to classify land cover, incorporating both temporal and spectral variety to achieve precise and reliable results. The image collections consisted of Sentinel-1 (S1), Sentinel-2 (S2), and Landsat-8 (L8) from 2015 through 2023. The Sentinel-1 mission is an operational radar satellite mission managed by the European Space Agency (ESA). Providing synthetic aperture radar (SAR) imagery with diverse polarization modes renders it highly helpful for land cover classification, primarily owing to its capacity to operate well in all weather conditions. The investigated area was provided with Sentinel-1 data from the Copernicus S1 GRD image collection. This framework is based on interferometric wide-swath (IW) GRD images. These images guarantee full information detail with a 10 m pixel spacing, a spatial resolution of 20-22 m, and a temporal resolution of 6-12 days (Wang et al. 2020).

In addition, the Sentinel-2 satellite project, developed by the European Space Agency (ESA), offers high-resolution optical imaging in different spectral bands. Using Sentinel-2

<sup>1</sup>KLHK. (2024). SiPongi (Forest and Forestry Monitoring System), Burnt Area Calculation. <https://sipongi.menlhk.go.id/indikasi-luas-kebakaran>



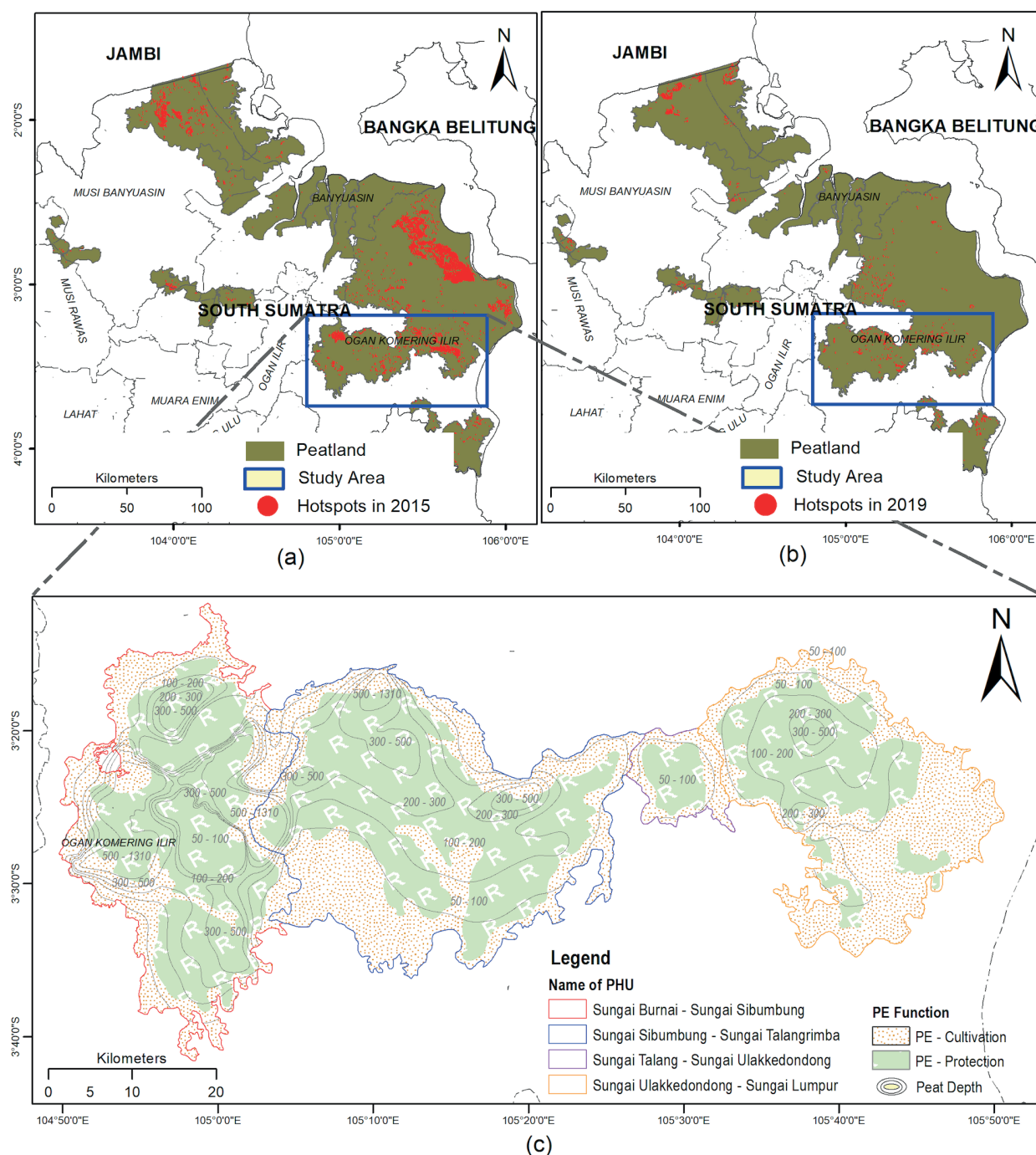


**Fig. 1. (a), (b) Fire hotspots over the PHUs of South Sumatra in 2015 and 2019, respectively and (c) peat ecosystem functions of the study area (Peat Restoration Agency 2017) and peat thickness (BBSDL 2019)**

data's multispectral characteristics enables the identification of significant insights related to land cover features. The Sentinel-2 image for our investigation was sourced from the Copernicus S2 level-1 image collection covering the study period. Moreover, the Landsat-8 satellite, jointly operated by the United States Geological Survey (USGS) and NASA, offers optical imagery with a moderate resolution. The use of Landsat-8 data is critical for ongoing land cover monitoring and long-term change detection. The Landsat-8 Surface Reflectance was used from the USGS Landsat 8, Collection 2, Tier 1 dataset image.

## Methodology

### Preprocessing

The Ground Range Detected (GRD) scenes are a collection of images that have been processed using the Sentinel-1 Toolbox. This processing generates a calibrated

and ortho-corrected product made available on the Google Earth Engine (GEE) platform. In our study, we opted for dual polarization modes, specifically VV (vertical-vertical) and VH (vertical-horizontal). In addition, we implemented an improved Lee speckle filter to effectively eliminate speckle noises. This step is crucial in preprocessing synthetic aperture radar (SAR) images. The collection of processed S1 images was converted to a linear power or decibel (dB) scale using the sigma naught ( $\sigma^0$ ) parameter. We derived two indices from S1, namely the radar vegetation index (RVI) (Kim et al. 2012) and the normalized ratio procedure between bands (NRPB) (Filgueiras et al. 2019), which we added to an input image composite.

The Copernicus S2 level-1 image has been orthorectified and radiometrically corrected, which has produced top-of-atmosphere reflectance values (Gatti et al. 2015). It was decided to use Bands 2 to 8, each with an initial spatial resolution of 10 meters. Band QA60 from the S2 1C product was used in an automated cloud masking technique to

ensure data quality (Carrasco et al. 2019). This procedure successfully masked both opaque and cirrus clouds. Clouds and shadows were also masked from Landsat 8 imagery in GEE using the Quality Assessment ("QA\_PIXEL") band to mask out pixels with clouds and shadows (Zhen et al. 2023). To create a cloud-free composite image from S1 and S2, we used the median to combine multiple cloud-masked images into one representative image for a year. On the other hand, the mean was used to create an annual S1 image composite.

We calculated the Normalized Difference Vegetation Index (NDVI), Normalized Difference Water Index (NDWI), and Normalized Difference Built-Up Index (NDBI) from the optical S2 and L8 data to increase the accuracy of land cover classification. Besides these auxiliary data, the Inverted Red-Edge Chlorophyll Index (IRECI) and Sentinel-2 Red-Edge Position (S2REP) were calculated from S2 imagery (Frampton et al. 2013). The S1 SAR and S2/L8 optical data, along with their calculated indices, were combined into a yearly composite dataset.

After creating the yearly composite, we applied Principal Component Analysis (PCA) based on the composite. It transformed the original bands into orthogonal or principal components, ranked by their variance. This statistical technique compresses data from many bands into fewer uncorrelated bands. The PCA is also advantageous in improving supervised classification results (Ali et al. 2019). Prior to sampling training points, we added the first three principal component bands to the original composite. We can capture various spectral and structural information about the land cover classes by incorporating 34 bands and indices from multiple sensors and 3 PCA components. The more bands can lead to a more discriminative dataset for classification.

### Land Cover Classification

The eight major land cover classifications are tree cover, shrubland, grassland, farmland, built-up, bare/sparse vegetation, water bodies, and herbaceous vegetation. Peat forests, oil palm plantations, rubber plantations, and mangroves were classified as tree cover. We classified shrubs as woody perennial plants with persistent, woody stems and no single, well-defined main stem that grow to a height of less than 5 meters. Grass is any geographical area dominated by natural plants (with no persistent branches or shoots above ground and no definite hard structure). Grasslands include grasslands, prairies, steppes, savannahs, and pastures. Cropland is cultivated land that can be harvested at least once within a year of the first sowing or planting. Buildings, roads, and other manufactured structures, such as railroads, inhabit built-up areas. Furthermore, water class is used to classify different aquatic settings, such as fishponds, rivers, and other bodies of water. Herbaceous wetlands are characterized by natural herbaceous vegetation (coverage of 10% or greater) that is permanently or frequently inundated by fresh or brackish water.

We created 282 feature collections with points representing pixels in those classes. These samples of feature collection have a property called landcover, with values from 1 to 8 representing tree cover, shrubland, grassland, farmland, built-up, bare/sparse vegetation, water bodies, and herbaceous vegetation, respectively. These samples were collected from the RGB composite of the optical imagery and field observation. Furthermore, the classification accuracy was quantitatively estimated

by dividing the samples into two random fractions – 70% for training the model and 30% for validation of the predictions.

The Random Forest classification process for peatland analysis in South Sumatra commences with the assembly of a comprehensive input dataset, which encompasses 34 bands, spectral indices, and three PCA-derived components (namely pc1, pc2, and pc3) from Sentinel-1, Sentinel-2, and Landsat-8 imagery. This rich dataset encapsulates a wide range of spectral and radar information for characterizing peatland vegetation and conditions. In the classification stage, a Random Forest method was employed, and notably, all available bands, indices, and PCA components were considered for each tree, totaling 36 features. This method ensures the model leverages all the input data, maximizing its inherent spectral and geographical variety.

After performing the classification, a feature importance analysis was carried out to determine the significance of each feature in distinguishing land over classes. This stage plays a crucial role in identifying the bands, indices, or PCA components that have the most impact on the classification process. By quantifying feature importance scores, we gained valuable insights into the critical elements that contribute to the characterization of peatlands. This, in turn, facilitated the selection and interpretation of features based on data-driven approaches.

The optimal model performance in the Random Forest classification process is dependent on the critical feature of hyperparameter adjustment. To get accurate and robust classification outcomes, it is crucial to precisely tune parameters such as the number of trees, variables per split, bagging fraction, minimum leaf population, maximum number of leaf nodes, and seeds. Exhaustive tuning efforts, often involving grid searches and cross-validation techniques, helped identify the parameter values that maximize classification accuracy while mitigating overfitting risks.

Finally, post-processing techniques are applied to the classification results to refine and enhance their quality. These post-processing steps may encompass spatial smoothing, majority filtering, or object-based analysis tailored to the unique characteristics of peatland regions. The objective is to produce visually coherent and accurate peatland maps suitable for subsequent ecological and environmental assessments or management decisions in South Sumatra's peatland areas.

### Mapping Burn Severity

Normalized Burn Ratio (NBR) is used to identify areas of burned vegetation. The NBR for the before and after fires was calculated utilizing optical images, either Landsat-8 or Sentinel-2, using Eq. (1) (Cocke et al. 2005). The NBR value is bounded between -1 and +1, with vegetation contributing the most and burned areas contributing the least. Burn severity can be estimated by calculating the differenced Normalized Burn Ratio (dNBR), as presented in Eq. (2). As shown in Table 1, the values of burn severity indices were categorized into seven distinct severity levels.

$$NBR = (NIR - SWIR) / (NIR + SWIR) \quad (1)$$

$$dNBR = NBR_{prefire} - NBR_{postfire} \quad (2)$$

Table 1. Seven burned severity classes

No	Severity Level	Range
1.	Enhanced Regrowth, High	< -500
2.	Enhanced Regrowth, Low	-250 to -100
3.	Low Severity	-100 to 100
4.	Unburned	100 to 270
5.	Moderate-low Severity	270 to 440
6.	Moderate-high Severity	440 to 660
7.	High Severity	> 660

## RESULTS

### Optimum parameters and feature importance

We optimized critical hyperparameters in the Random Forest classification context, including decision trees, variables, bagging fraction, leaf population, nodes, and seed value. This step identified the optimum values within defined ranges to assess their influence on classification results. The results were significant, revealing the specific parameter values that, through experimentation and analysis, were found to optimize the Random Forest classification model.

An example of parameter selection for classifying the land cover in 2020 is illustrated in Fig. 2. The study

determined that the ideal number of decision trees in the Random Forest ensemble is 270. For the number of variables considered at each split, 15 was identified as the optimal value. The bagging fraction, which controls the proportion of the training data used for building individual trees, performed optimally at 0.9. Regarding the minimum leaf population, the analysis revealed that a minimum of one sample must be present at a leaf node for optimal results. The minimum number of leaf nodes, which indicates the number of terminal nodes in a tree, was observed to be most effective at 100. Lastly, the seed value, which can impact the randomness in the Random Forest, was determined to yield the best results at a value of 301.

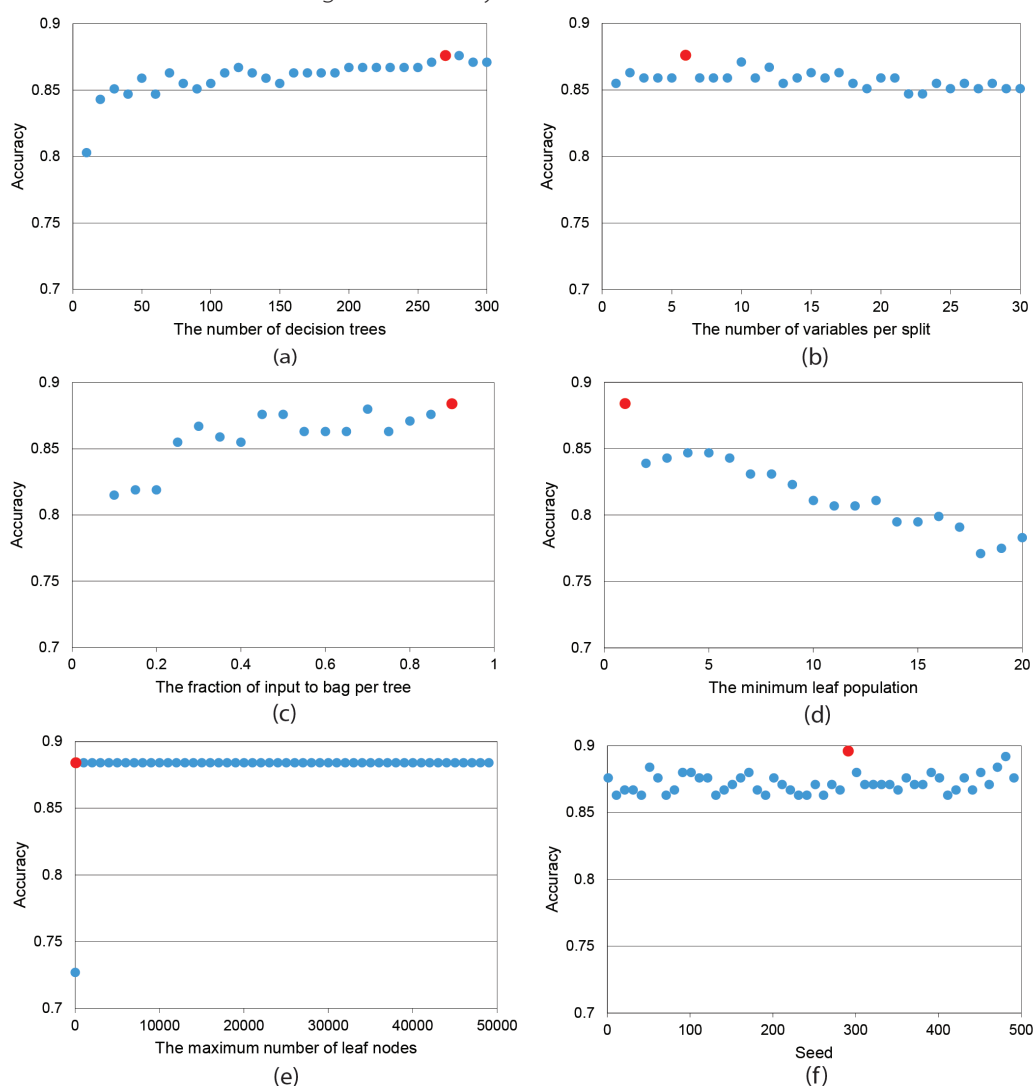


Fig. 2. Selected optimum parameter for the random forest classification



In the context of Random Forest classification analysis, figuring out how discriminative a set of input features from different sources is requires figuring out how relevant each feature is. As shown in Fig. 3, the relative relevance scores reveal unique patterns among these characteristics, offering information on their contributions to land cover classification.

The Sentinel-2 dataset encompasses a collection of spectral bands (B1 to B12) and associated indices (IRECI, S2REP, NDBI of S2, NDVI of S2, NDWI of S2) demonstrating varied significance levels. Bands B5 and B11 significantly have noteworthy relative significance ratings of 3.033 and 3.24, respectively. These bands demonstrate exceptional proficiency in gathering crucial vegetation data, which is fundamental for distinguishing different land cover types. Indices such as the Normalized Difference Vegetation Index (NDVI) derived from Sentinel-2 satellite imagery, which has been assigned a relative relevance value of 2.85, are known to have a substantial impact on assessing the health of vegetation.

The Landsat-8 dataset exhibits a collection of significant attributes, notably the surface reflectance bands (SR\_B1 to SR\_B7) and indices (NDVI of L8, NDWI of L8, NDBI of L8). SR\_B3 and SR\_B1 are significantly influential, as indicated by their respective relative significance ratings of 3.522 and 3.301. These bands are very important for accurately classifying different types of land cover and describing the land surface's characteristics. An important indication of water-related land cover is the Normalized Difference Water Index (NDWI) produced from Landsat 8 satellite images, with a relative relevance score of 3.047.

Using synthetic aperture radar (SAR) data obtained from Sentinel-1 provides distinctive characteristics with significant relative significance. The VH (Vertical Transmit and Horizontal Receive) method stands out significantly, as indicated by its relative relevance score of 3.205. The (VV – VH) attribute, which denotes the disparity between VV and VH, holds significant significance, as evidenced by its score of 3.115. The SAR features demonstrate exceptional capability in effectively penetrating cloud cover and offering valuable observations regarding surface parameters.

PCA combines Sentinel-1, Sentinel-2, and Landsat-8 data to produce three main components: pc1, pc2, and pc3. Each component contributes to the classification process, with pc1 having a relative importance value of 2.71, pc2 having a score of 2.835, and pc3 having a score of 2.893. These PCA-derived components represent the

combination of data from several sources, which jointly improves the classification process.

### Land cover accuracy

The high Overall Accuracy (OA) values recorded over several years represent the overall performance of the land cover classification model, as presented in Table 2. These OA values, which range from 76.47% to 91.03%, reflect the model's broad ability to accurately categorize pixels across all land cover categories. It implies that the model adequately represents the landscape's complexity and delivers trustworthy forecasts for diverse land cover types. The Kappa values, which range from 0.71 to 0.89, further emphasize the model's dependability. These results indicate a moderate to significant agreement between observed and anticipated classifications, validating the model's consistency and accuracy in land cover classification.

Across multiple land cover types, the classification model displays remarkable accuracy concerning Producer's Accuracy (PA) and User's Accuracy (UA). The model consistently yields high PA and UA values for tree cover, demonstrating a strong capacity to accurately identify and categorize pixels in this category. This accuracy shows the model's consistency in delivering correct findings and the high likelihood that pixels identified as tree cover represent such vegetation.

The model's accuracy in recognizing shrublands varies with moderate to high PA and UA values, suggesting that environmental conditions or land cover changes may affect its precision. It has reasonable accuracy in categorizing grassland and consistently obtains high PA and UA values, demonstrating its ability to distinguish agriculture from other land cover categories. The model also reliably and accurately identifies built-up regions, demonstrating its dependability in detecting urban or developed areas. However, the accuracy of categorizing bare or sparse vegetation varies, potentially influenced by environmental variables or changes in land cover. The model also reliably classifies water bodies with high PA and UA values, demonstrating its ability to differentiate aquatic characteristics from other land cover categories. For herbaceous wetlands, the model consistently shows high PA and UA values, demonstrating its consistent recognition of these regions over time.

The high OA and Kappa values show that the land cover classification model is accurate and consistent. Over numerous years, the model's consistently high PA and

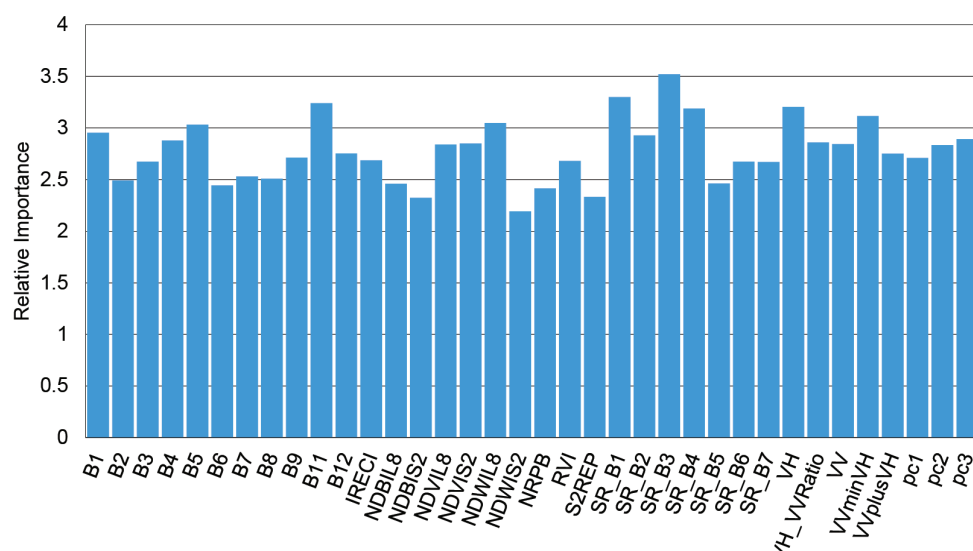


Fig. 3. Relative importance of features as inputs for random forest classification

Table 2. Accuracy measures of land cover classification

Year	Kappa	OA	Tree Cover		Shrubland		Grassland		Cropland		Built-up		Bare / sparse vegetation		Water bodies		Herbaceous Wetland	
			PA	UA	PA	UA	PA	UA	PA	UA	PA	UA	PA	UA	PA	UA	PA	UA
2015	0.74	0.78	0.89	0.71	0.62	0.81	0.54	0.72	0.82	0.93	0.70	0.88	0.40	0.38	1.00	1.00	0.92	0.92
2016	0.71	0.76	0.86	0.80	0.57	0.76	0.67	0.67	1.00	0.75	0.89	0.57	0.50	0.60	1.00	0.95	0.83	0.94
2017	0.76	0.81	0.83	0.78	0.63	0.79	0.53	0.40	1.00	0.92	1.00	0.83	0.48	0.64	1.00	1.00	0.90	1.00
2018	0.81	0.84	0.89	0.84	0.73	0.86	0.69	0.77	1.00	1.00	0.89	0.67	0.65	0.67	1.00	1.00	1.00	0.92
2019	0.81	0.84	0.92	0.79	0.84	0.89	0.82	0.67	0.61	1.00	0.88	0.88	0.58	0.82	1.00	1.00	1.00	1.00
2020	0.89	0.91	0.91	0.94	0.84	0.89	0.96	0.79	0.86	1.00	0.90	0.82	0.77	0.79	1.00	1.00	1.00	1.00
2021	0.87	0.89	0.92	0.87	0.84	0.84	0.96	0.77	0.95	0.95	1.00	0.92	0.60	0.95	0.97	1.00	1.00	0.94
2022	0.81	0.85	0.85	0.73	0.67	0.80	0.72	0.78	0.94	0.88	0.75	0.90	0.76	0.81	1.00	1.00	1.00	0.92
2023	0.84	0.87	0.94	0.89	0.80	0.80	0.89	0.61	0.47	1.00	0.77	0.77	0.72	0.81	1.00	0.98	0.91	1.00

UA values across land cover categories demonstrate its accuracy in identifying and classifying various landscape elements. This result shows that the model captures the dynamics of land cover patterns and provides reliable insights for numerous applications.

### Spatiotemporal land cover dynamics

The land cover from 2015 to 2023 is presented in Fig. 4, as determined through the application of Random Forest classification. The spatial and temporal distribution of land cover categories exhibited variation. The tree covers in PHU S. Burnai – S. Sibumbung are primarily comprised of oil palm and rubber plantations, as observed from the field investigation. In contrast, the region of PHU S. Sibumbung - S. Talangrimba was mainly characterized by peatland forest, with a comparatively smaller portion dedicated to plantation activities in the southern part of this PHU.

Peatland regions in four PHUs have exhibited notable changes in land cover. In 2015, an extensive expanse of trees was observed in PHU S. Burnai – S. Sibumbung, amounting to about 16,050 hectares consisting of most oil palm plantations, rubber plantations, and small peat forests. However, throughout the years, a significant reduction in tree coverage has been witnessed, which could be attributed to various factors such as land conversion for plantation purposes and natural events like the El Niño phenomenon, which can contribute to forest fires and deforestation. This decline in tree coverage coincides with an augmentation in shrubland, grassland, and built-up areas, indicating land conversion for plantations, settlements, and other land uses. Additionally, the presence of cloud cover in different years suggests the existence of climatic variations that could potentially impact the detection and analysis of land cover.

In 2019, after the occurrence of the El Niño phenomenon in 2015, a decline in the extent of forested areas was observed in most locations, and this pattern persisted throughout the year 2020. The El Niño phenomenon frequently induces arid conditions, rendering the peatlands more vulnerable to fires, potentially impacting forested areas' extent. However, there was an expansion in grassland, shrubland, and built-up areas, particularly in the regions of KHG Sungai Sibumbung – Sungai Talangrimba and KHG Sungai Ulakkedondong – Sungai Lumpur. These alterations may indicate changes in land utilization, such as the expansion of plantation activities,

settlement development, or changes in vegetation types. The conversion of land for agricultural purposes might also contribute to the augmentation of cropland.

The dynamics of land cover appear to be improving in 2021. Several sites had an increase in tree covers, suggesting the possibility of afforestation or natural regeneration, which is encouraging for attempts to conserve peatlands. Other land cover types, such as grassland and shrubland, appear to be expanding, possibly due to continued land use changes and plantation preparation. Furthermore, there was an increase in tree cover in 2023, particularly in KHG Sungai Sibumbung - Sungai Talangrimba, which may result from natural regeneration of forests or plantation growth. It is critical to monitor these trends to ensure that conservation efforts involve the restoration of peat forests and are sustainable.

The relationship between land cover types is dynamic and impacted by various factors, including human activity, conservation initiatives, and climatic phenomena like El Niño. Tree cover can assist in preserving soil moisture and reduce the risk of fire, it is essential for peatland ecosystems, including oil palm and rubber plantations. Peatland conservation faces obstacles posed by expansion into alternative land cover types, specifically settlements and agricultural areas. Restoration programs, climate resilience plans, and sustainable land management techniques are crucial for preserving a healthy balance and safeguarding these essential ecosystems.

The temporal analysis of land cover classes for the overall study area spanning from 2015 to 2023 is presented in Fig. 5. Several noteworthy tendencies can be found in a few of these classes. The tree cover displayed notable temporal fluctuations, with values ranging from a minimum of 40.02% in 2016 to a maximum of 53.12% in 2019. The increase in tree cover in 2019 is indicated as a massive expansion of the oil palm plantation in PHU S. Burnai – S. Sibumbung, which can be seen on the land cover map in Fig. 4. Nevertheless, the decline to 43.56% in 2023 prompts inquiries regarding potential influences such as deforestation or natural disruptions impacting the extent of tree coverage.

In contrast, the shrubland class exhibited steady percentages, ranging from 5.89% to 14.79%, with no significant increasing or decreasing trend. It suggests that there is a stable and persistent land cover within this classification. The data reveals a progressive rise in grassland proportions, commencing at 12.08% in 2015 and



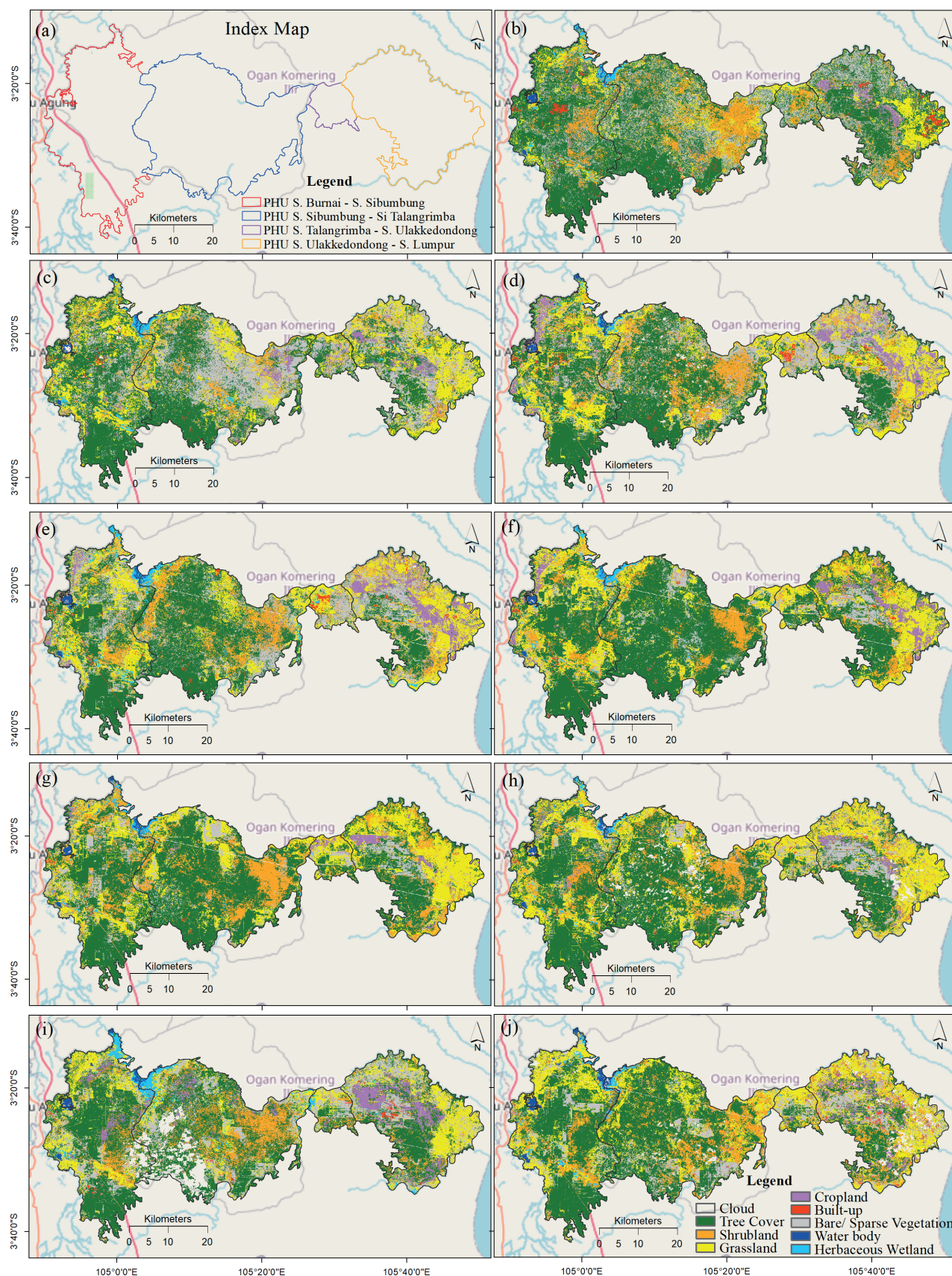
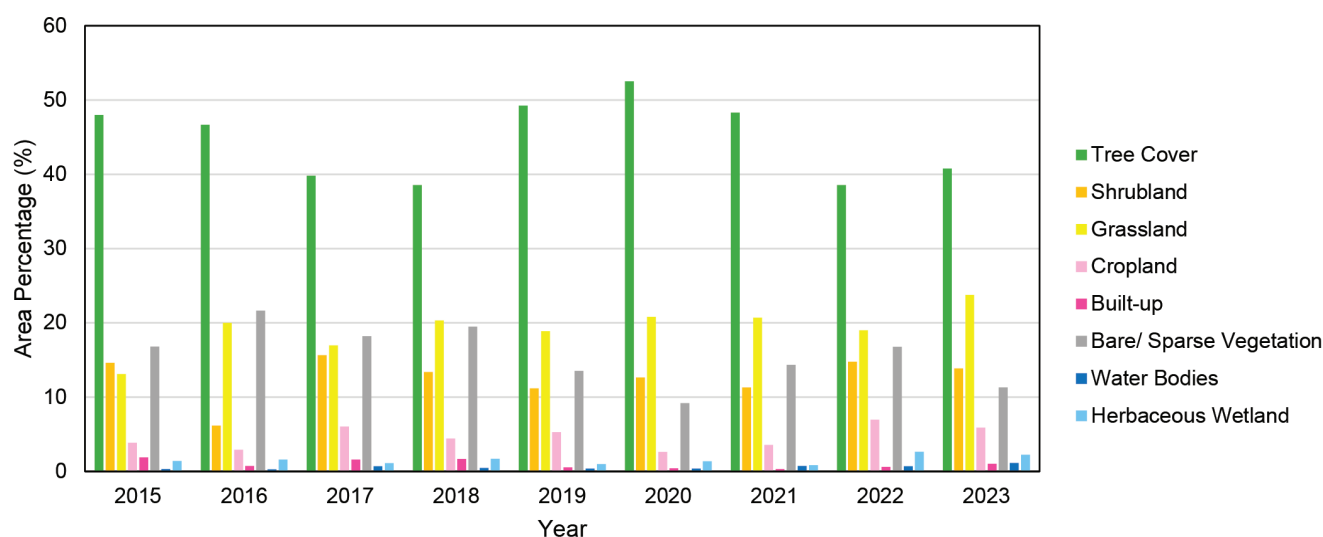


Fig. 4. (a) PHU areas and (b) – (j) classified land cover from random forest method for a period 2015 – 2023, respectively



**Fig. 5. The variation of land cover percentages for each class from 2015 to 2023**

culminating at 24.07% in 2023. This observation implies a potential increase in the extent of grassland ecosystems, possibly driven by alterations in land use patterns, such as changes in forested or shrubland areas into grasslands. Over the observed period, the cropland percentages consistently fluctuated within the 2.04% to 6.23% range. The observed consistency is likely attributable to consistent agricultural techniques or land use policies. The percentage of built-up regions witnessed a marginal rise from 0.36% in 2020 to 0.96% in 2023, indicating a continuing trend of land clearing, especially for plantations. The trend is significant in environmental planning and land use control. The water bodies exhibited notable stability, ranging from 0.34% to 1.13%. This observation suggests that these hydrological features can endure and persist within the broader landscape. The proportions of herbaceous wetlands fluctuated, increasing from 0.36% in 2015 to 1.43% in 2016, followed by subsequent modest fluctuations.

### Spatiotemporal Burn Severity Levels

The burnt severity maps for the four-peat hydrological units in the study region from 2015 to 2023 are presented in Fig. 6. PHUs with high fire severity occurred in small areas in S. Burnai-Sibumbung, S. Talangrimba, and S. Ulakkedondong – S. Lumpur, respectively, in 2015, 2019, and 2023. Meanwhile, the PHU with the most significant percentage of areas experiencing high severity is PHU S. Burnai-S. Sibumbung. This severity corresponded to years of El Niño, which caused a severe drought.

Furthermore, a moderate-high severity level had been in a slightly larger area than the high severity level. This severity occurred in the largest region in 2015, especially PHU S. Burnai-S. Sibumbung. Fires of high-moderate severity occurred over all PHUs almost yearly during the study period, even in a tiny percentage of the area. In addition, the trend of the percentages of regions with moderate-low severity was almost the same as that with moderate-high severity, but the percentages were slightly higher. Meanwhile, the low severity of fires had stayed stable over time.

On the contrary, in 2015, 2019, and 2023, as expected, the area did not burn less compared to other years. Unburned areas imply fire resistance and a stable, ecologically stable ecosystem. Meanwhile, low levels of regrowth grew in some PHUs but remained consistent in others. Enhanced regrowth low occurrences were highest in PHU S. Sibumbung-S. Talangrimba and S.

Talang-S. Ulakkedondong, but enhanced regrowth high burns were rare and variable. Enhanced regrowth high, identical to enhanced regrowth low, was highest in PHU S. Sibumbung-S. Talangrimba and S. Ulakkedondong-S. Lumpur.

The analysis of burn severity trends from 2015 to 2023 reveals interesting patterns in the temporal distribution of burn severity classifications, as depicted in Fig. 7. Notably, the proportion of high-severity burn regions peaked in 2015 at 2.01% of the landscape. Following that, there was a steady fall, reaching a low of 0.11% in 2017 and 2020. However, there was a modest increase in high-severity burn regions in 2023, recording at 0.95%. Unburned areas, which began at 49.10% in 2015, fluctuated but generally showed an increasing trend in succeeding years, indicating a continuous recovery process.

The data also shows that the trend in moderate-high, moderate-low, and low-severity burn areas is dropping. This decrease indicates a transition from moderate to low burn severity, indicating that these areas are still recovering. Similarly, from 2015 to 2018, the categories of Enhanced Regrowth Low and Enhanced Regrowth High showed constant growth, indicating a period of regrowth and recovery in these areas, followed by minimal changes in succeeding years.

A remarkable contrast arises when comparing 2015 to 2023: whereas high-severity burns peaked at 2.01% in 2015, unburned land accounted for the highest proportion at 69.46% in 2018, indicating significant progress in ecological restoration. This shift reflects a steady tendency toward recovery, as seen by a decrease in the proportions of high and moderate burn severity categories and an increase in unburned and regrowth areas.

### DISCUSSION

The relationship between land cover dynamics and fire severity levels exposes interrelated environmental processes and their long-term implications. This study's land cover classification model consistently categorizes different landscape aspects with high OA and Kappa values, demonstrating its dependability in capturing landscape complexity. While the model succeeds at identifying different land cover types such as tree cover, shrubland, grassland, and built-up areas, the model's varying accuracy in recognizing shrublands and sparse vegetation implies susceptibility to environmental shifts or changes in land cover of the study area.



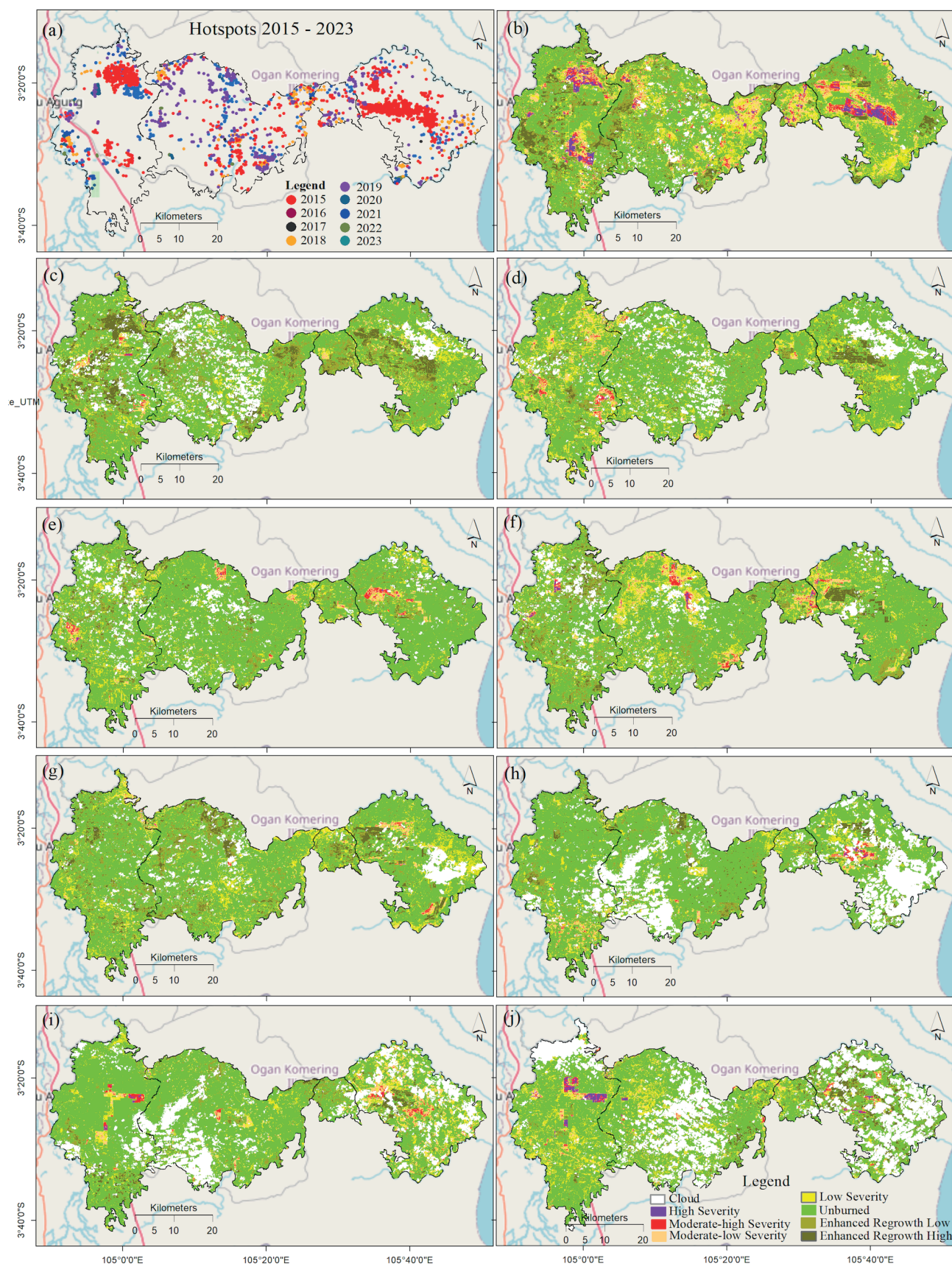
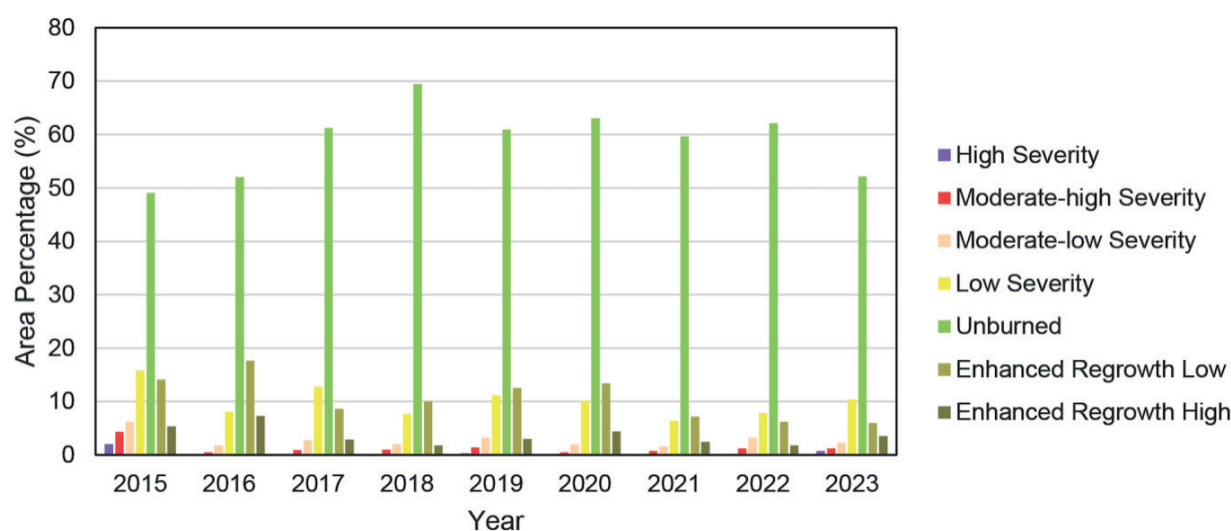


Fig. 6. (a) Fire hotspots and (b) – (j) burned severity in the study area from 2015–2023



**Fig. 7. The variation of area percentages of burn severity from 2015 to 2023**

Temporal assessments of land cover transformations reveal subtle changes in tree cover, shrubland, grassland, and built-up areas, particularly in peatland areas. Declines in tree cover and increases in shrubland, grassland, and built-up areas suggest land conversions for plantations or settlements. The peatland conversion to oil-palm plantations also occurred in other sites, such as Riau Province, Indonesia (Numata et al. 2022), Kalimantan, Indonesia, and Peninsular Malaysia (Miettinen et al. 2016). Deforestation and land conversion in peatlands are causing significant loss of natural forest cover, greenhouse gas emissions, and habitat loss for variety of species. In addition, reduced tree cover during El Niño episodes suggests a vulnerability to fires and probable deforestation in peatlands. Peatlands have always had fire as an inherent component of their ecosystems. Agricultural techniques and land clearance are two examples of human activities that have contributed to the dramatic increase in the frequency and severity of flames in the last several centuries (Cole et al. 2019). The ability of peatlands to withstand fire is determined by variables such as the frequency and intensity, as well as the extent of human interference. Undisturbed peatlands demonstrate inherent resilience, but human activities diminish their ability to recuperate after fires. Nonetheless, observed increases in tree cover in some years suggest afforestation or regeneration initiatives are critical for peatland conservation. These variations highlight the dynamic character of landscapes influenced by human activity, conservation efforts, and climatic variations such as El Niño.

The burn severity patterns reported in this study are consistent with the findings of prior research on fire dynamics in tropical peatlands (Page et al. 2009). El Niño events have a substantial impact on fires in Southeast Asian peatlands. These events increase both the frequency and intensity of fires in the region. The fires are more severe during El Niño because of prolonged drought and lower water tables. These conditions make the peat substrates more prone to burning. A significant correlation exists between drought conditions worsened by El Niño occurrences and the increased intensity and spread of fires in tropical peatland regions (Schmidt et al. 2024; Turetsky et al. 2015).

High fire severity during El Niño-induced droughts corresponds to environmental stress, with PHU S. Burnai–S. Sibumbung having the most significant percentage of high-severity burns. Moderate-high severity covers a broader area than high severity, with moderate-low severity having

slightly higher proportions. Low-severity fires maintain steady levels over time. Severe fires frequently cause significant changes in the plant communities' composition, promoting the growth of species that are more suited to intense disturbances. On the other hand, fires with minimal intensity typically maintain the plant community's current structure, enabling faster vegetation restoration before the fire (Schmidt et al. 2024). Unburned regions that remain steady over time demonstrate ecological stability and fire tolerance in specific ecosystems. Low-regrowth regions show different tendencies throughout PHUs, with enhanced regrowth levels more prominent in some locales. From 2015 to 2023, the dynamics of burn severity showed a decline in high-severity burn zones, followed by a minor increase in 2023. Moderate-high, moderate-low, and low-intensity burn zones exhibit falling patterns, indicating an ongoing recovery process. The difference between 2015 and 2023, with high-severity burns peaking in 2015 and unburned land reaching its highest share in 2018, demonstrates a persistent trend toward recovery. It provides critical insights into wildfire consequences and ecosystem recovery, aiding in land management decisions and strategic decisions about the recovery and preservation of ecosystems.

This study highlights the importance of understanding the relationship between land cover types and ecosystem dynamics in peatlands. It provides valuable information for local government, BRG, and other stakeholders involved in further restoration programs. Some of the programs must include rewetting drained peatlands, revegetating the landscape, and preparing peatlands without fire. To disable drainage systems, it needs to backfill and obstruct canals. The study underscores the importance of prioritizing restoration efforts in PHU S. Burnai–S. Sibumbung, an area with the highest proportion of burns classified as high severity. Targeted fire prevention and management methods, as well as reforestation and afforestation efforts, are crucial in this area. Planting native tree species that retain soil moisture and reduce fire danger is important. Sustainable land management methods that improve peatland resilience to climate fluctuations, particularly droughts, should be integrated into restoration initiatives. Hydrological restoration measures are also important in mitigating the impacts of climate change on peatlands. Implementing a monitoring system will allow stakeholders to track changes in land cover and fire severity, making timely adjustments to restoration programs. Additionally, engaging the community and educating them on peatland



conservation will generate support for restoration and promote sustainable livelihoods that protect peatland integrity. Peatlands, especially those in the Middle Taiga zone of West Siberia, are important carbon sinks, as (Dyukarev et al. 2019) shown by studying the carbon dynamics of peatland ecosystems. This realization emphasizes the need to preserve intact peatland cover in tropical areas, such as OKI peatland, to lessen the negative impacts of fire occurrences and changes in land cover on carbon sequestration.

## CONCLUSIONS

We have successfully performed dynamics of the land cover and burn severity in OKI peatland over the period of 2015 to 2023. The random forest algorithm accurately classified land cover, and the differenced Normalized Burn Ratio (dNBR) robustly delineated burn severity. We summarize our findings from the results as follows:

El Niño-induced drought in 2015 led to high temperatures and increased fire hotspots, causing significant tree cover loss and increased bare/sparse vegetation. In addition, the 2019 El Niño event caused another spike in fire hotspots, reducing unburned areas and increasing burn severity.

Human activities, including oil-palm plantations and agricultural expansion, exacerbated the degradation of natural ecosystems and increased fire risk.

Restoration activities from 2016 to 2020 mitigated the effects of the 2015 drought, resulting in fewer fire hotspots. Post-restoration, tree cover fluctuated, with minor fluctuations and a possible resurgence of fire activity.

The need for sustainable land management practices and stricter regulations is underscored, emphasizing the need for continuous adaptive management to ensure the long-term sustainability of both natural and human-modified landscapes. ■

## REFERENCES

- Ali U.A.M.E., Hossain M.A. and Islam M.R. (2019). Analysis of PCA Based Feature Extraction Methods for Classification of Hyperspectral Image. The 2<sup>nd</sup> International Conference on Innovation in Engineering and Technology (ICIET), Dhaka, Bangladesh. DOI: 10.1109/ICIET48527.2019.9290629
- Badan Restorasi Gambut. (2017). Lembar Pengesahan Rencana Restorasi Ekosistem Gambut 7 (Tujuh) Provinsi, Issue September.
- BBSDLP. (2019). Map of Peatland of Sumatra Island, Scale 1:50,000.
- Biancalani R. and Avagyan A. (2014). Towards Climate-Responsible Peatlands Management. In: Mitigation of Climate Change in Agriculture Series 9. Rome: Food and Agriculture Organization of the United Nations (FAO), <http://www.fao.org/3/a-i4029e.pdf>
- Carrasco L., O'Neil A., Morton R. and Rowland C. (2019). Evaluating Combinations of Temporally Aggregated Sentinel-1, Sentinel-2 and Landsat 8 for Land Cover Mapping with Google Earth Engine. *Remote Sensing*, 11(3), 288. DOI: 10.3390/rs11030288
- Cocke A.E., Fulé P.Z. and Crouse J.E. (2005). Comparison of Burn Severity Assessments Using Differenced Normalized Burn Ratio and Ground Data. *International Journal of Wildland Fire*, 14(2), 189–198. DOI: 10.1071/WF04010
- Cole L.E.S., Bhagwat S.A. and Willis K.J. (2019). Fire in the Swamp Forest: Palaeoecological Insights Into Natural and Human-Induced Burning in Intact Tropical Peatlands. *Frontiers in Forests and Global Change*, 2(August), 1–15. DOI: 10.3389/ffgc.2019.00048
- Dohong A. (2019). Restoring Degraded Peatland in Indonesia: the 3R Approach. Parish, F., Yan, L. S., Zainuddin, M. F. & Giesen, W.(Eds.) RSPO Manual on Best Management Practices (BMPs) for Management and Rehabilitation of Peatlands. 2<sup>nd</sup> Ed. Kuala Lumpur, RSPO, Kuala Lumpur, 57, 2016–2017.
- Dyukarev E.A., Godovnikov E.A., Karpov D.V., Kurakov S.A., Lapshina E.D., Filippov I.V., Filippova N.V. and Zarov E.A. (2019). Net Ecosystem Exchange, Gross Primary Production and Ecosystem Respiration in Ridge-Hollow Complex at Mukhrino Bog. *Geography, Environment, Sustainability*, 12(2), 227–244. DOI: 10.24057/2071-9388-2018-77
- Filgueiras R., Mantovani E.C., Althoff D., Filho E.I.F. and Cunha F.F.d. (2019). Crop NDVI Monitoring Based on Sentinel 1. *Remote Sensing*, 11(12). DOI: 10.3390/rs11121441
- Frampton W.J., Dash J., Watmough G. and Milton E.J. (2013). Evaluating the Capabilities of Sentinel-2 for Quantitative Estimation of Biophysical Variables in Vegetation. *ISPRS Journal of Photogrammetry and Remote Sensing*, 82, 83–92. DOI: 10.1016/j.isprsjprs.2013.04.007
- Gatti A., Naud C., Castellani C., Carriero F., Bertolini A., Nasuti C. and Carriero F. (2015). Sentinel-2 Products Specification Document. Thales Alenia Space, 1–487.
- Goldstein J.E., Graham L., Ansori S., Vetrina Y., Thomas A., Applegate G., Vayda A.P., Saharjo B.H. and Cochrane M.A. (2020). Beyond Slash-and-Burn: The Roles of Human Activities, Altered Hydrology and Fuels in Peat Fires in Central Kalimantan, Indonesia. *Singapore Journal of Tropical Geography*, 41(2), 190–208. DOI: 10.1111/sjtjg.12319
- Gomarasca M.A., Giardino C., Bresciani M., Caroli G.D., Sandu C., Tornato A., Spizzichino D., Valentini E., Taramelli A. and Tonolo F.G. (2019). Copernicus Sentinel Missions for Water Resources. The 6th International Conference on Space Science and Communication (IconSpac), Italy.
- Hapsari K.A., Biagioni S., Jennerjahn T.C., Reimer P., Saad A., Sabiham S. and Behling H. (2018). Resilience of A Peatland in Central Sumatra, Indonesia to Past Anthropogenic Disturbance: Improving Conservation and Restoration Designs Using Palaeoecology. *Journal of Ecology*, 106(6), 2473–2490. DOI: 10.1111/1365-2745.13000
- Harrison M.E., Wijedasa L.S., Cole L.E.S., Cheyne S.M., Choiruzzad S.A.B., Chua L., Dargie G.C., Ewango C.E.N., Honorio C.E.N., Ifo S.A., Imron M.A., Kopansky D., Lestaris T., O'Reilly P.J., van Offelen J., Refisch J., Roucoux K., Sugardjito J., Thornton S.A. and Page S. (2020). Tropical Peatlands and Their Conservation Are Important in the Context of COVID-19 and Potential Future (Zoonotic) Disease Pandemics. *PeerJ*, 1–43. DOI: 10.7717/peerj.10283
- Kankaku Y., Suzuki S. and Shimada M. (2015). ALOS-2 First Year Operation Result. *IEEE International Geoscience and Remote Sensing Symposium (IGARSS)*, 2, 4121–4124.
- Khakim M.Y.N., Bama A.A. and Tsuji T. (2022). Spatiotemporal Variations of Soil Moisture and Groundwater Level in a South Sumatra Peatland, Indonesia During 2015–2018. *Geography, Environment, Sustainability*, 15(2), 58–70. DOI: 10.24057/2071-9388-2021-137
- Khakim M.Y.N., Bama A.A., Yustian I., Poerwono P., Tsuji T. and Matsuoka T. (2020). Peatland Subsidence and Vegetation Cover Degradation as Impacts of the 2015 El Niño Event Revealed by Sentinel-1A SAR Data. *International Journal of Applied Earth Observation and Geoinformation*, 84(August 2019), 101953. DOI: 10.1016/j.jag.2019.101953
- Kim Y., Jackson T., Bindlish R., Lee H. and Hong S. (2012). Radar Vegetation Index For Estimating the Vegetation Water Content of Rice and Soybean. *IEEE Geoscience and Remote Sensing Letters*, 9(4), 564–568. DOI: 10.1109/LGRS.2011.2174772
- Loveland T.R. and Irons J.R. (2016). Landsat 8: The plans, the Reality, and the Legacy. *Remote Sensing of Environment*, 185, 1–6. DOI: 10.1016/j.rse.2016.07.033

- Miettinen J. and Liew S.C. (2010). Status of Peatland Degradation and Development in Sumatra and Kalimantan. *Ambio*, 39(5), 394–401. DOI: 10.1007/s13280-010-0051-2
- Miettinen J., Shi C. and Liew S.C. (2016). Land Cover Distribution in the Peatlands of Peninsular Malaysia, Sumatra and Borneo in 2015 with Changes Since 1990. *Global Ecology and Conservation*, 6, 67–78. DOI: 10.1016/j.gecco.2016.02.004
- Novero A.U., Pasaporte M.S., Aurelio R.M., Madanguit C.J.G., Tinoy M.R.M., Luayon M.S., Oñez J.P.L., Daquiado E.G.B., Diez J.M.A., Ordaneza J.E., Riños L.J., Capin N.C., Pototan B.L., Tan H.G., Polinar M.D.O., Nebres D.I. and Nañola C.L. (2019). The Use of Light Detection And Ranging (LiDAR) Technology and GIS in the Assessment and Mapping of Bioresources in Davao Region, Mindanao Island, Philippines. *Remote Sensing Applications: Society and Environment*, 13, 1–11. DOI: 10.1016/j.rsase.2018.10.011
- Numata I., Elmore A.J., Cochrane M.A., Wang C., Zhao J. and Zhang X. (2022). Deforestation, Plantation-Related Land Cover Dynamics and Oil Palm Age-Structure Change During 1990–2020 in Riau Province, Indonesia. *Environmental Research Letters*, 17(9). DOI: 10.1088/1748-9326/ac8a61
- Osaki M. and Tsuji N. (2016). Peatland Fire Occurrence. *Tropical Peatland Ecosystems*, Springer Japan. 377–395. DOI: 10.1007/978-4-431-55681-7\_25
- Osman K.T. (2018). Peat Soil. In: *Management of Soil Problems*. Springer International Publishing AG, part of Springer Nature. DOI: 10.1007/978-3-319-75527-4\_7
- Page S., Hoschilo A., Langner A., Tansey K., Siegert F., Limin S. and Rieley J. (2009). Tropical peatland fires in Southeast Asia. *Tropical Fire Ecology*, 263–287. DOI: 10.1007/978-3-540-77381-8\_9
- Panetti A., Rostan F., Abbate M.L. and Bruno C. (2014). Copernicus Sentinel-1 Satellite and C-SAR Instrument. *IEEE Geoscience and Remote Sensing Symposium*, 1, 1461–1464. DOI: 10.1109/IGARSS.2014.6946712
- Peat Restoration Agency. (2017). Data Acquisition and Thematic Mapping in KHG Area of Cawang - Lalang River and KHG of Sugihan - Saleh River. Final Report.
- Picotte J.J., Cansler C.A., Kolden C.A., Lutz J.A., Key C., Benson N.C. and Robertson K.M. (2021). Determination of Burn Severity Models Ranging from Regional to National Scales for the Conterminous United States. *Remote Sensing of Environment*, 263(May 2020), 112569. DOI: 10.1016/j.rse.2021.112569
- Peat Restoration Agency, Pub. L. No. 1 (2016).
- Pu R. (2021). Mapping Tree Species Using Advanced Remote Sensing Technologies: A State-of-the-Art Review and Perspective. *Journal of Remote Sensing*, 2021. DOI: 10.34133/2021/9812624
- Schmidt A., Ellsworth L.M., Boisen G.A., Novita N., Malik A., Gangga A., Albar I., Nurhayati A.D., Ritonga R.P., Asyhari A. and Kauffman J.B. (2024). Fire Frequency, Intensity, and Burn Severity in Kalimantan's Threatened Peatland Areas over Two Decades. *Frontiers in Forests and Global Change*, 7(February), 1–16. DOI: 10.3389/ffgc.2024.1221797
- Shirvani Z., Abdi O. and Buchroithner M. (2019). A Synergetic Analysis of Sentinel-1 and -2 for Mapping Historical Landslides Using Object-Oriented Random Forest in the Hyrcanian Forests. *Remote Sensing*, 11(19). DOI: 10.3390/rs11192300
- Sirin A. and Medvedeva M. (2022). Remote Sensing Mapping of Peat-Fire-Burnt Areas: Identification among Other Wildfires. *Remote Sensing*, 14(1). DOI: 10.3390/rs14010194
- Turetsky M.R., Benscoter B., Page S., Rein G., Van Der Werf G.R. and Watts A. (2015). Global Vulnerability of Peatlands to Fire and Carbon Loss. *Nature Geoscience*, 8(1), 11–14. DOI: 10.1038/ngeo2325
- Usup A., Hashimoto Y., Takahashi H. and Hayasaka H. (2004). Combustion and Thermal Characteristics of Peat Fire in Tropical Peatland in Central Kalimantan, Indonesia. *Tropics*, 14(1), 1–19. DOI: 10.3759/tropics.14.1
- Wang J., Xiao X., Liu L., Wu X., Qin Y., Steiner J.L. and Dong J. (2020). Mapping Sugarcane Plantation Dynamics in Guangxi, China, by Time Series Sentinel-1, Sentinel-2 and Landsat images. *Remote Sensing of Environment*, 247(June), 111951. DOI: 10.1016/j.rse.2020.111951
- Zhen Z., Quackenbush L.J. and Zhang L. (2016). Trends in Automatic Individual Tree Crown Detection and Delineation-Evolution of LiDAR Data. *Remote Sensing*, 8(4), 1–26. DOI: 10.3390/rs8040333
- Zhen Z., Chen S., Yin T. and Gastellu-etchegorry J. (2023). Globally Quantitative Analysis of the Impact of Atmosphere and Spectral Response Function on 2-Band Enhanced Vegetation Index ( EVI2 ) over Sentinel-2 and Landsat-8. *ISPRS Journal of Photogrammetry and Remote Sensing*. 205(November 2023), 206–226. DOI: 10.1016/j.isprsjprs.2023.09.024



# STATISTICAL MODELING OF THE EFFECTS OF WIND SPEED, AIR TEMPERATURE AND RELATIVE HUMIDITY ON THE CONCENTRATION OF CARBON MONOXIDE IN THE URBAN ATMOSPHERE

**Gleb G. Alexandrov<sup>1\*</sup>, Alexander S. Ginzburg<sup>1</sup>**

<sup>1</sup> A.M. Obukhov Institute of Atmospheric Physics Russian Academy of Sciences, Pyzhevsky per, 3, Moscow, 119017, Russia

\*Corresponding author: [gleb@ifaran.ru](mailto:gleb@ifaran.ru)

Received: August 21<sup>st</sup> 2023 / Accepted: July 25<sup>th</sup> 2024 / Published: October 1<sup>st</sup> 2024

<https://doi.org/10.24057/2071-9388-2024-3012>

**ABSTRACT.** The high carbon monoxide content in the urban atmosphere is one of the most important indicators of poor air quality in megacities such as Moscow. This study is to evaluate the importance of wind speed, air temperature, and relative air humidity for predicting the concentrations of carbon monoxide for the day ahead using a simplified one-dimensional quasistationary statistical model. It is shown that the concentration of carbon monoxide in the Moscow atmosphere is determined by a combination of internal (previous days CO concentration) and external (meteorological conditions) factors. The variation of carbon monoxide concentration at one station differs from the variation at another station due to the differences in local conditions. Taking into account wind speed and air temperature increases the predictive value of the one-dimensional quasi-stationary statistical model for most of the stations. In contrast to wind, relative air humidity decreases the predictive value of the model for most of the stations. This means that meteorological factors considered in this study could have different effects on predicting carbon monoxide concentration in the case of Moscow. The data from the Balchug weather station, located in the city center, offers a more accurate CO concentration forecast for most Moscow stations compared to the VDNKh weather station. For a more complete description of the influence of meteorological conditions on the predicted low concentration of gases, it is useful to take into account the model wind direction, surface air pressure, and the intensity of mixing in the urban boundary layer.

**KEYWORDS:** statistical forecasting, regression-autoregression model, urban air, atmospheric pollution, carbon monoxide, meteorological factors

**CITATION:** Alexandrov G. G., Ginzburg A. S. (2024). Statistical Modeling Of The Effects Of Wind Speed, Air Temperature And Relative Humidity On The Concentration Of Carbon Monoxide In The Urban Atmosphere. *Geography, Environment, Sustainability*, 3(17), 19-34

<https://doi.org/10.24057/2071-9388-2024-3012>

**ACKNOWLEDGEMENTS:** The authors are grateful to the “Mosecomonitoring” for providing data, reviewers and editor for constructive comments. This work was supported by a part of State Task registration number 1021032424681-6-1.5.10;1.5.8;1.6.19.

**Conflict of interests:** The authors reported no potential conflict of interest.

## INTRODUCTION

Modeling and forecasting the content of gas pollutants in the urban atmosphere is one of the most important, interesting, and difficult problems of urban meteorology. As is known, the concentrations of gaseous pollutants in urban air are determined by the magnitude and spatial distribution of their emissions from stationary and mobile sources, atmospheric diffusion, and mesoscale meteorological processes. The assessment of the influence of meteorological factors on the measured and predicted concentrations of gas pollution is a rather non-trivial research task due to the uncertainty of the spatial and temporal variability of emissions and their propagation conditions. Modern meteorological models (WRF, COSMO,

ICON, etc.) may not always justify their use due to the complex configuration of the urban surface layer and the multitude of stationary and mobile sources of gas pollution in megacities like Moscow. In many large cities around the world, especially in South and Southeast Asia, machine learning methods based on multiple regression and autoregression equations are widely used for short-term forecasting of urban air pollution, which give results comparable to those of meteorological models but require significantly lower computational costs. In Russia, the methods for calculating the dispersion of emissions of polluting substances in atmospheric air were approved by the Order of the Ministry of Natural Resources and Ecology (Order No. 273 from June 6, 2017) replacing the “Methodology for calculating concentrations of harmful

substances, contained in emissions from enterprises, in the atmospheric air" (OND-86) that had been valid since 1986. Urban transport is the primary source of carbon monoxide. The spatial and temporal distribution of this CO source is difficult to describe in sufficient detail for numerical modeling. Thus, for example, the decrease in the concentration of CO in Moscow due to a sharp decrease in ground transport flows during the lockdown associated with the COVID-19 pandemic was much stronger in residential areas than near highways (Ginzburg et al. 2020). Due to the complex pattern of CO sources, in previous works (Demchenko et al. 2015; Zavalishin et al. 2018) co-authored by the authors of this article, the method of multiple regression-autoregression was suggested for using in short-term forecasting of the average daily concentration of CO and other gas and aerosol pollutants in the urban atmosphere and to address the effect of the main meteorological factors (temperature, wind speed and air humidity).

The carbon monoxide increase in an urban environment leads to the formation of tropospheric ozone and serves as an indicator of global atmospheric changes (Grechko et al. 2009). Variations in carbon monoxide concentration in the Moscow air basin are significantly affected by meteorological conditions (Vilfand et al. 2014; Golitsyn et al. 2015; Kuznetsova 2010; Demchenko et al. 2015; Elansky et al. 2015; Rakitin et al. 2021) such as wind speed (Grechko et al. 2009, Demchenko et al. 2015, Elansky et al. 2015, Rakitin et al. 2021, Berlyand, 1991, Comrie & Diem 1999, Đurić & Vujović 2020, Li, R. et al. 2020, Ruan 2021), air temperature (Benavides et al. 2019, Berlyand 1991, Comrie & Diem 1999, Czerwińska & Wielgosiński 2020, Đurić & Vujović 2020, Li et al. 2020, Ruan et al. 2021), air humidity (Comrie & Diem 1999), and atmospheric pressure (Comrie & Diem 1999, Czerwińska & Wielgosiński 2020, Ruan et al. 2021).

Besides, carbon monoxide variations reflect the weekly cycle of economic and business activity (Gorchakov et al. 2010a). On weekends, the concentration of carbon monoxide decreases (Gorchakov et al. 2006) to an average of 87.5% of the concentration on weekdays (Gorchakov et al. 2010b). The factors that determine "calendar" variability (Gorchakov et al. 2010c) are included in a non-linear regression-autoregression model developed for reproducing the temporal evolution of the observed concentrations of various pollutants in the Moscow air basin (Demchenko et al. 2015).

Modeling the temporal evolution of air pollutants in the urban atmosphere serves for many purposes: for making forecasts of their concentrations at different time scales (Arya 1990, Baklanov et al. 2007), for air quality management, and for relating the concentrations observed at stationary or mobile monitoring stations to the intensity and localization of emission sources (Bornstein, Johnson 1977). The models of the temporal evolution of air pollutants may be divided into statistical, simplified one-dimensional quasi-stationary models (Berlyand 1985), integral box models (Agirre-Basurko et al. 2006, Poggi, Portier 2011), and Euler or Lagrangian three-dimensional photochemical models (Arya 1990, Revokatova et al. 2012) such as the COSMO-ART model, which is used by The Russian Federal Service for Hydrometeorology and Environmental Monitoring (Roshydromet) (Revokatova et al. 2012). Statistical models, in contrast to three-dimensional models, do not require information on the intensity of emission sources. Obtaining such information is a difficult task. Statistical models are also much more computationally effective. Some studies (Dias-Robles et al. 2008, Gardner, Dorling 1998) also demonstrate that

the accuracy of statistical and three-dimensional models practically do not differ when they are used to predict the concentrations of pollutants for the upcoming day.

However, due to regional variations in the relationship between air pollution and meteorological conditions, the performance of a statistical model depends on the factors taken into consideration (Liu et al. 2020). This study is to reveal the contribution of such meteorological factors as wind speed, air temperature, and air humidity to the ability of a regression-autoregression model to reproduce the observed carbon monoxide concentrations.

## MATERIALS AND METHODS

The prognostic equation of nonlinear regression-autoregression proposed by Demchenko et al. (2015) includes both external and internal factors. The internal factors include the concentrations of atmospheric pollutants for the days during a certain period preceding the day for which the forecast is made, and the external factors include meteorological factors.

The simplest way to predict any pollutant concentration on the one day ahead is using so-called inertial forecast, that is, to assume that tomorrow there will be the same concentration as today. It means that if in day before measured concentration is  $y_{i-1}$ , in the next day concentration  $Y_i = y_{i-1}$ . Below this forecast will be called "inertial".

In simplest autoregression model the one day ahead prediction of a pollutant concentration  $Y_i$  is based on the measured concentrations on the two previous days  $y_{i-1}$  and  $y_{i-2}$ .

The model will be represented by the following Eq. (1):

$$Y_i = a_1 y_{i-1} + a_2 y_{i-2} \quad (1)$$

where  $a_1$  and  $a_2$  are the coefficients that provide the best approximation in terms of the standard deviation of the predicted values from the observed values,  $Y_i$  is predicted value of CO concentration for the  $i$ -th day,  $y_{i-1}$  and  $y_{i-2}$  are concentrations of pollutant of previous 2 days,  $i$  is the index of the array containing the observed values of CO concentrations.

To study the role of wind speed, a term describing the effect of wind speed is added to the right side of Eq. (1) (Eq. (2)):

$$Y_i = a_1 y_{i-1} + a_2 y_{i-2} + a_3 (v_i + a_4) \quad (2)$$

where  $v_i$  is the average daily wind speed (m/s) at the day of forecast,  $a_1$ ,  $a_2$ ,  $a_3$  and  $a_4$  are the coefficients that provide the best approximation in terms of the standard deviation of the predicted values from the observed values.  $a_4$  – additional coefficient for better accounting of calm conditions.

To study the role of air temperature (°C) a term describing the effect of air temperature is added to the right side of Eq. (2) (Eq. (3)):

$$Y_i = a_1 y_{i-1} + a_2 y_{i-2} + a_3 (v_i + a_4) + a_5 T_i \quad (3)$$

where  $T_i$  – the daily mean air temperature,  $a_1$ ,  $a_2$ ,  $a_3$ ,  $a_4$  and  $a_5$  are the coefficients that provide the best approximation in terms of the standard deviation of the predicted values from the observed values.

To study the role of relative air humidity (%), a term describing the effect of relative air humidity was added to the right side of Eq. (3) (Eq. (4)):

$$Y_i = a_1 y_{i-1} + a_2 y_{i-2} + a_3 (v_i + a_4) + a_5 T_i + a_6 u_i \quad (4)$$

where  $u_i$  is the average daily air humidity,  $a_1$ ,  $a_2$ ,  $a_3$ ,  $a_4$ ,  $a_5$  and  $a_6$  are the coefficients that provide the best approximation in terms of the standard deviation of the predicted values from the observed values.

For a more complete consideration of the influence of meteorological conditions on the predicted concentration of gaseous pollution, it is helpful to include in the statistical model wind direction, surface air pressure, and preferably temperature at a certain height (for example, on the Ostankino tower), verbal gradations of stratification types (unstable, stable, weakly stable) and mixing intensity (intense, moderate, weak, strong). However, it is difficult to consider all these factors within the framework of a single article. This is the subject of further research and publications.

The observed values of carbon monoxide concentrations are provided by the Budgetary Environmental Protection Institution "Mosecomonitoring". The air quality monitoring system includes a network of automatic air pollution monitoring stations (AAPMS), specialized meteorological complexes for monitoring dispersion conditions, mobile laboratories, and an analytical laboratory accredited for laboratory analysis of a wide range of pollutants in the air. The atmospheric air pollution monitoring system in Moscow contains a network of 56 stationary automatic air

pollution monitoring stations, which allow continuous and round-the-clock monitoring of more than 20 atmospheric pollution parameters (Fig. 1). In addition, there is a high-altitude air pollution control station at the Ostankino television tower. These automated air pollution control stations are located throughout the city and cover all functional areas: areas under the influence of major roads, sleeping areas, areas located at a distance from emission sources (suitable for background monitoring), areas affected by emissions from large industrial facilities.

To analyze the contribution of meteorological factors, we used two datasets representing different patterns of city lifestyle. The first dataset contains the data for May-July 2020. The COVID restrictions had an impact on lifestyle during this period. The second dataset contains the data for May-July 2021. During this period, Moscow citizens came back to their usual lifestyle.

Each period was divided into a training sub-period (May-June) and a prediction sub-period (July). The training sub-period is used to determine the coefficients of the Eq. (1-4) and to evaluate how well the model fits the



Fig. 1. Map of Automated air pollution control stations in Moscow

(map used as a source available by link [https://commons.wikimedia.org/wiki/File:Msk\\_blank.svg?uselang=ru](https://commons.wikimedia.org/wiki/File:Msk_blank.svg?uselang=ru))

observations that were used for its training. The prediction sub-period is used to evaluate how well the model predicts observations that were not used for its training.

The meteorological data for the WMO station №27612 (VDNKh) which is usually considered a representative station for Moscow, and for the WMO station №27605 (Balchug), located in the city center, were taken from the RP5 website (<https://rp5.ru/>). The code (R script) and primary data used in calculations are available upon request to the corresponding author.

## RESULTS

The values of carbon monoxide concentration predicted with Eq. (1) correlate quite well with the observed ones (Table A.1). For example, at Zelenograd-6 station, the correlation coefficient is equal to 0.76, at MSU station, it is 0.85, at Chayanov, it is 0.78, and at half of the stations it exceeds 0.51.

One may slightly increase the correlation coefficient between the predicted and observed values of carbon monoxide concentrations by taking into account the factor of wind speed (Table A.1), Eq. (2). For example, at the MSU station, the correlation coefficient increases from 0.85 to 0.86, and at Chayanov, from 0.78 to 0.79. The exception is the Zvenigorod station, where the correlation coefficient increases from 0.03 to 0.43, and the Dolgoprudnaya station, where the correlation coefficient increases from 0.18 to 0.28.

If the air temperature (Table A.1) is also taken into account, Eq. (3) slightly improves the match between predicted and observed values compared to Eq. (2). The correlation coefficient increases by 0.15 at Dolgoprudnaya and by 0.12 at Sukharevskaya station; in most other cases, the increase does not exceed 0.02.

Considering additionally the factor of humidity (Table A.1), Eq. (4), has an even stronger effect: the correlation coefficient increases by 0.04 at most stations. The highest increase is achieved at the Lyublino station (by 0.17), the Dolgoprudnaya station (by 0.11) and the Glebovskaya station (by 0.10).

The Eq. (4), which includes wind speed, temperature, and relative humidity, reproduces well the concentrations observed at some stations (Fig. 2) and significantly increases the correlation between predicted and observed

values compared to the Eq. (1), which does not include meteorological predictors: the correlation coefficient increases by 0.08 at most stations. In the case of Zvenigorod station, the correlation coefficient increases from 0.03 to 0.51, at the Dolgoprudnaya from 0.18 to 0.53, at the Lyublino from 0.24 to 0.50, at the Sukharevskaya from 0.50 to 0.71, at the station Spiridonovka from 0.39 to 0.55, and the median of the correlation coefficient increased to 0.59.

The results obtained using meteorological data from the Balchug station improved the average forecast results (July 2020 and 2021). For July 2020 with meteorological data from the VDNKh station (Table A.3), the maximum average correlation among all 4 types of models was 0.46 (Eq. (1)), but with meteorological data from the Balchug (Table A.5) it became 0.58 (Eq. (2)), exceeding the inertial forecast, which was 0.46, by 0.12 points.

For July 2021, we got almost the same results with meteorological data from the VDNKh station (Table A.4). The highest average correlation between all 4 types of models was 0.35 (Eq. (1)), but it rose to 0.56 (Eq. (2)) with meteorological data from the Balchug (Table A.6), which was 0.15 points higher than the inertial forecast of 0.41.

The observations show that the pattern of changes in carbon monoxide concentration varies from station to station. To find out if there was any connection between these patterns, we divided stations by administrative districts to see the correlation between stations. Stations were divided into 5 groups: northern districts (Table 1), Zelenograd district (Table 2), Eastern and Central administrative districts (Table 3) and Southern districts (Table 4). Carbon monoxide concentrations at the stations of the South-West Administrative District (Butlerova and Cheryomushki) correlate well with each other (Table 1). The South-Eastern Administrative District's stations (Veshnyaki, Lyublino, and Maryinsky Park) exhibit a similar correlation. As to the stations of the South Administrative District (Biryulyovo, Guryevskiy passage, Shabolovka), only Guryevskiy passage and Shabolovka correlate well with each other. The way that CO concentration changes over time at the Biryulyovo station is very different from how it changes at stations in the South Administrative District and in the southern parts of Moscow. As shown in Table 1, concentration changes at these stations (with the exception of Biryulyovo) are well correlated.

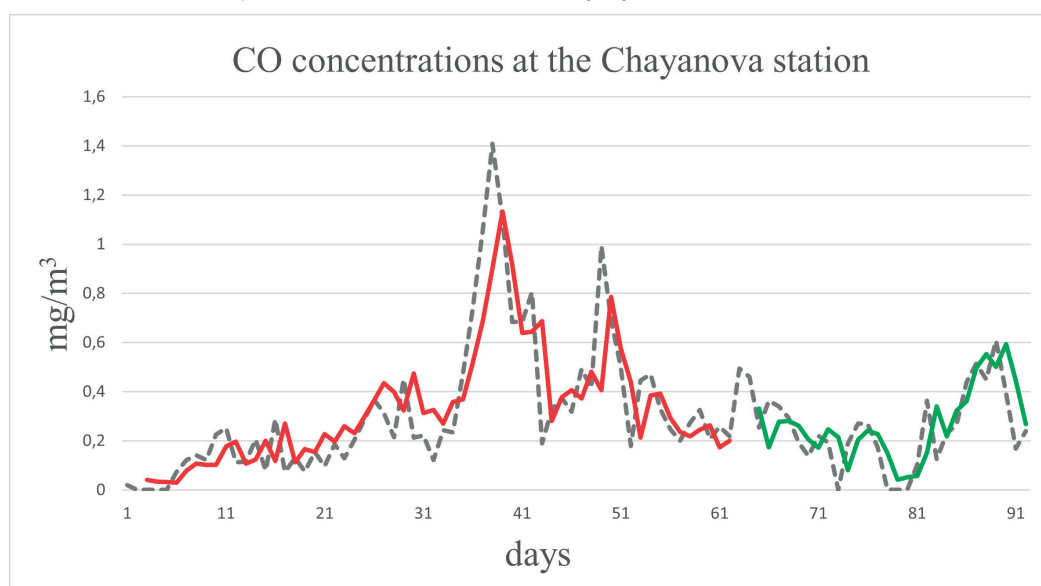


Fig. 2. CO concentrations at the Chayanova station in the period from May to July 2020: the gray dotted line is the observed values; the red line is the simulated values for the period from May to June; and the green line is the values for July (calculated with Eq. (4))



**Table 1. Coefficients of pairwise correlation between changes in carbon monoxide concentration at the stations in the southern part of Moscow**

Number and name of a station		1	2	3	4	5	6	7	8
1	Biryulyovo	1	0.53	0.41	0.25	0.45	0.44	0.50	0.34
2	Guryevskiy passage	0.53	1	0.71	0.76	0.77	0.67	0.63	0.68
3	Shabolovka	0.41	0.71	1	0.79	0.66	0.72	0.76	0.81
4	Veshnyaki	0.25	0.76	0.79	1	0.74	0.70	0.75	0.75
5	Lublino	0.45	0.77	0.66	0.74	1	0.81	0.59	0.72
6	Maryinsky park	0.44	0.67	0.72	0.70	0.81	1	0.59	0.74
7	Butlerova	0.50	0.63	0.76	0.75	0.59	0.59	1	0.74
8	Cheryomushki	0.34	0.68	0.81	0.75	0.72	0.74	0.74	1

The measurements at Zelenograd stations also correlate well with each other (Table 2).

However, the measurements at the stations of the Central Administrative District (Kazakova, Spiridonovka, Chayanova) do not correlate well with each other (Table 3a), as do the measurements at the stations of the Eastern Administrative District (Table 3b) and at the stations in the northern part of Moscow (Table 4).

The measurements at WAD stations (MSU and Tolbukhina) do not correlate well with each other ( $R=0.66$ ). However, it is noteworthy that the MSU station's measurements exhibit a strong correlation with those from stations in other districts, specifically Ostankino (NEAD),  $R=0.77$ , Letnaya (NWAD),  $R=0.78$ , Kazakova (CAD),  $R=0.7$ , Shabolovka (SAD),  $R=0.77$ , Veshnyaki (SEAD),  $R=0.81$ , Cheryomushki (SWAD),  $R=0.77$ . In the worst scenario, the correlation coefficient between the measurements at the

MSU station and the Kozhukhovo station is 0.25. However, measurements at the Kozhukhovo station generally correlate poorly with measurements at other stations in Moscow: the correlation coefficient does not exceed 0.49, and the median correlation coefficient is 0.3.

Another station where the measurements correlate poorly with those at other stations is the Biryulyovo station: the correlation coefficient does not exceed 0.51, and the median of the correlation coefficient is 0.25.

The measurements at the Losiny Ostrov station, located on a territory whose characteristics differ significantly from other observation zones, correlate better with measurements at other stations than measurements at Biryulyovo station: the median of the correlation coefficient is 0.53, and its maximum value is 0.7.

If we do not take into account the measurements at Biryulyovo, Kozhukhovo, Kosino, MADI, Polyarnaya,

**Table 2. Pairwise correlation coefficients between changes in carbon monoxide concentration at Zelenograd stations**

Number and name of a station		1	2	3
1	Zelenograd-mr 11	1	0.79	0.75
2	Zelenograd-mr 16	0.79	1	0.75
3	Zelenograd-mr 6	0.75	0.75	1

**Table 3. Coefficients of pairwise correlation between changes in carbon monoxide concentration at the stations of the Central Administrative District (CAD) (a) and the Eastern Administrative District (EAD) (b)**

Number and name of a EAD station (a)					Number and name of a CAD station (b)			
1	2	3	4	5	1	2	3	4
1	Kozhukhovo	1	0.49	0.36	Kazakova			
2	Kosino	0.49	1	0.40	Spiridonovka			
3	Losiny Ostrov	0.36	0.40	1	Chayanova			

**Table 4. Coefficients of pairwise correlation between changes in carbon monoxide concentration at stations in the northern part of Moscow**

Number and name of a station		1	2	3	4	5	6
1	Dolgoprudnaya	1	0.52	0.79	0.72	0.79	0.44
2	MADI	0.52	1	0.52	0.25	0.51	0.39
3	Ostankino	0.79	0.52	1	0.55	0.75	0.54
4	Polyarnaya	0.72	0.25	0.55	1	0.60	0.33
5	Letnaya	0.79	0.51	0.75	0.60	1	0.47
6	Turistskaya	0.44	0.39	0.54	0.33	0.47	1

Touristskaya, Chayanova stations, where the median of the correlation coefficient with measurements at other stations does not exceed 0.51, then we can say that the measurements at the remaining stations (Losiny Ostrov, Moscow State University, Tolbukhina, Dolgoprudny, Ostankino, Letnaya, Kazakova, Spiridonovka, Guryevskiy passage, Shabolovka, Lyublino, Maryinsky park, Butlerova, Cheryomushki) correlate well with each other: the medians of the correlation coefficient vary from 0.59, in the case of Losiny Ostrov station, to 0.74, in the case of the Veshnyaki station, and its smallest values vary from 0.47, in the case of the Spiridonovka station, to 0.64, in the case of the Veshnyaki station.

The absence of a pronounced spatial correlation between the stations supports the opinion (Dias-Robles et al. 2008, Gardner, Dorling 1998) that simplified onedimensional quasi-stationary statistical models are not less suitable than three-dimensional models for predicting the concentrations of pollutants for the day ahead. This

means that each station can be analyzed and studied independently from the others.

We should keep in mind that the zones in which AAPMS is located determine its classification, given that changes in CO concentration by stations are independent. There are 3 types of zones: residential and natural, nonresidential (near highways) and mixed zones. Comparing predicted carbon monoxide concentrations for July 2020 and 2021 it is obvious that, in general, the correlation between the observed and predicted carbon monoxide concentrations for the prediction sub-period is stronger in the case of the station located in a residential and natural zone (Fig. 1) as can be seen from Tables 5 and 6.

## DISCUSSION AND CONCLUSION

The application of the proposed statistical model with the account of different numbers of meteorological factors provides quite a complicated heterogeneous picture.

**Table 5. Correlation between observed and predicted carbon monoxide concentrations for July 2020 (prediction sub-period) by zones**

Station name	Correlation coefficient				
	Equation (1)	Equation (2) with $v_i$	Equation (3) with $v, T$	Equation (4) with $v, T$ and $u$	Inertial
Residential and natural zone					
Shabolovka	0.44	0.56	0.56	0.58	0.46
Losiny Ostrov	0.65	0.70	0.70	0.60	0.62
Tolbukhina	0.50	0.56	0.59	0.60	0.52
Median	0.50	0.56	0.59	0.60	0.52
Average	0.53	0.61	0.62	0.59	0.53
Nonresidential zone (near highways)					
Sukharevskaya	0.5	0.57	-0.19	0.12	0.62
Kozhukhovskiy passage	0.37	0.43	0.35	0.38	0.41
Zvenigorod	0.36	-0.02	-0.03	-0.04	0.36
Gagarin sq.	0.64	0.67	0.68	0.67	0.66
Median	0.44	0.50	0.16	0.25	0.52
Average	0.47	0.41	0.20	0.28	0.51
Mixed zone					
Maryino	0.21	0.01	0.2	-0.08	0.2
Glebovskaya	0.4	0.43	0.47	0.26	0.47
Lublino	0.18	0.2	0.22	0.02	0.18
Dolgoprudnaya	0.5	0.16	0.27	-0.06	0.42
Polyarnaya	0.65	0.64	0.66	0.62	0.64
Kozhukhovo	0.29	0.28	0.21	0.21	0.3
Median	0.35	0.24	0.25	0.12	0.36
Average	0.37	0.29	0.34	0.16	0.37

Table 6. Correlation between observed and predicted carbon monoxide concentrations for July 2021 (prediction sub-period) by zones

Station name	Correlation coefficient				
	Equation (1)	Equation (2) with $v_i$	Equation (3) with $v_i, T$	Equation (4) with $v_i, T$ and $u$	Inertial
Residential zone					
Shabolovka	0.55	0.3	0.28	0.13	0.62
Losiny Ostrov	0.58	0.42	0.43	0.42	0.6
Tolbukhina	0.44	0.39	0.4	0.41	0.48
Median	0.55	0.39	0.40	0.41	0.60
Average	0.52	0.37	0.37	0.32	0.57
Nonresidential zone (near highways)					
Sukharevskaya	0.17	0.26	0.25	-0.05	0.3
Kozhukhovsky passage	0.53	0.5	0.5	0.46	0.6
Zvenigorod	0.23	0.31	0.32	0.28	0.32
Gagarin sq.	0.38	0.52	0.53	0.43	0.52
Median	0.31	0.41	0.41	0.36	0.42
Average	0.33	0.40	0.40	0.28	0.44
Mixed zone					
Maryino	0.18	0.16	0.12	0.13	0.2
Glebovskaya	0.2	0.27	0.27	0.25	0.29
Lublino	0.08	-0.04	-0.03	-0.01	0.13
Dolgoprudnaya	0.48	0.53	0.5	0.56	0.62
Polyarnaya	0.52	0.51	0.53	0.44	0.4
Kozhukhovo	0.02	0.08	0.07	0.11	0.16
Median	0.19	0.22	0.20	0.19	0.25
Average	0.25	0.25	0.24	0.25	0.30

Nevertheless, taking into account meteorological predictors such as wind speed, air temperature, and relative humidity increase the correlation between predicted and observed carbon monoxide concentrations. The addition of wind (Eq. (2)) increases the correlation coefficient between observed and modeled values by 0.0–0.4, adding temperature (Eq. (3)) increases the correlation coefficient by another 0.0–0.14, adding relative humidity (Eq. (4)) increases the correlation coefficient by another 0.0–0.17. It should be noted here that the effect of meteorological predictors is more pronounced at some stations than at others. For example, in the case of the station Sukharevskaya, the addition of meteorological predictors increases the correlation coefficient from 0.5 to 0.71 (Table A.1), and in the case of the MSU station, from 0.85 to 0.86 (Table A.1). To increase clarity, replace with: The effect of weather forecasters can change from year to year. For example, adding temperature raises the correlation coefficient between observed and modeled values in

2021 by 0.02–0.21; adding wind raises it by 0.00–0.07; and adding humidity raises it by 0.00–0.03. For example, in the case of the station Sukharevskaya, the correlation coefficient increases from 0.4 to 0.5 (Table A.2), and in the case of the MSU station, from 0.18 to 0.26 (Table A.2). Interannual variability in the intensity of economic activity might explain the interannual variability in the effect of meteorological predictors: in the period from May to June 2020, there were epidemiological restrictions on economic activity in Moscow (Ginzburg et al. 2020).

However, it is difficult to draw an unambiguous conclusion about the role of meteorological predictors for all stations when the equations were applied for periods that were not used in determining the coefficients. In some cases, adding relative humidity to the number of meteorological predictors reduces the correlation coefficient between predicted and observed values in July to negligible (and even negative) values. The addition of wind increases the correlation coefficient between

observed and predicted values at 12 stations in July 2020 (Table A.3) by 0.0–0.12, and decreases by 0.01–0.38 at 6 stations; the addition of temperature increases the correlation coefficient by 0.0–0.19 at 13 stations and decreases by 0.01–0.76 at 5 stations; the addition of relative humidity increases the correlation coefficient by 0.0–0.31 at half of the stations and reduces by 0.01–0.33 the other half of the stations (Table A.3). In July 2021 (Table A.4) the addition of wind increases the correlation coefficient at 16 stations out of 28 stations by 0.0–0.14, and decreases by 0.01–0.25 at 12 stations; the addition of temperature increases the correlation coefficient by 0.0–0.04 at 18 stations and decreases by 0.01–0.05 at 10 stations; the addition of relative humidity increases the correlation coefficient by 0.0–0.09 at 13 stations and decreases by 0.01–0.3 at 15 stations (Table A.4). Almost the same result is obtained with RMSE (Table A.3, A.4), adding relative humidity (Eq. (4)) makes model worst then not adding any meteorological predictors (Eq.1). The correlation between the observed and predicted carbon monoxide concentrations for the training sub-periods of 2020 (Table A1) and 2021 (Table A.2) provided by the inertial forecast is weaker than that provided by any of the Eq. (1–4). As to the prediction sub-periods, at least one of Eq. (1–4) outperforms the inertial forecast at 15 out of 16 stations in 2020 (Table A.3) and at 10 out of 28 stations in 2021 (Table A.4). At all stations in 2020 (Table A.3) and at 23 of the 28 stations in 2021 (Table A.4), at least one of Eq. (1–4) does better than the inertial forecast in terms of RMSE. The correlation between the observed and predicted carbon monoxide concentrations for the prediction sub-periods provided by the Eq. (4) is weaker than that provided by any of the Eq. (1–3) at 8 out of 16 stations in 2020 (Table A.3) and at 14 out of 28 stations in 2021 (Table A.4). Hence, taking into account air humidity may reduce the prognostic value of a model. The RMSE provided by Eq. (4) is higher than that provided by any of Eq. (1–3) at the 4 out of 16 stations in 2020 (Table A.3) and at the 10 out of 28 stations in 2021 (Table A.4). This trend remains for meteorological data from Balchug, too. For 7 out of 16 stations, adding humidity worsened the correlation coefficient; for 5 out of 16 stations it improved, and for 4 stations, it remained unchanged. There were also exceptions at stations Shabolovka and Kozhukhovo. A gradual improvement was observed with the addition of meteorological parameters; the correlation coefficient increased from 0.44 to 0.68 and from 0.29 to 0.37, respectively. In the case of Dolgoprudnaya station, the correlation for Eq. (2) was 0.56, but when temperature and humidity were added, the correlation coefficient dropped to 0.29. This is also an isolated case, but the meteorological data from VDNKh showed a sharp drop in the correlation coefficient when adding meteorological parameters. The trend that

adding humidity worsens the forecast also continues for 2021 and is revealed even more clearly. For 19 out of 27 stations, the addition of humidity led to a worsening of the forecast, and at 4 out of 27 to an improvement; at 4 stations there was no change. Stations Shabolovka and Kazakova, as in 2020, show a trend towards improving the forecast with the addition of meteorological parameters. At station Butlerova, with the addition of humidity, the correlation coefficient increased from 0.08 to 0.24, but this is rather an exception. For 2020 and 2021, we can conclude that changes in weather data led to a significant improvement in the forecast, but adding humidity is not recommended, since (in 70% of cases for the period in 2021), this leads to its deterioration. Hence, taking into account air humidity may reduce the prognostic value of a model.

Therefore, adding relative air humidity to the list of meteorological predictors doesn't seem like a good way to improve a long-range forecast, since it makes the model less accurate most of the time. The inclusion of air temperature in the number of meteorological predictors increased the predictive value of the model at most stations, making it suitable for improving a long-range forecast of carbon monoxide concentration. Wind speed, similarly to air temperature, is shown to be a significant predictor of CO concentration in Moscow.

The wind speed, air temperature and relative humidity are not the only meteorological factors that may improve the accuracy of CO concentration forecast. There are some factors that describe weather conditions verbally (Kuznetsova 2021) that are hard to add to the model. For a more complete consideration of the influence of meteorological conditions on the predicted concentration of gaseous pollution, it is necessary to include in the statistical model wind direction, surface air pressure, and preferably temperature at a certain height (for example, on the Ostankino tower), verbal gradations of stratification types (unstable, stable, weakly stable) and mixing intensity (intense, moderate, weak, strong). However, it is difficult to consider all these factors within the framework of a single article. Further research is needed to understand why some meteorological factors may reduce the accuracy of CO concentration forecast provided by the statistical model. The results of this study suggest that the role of meteorological factors in explaining the observed variability of CO concentrations may fundamentally differ from their role in predicting the changes in CO concentrations for the day ahead: the comprehensive consideration of meteorological factors definitely improves the explanatory value of a model, but to improve the prognostic value of the model, it might be better to exclude some of the meteorological factors from consideration. ■



## REFERENCES

- Agirre-Basurko E., Ibarra-Berastedi G., Madariaga I. (2006). Regression and multilayer perception-based models to forecast O<sub>3</sub> and NO<sub>2</sub> levels in Bilbao area. *Environmental Modelling & Software*, 21(4), 430-446, DOI:10.1016/j.envsoft.2004.07.008.
- Arya S.P. (1990). *Air pollution meteorology and dispersion*. Oxford: Oxford University Press.
- Baklanov A., Hanninen O., Stordal L.H. et al. (2007). Integrated systems for forecasting urban meteorology, air pollution, and population exposure. *Atmospheric Chemistry and Physics*, 7(3), 855-874, DOI:10.5194/acp-7-855-2007.
- Benavides, J., Snyder, M., Guevara, M., Soret, A., Pérez García-Pando, C., Amato, F., & Jorba, O. (2019). CALIOPE-Urban v1.0: coupling R-LINE with a mesoscale air quality modelling system for urban air quality forecasts over Barcelona city (Spain). *Geoscientific Model Development*, 12(7), 2811-2835, DOI:10.5194/gmd-12-2811-2019.
- Berlyand M.E. (1985). *Forecast and regulation of atmospheric pollution*. Leningrad: Gidrometeoizdat.
- Berlyand M.E. (1991). Statistical methods of air pollution forecasting. In: *Prediction and Regulation of Air Pollution*. Atmospheric Sciences Library, vol 14. Dordrecht: Springer, 159-201, DOI:10.1007/978-94-011-3768-3\_6.
- Bornstein R.D. and Johnson D.S. (1977). Urban – rural wind velocity differences. *Atmospheric Environment*, 11(7), 597-604, DOI:10.1016/0004-6981(77)90112-3.
- Comrie A. C. and Diem J. E. (1999). Climatology and forecast modeling of ambient carbon monoxide in Phoenix, Arizona. *Atmospheric Environment*, 33(30), 5023-5036, DOI:10.1016/S1352-2310(99)00314-3.
- Czerwiński J. and Wielosiński G. (2020). The effect of selected meteorological factors on the process of « Polish smog » formation. *Journal of Ecological Engineering*, 21(1), 180-187, DOI:10.12911/22998993/112764.
- Demchenko P.F., Ginzburg A.S., Aleksandrov G.G., Gorchakov G.I., Zavalishin N.N., Yudin N.I., Vereskov A.I., Zakharova P.V. and Lezina E.A. (2015). Statistical modeling of average daily concentration of pollutants in the atmosphere over Moscow megalopolis by the multiple regression method. *Russian Meteorology and Hydrology*, 40, 658-666, DOI:10.3103/S1068373915100039.
- Dias-Robles L.A., Ortega J.C., Fu J.S., Reed G.D., Chow J.C., Watson J.G. and Moncada-Herrera J.A. (2008). A Hybrid ARIMA and artificial neural networks model to forecast particulate matter in urban areas: the case of Temuco, Chile. *Atmospheric Environment*, 42(35), 8331 – 8340, DOI:10.1016/j.atmosenv.2008.07.020.
- Đurić M and Vujović D. (2020). Short-term forecasting of air pollution index in Belgrade, Serbia. *Meteorological Applications*, 27(5), 1946, DOI:10.1002/met.1946.
- Elansky N.F., Belikov I.B., Skorokhod A.I., Lokoshchenko M.A. and Trifanova A.V. (2015). On contents of trace gases in the atmospheric surface layer over Moscow. *Izvestiya, Atmospheric and Oceanic Physics*, 51(1), 30-41, DOI:10.1134/S000143381501003X.
- Gardner M.W. and Dorling S.R. (1998). *Artificial Neural Networks (the Multilayer Perceptron) – a Review of applications in the atmospheric sciences*. *Atmospheric Environment*, 32(14-15), 2627-2636, DOI:10.1016/S1352-2310(97)00447-0.
- Ginzburg A.S., Semenov V.A., Semutnikova E.G., Aleshina M.A., Zakharova P.V. and Lezina E.A. (2020). Impact of COVID-19 Lockdown on Air Quality in Moscow. *Doklady Earth Sciences*, 495, 862–866, DOI:10.1134/S1028334X20110069.
- Golitsyn G.S., Grechko E.I., Dzhola A.V., Emilenko A.S., Kopeikin V.M., Rakitin V.S., Safronov A.N., Fokeeva E.V., Wang G. and Wang P. (2015). Studying the pollution of Moscow and Beijing atmospheres with carbon monoxide and aerosol. *Izvestiya, Atmospheric and Oceanic Physics*, 51, 1-11, DOI:10.1134/S0001433815010041.
- Gorchakov G.I., Zotkin E.V., Karpov A.V., Ul'yanenko A.V., Semutnikova E.G. and Lezina E.A. (2006). Variations in gaseous pollutants in the air basin of Moscow. *Izvestiya, Atmospheric and Oceanic Physics*, 42, 156-170, DOI:10.1134/S0001433806020046.
- Gorchakov G.I., Karpov A.V., Kolesnikova A.B., Baikova E.S., Semutnikova E.G. and Zadorozhnaya O.S. (2010a). Weekly cycle of air pollution in Moscow: quantitative characteristics and refinement of the method of statistical forecasting of impurity concentrations. *Optics of the atmosphere and the ocean*, 23(9), 784-792, (in Russian with English summary).
- Gorchakov G.I., Anoshin B.A., Karpov A.V., Kolesnikova A.B. and Semutnikova E.G. (2010b). Statistical prediction of the pollution of the urban atmosphere. 1. Statistical regularities of the interdiurnal variations of the carbon monoxide and nitrogen oxide concentrations. *Atmospheric and Oceanic Optics*, 23(4), 309-316, DOI:10.1134/S102485601004010X.
- Gorchakov G.I., Anoshin B.A., Karpov A.V., Kolesnikova A.B. and Semutnikova E.G. (2010c). Statistical prediction of the urban atmosphere contamination. 2. Forecasting method of the interdiurnal and intradiurnal concentration variability of the carbon monoxide and nitrogen oxides. *Atmospheric and Oceanic Optics*, 23(5), 396-403, DOI:10.1134/S102485601005009X.
- Grechko E.I., Dzhola A.V., Rakitin V.S., Fokeeva E.V. and Kuznetsov R.D. (2009). Variation of the carbon monoxide total column and atmospheric boundary layer parameters in the center of Moscow. *Atmospheric and Oceanic Optics*, 22(3), 203-208, DOI:10.1134/S1024856009020110.
- Kuznetsova I.N. (2012). The effect of meteorology on air pollution in Moscow during the summer episodes of 2010. *Izvestiya, Atmospheric and Oceanic Physics*, 48(5), 504-515, DOI:10.1134/S0001433812050052.
- Kuznetsova I.N., Tkacheva Yu.V., Shalygina I.Yu. and Nakhaev M.I. (2021). Forecasting a meteorological indicator of pollutant dispersion in surface air. *Hydrometeorological Research and Forecasting*, 3(381), 131-149, (in Russian with English summary), DOI:10.37162/2618-9631-2021-3-131-149.
- Li R., Wang Z., Cui L., Fu H., Zhang L., Kong L. and Chen J. (2019). Air pollution characteristics in China during 2015–2016: Spatiotemporal variations and key meteorological factors. *Science of the total environment*, 648, 902-915, DOI:10.1016/j.scitotenv.2018.08.181.
- Liu Y., Zhou Y. and Lu J. (2020). Exploring the relationship between air pollution and meteorological conditions in China under environmental governance. *Scientific reports*, 10(1), 14518, DOI:10.1038/s41598-020-71338-7.
- Poggi J.M. and Portier B. (2011). PM<sub>10</sub> forecasting using clusterwise regression. *Atmospheric Environment*, 45(38), 7005-7014, DOI:10.1016/j.atmosenv.2011.09.016.
- Rakitin V.S., Elansky N.F., Skorokhod A.I., Dzhola A.V., Rakitina A.V., Shilkin A.V., Kirillova N.S. and Kazakov A.V. (2021). Long-term tendencies of carbon monoxide in the atmosphere of the Moscow megapolis. *Izvestiya, Atmospheric and Oceanic Physics*, 57(1), 116-125, DOI:10.1134/S0001433821010102.
- Revokatova, A. P., Surkova, G. V., Kirsanov A.A. and Rivin G.S. (2012). Forecast of air pollution in the Moscow region using the COSMO-ART model. *Bulletin of Moscow University Series 5 Geography*, 4, 25-32, (in Russian with English summary).
- Ruan H. L., Deng W. S., Wang Y., Chen J. B., Hong W. L., Ye S. S. and Hu Z. J. (2021). Carbon monoxide poisoning: a prediction model using meteorological factors and air pollutant. *BMC proceedings*, 15, 1-9, DOI:10.1186/s12919-021-00206-7.

Vilfand R.M., Kuznetsova I.N., Shalygina I.Yu., Zvyagintsev A.M., Nakhaev M.I., Zakharova P.V. and Lapchenko V.A. (2014). Monitoring and forecasting of air quality in the Moscow region. *Biosphere*, 6(4), 339-351, (in Russian with English summary), DOI:10.24855/biosfera.v6i4.178.

Zavalishin N.N., Ginzburg A.S. and Alexandrov G.G. (2018). Statistical forecasting method for atmospheric air pollution in megapolises: Moscow case study. International conference and early career scientist's school on environmental observations, modeling and information systems: ENVIROMIS-2018, 302-305, (in Russian with English summary).

## APPENDICES

**Table A.1. Correlation and RMSE values between observed and predicted values of carbon monoxide concentrations for May–June 2020 (training sub-period) based on data from the VDHKh weather station.**

Station name	Correlation coefficient / RMSE				
	Equation (1)	Equation (2) with $v_i$	Equation (3) with $v, T$	Equation (4) with $v, T$ and $u$	Inertial
Sukharevskaya	0.50 / 0.119	0.51 / 0.110	0.63 / 0.099	0.71 / 0.089	0.50 / 0.127
Shabolovka	0.48 / 0.085	0.51 / 0.075	0.55 / 0.073	0.57 / 0.072	0.47 / 0.088
Kazakova	0.49 / 0.088	0.52 / 0.079	0.55 / 0.077	0.59 / 0.075	0.49 / 0.092
Maryino	0.29 / 0.084	0.35 / 0.075	0.36 / 0.075	0.42 / 0.073	0.30 / 0.097
Zelenograd 6	0.76 / 0.084	0.76 / 0.080	0.77 / 0.079	0.79 / 0.076	0.75 / 0.086
Zelenograd 11	0.51 / 0.065	0.51 / 0.061	0.51 / 0.060	0.55 / 0.059	0.50 / 0.071
MADI	0.22 / 0.182	0.27 / 0.156	0.28 / 0.155	0.29 / 0.155	0.26 / 0.199
Biryulyovo	0.65 / 0.143	0.68 / 0.131	0.70 / 0.127	0.72 / 0.124	0.65 / 0.152
Moscow State University (MSU)	0.85 / 0.090	0.86 / 0.084	0.86 / 0.082	0.86 / 0.077	0.82 / 0.090
Butlerova	0.63 / 0.052	0.64 / 0.048	0.66 / 0.048	0.71 / 0.045	0.61 / 0.053
Losiny Ostrov	0.64 / 0.124	0.65 / 0.113	0.65 / 0.112	0.71 / 0.105	0.66 / 0.135
Glebovskaya	0.43 / 0.172	0.44 / 0.146	0.46 / 0.145	0.56 / 0.133	0.42 / 0.184
Lublino	0.24 / 0.09	0.30 / 0.084	0.33 / 0.082	0.50 / 0.077	0.28 / 0.090
Chayanova	0.78 / 0.183	0.79 / 0.175	0.80 / 0.171	0.81 / 0.168	0.79 / 0.189
Tolbukhina	0.37 / 0.112	0.41 / 0.097	0.46 / 0.094	0.49 / 0.093	0.39 / 0.117
Dolgoprudnaya	0.18 / 0.093	0.28 / 0.081	0.42 / 0.076	0.53 / 0.071	0.21 / 0.106
Narodnogo opolcheniya	0.56 / 0.186	0.56 / 0.172	0.57 / 0.171	0.63 / 0.161	0.54 / 0.195
Polyarnaya	0.66 / 0.078	0.69 / 0.069	0.69 / 0.068	0.72 / 0.066	0.63 / 0.080
Spiridonovka	0.39 / 0.109	0.44 / 0.094	0.53 / 0.089	0.55 / 0.088	0.46 / 0.109
Kozhukhovsky passage	0.52 / 0.109	0.53 / 0.094	0.58 / 0.089	0.62 / 0.088	0.52 / 0.107
Ostankino	0.53 / 0.193	0.54 / 0.175	0.56 / 0.168	0.58 / 0.162	0.52 / 0.202
Zvenigorod	0.03 / 0.074	0.43 / 0.067	0.43 / 0.066	0.51 / 0.065	0.17 / 0.077
Kozhukhovo	0.41 / 0.127	0.47 / 0.094	0.50 / 0.094	0.51 / 0.089	0.43 / 0.150
Gagarin sq.	0.51 / 0.103	0.52 / 0.089	0.54 / 0.087	0.59 / 0.087	0.53 / 0.108
Median	0.51 / 0.109	0.52 / 0.094	0.55 / 0.089	0.59 / 0.088	0.50 / 0.108
Average	0.48 / 0.116	0.53 / 0.103	0.56 / 0.101	0.61 / 0.097	0.50 / 0.122

**Table A.2. Correlation and RMSE values between observed and predicted carbon monoxide concentrations for May-June 2021 (training sub-period) based on data from the VDHKh weather station.**

Station name	Correlation coefficient / RMSE value				
	Equation (1)	Equation (2) with $v_i$	Equation (3) with $v, T$	Equation (4) with $v, T$ and $u$	Inertial
Sukharevskaya	0.40 / 0.147	0.47 / 0.127	0.49 / 0.126	0.50 / 0.125	0.38 / 0.161
Shabolovka	0.30 / 0.117	0.35 / 0.103	0.38 / 0.102	0.38 / 0.102	0.27 / 0.130
Kazakova	0.27 / 0.136	0.33 / 0.12	0.33 / 0.120	0.36 / 0.119	0.24 / 0.154
Maryino	0.40 / 0.144	0.45 / 0.129	0.47 / 0.128	0.47 / 0.127	0.37 / 0.165
Zelenograd 6	0.40 / 0.112	0.41 / 0.103	0.42 / 0.102	0.42 / 0.102	0.34 / 0.128
Zelenograd 11	0.51 / 0.112	0.52 / 0.104	0.52 / 0.103	0.52 / 0.103	0.50 / 0.123
Zelenograd 16	0.51 / 0.141	0.56 / 0.122	0.56 / 0.122	0.58 / 0.121	0.53 / 0.142
MADI	0.45 / 0.153	0.45 / 0.141	0.50 / 0.138	0.51 / 0.136	0.41 / 0.169
Biryulyovo	0.49 / 0.124	0.52 / 0.111	0.52 / 0.111	0.52 / 0.111	0.50 / 0.131
Moscow State University (MSU)	0.18 / 0.088	0.25 / 0.077	0.26 / 0.077	0.26 / 0.077	-0.12 / 0.118
Butlerova	0.08 / 0.147	0.24 / 0.119	0.31 / 0.117	0.32 / 0.116	0.17 / 0.156
Losiny Ostrov	0.35 / 0.082	0.40 / 0.073	0.40 / 0.073	0.40 / 0.073	0.32 / 0.089
Glebovskaya	0.46 / 0.104	0.47 / 0.096	0.47 / 0.096	0.47 / 0.096	0.47 / 0.112
Lublino	0.18 / 0.202	0.39 / 0.162	0.40 / 0.161	0.40 / 0.161	0.20 / 0.223
Ak. Anokhina	0.28 / 0.141	0.33 / 0.123	0.36 / 0.122	0.37 / 0.121	0.26 / 0.159
Chayanova	0.43 / 0.108	0.50 / 0.093	0.51 / 0.093	0.51 / 0.093	0.44 / 0.113
Tolbukhina	0.41 / 0.122	0.47 / 0.107	0.48 / 0.107	0.48 / 0.107	0.37 / 0.135
Veshnyaki	0.66 / 0.121	0.68 / 0.111	0.68 / 0.110	0.69 / 0.110	0.66 / 0.127
Dolgoprudnaya	0.31 / 0.119	0.46 / 0.102	0.47 / 0.102	0.47 / 0.101	0.32 / 0.135
Koptevsky	0.54 / 0.216	0.54 / 0.203	0.56 / 0.201	0.56 / 0.201	0.49 / 0.237
Polyarnaya	0.49 / 0.207	0.54 / 0.182	0.56 / 0.179	0.57 / 0.178	0.51 / 0.216
Cheryomushki	0.36 / 0.104	0.39 / 0.093	0.39 / 0.093	0.39 / 0.093	0.33 / 0.117
Touristskaya	0.27 / 0.113	0.31 / 0.099	0.31 / 0.099	0.31 / 0.099	0.25 / 0.129
Spiridonovka	0.40 / 0.097	0.44 / 0.086	0.44 / 0.086	0.44 / 0.086	0.39 / 0.105
Kozhukhovskiy passage	0.67 / 0.128	0.68 / 0.12	0.68 / 0.120	0.68 / 0.120	0.64 / 0.140
Ostankino	0.28 / 0.095	0.32 / 0.084	0.33 / 0.083	0.34 / 0.083	0.18 / 0.104
Zvenigorod	0.30 / 0.162	0.40 / 0.138	0.41 / 0.138	0.41 / 0.137	0.33 / 0.173
Kozhukhovo	0.32 / 0.109	0.37 / 0.096	0.38 / 0.096	0.39 / 0.095	0.30 / 0.120
Gagarin sq.	0.34 / 0.196	0.40 / 0.169	0.40 / 0.169	0.41 / 0.169	0.36 / 0.207
Khamovniki	0.51 / 0.238	0.52 / 0.22	0.52 / 0.219	0.52 / 0.218	0.50 / 0.254
Kapotnya	0.69 / 0.101	0.71 / 0.093	0.72 / 0.091	0.72 / 0.091	0.69 / 0.106
Median	0.40 / 0.122	0.45 / 0.111	0.47 / 0.110	0.47 / 0.110	0.37 / 0.135
Average	0.39 / 0.135	0.45 / 0.120	0.46 / 0.119	0.46 / 0.118	0.37 / 0.148

**Table A.3. Correlation and RMSE values between observed and predicted carbon monoxide concentrations for July 2020 (prediction sub-period) based on data from the VDHKh weather station.**

Station name	Correlation coefficient / RMSE value				
	Equation (1)	Equation (2) with $v_i$	Equation (3) with $v, T$	Equation (4) with $v, T$ and $u$	Inertial
Shabolovka	0.44 / 0.11	0.56 / 0.091	0.56 / 0.104	0.58 / 0.089	0.46 / 0.112
Maryino	0.21 / 0.065	0.01 / 0.062	0.20 / 0.059	-0.08 / 0.088	0.20 / 0.075
MADI	0.31 / 0.219	0.27 / 0.206	0.36 / 0.217	0.33 / 0.207	0.31 / 0.232
Losiny Ostrov	0.65 / 0.066	0.70 / 0.060	0.70 / 0.061	0.60 / 0.077	0.62 / 0.072
Glebovskaya	0.40 / 0.172	0.43 / 0.158	0.47 / 0.177	0.26 / 0.169	0.47 / 0.171
Lublino	0.18 / 0.185	0.20 / 0.175	0.22 / 0.213	0.02 / 0.190	0.18 / 0.203
Chayanova	0.62 / 0.129	0.65 / 0.127	0.67 / 0.154	0.69 / 0.119	0.61 / 0.140
Tolbukhina	0.50 / 0.117	0.56 / 0.105	0.59 / 0.133	0.60 / 0.107	0.52 / 0.118
Dolgoprudnaya	0.50 / 0.126	0.16 / 0.146	0.27 / 0.203	-0.06 / 0.171	0.42 / 0.146
Narodnogo opolcheniya	0.72 / 0.217	0.76 / 0.207	0.76 / 0.206	0.78 / 0.312	0.76 / 0.209
Polyarnaya	0.65 / 0.155	0.64 / 0.148	0.66 / 0.157	0.62 / 0.145	0.64 / 0.152
Spiridonovka	0.46 / 0.142	0.46 / 0.136	0.42 / 0.221	0.45 / 0.176	0.44 / 0.154
Kozhukhovsky passage	0.37 / 0.183	0.43 / 0.158	0.35 / 0.251	0.38 / 0.167	0.41 / 0.188
Zvenigorod	0.36 / 0.101	-0.02 / 0.119	-0.03 / 0.113	-0.04 / 0.183	0.36 / 0.114
Kozhukhovo	0.29 / 0.109	0.28 / 0.099	0.21 / 0.125	0.21 / 0.110	0.31 / 0.114
Gagarin sq.	0.64 / 0.135	0.67 / 0.126	0.68 / 0.138	0.67 / 0.131	0.66 / 0.137
Median	0.45 / 0.132	0.45 / 0.132	0.45 / 0.156	0.42 / 0.156	0.45 / 0.143
Average	0.46 / 0.139	0.42 / 0.133	0.44 / 0.158	0.38 / 0.153	0.46 / 0.146

**Table A.4. Correlation and RMSE values between observed and predicted carbon monoxide concentrations for July 2021 (prediction sub-period) based on data from the VDHKh weather station.**

Station name	Correlation coefficient / RMSE value				
	Equation (1)	Equation (2) with $v_i$	Equation (3) with $v, T$	Equation (4) with $v, T$ and $u$	Inertial
Sukharevskaya	0.17 / 0.214	0.26 / 0.181	0.25 / 0.180	-0.05 / 0.241	0.30 / 0.211
Shabolovka	0.55 / 0.065	0.30 / 0.073	0.28 / 0.070	0.13 / 0.071	0.62 / 0.064
Kazakova	0.35 / 0.122	0.33 / 0.107	0.34 / 0.107	0.29 / 0.147	0.38 / 0.140
Maryino	0.18 / 0.153	0.16 / 0.133	0.12 / 0.135	0.13 / 0.145	0.20 / 0.169
Zelenograd 6	0.40 / 0.131	0.41 / 0.116	0.38 / 0.117	0.38 / 0.117	0.49 / 0.135
Zelenograd 11	0.35 / 0.093	0.35 / 0.085	0.35 / 0.086	0.33 / 0.093	0.35 / 0.099
Zelenograd 16	0.63 / 0.188	0.71 / 0.163	0.71 / 0.164	0.67 / 0.198	0.65 / 0.184
Biryulyovo	0.29 / 0.122	0.32 / 0.106	0.32 / 0.106	0.33 / 0.108	0.36 / 0.122
Moscow State University (MSU)	0.20 / 0.106	0.06 / 0.098	0.06 / 0.099	0.07 / 0.104	0.13 / 0.125
Butlerova	0.07 / 0.120	-0.16 / 0.115	-0.21 / 0.130	-0.12 / 0.111	0.04 / 0.136
Losiny Ostrov	0.58 / 0.047	0.42 / 0.064	0.43 / 0.063	0.42 / 0.061	0.60 / 0.048
Glebovskaya	0.20 / 0.150	0.27 / 0.136	0.27 / 0.135	0.25 / 0.138	0.29 / 0.153
Lublino	0.08 / 0.230	-0.04 / 0.199	-0.03 / 0.199	-0.01 / 0.198	0.13 / 0.246
Ak. Anokhina	0.39 / 0.127	0.47 / 0.116	0.46 / 0.125	0.34 / 0.113	0.54 / 0.120
Chayanova	0.52 / 0.114	0.56 / 0.105	0.56 / 0.103	0.56 / 0.106	0.56 / 0.117
Tolbukhina	0.44 / 0.134	0.39 / 0.124	0.40 / 0.124	0.41 / 0.123	0.48 / 0.139
Dolgoprudnaya	0.48 / 0.149	0.53 / 0.140	0.50 / 0.140	0.56 / 0.136	0.62 / 0.135
Koptevsky	0.12 / 0.193	0.15 / 0.176	0.13 / 0.184	0.17 / 0.199	0.24 / 0.210
Polyarnaya	0.52 / 0.191	0.51 / 0.166	0.53 / 0.164	0.44 / 0.229	0.40 / 0.195
Cheryomushki	0.37 / 0.092	0.39 / 0.092	0.39 / 0.092	0.34 / 0.092	0.71 / 0.079
Touristskaya	0.58 / 0.112	0.54 / 0.106	0.53 / 0.106	0.53 / 0.105	0.53 / 0.110
Kozhukhovskiy passage	0.53 / 0.140	0.50 / 0.132	0.50 / 0.131	0.46 / 0.156	0.60 / 0.131
Ostankino	0.40 / 0.088	0.45 / 0.080	0.49 / 0.080	0.58 / 0.075	0.45 / 0.091
Zvenigorod	0.23 / 0.184	0.31 / 0.155	0.32 / 0.156	0.28 / 0.184	0.32 / 0.188
Kozhukhovo	0.02 / 0.119	0.08 / 0.107	0.07 / 0.104	0.11 / 0.145	0.16 / 0.123
Gagarin sq.	0.38 / 0.211	0.52 / 0.209	0.53 / 0.208	0.43 / 0.272	0.52 / 0.194
Khamovniki	0.42 / 0.167	0.43 / 0.148	0.45 / 0.150	0.32 / 0.211	0.47 / 0.169
Kapotnya	0.37 / 0.124	0.36 / 0.113	0.36 / 0.113	0.34 / 0.130	0.39 / 0.126
Median	0.38 / 0.129	0.38 / 0.116	0.37 / 0.124	0.34 / 0.133	0.43 / 0.135
Average	0.35 / 0.139	0.34 / 0.127	0.34 / 0.127	0.31 / 0.143	0.41 / 0.141

**Table A.5. Correlation and RMSE values between observed and predicted carbon monoxide concentrations for July 2020 (prediction sub-period) based on data from the Balchug weather station.**

Station name	Correlation coefficient / RMSE value				
	Equation (1)	Equation (2) with $v_i$	Equation (3) with $v, T$	Equation (4) with $v, T$ and $u$	Inertial
Shabolovka	0.44 / 0.110	0.66 / 0.083	0.66 / 0.083	0.68 / 0.083	0.46 / 0.112
Maryino	0.21 / 0.065	0.48 / 0.054	0.50 / 0.061	0.54 / 0.057	0.20 / 0.075
MADI	0.31 / 0.219	0.44 / 0.193	0.40 / 0.193	0.33 / 0.195	0.31 / 0.232
Losiny Ostrov	0.65 / 0.066	0.74 / 0.056	0.75 / 0.056	0.74 / 0.057	0.62 / 0.072
Glebovskaya	0.4 / 0.172	0.64 / 0.135	0.66 / 0.135	0.66 / 0.135	0.47 / 0.171
Lublino	0.18 / 0.185	0.3 / 0.168	0.34 / 0.162	0.35 / 0.159	0.18 / 0.203
Chayanova	0.62 / 0.129	0.67 / 0.127	0.67 / 0.128	0.66 / 0.133	0.61 / 0.140
Tolbukhina	0.5 / 0.117	0.69 / 0.092	0.69 / 0.094	0.68 / 0.095	0.52 / 0.118
Dolgoprudnaya	0.5 / 0.126	0.56 / 0.130	0.29 / 0.137	0.29 / 0.137	0.42 / 0.146
Narodnogo opolcheniya	0.72 / 0.217	0.73 / 0.212	0.72 / 0.219	0.75 / 0.205	0.76 / 0.209
Polyarnaya	0.65 / 0.155	0.74 / 0.134	0.73 / 0.135	0.74 / 0.134	0.64 / 0.152
Spiridonovka	0.46 / 0.142	0.46 / 0.138	0.46 / 0.138	0.46 / 0.138	0.44 / 0.154
Kozhukhovsky passage	0.37 / 0.183	0.6 / 0.141	0.63 / 0.137	0.64 / 0.137	0.41 / 0.188
Zvenigorod	0.36 / 0.101	0.43 / 0.113	0.38 / 0.149	0.42 / 0.144	0.36 / 0.114
Kozhukhovo	0.29 / 0.109	0.35 / 0.096	0.37 / 0.093	0.37 / 0.094	0.31 / 0.114
Gagarin sq.	0.64 / 0.135	0.75 / 0.112	0.75 / 0.117	0.74 / 0.122	0.66 / 0.137
Median	0.45 / 0.132	0.62 / 0.128	0.64 / 0.135	0.65 / 0.135	0.45 / 0.143
Average	0.46 / 0.139	0.58 / 0.124	0.56 / 0.127	0.56 / 0.127	0.46 / 0.146

**Table A.6. Correlation and RMSE values between observed and predicted carbon monoxide concentrations for July 2021 (prediction sub-period) based on data from the Balchug weather station.**

Station name	Correlation coefficient / RMSE value				
	Equation (1)	Equation (2) with $v_i$	Equation (3) with $v, T$	Equation (4) with $v, T$ and $u$	Inertial
Sukharevskaya	0.17 / 0.214	0.30 / 0.177	0.26 / 0.182	0.32 / 0.180	0.30 / 0.211
Shabolovka	0.55 / 0.065	0.75 / 0.049	0.74 / 0.062	0.75 / 0.066	0.62 / 0.064
Kazakova	0.35 / 0.122	0.51 / 0.102	0.49 / 0.100	0.47 / 0.102	0.38 / 0.140
Maryino	0.18 / 0.153	0.39 / 0.128	0.40 / 0.123	0.40 / 0.123	0.20 / 0.169
Zelenograd 6	0.40 / 0.131	0.64 / 0.100	0.64 / 0.099	0.69 / 0.094	0.49 / 0.135
Zelenograd 11	0.35 / 0.093	0.47 / 0.084	0.37 / 0.088	0.36 / 0.089	0.35 / 0.099
Zelenograd 16	0.63 / 0.188	0.67 / 0.171	0.43 / 0.207	0.45 / 0.205	0.65 / 0.184
Biryulyovo	0.29 / 0.122	0.63 / 0.092	0.58 / 0.090	0.58 / 0.089	0.36 / 0.122
Moscow State University (MSU)	0.20 / 0.106	0.47 / 0.090	0.39 / 0.086	0.40 / 0.086	0.13 / 0.125
Butlerova	0.07 / 0.120	0.08 / 0.118	0.08 / 0.120	0.24 / 0.112	0.04 / 0.136
Losiny Ostrov	0.58 / 0.047	0.77 / 0.046	0.81 / 0.057	0.80 / 0.056	0.60 / 0.048
Glebovskaya	0.20 / 0.150	0.37 / 0.130	0.37 / 0.130	0.35 / 0.131	0.29 / 0.153
Lublino	0.08 / 0.230	0.61 / 0.170	0.44 / 0.173	0.44 / 0.173	0.13 / 0.246
Ak. Anokhina	0.39 / 0.127	0.65 / 0.116	0.46 / 0.113	0.45 / 0.113	0.54 / 0.120
Chayanova	0.52 / 0.114	0.65 / 0.093	0.38 / 0.130	0.36 / 0.134	0.56 / 0.117
Tolbukhina	0.44 / 0.134	0.74 / 0.100	0.67 / 0.104	0.67 / 0.104	0.48 / 0.139
Dolgoprudnaya	0.48 / 0.149	0.67 / 0.133	0.59 / 0.136	0.54 / 0.138	0.62 / 0.135
Koptevsky	0.12 / 0.193	0.17 / 0.172	0.03 / 0.199	0.05 / 0.196	0.24 / 0.210
Polyarnaya	0.37 / 0.191	0.78 / 0.114	0.56 / 0.170	0.52 / 0.180	0.40 / 0.195
Cheryomushki	0.58 / 0.092	0.81 / 0.076	0.78 / 0.072	0.70 / 0.079	0.71 / 0.079
Touristskaya	0.43 / 0.112	0.81 / 0.088	0.61 / 0.092	0.62 / 0.090	0.53 / 0.110
Kozhukhovskiy passage	0.53 / 0.140	0.70 / 0.110	0.74 / 0.108	0.74 / 0.108	0.60 / 0.131
Ostankino	0.40 / 0.088	0.57 / 0.073	0.57 / 0.073	0.64 / 0.069	0.45 / 0.091
Zvenigorod	0.23 / 0.184	0.30 / 0.162	0.34 / 0.155	0.34 / 0.155	0.32 / 0.188
Kozhukhovo	0.02 / 0.119	0.47 / 0.089	0.47 / 0.094	0.48 / 0.094	0.16 / 0.123
Gagarin sq.	0.38 / 0.211	0.54 / 0.193	0.49 / 0.261	0.51 / 0.261	0.52 / 0.194
Kapotnya	0.37 / 0.124	0.68 / 0.091	0.64 / 0.090	0.62 / 0.093	0.39 / 0.126
Median	0.37 / 0.127	0.63 / 0.102	0.49 / 0.108	0.48 / 0.108	0.43 / 0.135
Average	0.35 / 0.138	0.56 / 0.114	0.49 / 0.123	0.50 / 0.123	0.41 / 0.141



# CONTEMPORARY PROBLEMS OF SETTLEMENT IN THE ETHNIC PLAIN VILLAGES OF THE NORTHWESTERN REGIONS OF AZERBAIJAN (ON THE EXAMPLE OF THE BALAKAN ADMINISTRATIVE DISTRICT)

**Bayimkhanim A. Huseynova\***

Institute of Geography, Huseyn Javid Avenue 115, Baku, AZ1143, Azerbaijan

\*Corresponding author: nane\_huseynova@yahoo.com

Received: October 22<sup>nd</sup> 2023 / Accepted: July 25<sup>th</sup> 2024 / Published: October 1<sup>st</sup> 2024

<https://doi.org/10.24057/2071-9388-2024-3102>

**ABSTRACT.** The geographical position of the region, ethnic composition, acceleration of the process of polarization among rural settlements, and other factors increase the relevance of the research. The subject of the research is the study of rural settlement problems, and the object of the research is the villages and ethnic minorities of the Balakan district. The study aims to reveal the modern problems of the settlement of ethnic minorities and the formation of rural agglomerations, to study the causes of the emptying of some villages, and to prepare a rural development model to prevent the problems. To conduct research, the literature and statistical materials were analyzed, as well as cartographic, comparative analysis, SWOT, and modelling methods were used. Moreover, a field investigation was conducted in the research area. It was revealed that although a majority of the rural population settles in villages with a high demographic potential, villages with a weak demographic potential, due to their higher number, play a major role in the settlement system. Moreover, some villages form rural agglomerations, while some of them lose their population due to socioeconomic challenges. Due to the intense migration processes, some villages have turned into endangered villages (Mazimustu, Goyrujuluk), and even some villages are on the brink of extinction (Bayrambina, Mazimchay, Abjit). Studying the regulation of rural settlement in the region is of practical importance in terms of ensuring the equal development of the region, ensuring the security of the borders, and protecting ethnic minorities. However, there is still a need for serious research in this field.

**KEYWORDS:** Balakan district, ethnic minorities, plain villages, depopulation, rural agglomeration, rural development model

**CITATION:** Huseynova B. A. (2024). Contemporary Problems Of Settlement In The Ethnic Plain Villages Of The Northwestern Regions Of Azerbaijan (On The Example Of The Balakan Administrative District). *Geography, Environment, Sustainability*, 3(17), 35-46

<https://doi.org/10.24057/2071-9388-2024-3102>

**ACKNOWLEDGEMENTS:** The author would like to acknowledge Azercosmos for the satellite images and the ethnic minorities participating in the survey in the research area.

**Conflict of interests:** The authors reported no potential conflict of interest.

## INTRODUCTION

Azerbaijan is distinguished by the diversity of its national-ethnic composition (Muradov 2021). The region covering the northwestern zone of the country is particularly distinguished by its multi-ethnicity, and it stands in second place after the Guba-Khachmaz economic region in terms of its ethnicity. Thus, the Udis and Inghilois, who are among the exotic peoples of the world and were ethnic groups of ancient Caucasian Albania; Tsakhurs, Avars, and many other ethnic peoples, who are known as Dagestani people, have settled in these areas. Generally speaking, almost all Tsakhurs, Udis, and Avars living in Azerbaijan reside in the country's northwestern region (Huseynova 2021a). The Shaki-Zagatala economic region covers the majority of the country's northwestern zone. This economic region includes 6 administrative districts (Balakan, Gakh, Gabala, Oghuz, Shaki, and Zagatala) covering 10.2% of the

country's territory (Huseynova 2021). Stretching along the southern slope of the Greater Caucasus Mountains, this region primarily consists of mountainous areas, with only up to 20% composed of plains (Huseynova 2021b). Balakan district, which is a research object, is the only district in the region where the population settles only in plain areas (Distribution of population and problems of demographic development in the Shaki-Zagatala economic region).

Azerbaijan was among the world's moderately urbanized countries, meaning that almost half of the country's population settled in rural settlements (Geography of the Republic of Azerbaijan). Despite this figure rising to 54.6 in 2023 and the country being included in the states with a moderately high urbanization level, the figure is still lower compared to developed countries (Demographic Indicators of Azerbaijan 2023). This means that rural settlements are of special importance in the country's settlement system. Balakan administrative district

is one of the least urbanized in the country. The majority of the population in the region lives in rural settlements. The district's location in the far north-west of the country, along with its mixed ethnic composition and the special role of rural settlements in population settlement, underscores the significance of conducting research in this area. At the same time, the rapid progress of the polarization process between rural settlements, that is, the growth of some villages by forming large agglomerations, and the depopulation of some villages, increases the actuality of the research. The subject of the research is the study of the settlement problems of minority ethnic groups in the Balakan district, and the object of the research is the villages of the Balakan district and the minority ethnic groups living there.

As in other countries of the world, the main part of the rural population in Azerbaijan engages in agriculture and related fields (Eminov 2005). Therefore, the availability of arable land resources, an irrigation system for agriculture, and favorable social infrastructure in rural areas are very important factors. However, problems in this direction remain in the country.

Generally, the rural population encounters numerous socioeconomic and environmental problems in the context of climate change, poverty, geographical distance, and other factors (Mihai and Iatu 2020). These problems lead to irregular settlement of the population in the country, including any region, and the emergence of demographic problems.

The settlement problem in the study area manifests itself primarily in the form of settlement polarization. In other words, in some areas, the geographic concentration of the population has accelerated, and large rural agglomerations are emerging, while in other areas, the process of depopulation has flourished. Generally, in many regions of Azerbaijan, villages form village agglomerations. This process takes place in both mountainous and plain areas. Considering that the settlements of the research area are located in plain areas (except for 1 village), attention was paid to agglomerations formed in plain villages. Strong socioeconomic and transport relations between villages and each other, as well as their strong demographic potential, have created conditions for the formation of rural agglomerations. In such areas, the migration process is slower. However, the strong migration process in small villages has resulted in their emptying.

Migration plays an important role in the region's settlement. It is known that in many countries around the world, migrations are mainly from rural to urban areas. The rural population considers leaving their place of residence as the main way to change their economic activity to lead a better life (Adamowicz 2022). This laid the foundation for the migration of the rural population from the village to urban places. As a result, there are negative trends in the demographic indicators of the population, and serious problems arise in the settlement. The emergence of such problems in the region located in the border zone can also create problems for the security of the border zone. It is necessary to prepare a special sustainable rural development model that prevent the emergence of such problems by regulating the ethno-demographic situation and settlement in the region. Achieving sustainable and balanced development in rural areas entails enhancing the living conditions of the rural population and creating favorable work environments, all while safeguarding the natural environment, landscape, and cultural heritage of the region. That is, the sustainable rural development concept approach aims to reconcile environmental, economic, and

social rights, utilizing an appropriate development strategy that not only improves the population's living conditions comprehensively, but also maintains healthy and robust rural communities capable of economic activity while preserving their values (Adamowicz and Magdalena 2018).

The primary goal of the research is to analyze the changes in the modern state of settlement in rural settlements, to reveal the modern problems of the settlement of ethnic groups, the formation of rural agglomerations (the reason for its formation, typology and classification), and to study the causes of the emptying of some villages and prepare a rural development model to prevent the problems that have arisen.

To achieve this goal, the following tasks have been set:

1. Determining the region's ethnically diverse rural settlements and their national-ethnic composition, transferring the data to the map;
2. Analysis of migration factors in the administrative district and its impact on the settlement system;
3. Study of population changes in the years 1999-2019 based on the grouping of villages in the region and the distribution of the population by altitude zones;
4. Analysis of the reasons for the formation of large rural agglomerations and their typology;
5. Revealing the factors that lead to the decrease in population in the villages that have been emptied and are in danger of depopulation;
6. Development of a rural development model to eliminate problems in rural settlement.

The scientific novelty of the research work includes:

1. For the first time, the ethno-demographic situation of the population in the Balakan district was studied by surveying the district level;
2. The modern settlement of the population in the district was compared with previous years and the reasons for the differences were investigated;
3. For the first time, the emergence causes of rural agglomerations, their typology and characteristics were studied;
4. Issues of population decline in villages and their causes were investigated;
5. A development model was developed to eliminate the problems arising in the settlement system of the region.

The database for the research work is based on 3 sources. The first source is obtaining theoretical knowledge from literature materials, collecting information about village settlements, and analyzing of statistical material; the second source is satellite images of the district; and the third source is the results of survey materials.

## MATERIALS AND METHODS

The Balakan administrative district, which is a part of the Shaki-Zagatala economic district, is located in the remote northwestern part of the Republic of Azerbaijan. The total area of the region is 923 km<sup>2</sup>. The region is surrounded by the Russian Federation (Republic of Dagestan) from the north, Georgia from the west and southwest, and the Zagatala district from the east (Fig.1). According to the latest statistics (2023), the population of the region is 100,2 thousand people (Demographic Indicators of Azerbaijan 2023). The main part of the population of the district is composed of Azerbaijanis (74.5%), a part of Avars (23.5%), and the rest of Inghilois, Russian, and other ethnic and national minorities (2%) (Census materials of the population of the Republic of Azerbaijan-2019). In total, there is 1 city

(Balakan city), 1 small town (Gabagchol), and 57 rural settlements in the district.

The research database is based on 3 main sources: statistics and literature materials; satellite images; field investigation. During the research process, to collect general information about the region, analyze theoretical materials, and study settlement in the area, the research works of authors who conducted research in this field and related fields in previous years were investigated. Numerous studies have been carried out in Azerbaijan on the ethnic composition of the population and settlement. In this field, Z.N. Eminov (2005), N.H. Ayyubov (2015) studied the settlement of the population in the Republic of Azerbaijan as altitude zones, R.N. Karimov (2016) researched the villages and village population of the Shaki-Zagatala economic region, Sh.M. Muradov (2013, 2022) studied the demographic, including the ethno-demographic situation in Azerbaijan, and G.J. Javadov (2000) studied the ethnic groups living in Azerbaijan and the change in their number. The places of residence of minority ethnic groups and their linguistic features were studied by J.M. Clifton, C. Tiessen (2005), W.M. Schulze (2013), and others. The research works of D. Sikorski, Latocha, R. Szmytkie, K. Kajdaneek, P. Miodonska, P. Tomczak (2020), A.A. Khan, M. Somunju (2013), A. Mahdi, M.H. Mahdi, M. Shafiei (2014), L. Ma, M. Chen, X. Che, F. Fang (2019), A. Vaishar, H. Vavrouchova, A. Leskova, V. Perinkova (2021) and others are important sources for obtaining information in the field of theoretical foundations of rural settlement and rural development models. Furthermore, statistical materials were analyzed to study the demographic situation.

The second main database of the research work is satellite images of the district covering the years 2017–2022 provided by Azercosmos. Satellite images were used to study the location of settlements in the region as well as their spatial and time changes. The data were compared with the data of the previous years before the

processed images were processed in the ArcGIS software. At this time, the comparative analysis method was used.

Finally, the last database was a survey of pre-selected rural settlements in the district to find out the reasons for the changes in the demographic situation and settlement of the population and to become more familiar with them. The survey process lasted for 1 week (02.01.2023–02.07.2023). Then the questionnaires were scrutinized and general results were obtained. Surveys were conducted in 30 villages, which are densely populated by Avars (Yeni Sharif, Sharif, Shambul, Meshashambul, Isakhligirma, etc.), Ititala village, inhabited by Inghiloi, Gamishtala, Garaveli, Gadashbina, Tulu, Talalar, Hetovlar, inhabited by Tsakhurs, Avars, and Azerbaijanis. 250 people took part in the survey process, and the respondents included both genders, different age groups, those engaged in various fields of activity, and different ethnic groups (Table 1).

The proposals, opinions, and comments of the local population were taken into account when developing a sustainable development model for rural settlements.

During the research work, several research methods were employed. To study the national-ethnic composition and migration processes in the region, the field research method; comparative analysis for the analysis of the statistical indicators of the population; and the cartographic method for transferring the obtained data to the map and to analyzing the maps were used. In addition to this, SWOT analysis and geographic modelling methods were used for grouping the measures intended to eliminate the problems.

## RESULTS AND DISCUSSION

Although the Balakan district covers areas from 140 meters above sea level to 3,123 meters, the population of the region is settled in areas up to 550 meters, that is, in the areas surrounding the Ganikh-Ayirchay valley of the

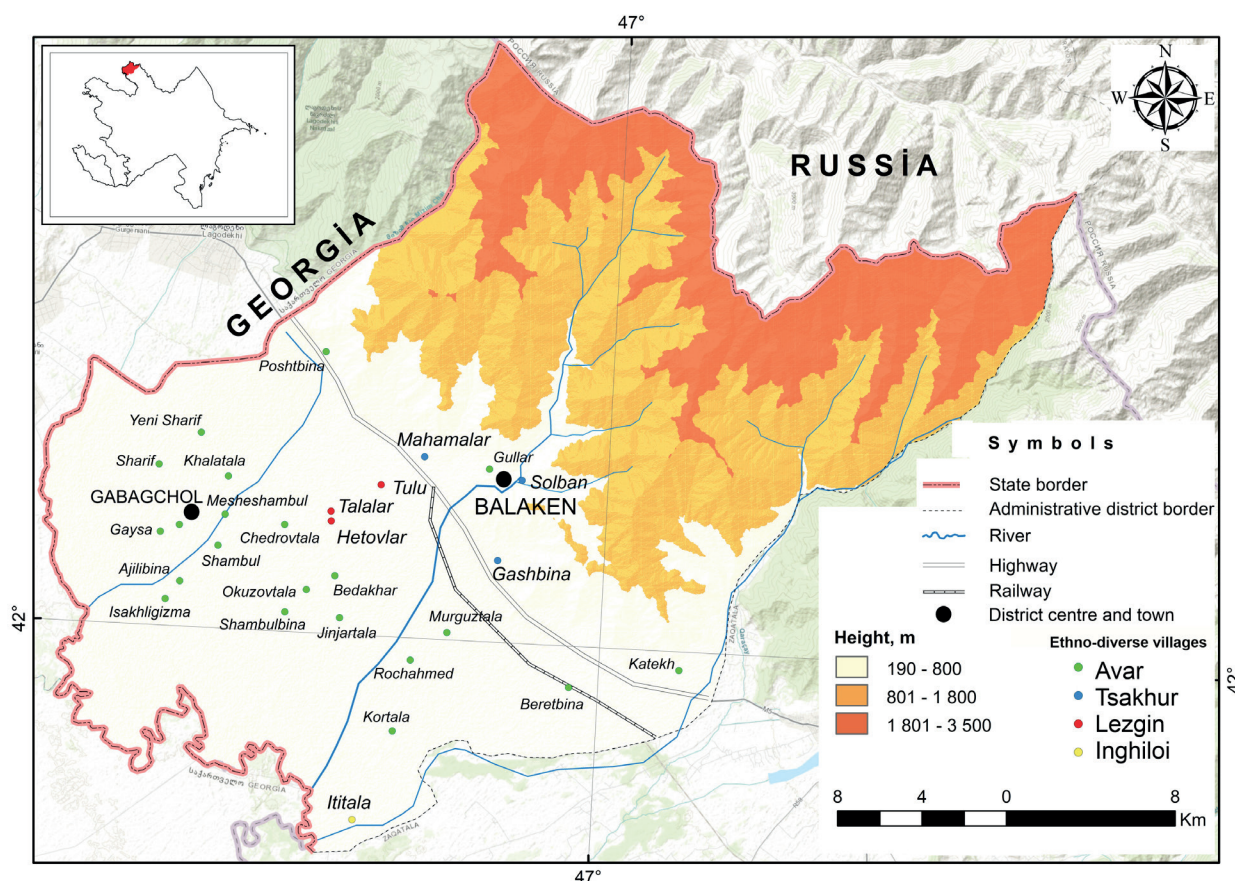


Fig. 1. Map of the study area



**Table 1. Composition of respondents participating in the survey**

Demographic features		Number of respondents	Share, %	Total
Sex composition	Female	115	46.0	250
	Male	135	54.0	
Age composition	15-24	28	11.2	250
	25-34	55	22.0	
	35-44	47	18.8	
	45-54	54	21.6	
	55-64	39	15.6	
	65 and over	27	10.8	
Occupation	Student	9	3.6	250
	Housewife	23	9.2	
	Agricultural sector	153	61.2	
	Industrial sector	9	3.6	
	Governmental sector	12	4.8	
	Private sector	5	2.0	
	Retiree	27	10.8	
	Unemployed	12	4.8	
Ethnicity	Avar	138	55.2	250
	Inghiloi	80	32.0	
	Tsakhur	12	4.8	
	Lezgin	20	8.0	

region and in the foothills. The region's middle and high mountainous areas are part of the Zagatala National State Reserve. The lowest settlement in the region is the village of Bayrambina, located at an altitude of 148 meters, and the highest settlement is the village of Mazimchay, located at an altitude of 558 meters. All the remaining villages are located lower than 500 meters.

Turning to the ethnic composition, Avars differ from the minority ethnic groups in the Balakan district in their share (23.5%). In addition, other minority ethnic groups, including the Inghiloi, Lezgins, and Tsakhurs, settled in the area as well. Thus, Sharif, Yeni Sharif, Shambul, Meshashambul, Isakhligirma, Gullar, Ajiliqbina, Mahamalar, Katekh, and several other villages of the region are densely populated by Avars; that is, these villages can be mainly considered Avar villages. Lezgins and Tsakhurs are sparsely settled in Tulu, Gasbina, Mahamalar, and other villages. The Inghiloi live only in the village of Ititala. The Muslims make up the majority of the Inghiloi in this village, having migrated from the Aliabad settlement in the Zagatala district (Encyclopedic dictionary of Azerbaijani toponyms).

Migration processes have a special role in the formation of the modern ethno-demographic situation of the population and settlement in the region (Huseynova 2022c). The area has been one of the most active migration districts in the country, both in modern and historical times. At the same time, the national-ethnic composition of this area became complicated as a result of those migration processes. According to some historical materials, the Inghiloi who settled in the Balakan district

are the descendants of the historical inhabitants of the Shaki-Zagatala region, that is, the descendants of the Gel tribe living in Ancient Caucasian Albania, but the migration of the Avars to the mentioned area dates back to the 15th and subsequent centuries (Geybullayev 1991; Javadov 2000). According to Abbasov (Abbasov et al. 2022), people have participated in migration processes since ancient times, and natural conditions pushed them to settle in other places.

In modern times, the rural population temporarily or permanently migrates to various places. This situation may have a positive or negative impact on their rural origin (Mendola 2010; Hidayat et al. 2022). There are various drivers of the emigration of the rural population, and this includes an economic situation (Cheng et al. 2006; Lyu et al. 2019; Marta et al. 2020), life satisfaction (Liu and Pan 2020), natural disasters (Berlemann and Steinhardt 2017; Gray and Mueller 2012; Ishtiaque and Nazem 2017), education (Crivello 2011), and finally, a political situation.

In the research area, migration processes happen mainly under the influence of socioeconomic factors. Regarding the shift in the migration balance over time, during the initial years of independence (following the collapse of the USSR), the deterioration of the socioeconomic and political conditions in all regions of the country, particularly the remote ones, led to a suspension of business operations. In other words, the difficulties of the transition period accelerated the process of migration out of the country during those years. As a result, the migration balance received a negative value. Moreover, in recent times,

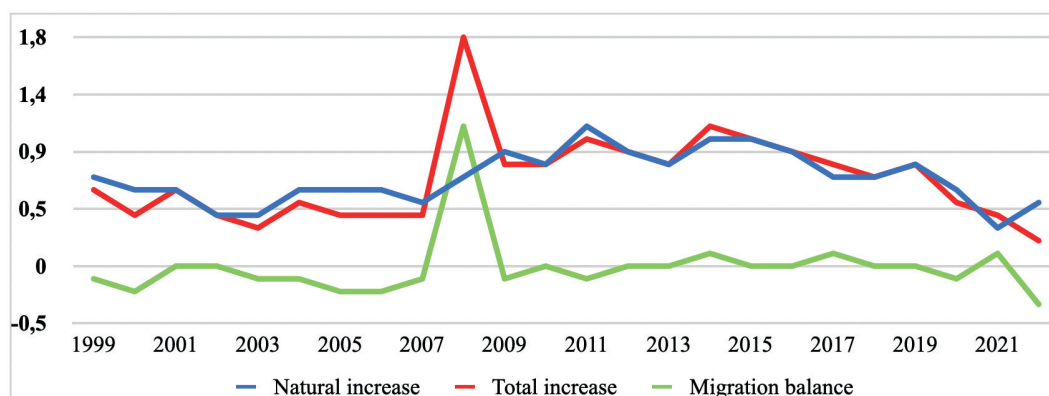


Fig. 2. Natural growth and migration of the total population in the administrative district from 1999-2022 (thousand people)

Source: "Population of Azerbaijan" statistical compilation-1999-2023.

the number of climate migrants has increased due to the drought, a decrease in the amount of precipitation, and other climate-induced factors. This situation is observed in the study area, according to the survey materials. However, in recent years, the migration balance in the region has remained stable and, in some cases, has received a positive value (Fig. 2).

However, it should be noted that sometimes the number of migrants is registered in the area of their residence, regardless of whether they migrated to Baku or neighboring countries, and their numbers are taken into account in the statistical materials because they are registered in the area of their residence. That is, receiving a positive evaluation of migration does not imply that it does not occur in the area. In the survey materials, it was recorded that migration is still intensive. In Balakan, internal migration is mainly in the direction of Baku city, and in external migration, Ingiloiis prefer migrating to Georgia; and Avars and Azerbaijanis prefer migrating to Russia (Fig. 3).

Balakan is one of the poorly urbanized administrative districts of the country (15.8%). The population is primarily concentrated in rural settlements. There are 57 villages, 1 city, and 1 small town in the administrative district (Demographic Indicators of Azerbaijan 2023).

In the village settlement system of the Balakan district, the main part of the villages is composed of village groups with a population of 501-1000, while the main part of the population is concentrated geographically in village groups with a population of 3001-5000. In recent years, serious problems have continued to appear in the Balakan district's rural settlement system. Having a special role in the dominance of small and medium-sized villages in the rural settlement system is among these problems. A large number of villages from this group in the rural settlement system, especially the large number of villages with a population of up to 200, increases the extinction risk of the village and accelerates the process of population polarization. In this type of small rural settlement, the

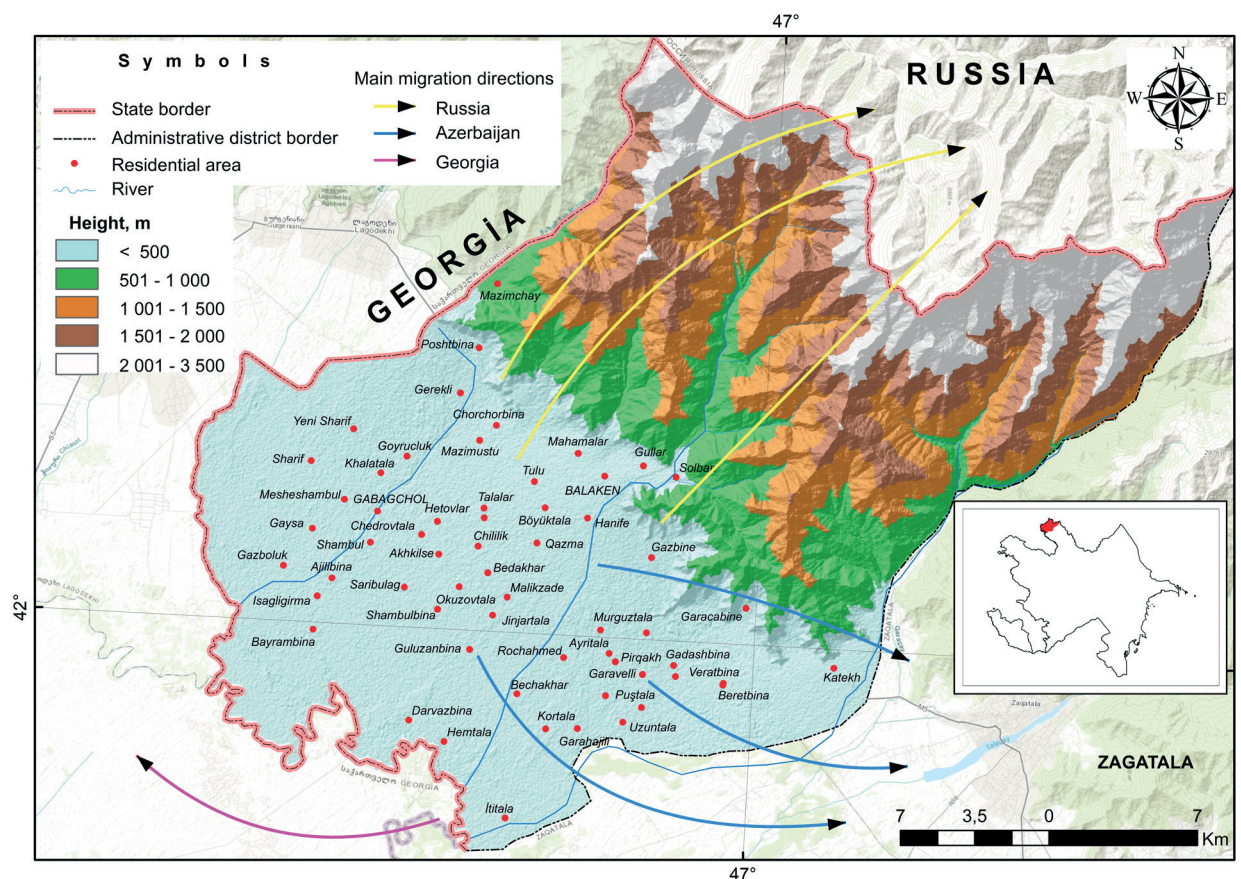


Fig. 3. Map of the direction of modern migration in the Balakan district

depopulation process is faster. This is due to the fact that either the population in these settlements decreases with demand and supply, or the opposite process occurs when the population's needs aren't satisfied, they decide to leave their current residence. Currently, 5 villages in the region (Goyamtala, Darvazbina, Abjit, Bayrambina, and Mazimgarishan) have no permanent population. In other words, these villages are used only for temporary living in the summer (Table 2). None of these mentioned villages have a suitable socioeconomic base for living. Interestingly, these uninhabited villages are located mainly in the border zone.

One of the important issues to be studied during the location of the population and settlements is the geopolitical study of the location of the population and settlements in the border zone, especially in ethno-diverse border regions. It is known that border areas differ in their problems and characteristics. In many countries, border areas are less populated, and such areas are not considered accessible in terms of providing basic facilities. In some areas where the ethnic composition is different, it can be a "hotbed of conflict". In other words, ethno-diverse border areas are relatively "active" areas from a political point of view. From a geopolitical point of view, as in all countries of the world, the protection of political stability in ethnically diverse settlements along the border is one of the important issues. In this regard, the demographic indicators of the population and population settlement in those areas should be kept under constant control.

As we mentioned earlier, even though the Balakan district covers different altitude zones and large areas, the population is mainly settled along the Ganikh-Ayrichay valley, which covers the southern zone of the region and covers heights of up to 500 meters, making it suitable for settlement and agriculture.

Turning to the location of residential areas according to altitude zones, although there are 4 rural residential areas in the altitude zone up to 200 meters, only Ititala village has a permanent population. The other 3 villages (Goyamtala, Darvazbina, and Bayrambina) have no permanent population (Fig. 4).

There is only 1 village in the mountainous area of the district. This is the village of Mazimchay, which has a medium demographic potential and whose population is growing

at a slow pace. As can be seen from the Table 3, the vast majority of the region's population and rural settlements are concentrated at an altitude of 200-500 meters. This indicates that the population and settlements in the area are not scattered but polarized. That is, the population is primarily concentrated in a specific altitude zone and area. This creates serious problems in the regulation of factors such as ensuring the security of the border zone in ethno-diverse regions, appropriating territories, using the potential of natural resources, and so on.

In the rural settlement system of the district, it is possible to find villages with both large ethno-demographic and weak ethno-demographic potential. As examples of large ethnic-rural settlements, Katekh, Hanifa, Tulu, and others can be cited. Unambiguously, villages in this group are mostly located close to the district center and each other and form large village agglomerations. These villages differ due to their proximity to each other and their strong socioeconomic base. The majority of the population of these villages with a large demographic potential is composed of Avars.

What is a rural agglomeration? Rural agglomerations, which manifest themselves more in developing countries, are the connections of villages located close to each other through strong economic, social, demographic, and transport links, and as a result, they are the development and growth of the villages.

Similarly, as in urban agglomerations, some settlements serve as main villages and satellites for rural agglomerations. Thus, as the village that plays the role of a main village develops, it also supports the development of surrounding villages. However, there is an important point here: when the typological indicators of the villages are the same, the development is faster; that is, rural agglomerations are formed. Rural agglomerations can be different according to their typology. Naturally, this diversity affects the strengthening of their relations, i.e., the formation of agglomeration. The typology of rural agglomerations in the northwestern region of Azerbaijan can be divided as follows:

1. as the population;

2. as the employment of the population (agricultural-oriented, agricultural products processing-oriented, tourism-oriented, etc.);

**Table 2. Changes in the number of village groups and the population of those villages in the Balakan administrative district**

Rural groups	1999		2009		2019		Increase or decrease of the number population (%)
	Number of villages	Number of population	Number of villages	Number of population	Number of villages	Number of population	
0-50	5	-	5	-	5	-	-
51-100	8	620	4	259	4	293	-52.7
101-200	2	236	7	903	7	1,108	+469.5
201-500	15	5,734	12	5,024	8	3,286	-42.7
501-1000	6	3,852	8	5,657	11	7,176	+86.3
1001-2000	5	7,938	3	4,535	5	7,524	-5.2
2001-3000	8	19,390	8	18,690	6	14,981	-3.6
3001-5000	5	18,448	7	25,611	8	29,370	+59.2
5000 and over	3	17,619	3	18,832	3	19,090	+8.3
Total	57	73,837	57	79,511	57	82,828	+12.2

Source: Census materials of the population of the Republic of Azerbaijan-1999, 2009, 2019



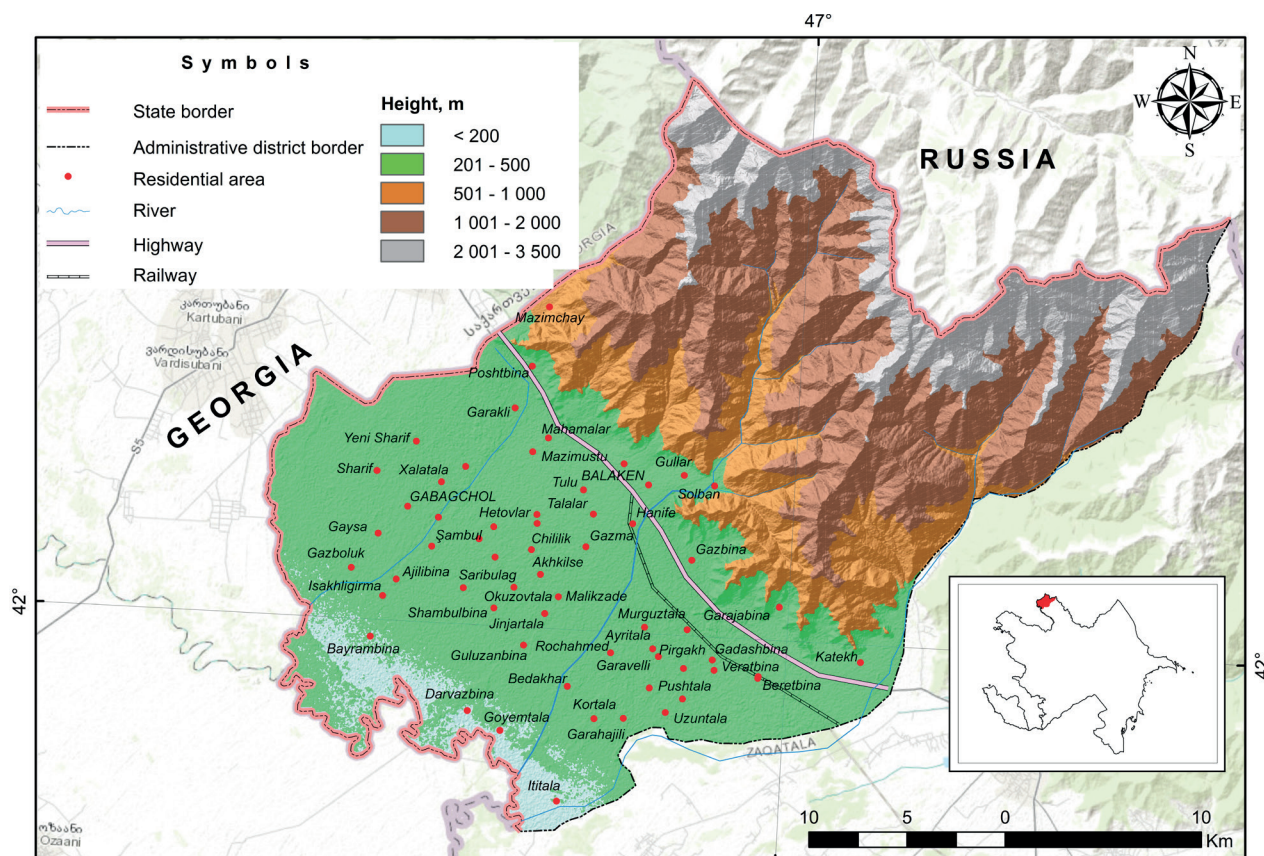


Fig. 4. Map of the location of settlements by altitude zones

Table 3. Change of settlements by altitude zones

Altitude zones	1999		2009		2019		Indicator of increase or decrease of the population (%)
	Number of villages	Number of population	Number of villages	Number of population	Number of villages	Number of population	
0-200*	4	2,029	4	2,240	4	2,504	+23.4
201-500	52	71,457	52	76,913	52	79,959	+11.9
500 and more	1	351	1	358	1	365	+4.0
Total	57	73,837	57	79,511	57	82,828	+12.2

\*In this altitude zone, there is no permanent population of three villages.

3. as national-ethnic composition;

4. as its integration into cities.

5 village agglomerations were formed in the Balakan administrative district (Fig. 5a):

- Rural agglomeration around the city of Balakan - Hanifa village (4,722 people), Gazma (2,749 people), Talalar (3,529 people), Tulu village (6,174 people), Mahamalar village (3,787 people), Gullar village (5,501 people);

- Sharif-Shambul village agglomerations - Sharif village (3,526 people), Yeni Sharif village (3,447 people), Khalatala (3,006 people), Meshashambul village (2,597 people), Gaysa village (3,787 people)

- Katekh-Mazikh village agglomeration - Katekh village (7,415 people), Mazikh village (1,653 people Zagatala district)

- Ititala (2,504 people) -Ashagi Chardakhlar (1,166 people Zagatala district)-Danachi (7,781 people Zagatala district) triangle

- Gerekli village agglomeration - Gerakli village (3,575 people).

From these agglomerations, the suburbs of Balakan (rural agglomeration around the city of Balakan) are distinguished by their proximity to the city center, strong

transport links with the city center, and high level of social infrastructure. Surely, these villages are distinguished by their strong demographic potential.

The main strength of the Sharif-Shambul agglomeration is the population employment, i.e., agriculture development. The main feature that connects these villages is strong transport and economic connections.

The main indicators that connect Katekh and Mazikh agglomerations are their proximity to each other despite being located far from the district center they belong to, their economic relations, and their national-ethnic composition.

The Ititala-Ashaghi Chardaglar-Danachi triangle has come close to each other mainly due to economic relations and national-ethnic composition.

The village of Gerekli is still under construction.

It is interesting that, despite being located in two different administrative districts, when a village in one district establishes strong ties with a village in the neighboring district, they can form village agglomerations. This can support the development of villages located in remote areas that are close to each other.



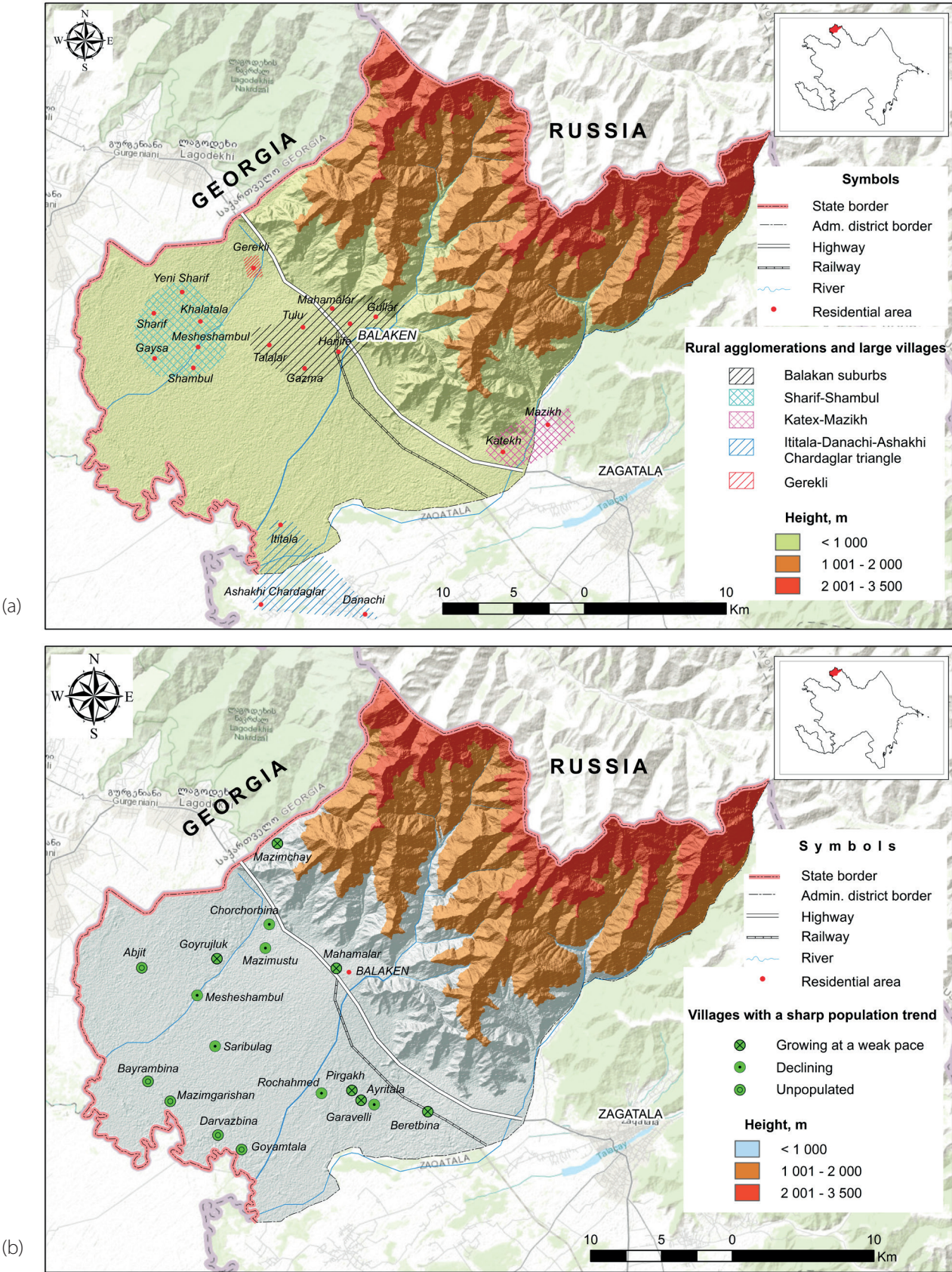


Fig. 5. (a) Village agglomerations; (b) Map of threatened, endangered and extinct villages

In some villages in the district, a serious decrease in population was recorded. The villages where the decrease was registered are mainly inhabited by Avars. Thus, from 1999–2019, the population decreased in 12 villages of the district, and in 2 villages, the village population was less than 100 people (Fig. 5b). In some villages in the district, the population is growing at a very slow pace. This may result in population decline in these villages in the following years (Table 4).

Villages with declining populations and slow growth are typically located far from the city center and off highways. These villages have relatively poor social infrastructure and are relatively unlivable. The main reason for the depopulation of these villages is the intensive migration from those areas, especially the lack of job opportunities in these villages, which has led to faster migration processes among young people. In this case, natural growth declines gradually. As a result, the population of the village decreases,

and these villages are included in the list of villages that are in danger of depopulation. Villages where depopulation is observed have many common characteristics, and the most important of them is that these villages have poor transport connections, are located far from the city center, and have a weak socioeconomic base.

Generally, there are two main reasons for the emptying out of rural settlements: human intervention and depopulation (Vaishar et al. 2021). The first case occurred in Azerbaijan in the 1960s. This was mainly related to the creation of a collective farm in USSR territory. In those years, all over the territory of the USSR, including the Azerbaijan SSR, small and very small villages were considered unpromising areas (Demographic development of villages in the Republic of Azerbaijan and settlement problems of rural population). As a result, in the Shaki-Zagatala economic region, the population living in mountain villages was relocated to plain villages. This resettlement policy has created serious problems in the settlement of the mountain villages. The second case, i.e., depopulation, was related to uneven socioeconomic development in the region or any area of the region, and this process is still ongoing. In Azerbaijan, the depopulation process takes place mainly in remote mountain villages and villages with poor social infrastructure.

In general, it should be noted that in recent years, the process of polarization between both homogeneous and heterogeneous types of settlements has continued to manifest itself in the country, and this process has gradually intensified in recent years. According to the statistics of the UN, although the gaps between the development of the countries in the world are decreasing, these gaps in the internal development of the country are gradually increasing and manifesting themselves in the settlement system of the country (Gao and Hu 2022). Especially in developing countries, including Azerbaijan, this manifests itself in the form of urban-rural gaps. However, it is interesting that in any region or part of the country,

these gaps are observed between both urban and rural settlements. That is, although large villages or large cities grow, small villages and small towns either grow at a slow pace, do not grow, or decline.

While urban settlements play an important role in providing living and working places for the population, and being a center of innovation and technology, rural settlements also play a special role in the settlement system. Rural settlements have increasingly become a "property" used by urban residents, entrepreneurs, and tourists, and as a result, villages are considered a public product of the population (Adamowicz 2022; Guzal 2018). Rural areas are also a "source" that provides food for people. In addition, rural areas are a source of labor resources used in urban areas, a refuge for endangered plant and animal species, natural landscapes, and areas in need of protection. Rural settlements are an important element of national and regional cultural heritage (Mihai and Iatu 2020). In general, rural settlements have a special role in agricultural production, environmental protection, and cultural heritage protection (Neal 2013). Considering the above, it can be concluded that villages have a very important role in the socio-economic and cultural life of the country. However, under the influence of various forms of rapid industrialization and urbanization in recent years, some rural settlements have begun to decline (Liu and Li 2017). Economic decline in rural areas, population decline or slowing growth, and development gaps between urban and rural settlements have become widespread, hindering sustainable regional development (Woods 2005). There is a great need to develop a rural development model in the region to prevent the acceleration and elimination of such problems.

Generally speaking, the development of sustainable development models is one of the most important factors for the regulation of rural settlements and demographic development in any area. Sustainable development refers to the totality of activities aimed at meeting the basic

**Table 3. Change of settlements by altitude zones**

№	Name of village	Altitude (meter)	Ethnic composition	Population			Share of decrease and increase 1999-2019 (%)
				1999	2009	2019	
1	Rochahmad	230	Avar	212	186	172	-18.9
2	Meshashambul	210	Avar	2,682	2,498	2,411	-10.1
4	Garaveli	232	Mixed*	386	384	385	-0.3
5	Saribulag	213	Mixed*	531	453	513	-3.4
6	Gullar	475	Mixed*	5,481	5,882	5,355	-2.3
7	Mahamalar	400	Avar	4,245	4,276	3,213	-24.3
8	Gasbina	290	Avar	1,716	2,238	1,140	-33.6
9	Mazimchay	558	Avar	351	358	323	-8.0
10	Goyrujluk	250	Mixed*	56	57	51	-8.9
11	Shambul	220	Avar	2,027	2,055	1,997	-1.5
12	Mazimustu	250	Mixed*	73	65	70	-4.1
Villages with slow population growth							
13	Solban	450	Avar	360	514	377	+4.7

\* The population of the mixed villages consists mainly of Azerbaijanis and Avars.

Source: Census materials of the population of the Republic of Azerbaijan-1999, 2009, 2019; field research materials.



needs of the population by conserving natural resources for future generations (Marsden 2003). The sustainable rural development model prevents the polarization process in population settlements by reducing the gaps between settlements. At the same time, the model of sustainable rural development reduces the poverty level among the population in rural areas; that is, it serves to create new areas of income for the population, and as a result, the level of well-being of the rural population increases.

The experiences of foreign countries can be used to develop villages in Azerbaijan, especially those located in remote and border areas. However, it should not be forgotten that those experiences should be adapted to the local environment, or a development model should be established accordingly. Because the villages of every country or any of its regions have both similar and different problems. In such a case, a specific development plan for the area would be more appropriate. This plan should conform not only to the natural and geographical conditions of the area, but also to the lifestyle of the population living here. Of course, it is appropriate for sustainable development to use modern technological practices when establishing the development model. However, villages cannot be technologized all of a sudden. Because the technologization

of villages and the establishment of “smart settlements” is a process that requires serious time and resources.

In-situ urbanization is one of the main issues to be taken into consideration when establishing a rural development model. In-situ urbanization is a model of rural development, and it means bringing the living standard of the rural population to the urban level without turning the rural settlement into an urban settlement in terms of territory and population<sup>1</sup>. This form of urbanization has been used in recent years to prevent people from moving from villages to other settlements, especially to large cities with many job opportunities. This practice is used in Japan, China, Sri Lanka, and other countries around the world.

Before developing a sustainable development model for the region, it is necessary to get acquainted with the current situation of the region. For this, a SWOT analysis was used for the research region. SWOT analysis is one of the most basic tools used for strategic analysis of rural areas (Harbiankova nad Gertsberg 2022). Thanks to this method, the “strong” and “weak” aspects of the villages located in the research area; will be able to determine opportunities and threats (Fig. 6).

Regarding the results of the analysis, we can see that the region has rich soil, agro-climatic resources, and water

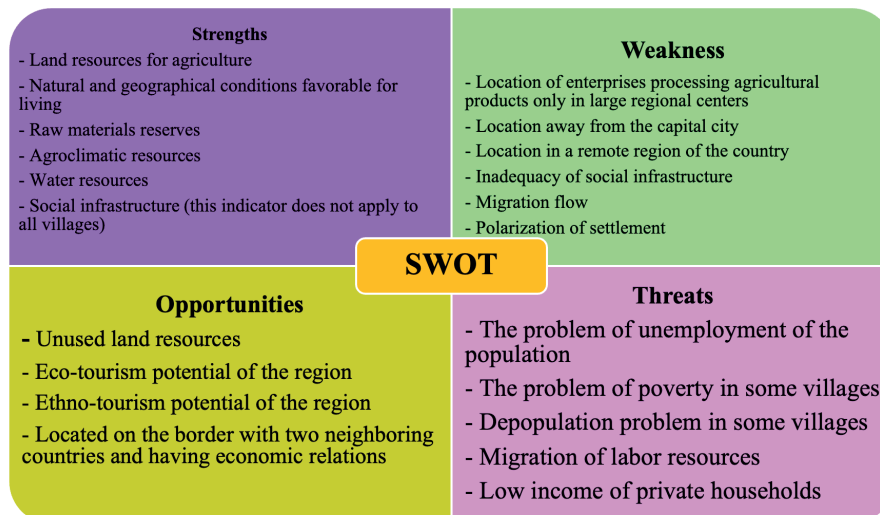


Fig. 6. Analysis of the villages of the Balakan administrative district by SWOT analysis

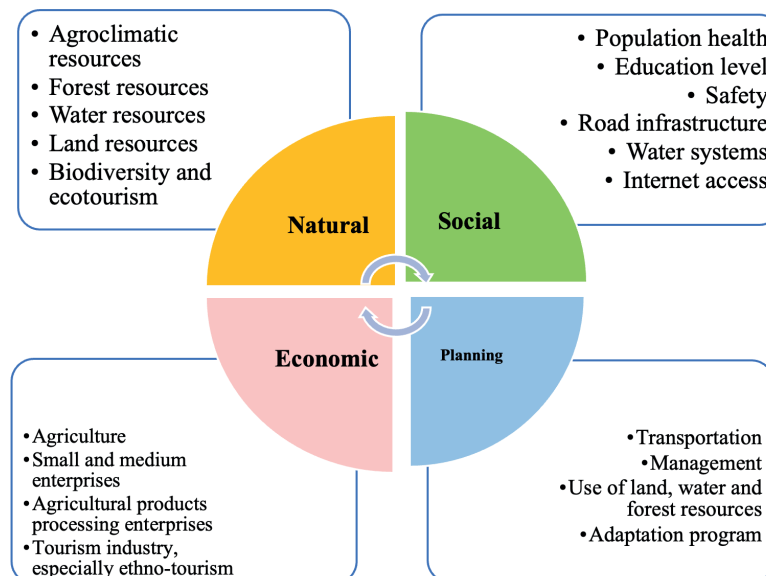


Fig. 7. Geographic modelling for a sustainable rural development

<sup>1</sup> World Social Report. Reconsidering Rural Development. (2021). Department of the Economic and Social Affairs of the United Nations, <https://desapublications.un.org>

resources for agriculture development. In addition, the state of social infrastructure in some large villages in the region is quite good. These are among the strengths of regional villages. However, the villages of the region have some weaknesses, which are manifested in the absence or remote location of enterprises processing agricultural products, in general, the location of the region in the remote part of the country, migration flows, population polarization, and several indicators. The presence of rich mountain-forest landscapes, historical-cultural monuments, and the settlement of ethnic minorities in the area indicate that various types of tourism can be developed in this region. In recent years, the state has taken some steps in the development of ecotourism and mountain and rural tourism in the region, and some tourist routes have been prepared. Especially in the villages of Mazimchay, Talalar, Ajiliqbina, Mahamalar, and others, there is potential for the development of various fields of tourism, especially eco- and ethnic tourism. Furthermore, the location on the border with the two countries, as well as the presence of a road to Tbilisi, the capital of Georgia, can strengthen economic relations between the two regions. Among the threats faced by the administrative region are the problems of unemployment in some areas and, as a result, the migration of young people to Baku city, the depopulation of some villages, and so on.

To develop a geographic model of sustainable rural development, the natural, socio-economic, and cultural potential and function of the area should be taken into account. For this, we will use 4 criteria: natural, social, economic, and planning (Fig. 7).

The establishment of a "rural development model" in ethno-diverse villages with declining and slow-growing populations in the study area was designed to serve the following goals (Huseynova 2023d) (Fig. 7):

1. Elimination of uneven socio-economic development and poverty in rural areas.
2. Eliminate the polarization problem of rural-rural and rural-urban dividends by developing technology.
3. Repopulation of villages with small ethnic groups to protect their ethnic diversity.

In the poorly urbanized and specialized Balakan administrative region of Azerbaijan, there is a great need to establish such development models to keep the population in place.

A logistical and profitable system should be established for the growth of interest in agriculture in the villages of the region. Because agriculture is an area where there may be risks to income. Among such risks, we can show examples of events such as drought, hail, flood, etc., which

occur as a result of natural disasters. Therefore, to ensure food security in the area, the state should pay special attention to this area. Therefore, it is important to use a multisectoral approach method when building a rural development model, and we have taken this method into account. A multisectoral approach to the development of villages is not only related to the rural economy but also to other additional areas, such as tourism, industry, transport, etc. (Hodge and Midmore 2008). Considering the ethnic composition of the region, we suggest that the population's income and job opportunities should be based not only on agriculture but also on ethnic tourism. In such a scenario, new job opportunities can be created for young people in this field in the region. To some extent, this can prevent the migration of young people.

Although the development of villages is proposed based on SWOT analysis in the research work, the issues of "Smart village development" have not been considered in the region. It is known that the studied area is an area where the urbanization level is very weak, and there is a great need to develop villages based on the concept of technology and smart rural development in such regions. To conduct research in the field of creating smart villages in the research region, first of all, a diagnostic assessment should be carried out in the area, and a smart village development concept should be built on its basis. One of the other important issues to be investigated in the region is to find out to what extent the problems that have manifested themselves in the context of climate change in recent years affect the settlement of the population.

## CONCLUSIONS

As a result of the conducted research, it became clear that the process of settlement polarization is underway in the research area, and this process manifests itself in the context of the creation of large rural agglomerations in some areas and the depopulation process in others. Along with the demographic factors, socioeconomic factors have played a significant role in such processes in the district. Demographic factors are mainly characterized by the intensification of migration processes; social and economic factors are mainly related to factors such as the inadequacy of social infrastructure and the income source of the population. There is a great need to carry out this research in the regions located in the border zone of the country, as well as in mountain villages. Because of the poor development of economic sectors in mountain villages and the intensity of difficulties in the social sphere, this process is going faster. ■

## REFERENCES

- Abbasov R., Karimov R., Jafarova N. (2022). *Ecosystem service in Azerbaijan*. Switzerland: Springer. DOI: <https://doi.org/10.1007/978-3-031-08770-7>
- Adamowicz M. (2022). Theoretical and practical rural development concepts. *Annals of the polish association of agricultural and agribusiness economists*, 12(3), 9-19, DOI: 10.5604/01.3001.0014.3452
- Adamowicz M. and Magdalena Z-L. (2018). New concepts for rural development in the strategies and policies of the European Union. *Economic and Regional Studies*, 11(3), 7-31.
- Berlemann M. and Max F. (2017). Climate Change, Natural Disasters, and Migration—A Survey of the Empirical Evidence. *CESifo Economic Studies*, 63, 353–385, DOI: <https://doi.org/10.1093/cesifo/ifx019>
- Census materials of the population of the Republic of Azerbaijan-1999. (2000). Baku: State Statistical Committee of Azerbaijan, volume IV.
- Census materials of the population of the Republic of Azerbaijan-2009. (2010). Baku: State Statistical Committee of Azerbaijan, volume XIX.
- Census materials of the population of the Republic of Azerbaijan-2019. (2022). Baku: State Statistical Committee of Azerbaijan, volume XXI.
- Cheng M., Qinghua Sh. and Limin M. (2006). An explanation of the motivation and obstacles affecting Rural-Urban migration: The case of China. *Frontiers of Economics in China*, 1, 576–96, DOI: <https://doi.org/10.1007/s11459-006-0021-6>
- Crivello G. (2011). 'Becoming somebody': Youth transitions through education and migration in Peru. *Journal of Youth Studies*, 14, 395–411, DOI: <https://doi.org/10.1080/13676261.2010.538043>
- Demographic development of villages in the Republic of Azerbaijan and settlement problems of rural population. (2021). Baku: Institute of Geography of ANAS.
- Demographic indicators of Azerbaijan. (2023). Baku: State Statistical Committee of Azerbaijan.
- Distribution of population and problems of demographic development in the Shaki-Zagatala economic region. (2016). Baku: Institute of Geography.
- Eminov Z.N. (2005). *Population of Azerbaijan*. Baku, Chirag publishing house.
- Encyclopedic dictionary of Azerbaijani toponyms. (2007). Baku: East-West.
- Gao B. and Hu Z. (2022). What Affects the Level of Rural Human Settlement? A Case Study of Tibet, China. *Sustainability*, 14(16):10445, 1-16, DOI: <https://doi.org/10.3390/su141610445>
- Geography of the Republic of Azerbaijan-Economic, social and political geography. (2015). Baku: Europe publication.
- Geybullayev, G.A. (1991). *To the ethnogenesis of Azerbaijanis*. Baku: Elm publication
- Guzal-Dec D. (2018). Intelligent development of the countryside – the concept of smart village: assumptions, possibilities and Implementation limitations. *Economic and Regional Studies*, 11 (3), 32-49, DOI: <https://doi.org/10.2478/ers-2018-0023>
- Harbiankova A. and Gertsberg L. (2022). Information Model for Sustainable Rural Development. *Energies*, 15(11):4009, 1-15, DOI: <https://doi.org/10.3390/en15114009>
- Hidayat, T., Onitsuka K., Sianipar C. and Hoshino S. (2022). Distance-Dependent Migration Intention of Villagers: Comparative Study of Peri-Urban and Remote Villages in Indonesia. *Administrative Sciences* 12:(48), 1-26, DOI: <https://doi.org/10.3390/admsci12020048>
- Hodge I. and Midmore P. (2008). Models of Rural Development and Approaches To Analysis Evaluation And Decision-Making. *Économie rurale*, 307, 23-38, DOI: <https://doi.org/10.4000/economierurale.406>
- Huseynova B.A. (2021). National-ethnic characteristics of demographic development in the northern regions of Azerbaijan (on the example of the Shaki-Zagatala economic-geographical region). *Geography and tourism*, Volume 64, 70-77, DOI: <https://doi.org/10.17721/2308-135X.2021.64.70-77>
- Huseynova B.A. (2021a). Transformation of rural ethno-settlements in Shaki-Zagatala economic-geographical region. *Geography and natural resources*, 2, 86-93.
- Huseynova B.A. (2021b). The tendency and improvement of settlements of ethnic minorities on altitude zones in the rural areas of the Shaki-Zagatala economic-geographical region. *Journal of Young Scientist*, 2, 112-120.
- Huseynova B.A. (2022c). Participation of ethnic minorities living in the north-western regions of the Republic of Azerbaijan in the migration process. *Geographical Bulletin*, 3(62), 45–57. DOI: 10.17072/2079-7877-2022-3-45-57.
- Huseynova B.A. (2023d). Depopulation of the Ethnic Diverse Mountain Villages in the Northwestern Part of Azerbaijan and the Development of a Sustainable Rural Development Model. *Regional Geosystems*, 47(1): 34–48. DOI: 10.52575/2712-7443-2023-47-1-34-48
- Javadov G.J. (2000). *Ethnic and national minorities of Azerbaijan*. Baku: Elm publication.
- Liu Q. and Haimin P. (2020). Investigation on life satisfaction of rural-to-urban migrant workers in China: A moderated mediation model. *International Journal of Environmental Research and Public Health*, 17, 24-54, DOI: <https://doi.org/10.3390/ijerph17072454>
- Liu Y. and Li Y. (2017). Revitalize the world's countryside. *Nature*, 548, 275–277, DOI: <https://doi.org/10.1038/548275a>.
- Lyu H., Zengchuan D., Mahendran R., Jaya K. and Saket P. (2019). Rural unemployment pushes migrants to urban areas in Jiangsu Province, China. *Palgrave Communications*, 5(1), 92, DOI: <https://doi.org/10.1057/s41599-019-0302-1>
- Marta J., Akhmad F., Bambang J. and Ernan R. (2020). Understanding migration motives and its impact on household welfare: Evidence from rural-urban migration in Indonesia. *Regional Studies, Regional Science*, 7, 118–32, DOI: <https://doi.org/10.1080/21681376.2020.1746194>
- Marsden T. (2003). *The condition of rural sustainability*. Assen, Netherlands: Royal Van Gorcum.
- Mendola M. (2010). Rural Out-Migration and Economic Development at Origin: A Review of The Evidence Mariapia. *Journal of International Development*, 24, 102–22, DOI: <https://doi.org/10.1002/jid.1684>
- Mihai F.C. and Iatu C. (2020). Sustainable Rural Development under Agenda 2030 // In M. J. Bastante-Ceca (Ed.), *Sustainability Assessment at the 21st century* London: IntechOpen Limited, 9-18, DOI: <https://doi.org/10.5772/intechopen.90161>
- Muradov Sh.M. (2021). *Demographic development of the Republic of Azerbaijan: historical changes, novel inclinations and, problems*. Baku: Elm and Bilik publication.
- Neal S. (2013). Transition Culture: Politics, localities and ruralities. *Journal of Rural Studies*, 32, 60–69, DOI: <https://doi.org/10.1016/j.rurstud.2013.04.001>
- Vaishar A., Vavrouchová H., Lešková A. and Perinková V. (2021). Depopulation and Extinction of Villages in Moravia and the Czech Part of Silesia since World War II. *Land*, 10(4):333, 1-18, DOI: <https://doi.org/10.3390/land10040333>
- Woods M. (2005). *Rural Geography: Processes, Responses, and Experiences in Rural Restructuring*. London: SAGE publication



# THE IMPACT OF GLOBAL AND REGIONAL CHALLENGES ON THE DECREASE IN TOURIST FLOWS

**Nikolai A. Grudtsyn<sup>1\*</sup>**

<sup>1</sup> St.Petersburg State University, 10th line V.I., 33-35, Saint-Peterburg, 199178, Russia

\*Corresponding author: [grudtcyn.nikolai@gmail.com](mailto:grudtcyn.nikolai@gmail.com)

Received: February 14<sup>th</sup> 2024 / Accepted: July 25<sup>th</sup> 2024 / Published: October 1<sup>st</sup> 2024

<https://doi.org/10.24057/2071-9388-2024-3253>

**ABSTRACT.** The article presents a comprehensive analysis of the impact of global and regional events on the dynamics of tourist flows. The primary reasons for the decrease in inbound tourist flows have been identified and categorized into three main groups: military-political class, economic class, and natural-technological class. Additionally, a hybrid class was identified, to which COVID-19 was assigned. The article is based on causal and comparative analysis, utilizing statistical data on tourist flows provided by the World Bank and UNWTO, as well as an assessment of similar patterns among countries worldwide. The main characteristics of tourist flows from 1995 to 2022 have been identified, pinpointing leaders among countries in increasing and decreasing the number of tourists per year. During the study, countries with similar patterns of tourist flow dynamics were identified. It was concluded that relying solely on quantitative analysis has limited applicability in identifying these patterns. Therefore, it is recommended that quantitative analysis be complemented with expert assessments for a more comprehensive understanding. The basic strategies for responding to the identified classes of causes were outlined. The research will benefit tourism professionals, governmental authorities, and researchers in socio-economic and political disciplines.

**KEYWORDS:** international events, trends, geopolitics, tourist flows, causal analysis, crisis management, strategic tourism planning

**CITATION:** Grudtsyn N. A. (2024). The Impact Of Global And Regional Challenges On The Decrease In Tourist Flows. *Geography, Environment, Sustainability*, 3(17), 47-63

<https://doi.org/10.24057/2071-9388-2024-3253>

**ACKNOWLEDGEMENTS:** The study was supported by the Russian Science Foundation grant № 23-28-00279, "Trajectories of Development of the Russian Medical Tourism Market in the Context of Global Reordering".

**Conflict of interests:** The author reported no potential conflict of interest.

## INTRODUCTION

Tourism is a complex phenomenon that plays a vital role in regions' and countries' development, acting as a catalyst for economic, social, and cultural progress (Creaco and Querini 2003). It generates revenue through direct tourist spending on accommodations, transportation, and other services. This capital has a cascading effect, stimulating other sectors such as hospitality, retail, and entertainment. Tourism not only creates job opportunities but also fosters entrepreneurship and infrastructure development to meet the growing demands of visitors. Beyond the economic impact, tourism promotes cross-cultural exchange (Reisinger & Turner 1998; Bakir et al. 2017), building connections and a deeper understanding of diverse communities and cultural groups. Sustainable tourism practices can encourage environmental conservation and the preservation of cultural heritage (Lusetyowati 2015), contributing not only to the overall well-being but also to the resilience of regions and countries.

In recent decades, the world has experienced a series of significant crises affecting all components of society's social and economic life, including the tourism sector. Changes in the geopolitical landscape, economic fluctuations, social transformations, public health challenges, and environmental issues all have a significant impact on

global tourism, directing tourist flows to new points of attraction or impeding them. For instance, international or regional economic conditions affect potential travelers' demand and purchasing power, and conflicts and revisions of visa policies can significantly alter a country's tourist appeal. The COVID-19 pandemic has vividly demonstrated how the rapid spread of disease can impact tourism, highlighting the importance of competent state and regional management and adaptation to new risks in the tourism industry (Zhong et al. 2022).

Research on tourist flows can be divided into several groups. The first includes studies of flows in specific countries and regions, such as Spain (Garin-Munoz & Amara 2000), Australia (Kulendran 1996), China (Mou et al. 2020), Europe (Jansen-Verbeke & Spee 1995) etc. The second group includes general patterns and trends of international interest (Williams and Zelinsky 1970; Yang and Wong 2013; World Tourism Organization and International Labour Organization 2013; Santana-Gallego et al. 2016; Klimova et al. 2017; Li and Cao 2018; Shao et al. 2020). The third group talks about specific reasons affecting the tourist flow, such as common (Gidebo 2021), natural (Hamilton et al. 2005; Rosselló et al. 2020), economic (Khalid et al. 2020) or geopolitical factors (Webster and Ivanov 2015). Additionally, we will examine several studies more precisely.

Khalid et al. (2020) examine the impact of economic and financial crises on international tourism flows across 200 countries from 1995 to 2010. Findings indicate that inflation crises reduce tourism flows in host and origin countries, while domestic debt crises boost tourism arrivals in host nations but negatively affect originating countries.

Chung et al. (2020) analyzed international tourism data from 124 countries between 2000 and 2013. They use cluster analysis and social network models to identify global tourism network structures, emphasizing that reduced transaction costs are more influential in attracting international tourists than natural and cultural attractions. The most comparable study in terms of data volume is Shao et al. (2020), whose research uses data on international tourist arrivals from 221 countries/regions between 1995 and 2018 and applies network analysis to explore the structure and evolution of these flows. It reveals that the network density of international tourist flows is increasing in Europe, East Asia, and North America.

The cited studies do not specifically address the niche targeted by this research. They offer valuable insights into the structure and evolution of international tourist flows or define and analyze specific causes of the reduction in tourist flow in various countries. However, the need for a more comprehensive analysis and classification of the reasons for the decrease in tourist flow across countries and territories remains relevant. This article *aims to identify the primary reasons for the significant decrease in tourist flows in various countries worldwide*.

Understanding dynamics, leveraging global best practices and adapting them to each country's unique circumstances and requirements is a valuable tool for enhancing competitiveness within the tourism sector. This may involve adopting successful management strategies for tourist flows, integrating innovative technologies, or implementing sustainable and environmentally responsible tourism practices. It is crucial to note that the primary aim of this study is not to propose specific and detailed strategies for response for each class of cause of decrease.

## MATERIALS AND METHODS

The study's analytical framework is based on different scientific theories and approaches: economic cycles, political instability, climate change models and disaster risk management, demographic transition, technological innovation, and diffusion. Economic downturns often lead to reduced travel spending, while political conflicts or terrorism can deter tourists from visiting certain regions due to safety concerns. Climate change and natural disasters can damage infrastructure and disrupt tourism, while demographic, religious, or cultural changes influence travel preferences.

### Methods

The study analyze global trends and specific country cases to understand and describe the overall state and dynamics of tourist flows worldwide. To achieve this, the study relies on various sources, including scientific articles, official reports, and news portals. The methodology employs comparative analysis to establish correlations and causations within tourism events, as well as case studies to understand the nuances of individual country scenarios. Statistical analysis is deployed to quantify these trends. At the same time, visualization techniques are used to map and interpret the data, offering a clear visual representation

of the current state and dynamics of the tourism industry. These methods, combined, provide a robust framework for comprehensively understanding the multifaceted nature of tourism trends.

### Data source

The combined dataset from the World Bank (WB) and the United Nations World Tourism Organization (UNWTO) is used for quantitative analysis. It contains information on the number of arriving international tourists (1995 – 2022; data for some countries for 2022 are still unavailable). According to the methodology, international inbound tourists are defined as the number of tourists travelling to a country different from where they usually reside for a period not exceeding 12 months, whose primary purpose of the visit is not an activity remunerated within the visited country. If data on the number of tourists is unavailable, the number of visitors displayed includes tourists, same-day visitors, cruise passengers, and crew members.

The dataset gathers data from various sources, including border statistics (police, immigration, etc.), border surveys, and tourist accommodation establishments. Some countries include the arrival of citizens living abroad, while others do not. Therefore, caution should be exercised when comparing arrivals across different countries.

This study uses the total number of inbound tourists, including same-day and overnight visitors. It is crucial to include both groups, as they can serve as significant economic, political, and cultural actors. Same-day and overnight tourists contribute differently to the tourism sector, with each group impacting local economies, cultural exchanges, and political landscapes in various ways. For instance, around 80% of visitors in Poland are same-day tourists, while in Paraguay, before 2003, more than 90% stayed there for less than a day. On the other hand, in Greece, more than 90% of tourists were overnight visitors in 2019. Excluding such a significant portion of tourists would result in an incomplete and potentially misleading analysis. While the author acknowledges that, at the country and region level, one group of tourists may have a more pronounced impact on the development of the tourism industry, using the total number of tourists is deemed appropriate for researching a global-scale dynamic.

The countries for the case studies emerged during discussions and were selected as follows: countries that experienced a decline in less than four separate years with an average number of tourist trips of less than 1.5 million per year and 'stable' were excluded. It was also decided that there should be at most five countries from various geographical regions to test the methodology without overloading it with data. As a result, Brazil, Egypt, Russia, Turkey, and Japan were selected. Additionally, Dominica was included as an example of one of the most unstable countries regarding tourist flows.

### Data preparation

At the preparatory stage, regional unions, country classifiers, countries, quasi-countries, and individual regions with zero indicators (Afghanistan, Channel Islands, Faroe Islands, Gibraltar, Isle of Man, etc.) were excluded from the data analysis. On the other hand, some overseas territories, such as Montserrat or the Northern Mariana Islands, were deliberately included in the dataset because, being located far from the main territory, they may have their own patterns of tourist behavior.

The dataset contains 339 missing values – 5.70% of the total dataset. Initially, attempts were made to fill these gaps using linear, cubic, and spline interpolations, but these methods were later abandoned due to the resulting distortions in the data. Linear interpolation was explicitly employed to identify patterns in percentage change dynamics while absolute values remained unfilled. The calculation model was adjusted to exclude the year following the missing data to maintain analysis integrity and reliability.

*Data analysis* is initiated by evaluating the overall state of global tourist flows, identifying years with more than a 5% change in incoming tourists. Subsequently, it combines the identification of countries with both unstable and stable tourist dynamics into one step. This involves distinguishing nations with significant fluctuations exceeding 5% from those showing stability or minor decreases in tourist flow (up to 10%).

Determining a decrease in the percentage of tourist flow in a country, which can be considered substantial, is quite challenging and depends on the study context, market specifics, and existing trends in the tourism industry. Among the factors to consider are the tourism sector's role in a country's economy, the dynamics of tourist flow in previous years, the level of dependence on international visitors, and government policies affecting tourism.

During the early stages of the study, we looked at groups of countries based on their income levels (Fig. 1) and discovered that the changes in tourist flows were only significantly higher than 5% once, in 2011. So, this level could be used as an appropriate threshold.

This approach is debatable, and we plan further to develop a more complex and comprehensive model that uses the share of tourism in a country's GDP and the result of the tourism dynamic in the previous year.

Technical tools used in analyzing and visualizing data include Python with libraries such as Pandas, Sklearn, Matplotlib, and Scipy, as well as Tableau Desktop 2024. The 'pdist' function and Euclidean distance are used to find groups of countries based on their tourist dynamics. The 'pdist' function calculates pairwise distances between observations in a dataset. The 'squareform' function converts the compact representation into a readable square distance matrix.

## RESULTS

### Overall state of tourist flows

Understanding long-term trends in tourist flows is critical for industry management. Identifying countries where tourism has consistently grown or declined can indicate successful tourism development strategies or problem areas that require attention. Fig. 2 displays the country's total number of positive and negative changes in tourist flows. The results point to a generally positive dynamic in international tourism. Armenia has observed a significant increase in tourist flow (24 times), while Dominica, the Northern Mariana Islands, Palau, Paraguay, and Venezuela faced a significant flow reduction (12 times). Countries with unstable dynamics are shown in Fig. 3. Such statistics may be of interest because they provide insights into the volatility and unpredictability of specific regions.

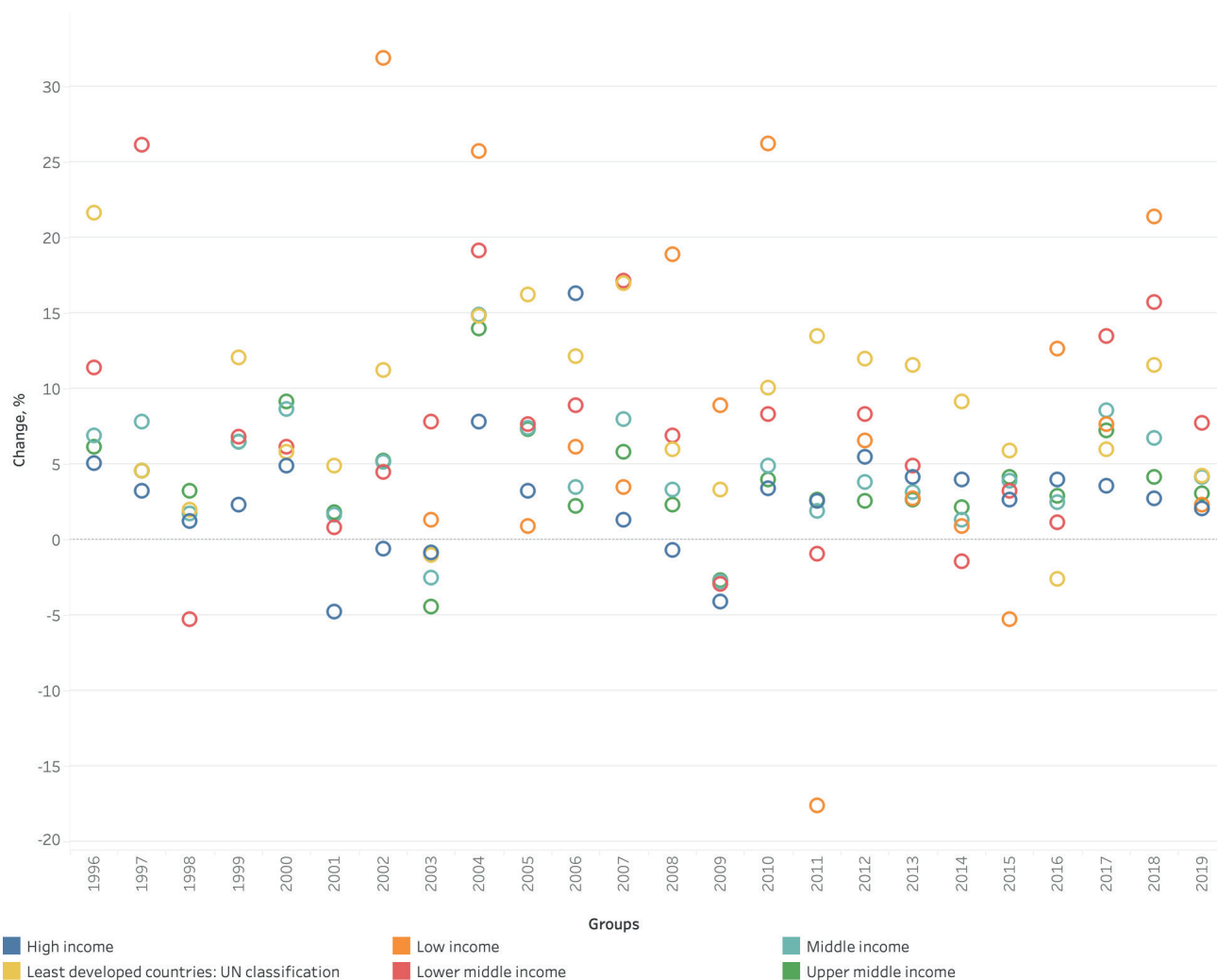
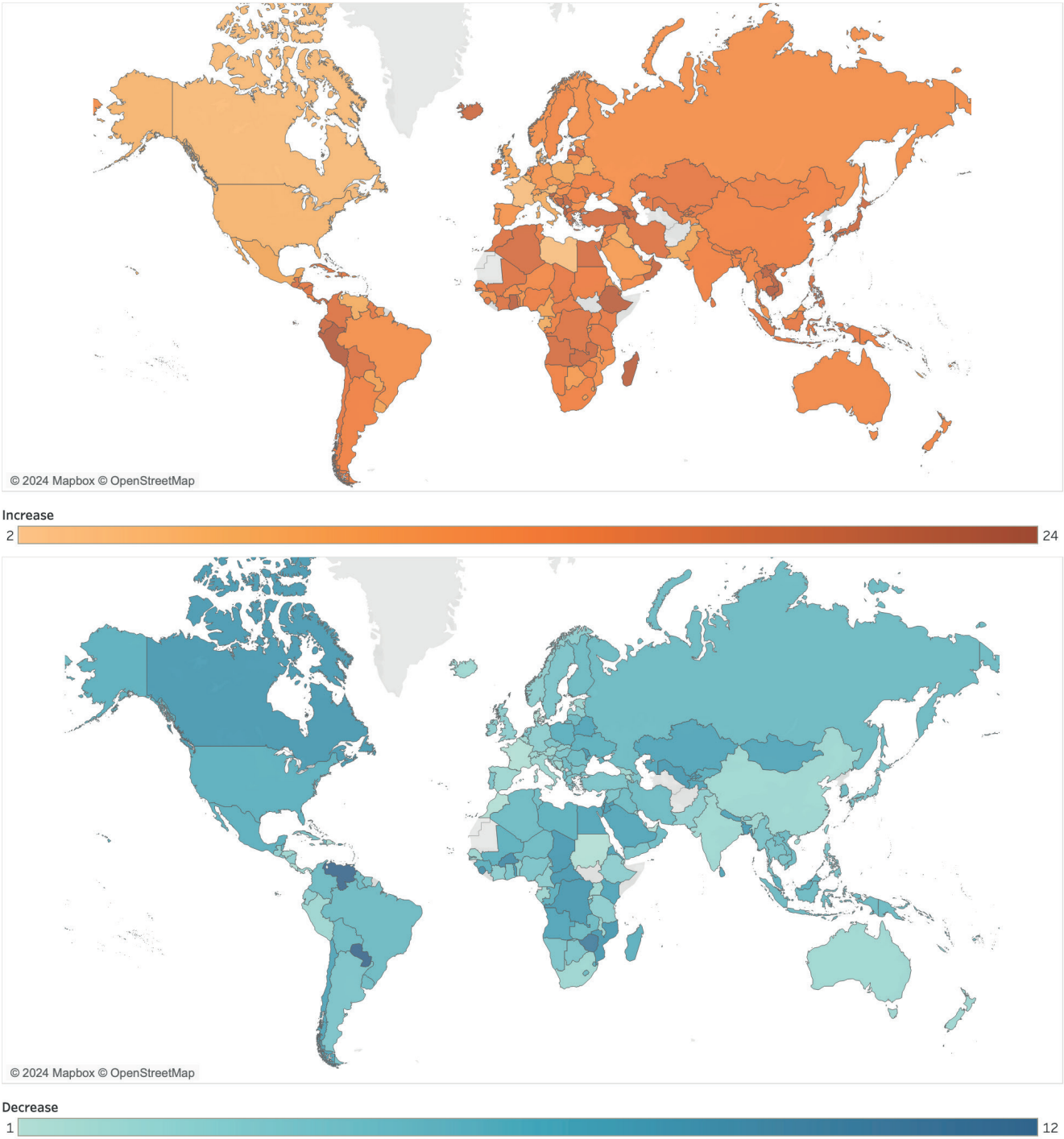


Fig. 1. Dynamics of tourist flow by groups of countries



**Fig. 2. Number of years with over 5% change in incoming tourist arrivals by country (1995-2022)**

Fig. 4 depicts countries with three groups of decreased tourist flows. In Fig. 5, we categorize countries (without COVID-19 years) into two groups based on the annual variation in tourist numbers: a decrease of less than 5% and from 5 to 10% annually. For example, France showed no significant decreases in tourist flow during the study period, indicating its resilience and attractiveness as a destination. Spain experienced a minor setback in 2009 with a 6% decrease in tourist numbers, likely due to the global financial crisis impacting travel behavior. On the other hand, the USA has experienced a decrease of several years below 10% annually (1998, 2001, 2002, 2009, 2011). This resilience in the face of economic and other challenges may highlight the adaptability of the tourism sectors in these countries.

We can observe in Figs. 4 and 5 that Europe (except the eastern part) is the most stable region regarding tourist

flows. Data on both stable and unstable dynamics in tourist flows informs decision-making in investment strategies, policy formulation, and itinerary and infrastructure creation. Moreover, it is recognized that higher instability implies higher risks and, consequently, the potential for higher returns for businesses operating in such environments. We have also identified values of decrease and increase in the number of tourists by country, in addition to the general trends discussed earlier (Table 1).

The data review indicates that the most significant changes in tourist numbers were connected to the COVID-19 pandemic. The growth in tourism in most countries is due to the low-base effect; for instance, Bhutan welcomed only one tourist who stayed for 113 days in 2001. Both Taiwan and Bhutan experienced a substantial decline for two consecutive years.

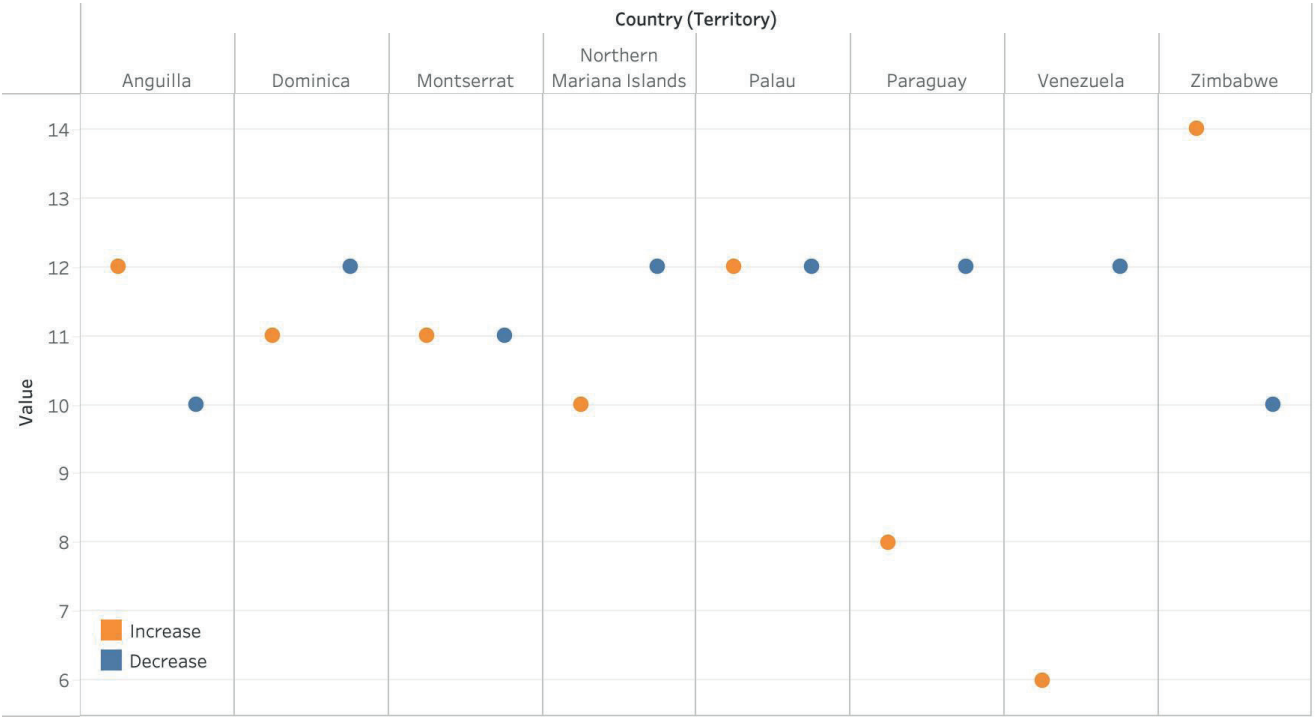


Fig. 3. Countries with unstable dynamics of tourist flows (1995 – 2019), increase or decrease, number of times

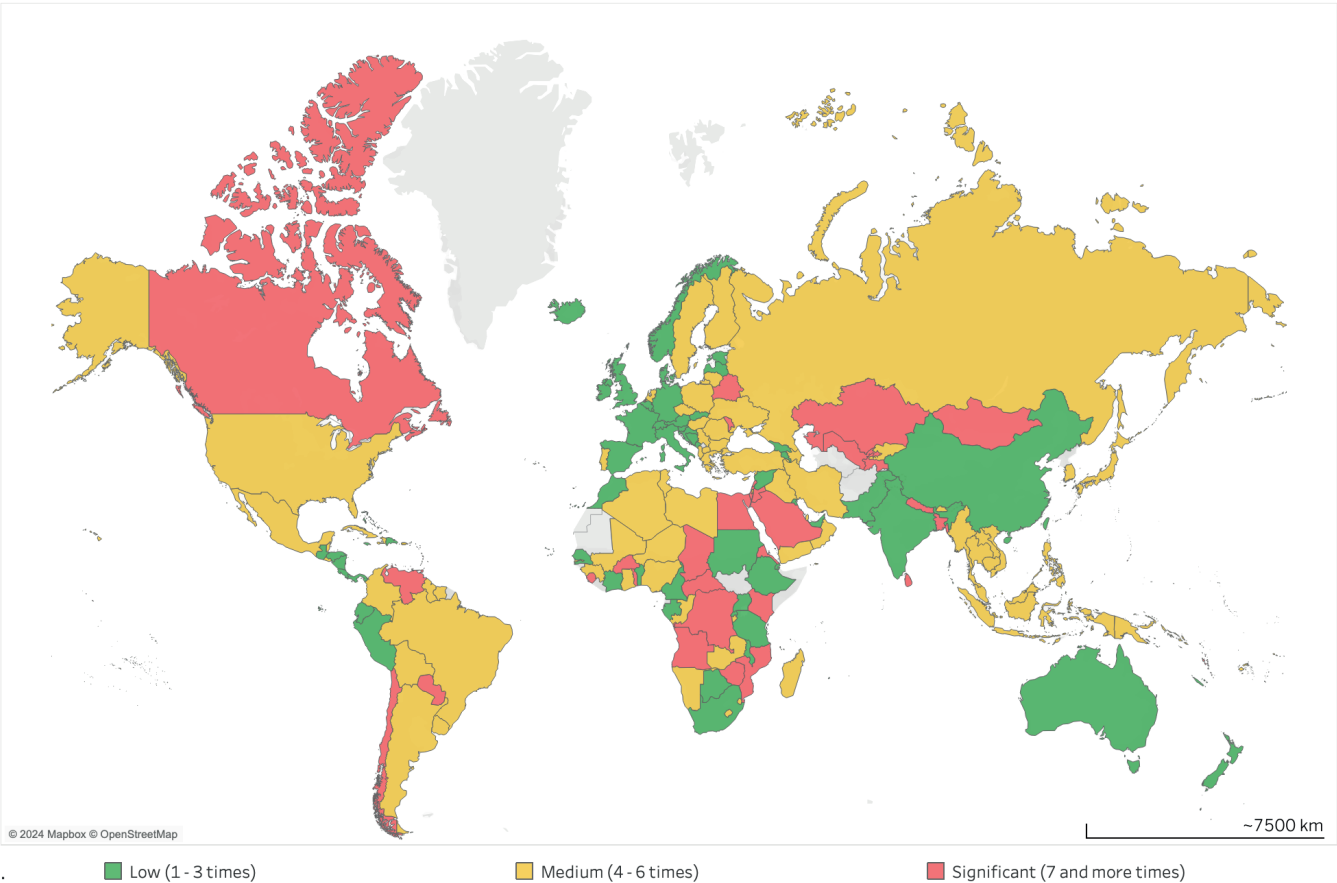


Fig. 4. Groups of countries by the level of decrease in tourist flow



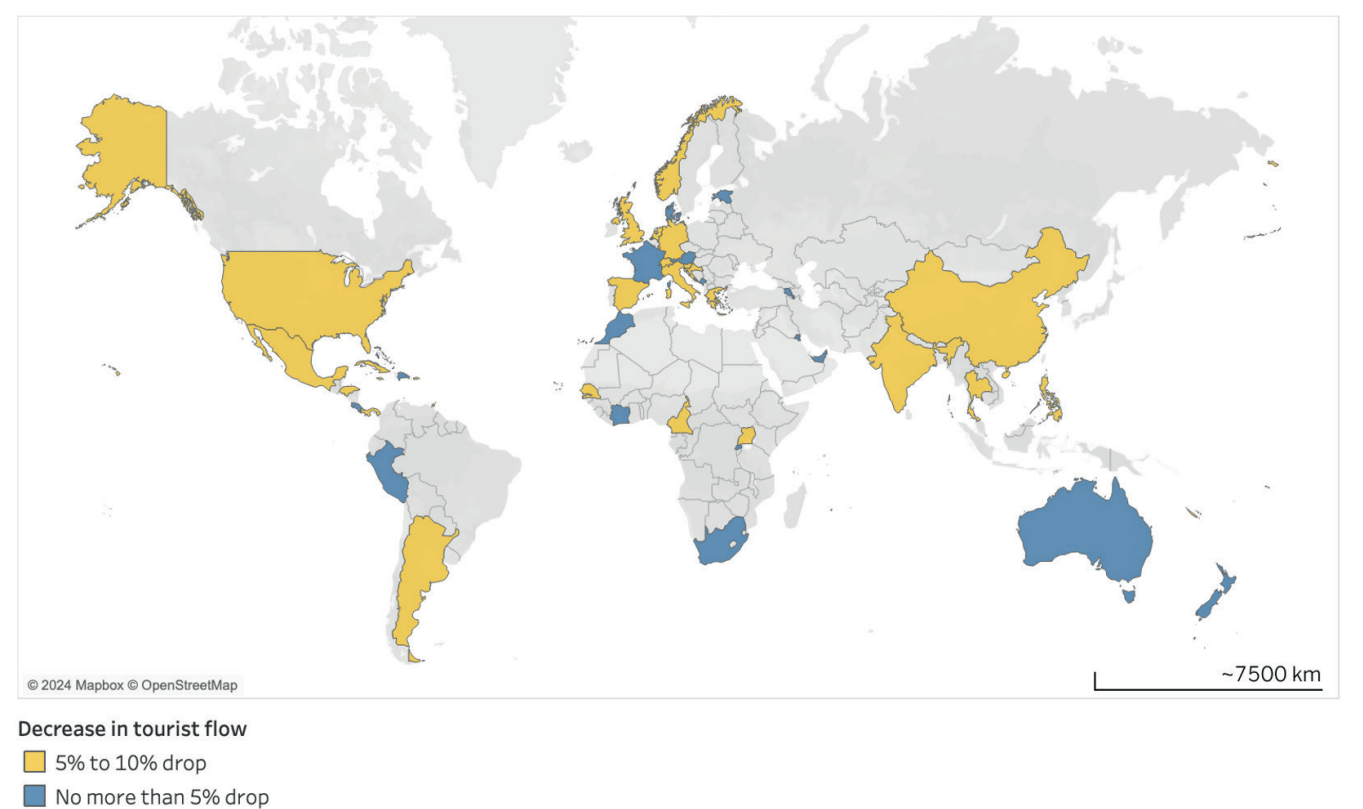


Fig. 5. Countries with annual tourist flow decrease of 0-5% and 5-10% (1995-2019)

Table 1. Top 20 countries with highest yearly increase and decrease in tourist arrivals

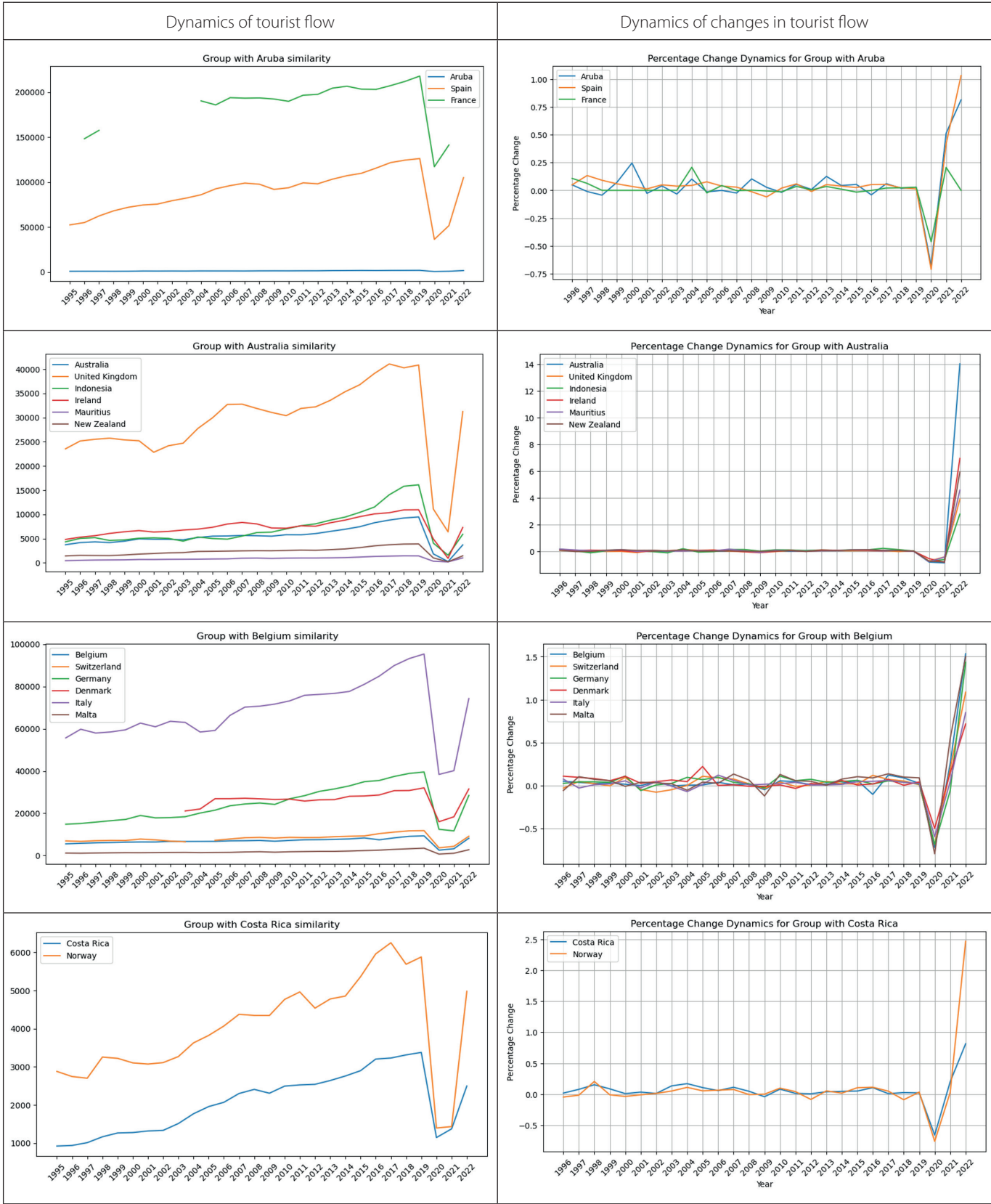
Nº	Country	Year	Increase, %	Country	Year	Decrease, %
1	Bhutan	2022	2,089,900	Tonga	2021	-100
2	Malaysia	2022	7360	Bhutan	2021	-99.997
3	Viet Nam	2022	2231.84	Hong Kong SAR, China	2021	-97.45
4	Fiji	2022	1937.5	Malaysia	2021	-96.884
5	Singapore	2022	1810.91	Marshall Islands	2021	-96.667
6	Samoa	2022	1533.33	Viet Nam	2021	-95.908
7	Philippines	2022	1518.29	American Samoa	2020	-95.313
8	Japan	2022	1457.72	Japan	2021	-94.023
9	Australia	2022	1401.63	Bermuda	2020	-93.665
10	Argentina	2022	1209.76	Hong Kong SAR, China	2020	-93.617
11	Cambodia	2022	1061.74	Tuvalu	2021	-93.333
12	Guinea	2011	991.67	Kiribati	2021	-92.857
13	Chile	2022	968.42	Thailand	2021	-92.402
14	Mongolia	2022	671.79	Bhutan	2020	-90.506
15	Northern Mariana Islands	2022	646.15	Taiwan	2021	-89.840
16	Libya	2008	616.98	Brunei Darussalam	2021	-89.729
17	Israel	2022	609.20	Mongolia	2020	-89.482
18	New Zealand	2022	592.75	Philippines	2021	-88.941
19	Hong Kong SAR, China	2022	564.84	Namibia	2020	-88.673
20	New Caledonia	2022	558.33	Taiwan	2020	-88.385

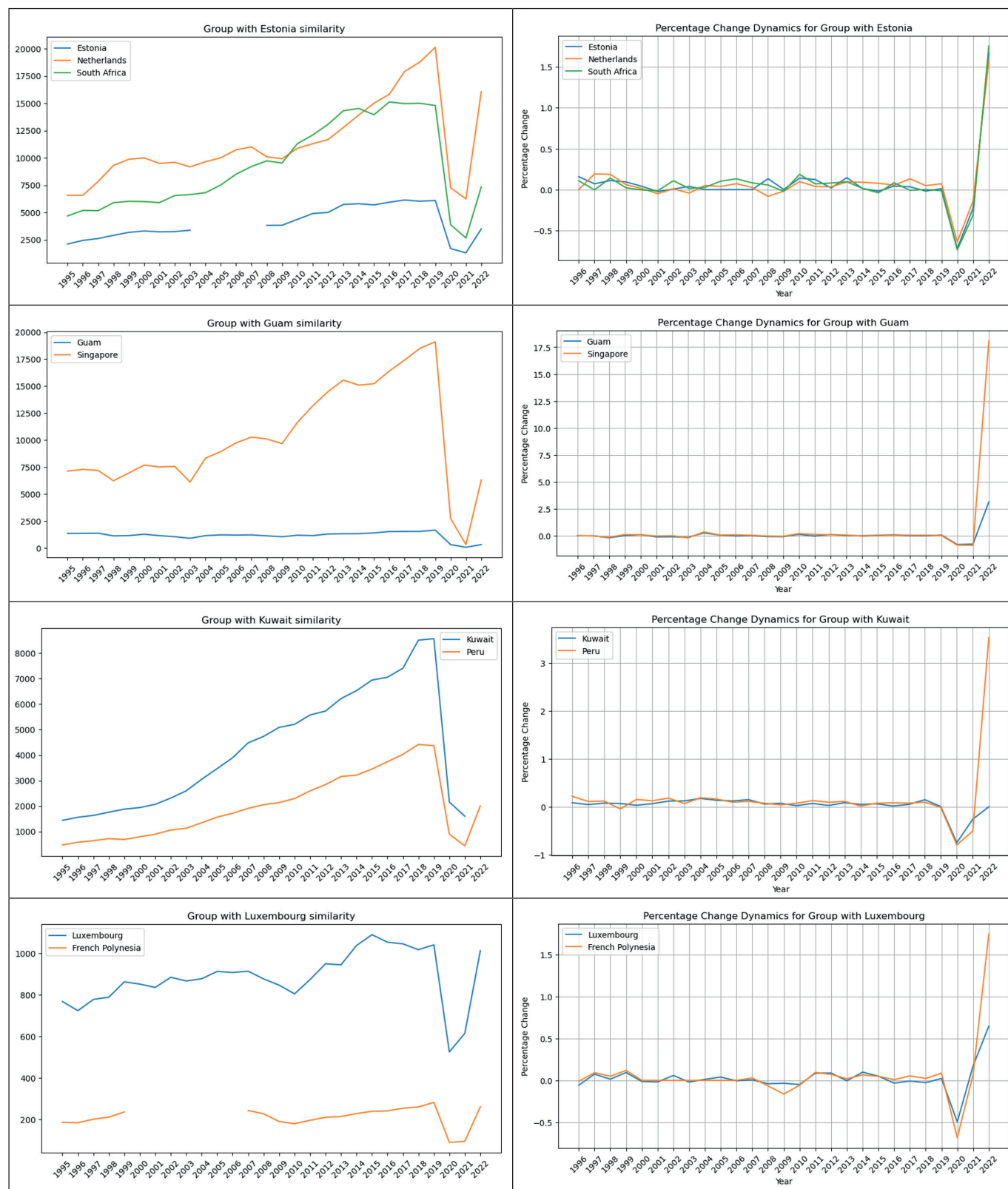
Patterns in tourist flow dynamics

We analyzed tourist flow dynamics quantitatively to identify countries with similar patterns (Table 2). The threshold was set at 0.095. Since we are working with normalized percentage changes, the data values have a similar scale. In this context, a threshold value around 0.1 is often an optimal choice, as it is flexible and reasonable. This value suggests that countries will be grouped if the distance between their normalized percentage changes is less than 9.5%.

According to Table 2, only a limited number of countries can be grouped, considering similar trends in tourist flows. Some countries, such as Germany, Denmark and Belgium, Australia and New Zealand or France and Spain, share similar socioeconomic and geographical characteristics. Meanwhile, affinity in the dynamics of tourist flows between countries such as Estonia and South Africa or Costa Rica and Norway seems more correlative than causal. Expert assessments should complement quantitative analysis to identify patterns in the dynamics of tourist flows, as the results suggest.

Table 2. Countries with similar patterns in tourist flow changes





The data also visually reaffirmed that the COVID-19 pandemic had a significant impact on the reduction of tourist flows in most countries. Then, to reduce the noise in the data, we decided to exclude the 2020–2022 years. This allowed us to lower the threshold to 0.65 and obtain results that more clearly reflect geographical patterns (Table 3).

### Classes of causes leading to a reduction in tourist flows

We identified the countries with the most noticeable reductions in tourist flows and examined the class of causes for each case (Table 4). This stage of the research allowed us to consider and assess the scale and primary factors behind

the substantial decrease in the number of tourists, which provided the opportunity to better understand the dynamics and resilience of the tourism markets in these regions.

Of the 20 cases, 14 belong to the military-political class and three each to the economic and natural-technological classes, respectively. Given the limited representation of the 2007–2009 years among the top 20 cases of decreased tourism flow, we decided to separately examine the impact of the global economic crisis on tourist flows across countries worldwide (Fig. 6). The results show that in 2008, the most significant decrease occurred in Kenya (33.79%) and in 2009 in Bangladesh (42.83%).

Table 3. Countries with similar dynamics in tourist flow changes (1996-2019)



Table 4. Top 20 countries with highest yearly decrease in tourist arrivals with class of causes (1996 - 2019)

Nº	Country	Year	Decrease, %	Class of Causes/ Comment
1	West Bank and Gaza	2001	-86.13	Military-political class // Conflict with Israel (Saleh 2003)
2	Iraq	1997	-70.59	Military-political class // Iraq and United Nations Special Commission UNSCOM tensions <sup>1</sup>
3	Central African Republic	2002	-70	Military-political class // Tension between Chad and CAR (Boutellis 2013)
4	Eritrea	1999	-69.68	Military-political class // The Eritrean-Ethiopian War (part of the Badme War) (Murphy 2016)
5	Yemen, Rep.	2015	-67.32	Military-political class // Yemen's civil war began in 2014 when Houthi insurgents took control of Yemen's capital and largest city, Sana'a, demanding lower fuel prices and a new government <sup>2</sup> .
6	Sierra Leone	1997	-63.64	Military-political class // Rebel declares himself head of state <sup>3</sup>
7	Madagascar	2002	-63.53	Military-political class // The post-electoral political crisis in 2002, which resulted in severe transportation disruptions <sup>4</sup>
8	Burundi	1997	-59.26	Military-political class // From 1996 to 2000, external aid dried up as a reaction to a military coup carried out in July 1996, during the 1993-2003 civil war. A few days after the July 1996 coup, Burundi was put under a total economic embargo. (Nkurunziza 2018)
9	Albania	1997	-58.54	Economic class // In early 1997, Albania's pyramid schemes collapsed, plunging the country into a deep economic and social crisis (Treichel 2002)

<sup>1</sup> <https://www.un.org/Depts/unscom/Chronology/chronologyframe.htm>

<sup>2</sup> <https://www.cfr.org/global-conflict-tracker/conflict/war-yemen>

<sup>3</sup> <http://edition.cnn.com/WORLD/9705/25/sierra.leone.pm/index.html>

<sup>4</sup> <https://documents1.worldbank.org/curated/en/994701467992523618/pdf/820250WP0P12800Box0379855B00PUBLIC0.pdf>

10	Madagascar	2009	-56.53	Military-political class // "The most recent incident, and one of the most damaging, has been the political unrest that emerged in March 2009" <sup>3</sup>
11	North Macedonia	2001	-55.80	Economic class // Poor and unstable economy of country (Iliev 2019)
12	Israel	2001	-54.38	Military-political class // Regional conflict (Saleh 2003)
13	Eritrea	1998	-54.15	Military-political class // The Eritrean-Ethiopian War (part of the Badme War) (Murphy 2016)
14	Montserrat	1996	-53.37	Natural-technological class// 1995 - The volcano erupts after being dormant for 500 years.1996 - The volcano continued to erupt and became more violent causing increased damage <sup>5</sup> .
15	Central African Republic	1998	-52.94	Military-political class // internal mutinies in previous years and in 1998 the final contingent of French troops leaving CAR (Berman and Lombard 2008)
16	Kyrgyz Republic	2010	-50.06	Military-political class // The 2010 political turmoil disrupted economic activity and negatively affected near-term growth prospects. (Kyrgyz Republic 2011)
17	Ukraine	2014	-49.18	Military-political class // Revolution, Civil war and conflict with Russia, Malaysia Airlines Flight 17 jet downing, 17 July 2014
18	Congo, Dem. Rep.	2002	-49.09	Natural-technological class <sup>6</sup> // But: war of 1998-2002 was characterized by mass displacement, collapse of health systems and food shortages <sup>7</sup>
19	Comoros	2007	-48.28	Natural-technological class// According to UNWTO data, there was a decrease from 28.5 to 15.2, while other sources, such as the Central Bank of Comoros, indicate only a 15% decrease, from 17 to 14.6 (Comoros, 2013). Despite the discrepancies in the data, the cause was identified as the Karthala volcano eruption (Global Volcanism 2007)
20	Bangladesh	2010	-47.94	Economic class // The tourism sector is experiencing numerous problems as a result of the global economic crisis (Haque 2015)

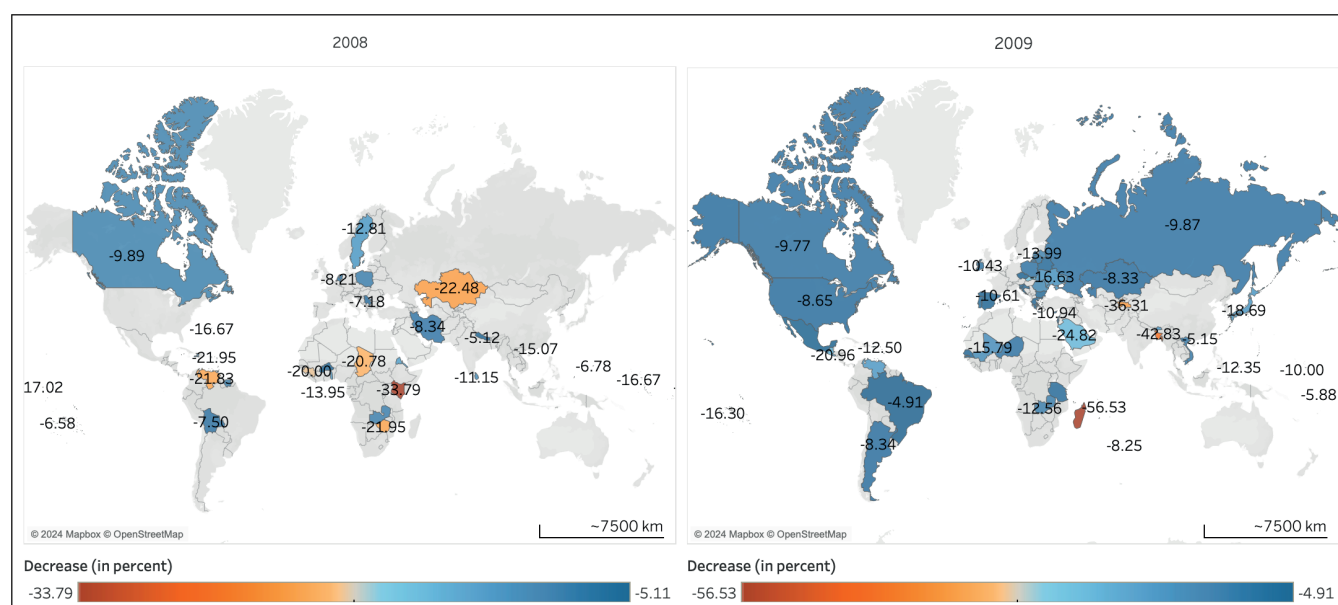


Fig. 6. Reduction in tourist flows by countries as a consequence of the Global financial crisis of 2007 – 2008

<sup>5</sup> <https://downstectonicprocesses.weebly.com/montserrat-a-case-study-of-a-volcanic-eruption.html>

<sup>6</sup> <https://earthobservatory.nasa.gov/images/9164/nyiragongo-volcano-erupts-in-the-congo>

<sup>7</sup> <https://www.rescue.org/sites/default/files/document/661/2006-7congomortalitysurvey.pdf>



The complex analysis allows us to conclude that over the last 30 years, the most significant reduction of international inbound tourism was caused by the COVID-19 pandemic, followed by the class of causes “military-political conflicts”, with economic class coming in third.

**Causal analysis of tourist flow dynamics in individual countries (case studies).** To assess the impact of different classes of causes of tourist flow decrease within individual countries, five countries were selected from different regions of the world: Brazil, Egypt, Russia, Turkey, and Japan, each with different tourist behavior patterns (Figs. 7, 8) and unique geopolitical, economic, and socio-cultural factors influencing tourism.

Due to Japan's growth, which created a significant distortion, we will also show Fig. 9 for the period from 1995 to 2019, which provides a clear visualization of complex dynamics for further analysis.

According to UNWTO data, there was a significant decrease in inbound tourism in Russia in 2016 (27%), but this figure only partly reflects reality. Since 2014 in Russia, tourist flows have been measured not by the number of tourists but by the number of trips, according to the ‘Official Statistical Methodology for Assessing the Number of Inbound and Outbound Tourist Trips’. As a result, according to the original methodology, there were 32,421,490 tourists in 2014, while the new methodology counted 25,437,893 trips. The drop was 21%, whereas the actual data is likely higher and may exceed UNWTO figures.

The obtained data reveal that general proportions of the class causes are maintained, while specific details are more pronounced at the country level. Out of 18 instances of decreased tourism flow, 10 are linked to military-political conflicts (56%), two to the natural-technological class (11%), and six to the economic class (33%). At the country level, different classes of causes can dominate in various countries, underscoring the significance of context-specific factors.

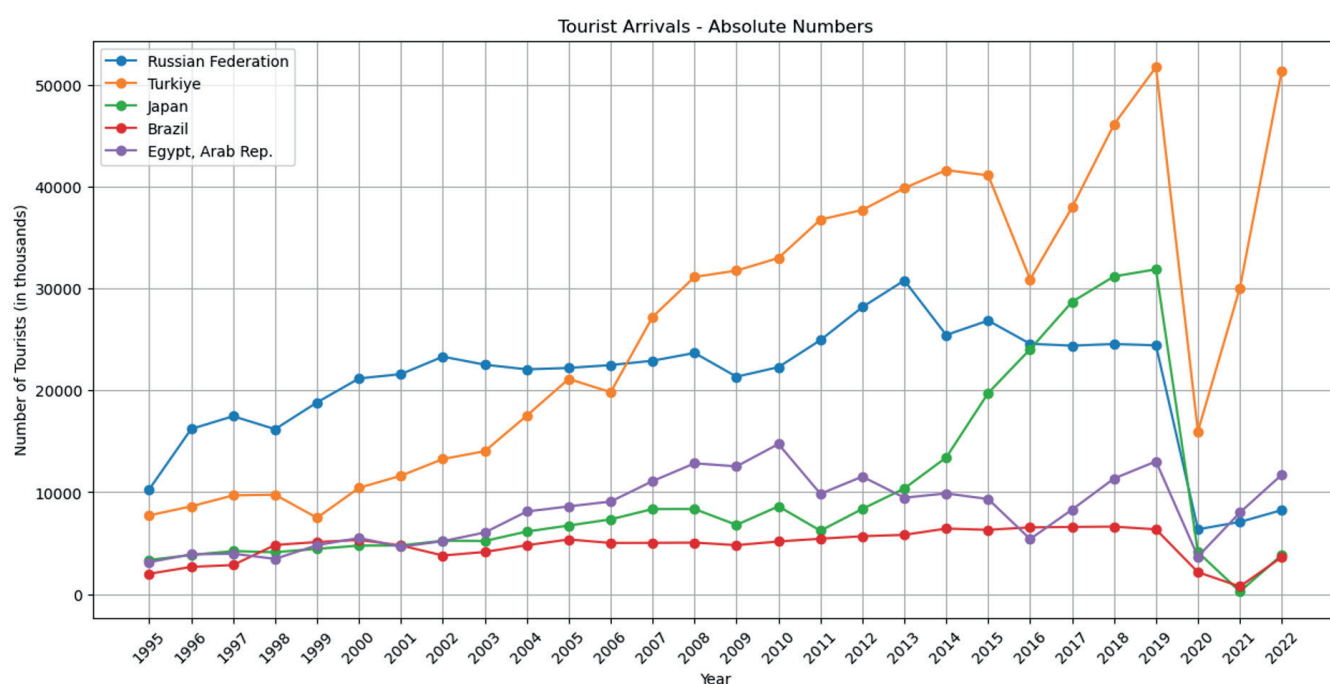


Fig. 7. The absolute number of tourists by individual countries (in thousands)

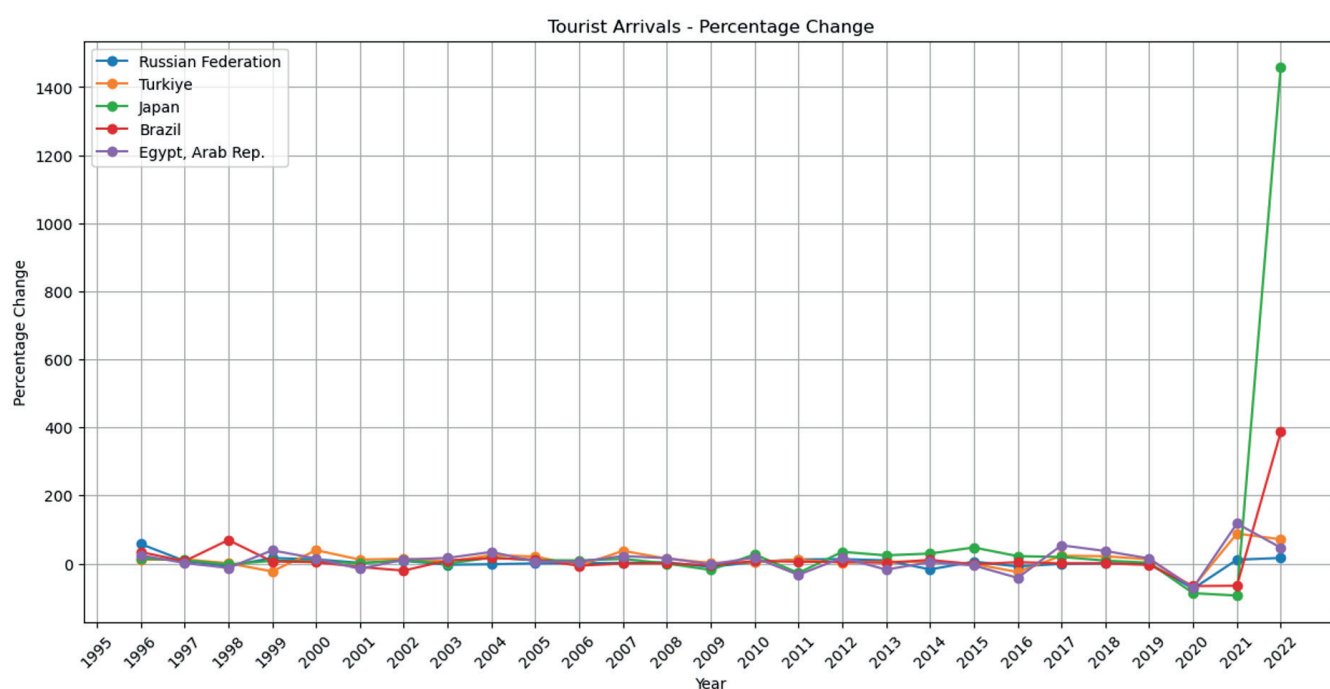
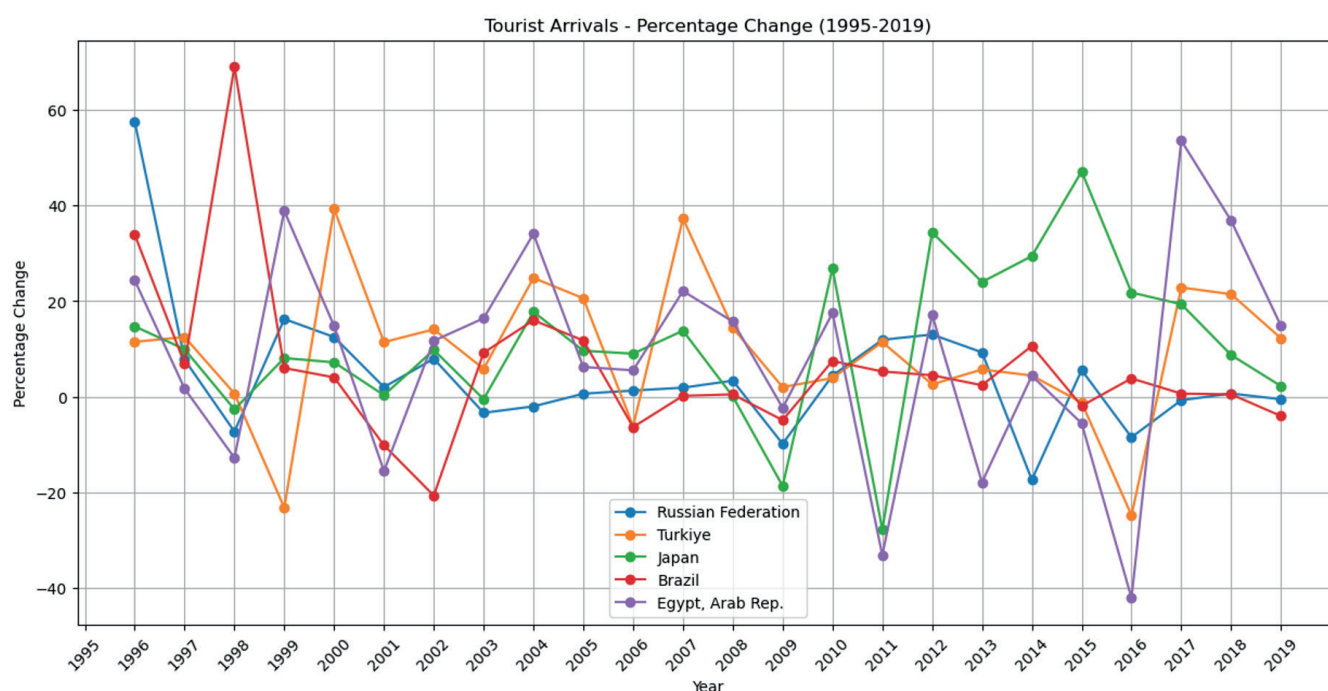


Fig. 8. Change in tourist flow by individual countries (in percent)



**Fig. 9. Change in tourist flow by individual countries in 1996 - 2019 (in percent)**

**Table 5. Reasons for the decline in tourist flow by individual countries**

Country	Year	Decrease (%)	Cause class // comment
Russia	1998	7,3%	Economic class // The underlying origins of the Russian crisis of 1998 are to be found in the country's economic structure, institutional environment and political processes <sup>8</sup>
	2008	9,87%	Military-political class // Conflict with Georgia and Global financial crisis
	2014	21,05%	Military-political class // Conflict with Ukraine and the associated initial period of sanctions (Dementiev and Andreev 2023)
	2016	8,5%	Military-political class // Conflict with Ukraine and the associated initial period of sanctions (Dementiev and Andreev 2023)
Egypt	1998	12,8%	Military-political class // In 1998 when tourist numbers decreased because of terrorism, the shares of Europe decreased drastically, while that of Middle East increased (The study on tourism..., 2000)
	2001	15,6%	Military-political class // Impact of political instability and terrorism in the tourism industry (Mody 2013)
	2011	33,1%	Military-political class Arab spring (Arruda 2018)
	2013	17,9%	Military-political class Arab Spring continued But there was a slight recovery in 2012
	2016	42,1%	Military-political class Decrease in the number of Russian tourists after a Russian aircraft crashed in October 2015, as well as to the decline in the number of tourists coming from Britain, Germany and Italy <sup>9</sup>
Japan	2009	18,7	Economic class // Consequences of the global economic crisis (Ishikawa 2011)
	2011	27,7	Natural-technological class // Earthquake and tsunami <sup>10</sup>

<sup>8</sup> <https://unctad.org/system/files/official-document/poirsd002.en.pdf>

<sup>9</sup> <https://www.middleeastmonitor.com/20170105-tourism-to-egypt-plummets-by-40-per-cent-in-2016/>

<sup>10</sup> <https://theconversation.com/making-it-safe-tourism-after-japans-earthquake-5691>

Turkey	1999	23,2%	Natural-technological class // Earthquake in the Marmara Region on 17 August 1999 (ÇİFTÇİ and BAYRAM 2021)
	2006	6,2%	Military-political class The most vital factor in the sudden change however was the political unrest the country experienced last year. There were strings of bombings by Kurdish rebels and this together with the nearby Lebanon/Israel conflict gave Turkey a reputation of being unsafe <sup>11</sup> .
	2016	24,8%	Military-political class // Turkey's previously booming tourism sector was gravely hit in the wake of a series of terrorist attacks and domestic political turmoil (Turkey's Economy 2017)
Brazil	2001	10,16%	Economic class // The fall of the flow of tourists to Argentina is related to the collapse of its economy from December 1, 2001
	2002	20,6%	Economic class // Due to the economic crisis that Argentina suffered in 2002, its participation in the influx of tourists to Brazil fell from 32.8 percent in 2000 to 19.24 percent in 2004. (Sobral et al 2007)
	2006	6,4%	Economic class // Varig Airlines bankruptcies - Varig was forced to cut 1.2 million international flights <sup>12</sup>
	2009	5%	Economic class // Global economic crisis

The case of Dominica was observed separately and clearly illustrates the issues related to distinguishing between tourists who stay in the country for more than one day and same-day tourists (Figs. 10, 11). Because the number of same-day visitors exceeds the number of overnight tourists by 2-5 times, the overall dynamics of tourist numbers follow the patterns of same-day visitors. Volatile tourist flow dynamics characterize Dominica: over the observed period, there were 11 years with a total number of tourists that increased by more than 5% and 12 years with a decrease of more than 5%.

As we can see from the graphs, the dynamics of the tourist flows are smooth for overnight tourists and do not raise questions, whereas, for same-day tourists (mostly cruise passengers), there are extreme fluctuations. In Dominica, the main class of reasons for the decrease is "natural-technological", such as hurricanes Lenny (1999), Ophelia (2011), Erika (2012), and Maria (2017), which deteriorated cruise activity. However, the country also faced economic crises, for example, in 2001–2002 (International Monetary Fund, 2011).

### The case studies allow us to draw several conclusions:

The analysis of tourist flow dynamics is sensitive to the chosen research methodology (total, overnight or same-day tourists). Significant changes in one indicator may not be prominently reflected when considering the other. The model for analyzing tourist flow dynamics should be comprehensive and include both types of tourists. The introduction of normalization coefficients, depending on the level of influence of every kind of tourist, might be necessary. This analytical model could help groups like government tourism boards, local businesses, and destination management organizations, make their marketing campaigns, infrastructure investments, and policy initiatives more suitable for the different wants and needs of tourists staying overnight and those visiting for the day.

Analyzing annual trends in tourist flow dynamics to determine the impact of specific cause classes is an overly generalized approach. This is evident in the example of hurricane seasonality in the Caribbean Sea, which

significantly impacts the tourism industry in a specific season. The same can apply to short-term military-political conflicts or terrorist acts. All this highlights the need for more granular time intervals for more accurate causal analysis.

Diversifying the tourism product and market segments is crucial, especially in regions heavily relying on a single type of tourism, such as cruise tourism in Dominica, where hurricanes, storms, and typhoons pose significant risks. While developing and promoting alternative forms of tourism is essential, devising strategies for mitigating the risks associated with such calamities is equally vital. This entails implementing robust disaster preparedness plans, enhancing infrastructure resilience, and fostering partnerships with local communities to ensure swift recovery and continuity of tourism activities in the aftermath of natural disasters.

### DISCUSSION AND CONCLUSION

The analysis of tourist flow dynamics at global and country levels is significant for state governance and tourism industry management. This understanding of dynamics empowers governments, tourism operators, and stakeholders to tailor effective strategies to attract and retain tourists, particularly during periods of decline.

Within this study's scope, three classes of causes are used: military-political class, economic class, and natural-technological class. We believe it is also worthwhile to introduce a fourth category — the hybrid class. This class is crucial for encompassing various complex cases, such as COVID-19, which, while primarily of natural origin, was also marked by economic challenges and individual countries' pursuit of geopolitical interests.

The objectives of this article do not include developing detailed strategies for addressing the identified causes of the decrease in tourist flows. However, it is important to outline basic directions that help respond effectively to tourism industry crises (Table 6).

By employing and developing these strategies, destination authorities can better manage and mitigate the various causes of the decrease in tourist flows, ensuring a more resilient and sustainable tourism industry. A logical continuation of this study would involve preparing more detailed and targeted

<sup>11</sup> <https://www.tourism-review.com/tourism-arrivals-in-turkey-dropped-dramatically-news176>

<sup>12</sup> <https://en.mercopress.com/2007/07/03/less-tourists-visited-brazil-in-2006-but-they-spent-more>

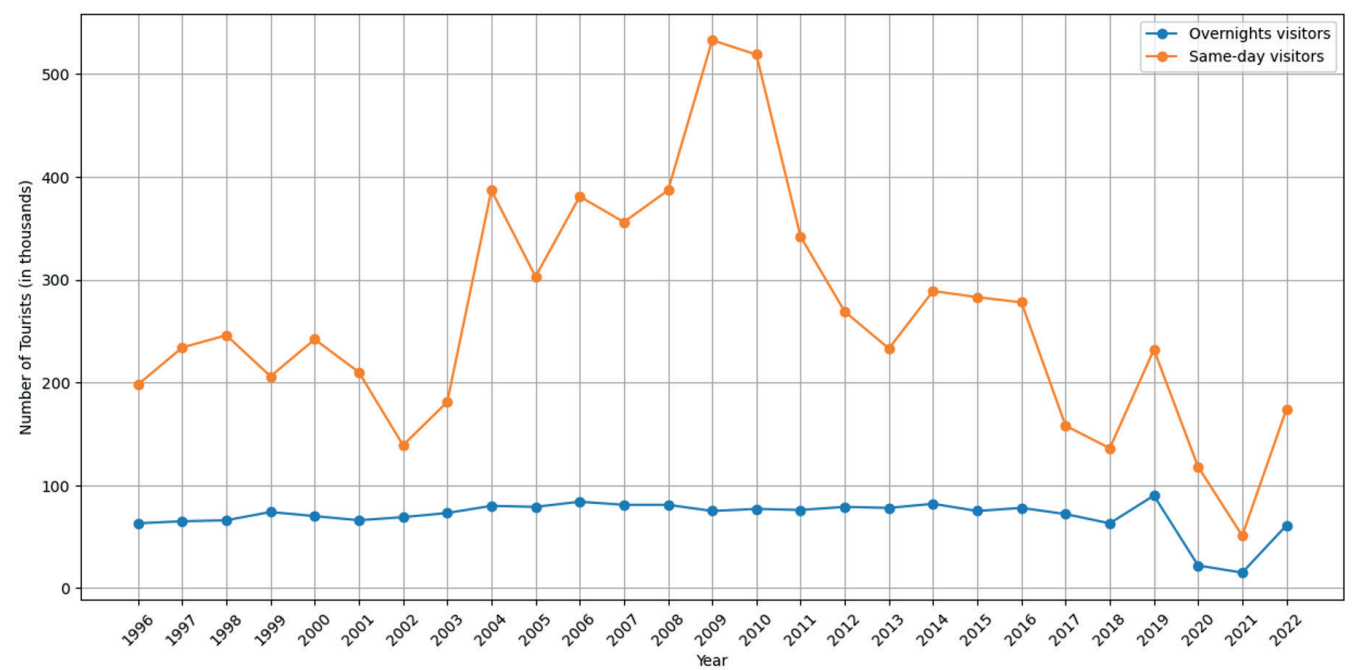


Fig. 10. The absolute number of tourists in Dominica (in thousands)

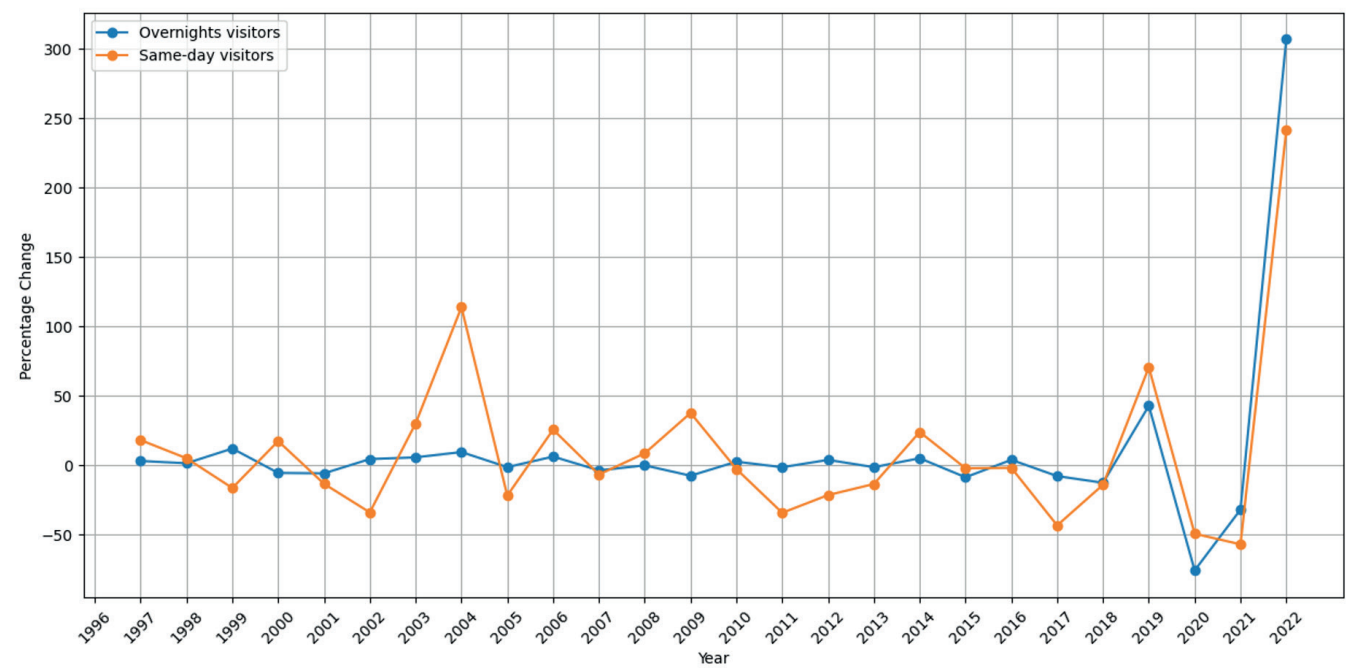


Fig. 11. Change in tourist flow in Dominica (in percent)

Table 6. Basic strategies for responding to the identified classes of causes

Military-political	Economic	Natural-technological	Hybrid
Engage in international diplomatic efforts to resolve conflicts and promote peace	Develop financial support mechanisms to support economy through collaboration between public and private sectors during downturns: tax breaks, subsidies, and financial aid for businesses	Conduct regular risk assessments and vulnerability analyses to identify and prioritize areas for intervention and develop disaster preparedness and response plans to mitigate the impact of risks	Establish comprehensive crisis management frameworks that address multilateral crises like pandemics, combining health, economic, and political strategies
Implement robust security measures to reassure tourists of their safety: increased police presence, improved surveillance, and security protocols at key tourist sites	Diversify the tourism products and services to appeal to different market segments and reduce dependency on specific economic factors	Invest in resilient infrastructure that can withstand natural or technological disasters	Promote international collaboration to address global challenges, exchanging information and resources in crisis situations



Develop a comprehensive crisis communication plan to provide timely and accurate information to tourists during political instability	Launch targeted marketing campaigns to promote tourism domestically and internationally, emphasizing affordability and value for money	Promote environmental sustainability initiatives to preserve natural attractions. Develop conservation efforts, sustainable tourism practices, and raising awareness among tourists and locals	Develop adaptive governance frameworks that allow for flexible and iterative decision-making processes, enabling governments to respond effectively to evolving and complex challenges in tourism industry
Develop tourist routes and programs showcasing the country's cultural and historical heritage to attract tourists despite the geopolitical situation.	Enhance long-term economic viability and resilience by promoting sustainable tourism practices, including investment in eco-tourism, cultural heritage preservation, and community-based tourism initiatives	Integrate technology-driven solutions for early warning systems and communication channels to promptly alert tourists and locals about potential natural or technological hazards	Implement proactive policy measures and facilitate collaborations between government agencies, private enterprises, and local communities to implement joint initiatives to enhance tourism resilience

recommendations. In further research, it is necessary to specify response options for stakeholders at different levels (global, regional, and local). When preparing sustainable tourism development strategies and analyzing risks and challenges for the industry, it is crucial to allocate responsibility for specific tasks and associated risks to the level that can best manage them.

One of the key limitations of this study in distinguishing the classes of reasons is the difficulty in precisely demarcating the economic and military-political causes that influence tourist flows. In the modern world, economic and political spheres are closely intertwined, and events in one can quickly and unpredictably affect the other. As a result, identifying purely economic reasons, such as financial crises or sudden economic downturns, can be complicated by the simultaneous presence of military-political factors, including conflicts, sanctions, or political instability. This interaction and influence of causes make the analysis less definitive and can lead to a conditional differentiation of causal factors. As a result, the article views these reasons as complementary rather than mutually exclusive factors.

Another limitation of this study is its exclusive focus on international tourism. In the negative scenarios unfolding within a country, domestic tourism might supplant international inbound tourism due to restrictions on the number of tourists able to travel abroad. This shift indicates that outbound tourism does not necessarily mirror the dynamics of inbound tourism under such circumstances. The following limitation arises from the fact that the analysis does not account for the possibility that a decrease in tourist flow may be a correction following a sharp increase in the previous year. Such an approach can lead to underestimating specific trends in the tourism industry.

In future research, it is important to continue analyzing the causes of the decrease in tourist flows while expanding the focus and deepening the understanding of the diverse factors that influence this process. One promising direction could be studying the influence of economic and political changes and natural and technological crises on tourism in different regions and within countries with different tourism specializations. It is important to consider key characteristics of countries, such as geographical features, expertise in certain types of tourism, or the overall level of development of the tourism industry (center-periphery).

Long-term trends and cyclicity in the tourism industry, such as periods of big growth followed by drops, could also be studied in a big way to learn more about how these cycles affect the stability of tourist markets. In addition, it would be helpful to study the tourism industry's response and adaptation to significant events, including natural disasters and pandemics, and to assess how various mitigation strategies can help manage such crises.

Researching the impact of consumer preferences and behavior changes on tourist flows will also be important, especially in light of growing interest in sustainable and environmentally responsible tourism. Analysis of how new trends in tourism, such as event, medical or cultural tourism, affect changes in tourist flows can provide valuable data for developing tourism industry strategies.

Quantitative analysis of similar patterns in tourist flows across the countries has revealed the remarkable diversity of the world's tourism landscape. Events unfold in various ways, showcasing the uniqueness of each country's trajectory. Identifying patterns over a long period may be less fruitful, as countries predominantly follow distinctive paths. Nevertheless, the patterns we observed demonstrate that geography matters.

Given that military-political conflicts are one of the leading causes of the decrease in tourist flow, it is critical to consider tourism's role in reducing geopolitical tension. As an international phenomenon, well-organized and managed tourism uniquely brings people and cultures together, promoting understanding and peaceful interaction between peoples. In this context, the following research may focus on analyzing international tourism as a tool of soft diplomacy and cultural exchange, reducing tension, and preventing conflicts. Studying successful examples of how tourism has contributed to peace and stability can provide valuable lessons for developing tourism and international relations strategies. An important aspect of such research is examining how tourism initiatives and programs can be integrated into broader diplomatic and peacekeeping efforts. Furthermore, it is critical to investigate how tourism strategies can be adapted to minimize risks associated with geopolitical conflicts, as well as how tourism can contribute to economic development and social progress in conflict-prone regions. This may involve exploring collaboration mechanisms between governmental and non-governmental organizations, local communities, and international tourism companies to create sustainable and peaceful tourist destinations.

A significant direction for future tourism research is the analysis of the impact of the COVID-19 pandemic, which has become a critical negative factor in the tourism industry. The pandemic has demonstrated the need for a deep interaction between healthcare systems and tourism to effectively deal with such global challenges. In this context, special attention should be given to developing and implementing strategies that can minimize health risks in international tourism. Particularly crucial is the development of medical tourism as one of the possible ways to enhance the level of the healthcare system and, simultaneously, the recovery and development of the tourism sector after the pandemic. Medical tourism provides medical services to foreign patients and creates conditions for safe and healthy travel, which becomes especially relevant during the pandemic. ■

## REFERENCES

- Bakir A., Wickens E., Boluk K., and Avgeli V. (2017). Cross-cultural issues in tourism and hospitality. *Tourism and Hospitality Research*, 17(3), 245–248.
- Berman E. G. and Lombard, L.N. (2008). *The Central African Republic and small arms*. Graduate Institute of International and Development Studies, Geneva.
- Boutellis A. (2013). Chad and the Central African Republic. In: Boulden, J. ed., *Responding to Conflict in Africa*. Palgrave Macmillan, New York. [https://doi.org/10.1057/9781137367587\\_7](https://doi.org/10.1057/9781137367587_7)
- ÇİFTÇİ, G. and BAYRAM, S. (2021). The Effects of Earthquakes on Tourism: Evidence from Turkey. *Journal of Tourism Leisure and Hospitality*, 3(2), 82–94. <http://dx.doi.org/10.48119/toleho.851669>
- Chung M. G., Herzberger A., Frank K. A., and Liu J. (2020). International Tourism Dynamics in a Globalized World: A Social Network Analysis Approach. *Journal of Travel Research*, 59(3), 387–403. <https://doi.org/10.1177/0047287519844834>
- Comoros. (2013). Tourism sector review. World Bank Group.
- Creaco S. and Querini G. (2003). The role of tourism in sustainable economic development, 43rd Congress of the European Regional Science Association: «Peripheries, Centres, and Spatial Development in the New Europe», 27th – 30th August 2003, Jyväskylä, Finland, European Regional Science Association (ERSA), Louvain-la-Neuve
- Dementiev V. S. and Andreev A. A. (2023). Dynamics of incoming and outgoing tourism in Russia in 2014–2022, *Pskov Journal of Regional Studies*, vol. 19, no. 1, pp. 56–72. (In Russian with English summary). DOI: <https://doi.org/10.37490/S221979310023983-4>
- Ferrera de Arruda, D. (2018–19). The Impact of the Arab Spring on Tourism.
- Garin-Munoz T. and Amaral T.P. (2000). An econometric model for international tourism flows to Spain. *Applied Economics Letters*, 7(8), pp.525–529. <https://doi.org/10.1080/13504850050033319>
- Gidebo H. B. (2021). Factors determining international tourist flow to tourism destinations: A systematic review. *Journal of Hospitality Management and Tourism*, 12(1), 9–17. <http://dx.doi.org/10.5897/JHMT2019.0276>
- Hamilton J. M., Maddison D. J. and Tol R. S.J. (2005). Effects of climate change on international tourism. *Climate research* 29, no. 3: 245–254.
- Haque Dr. (2015). The Impact of Economic Crisis on Tourism Industry: A Bangladesh Perspective. *International Research Journal of Engineering, IT & Scientific Research*, p. 2. <http://dx.doi.org/10.21744/irjeis.v1i1.29>
- Iliev D. (2019). Evolution and changes of tourism in Macedonia in the post-socialist period (1991–2018). *Journal of Geography, Politics and Society*, 9, 23–32. <https://doi.org/10.26881/jpgs.2019.3.04>
- International Monetary Fund. (2011). Dominica: Staff Report for the 2011 Article IV consultation. IMF Staff Country Reports, 2011(324), A001. <https://doi.org/10.5089/9781463924577.002.A001>
- Ishikawa, Y. (2011). Impact of the economic crisis on human mobility in Japan: a preliminary note. *Belgeo*, 3–4, pp. 129–148.
- Jansen-Verbeke, M. and Spee, R. (1995). A regional analysis of tourist flows within Europe. *Tourism Management*, 16(1), 73–80. [https://doi.org/10.1016/0261-5177\(95\)93433-W](https://doi.org/10.1016/0261-5177(95)93433-W)
- Khalid U., Okafor L. E., and Shafullah M. (2020). The effects of economic and financial crises on international tourist flows: A cross-country analysis. *Journal of Travel Research*, 59(2), 315–334. <https://doi.org/10.1177/0047287519834>
- Klimova T.B., Vishnevskaya E.V. and Anoprieva E.V. (2017). The structure and dynamics of tourist flows trends and determining factors. *Service in Russia and abroad*, 11(5 (75)), pp.6–18. <http://dx.doi.org/10.22412/1995-042X-11-5-1>
- Kulendran N. (1996). Modelling quarterly tourist flows to Australia using cointegration analysis. *Tourism Economics*, 2(3), pp.203–222. <https://doi.org/10.1177/135481669600200301>
- Kyrgyz Republic (2011). Article IV Consultation and Request for a Three-Year Arrangement Under the Extended Credit Facility. International Monetary Fund. <https://doi.org/10.5089/9781455280575.002>
- Li Y., and Cao H. (2018). Prediction for tourism flow based on LSTM neural network. *Procedia Computer Science*, 129, 277–283. <https://doi.org/10.1016/j.procs.2018.03.076>
- Lusetyowati T. (2015). Preservation and conservation through cultural heritage tourism. Case study: Musi Riverside Palembang. *Procedia-Social and Behavioral Sciences*, pp. 184, 401–406.
- Mody A. (2013). Impact of political instability and terrorism in the tourism industry of three middle-east countries: an econometric exploration.
- Mou N., Zheng Y., Makkonen, T., Yang T., Tang J. J. and Song Y. (2020). Tourists' digital footprint: The spatial patterns of tourist flows in Qingdao, China. *Tourism Management*, 81, 104151. <https://doi.org/10.1016/j.tourman.2020.104151>
- Murphy S. D. (2016). The Eritrean-Ethiopian War (1998–2000). *International Law and the Use of Force: A Case-Based Approach*, GWU Law School Public Law Research Paper №. 2016–52 <http://dx.doi.org/10.2139/ssrn.2856670>
- Nkurunziza J. D. (2018). The origin and persistence of state fragility in Burundi. The LSE-Oxford Commission on State Fragility, Growth and Development.
- Reisinger Y., and Turner L. (1998). Cross-cultural differences in tourism: A strategy for tourism marketers. *Journal of Travel & Tourism Marketing*, 7(4), 79–106.
- Roselló J., Becken S., and Santana-Gallego, M. (2020). The effects of natural disasters on international tourism: A global analysis. *Tourism Management*, 79, 104080. <https://doi.org/10.1016/j.tourman.2020.104080>
- Saleh B. (2003). The Itifada's impact on tourism in Israel: an interrupted time-series approach. Available at: <https://econwpa.ub.uni-muenchen.de/econ-wp/test/papers/9912/9912139.pdf> [Accessed 8 March. 2024].
- Santana-Gallego M., Ledesma-Rodríguez F. J. and Pérez-Rodríguez J. V. (2016). International trade and tourism flows: An extension of the gravity model. *Economic Modelling*, 52, 1026–1033. <https://doi.org/10.1016/j.econmod.2015.10.043>
- Scheyvens R., and Russell M. (2009). *Tourism and Poverty Reduction in the South Pacific*.
- Shao Y., Huang S.S., Wang Y., Li Z. and Luo M. (2020). Evolution of international tourist flows from 1995 to 2018: A network analysis perspective. *Tourism Management Perspectives*, 36, p.100752. <https://doi.org/10.1016/j.tmp.2020.100752>
- Sobral F., Peci A. and Souza G. (2007). An analysis of the dynamics of the tourism industry in Brazil: challenges and recommendations. *International Journal of Contemporary Hospitality Management*, 19(6), 507–512. <http://dx.doi.org/10.1108/09596110710775165>
- The study on tourism development projects in the Arab Republic of Egypt. (2002). Japan International Cooperation Agency (JICA) / Tourism Development Authority/ Ministry of Tourism/Egypt.
- Treichel V. (2002). Stabilization Policies and Structural Reforms in Albania Since 1997: Achievements And Remaining Challenges. IMF. <https://doi.org/10.5089/9781451974508.003>
- Webster C., and Ivanov S. (2015). Geopolitical drivers of future tourist flows. *Journal of Tourism Futures*, 1(1), 58–68. <https://doi.org/10.1108/JTF-12-2014-0022>

World Tourism Organization and International Labour Organization (2013), Economic Crisis, International Tourism Decline and its Impact on the Poor, UNWTO, Madrid.

Yang Y. and Wong K. K. (2012). A spatial econometric approach to model spillover effects in tourism flows. *Journal of Travel Research*, 51(6), 768-778. <https://doi.org/10.1177/0047287512437855>

Zhong L., Sun S., Law R. and Deng B. (2022). An investigation of international tourist flow modelling during the pandemic. *Current Issues in Tourism*, 25(12), 1910-1919.

# PETROLEUM HYDROCARBONS IN ARCTIC URBAN LAKE SEDIMENTS (MURMANSK, RUSSIA)

Vladimir A. Myazin<sup>1,2\*</sup>

<sup>1</sup> Peoples' Friendship University of Russia, Miklouho-Maklaya 6, Moscow, 117198, Russia

<sup>2</sup> Institute of the North Industrial Ecology Problems of Kola Science Center of Russian Academy of Science, Akademgorodok 14A, Apatity, 184209, Russia

\*Corresponding author: myazin\_va@pfur.ru

Received: July 31<sup>st</sup> 2023 / Accepted: July 25<sup>th</sup> 2024 / Published: October 1<sup>st</sup> 2024

<https://doi.org/10.24057/2071-9388-2024-2990>

**ABSTRACT.** The level of pollution of lake sediments located in the city of Murmansk (Russia) with petroleum hydrocarbons was studied. The most urban lakes can be classified as slightly polluted, representing the maximum acceptable risk for human health and ecosystems; Lake Yuzhnoe – as moderately polluted with a negative impact on the aquatic environment, and Lake Ledovoe located near the highway, gas station, and car service, – as dangerously polluted, posing a threat to human health and requiring remediation. The background content of organic compounds identified as petroleum hydrocarbons in the sediments of Murmansk lakes ranges from 76 to 307 mg TPH/kg. High background concentrations of hydrocarbons can be associated with a large amount of organic matter in the sediments of lakes. The standards for the content of hydrocarbons in sediments, developed for other regions, give an ambiguous assessment of their content in the sediments of lakes in Murmansk. It is not entirely correct to use the background content of hydrocarbons in the sediments of lakes in other regions, which differ in particle size distribution, content of organic matter, and chemical composition, to assess the degree of pollution. Additional research is needed to determine the content of hydrocarbons in the sediments of background lakes in the Murmansk region and to develop standards for the content of hydrocarbons in the bottom sediments of Arctic cities.

**KEYWORDS:** urban lakes, sediments, total petroleum hydrocarbons, Arctic

**CITATION:** Myazin V. A. (2024). Petroleum Hydrocarbons In Arctic Urban Lake Sediments (Murmansk, Russia). *Geography, Environment, Sustainability*, 3(17), 64-69

<https://doi.org/10.24057/2071-9388-2024-2990>

**ACKNOWLEDGEMENT:** Expedition work and sampling were supported by the state scientific program № 122022400109-7. The analysis of TPH content was funded by the Russian Science Foundation, project № 19-77-30012. Data analysis was supported by the Ministry of Science and Higher Education of the Russian Federation, project FSSF-2024-0023.

**Conflict of interests:** The authors reported no potential conflict of interest.

## INTRODUCTION

Lakes and rivers located in the city are always subject to strong negative anthropogenic impacts. Situated in the natural depressions of the area, they accumulate pollution from the adjacent territories. Petroleum hydrocarbons and heavy metals are two of the most common types of water pollution. These pollutants accumulate in sediments due to their high sorption capacity, fractionation characteristics in water and sediments, and biochemical stability.

Urban rivers and lakes often suffer from constant or regular discharges from enterprises, as well as spontaneous garbage dumps along the banks. Cienfuegos Bay (Cuba) receives up to 50 tons of high molecular weight petroleum hydrocarbons annually (Tolosa et al. 2009). In other countries, much attention was paid to studying the accumulation and transformation of TPH in sediments. In the sediments of Yuan Dan Lake (China) the TPH content is 1397 mg/kg, and in the sediments of Xiamen Harbour it is within the range of 133–943 mg/kg (Ou et al. 2004). The TPH concentrations in the samples from Lake Chao Hu, one of the most eutrophic lakes in China, varied from 11.9 to 325 mg/kg dry weight (Wang et al. 2012). In

Algoa Bay (Eastern Cape Province of South Africa) the TPH content varied from 45.07 to 307 µg/L in the water and from 0.72 to 27.03 mg/kg in the sediments (Adeniji et al. 2017a), but in the Buffalo River Estuary (East London, South Africa) the TPH content varied from 12.59 to 1100 mg/kg in the sediments, with the mean values of 209.81±63.82 mg/kg (Adeniji et al. 2017b). Studies in Nigeria have shown that the TPH content in the Qua Iboe River is from 90 to 250 µg/L in the water and from 270 to 830 mg/kg in the sediments (Inyang et al. 2018), while in the sediments of Ikoli Creek the TPH content ranges from 0.001 to 0.44 mg/kg (Ighariemu et al. 2019). The transfer of TPH from the surface of Crater Lake in North America led to its accumulation in the sediments (1440 mg/kg), especially in the places of ship mooring (Oros et al. 2007). In the sediments of the middle part of the Clyde estuary (Scotland), the TPH content varied from 34 to 4386 mg/kg (Vane et al. 2011). The study of Lake Zug (Switzerland) showed that the sediments near the densely populated northern end of the lake accumulate more hydrocarbons – up to 900 mg/kg, while in the central part of the lake, with a lower population density, the content of hydrocarbons did not exceed 50 mg/kg (Giger et al. 1974).



In the Arctic, negative impacts on aquatic ecosystems have more pronounced consequences. Severe climatic conditions contribute to high vulnerability and significantly reduce the rate of natural restoration of ecosystems under technogenic impact (Nøst et al. 1997; Zubova et al. 2020).

In Russia, TPH accumulation in the sediments of lakes and rivers is studied in oil-producing regions, mainly in Western Siberia (Vorobyev and Popkov 2005; Panicheva et al. 2013; Uvarova and Zakharova 2016). The high concentrations of TPH are characteristic of lake sediments located in industrial impact zones. After a terrible environmental disaster in 1994–1997, a full study of the oil spill's effects on the Pechora River ecosystem found that TPH levels were high, ranging from 360 to 1250 mg/kg in the river's mouth and delta. In that accident, 100 to 375 thousand tons of raw oil entered the water body ecosystem (Lukin and Dauvalter 1997; Lukin et al. 2000). The TPH content in the sediments of urban lakes was also assessed. The sediments of these lakes can accumulate up to 10,000 mg TPH/kg (Belkina et al. 2008; Ivanov et al. 2011; Ivanov 2012; Guzeeva 2014).

At the same time, insufficient attention has been paid to studying urban lakes in the Arctic zone. Among the six largest cities in the world located beyond the Arctic Circle, five are in the Russian Federation, in particular on the territory of the Murmansk region, where there is a high level of urbanization and a concentration of industrialized territories.

The aim of this study was to assess the content of petroleum hydrocarbons in the sediments of urban lakes in the Arctic.

## MATERIALS AND METHODS

### Study Area

Murmansk is the largest city located beyond the Arctic Circle in the world and one of the largest ports in Russia. The population of Murmansk is approximately 290,000 people. It is located on the rocky eastern coast of Kola Bay of the Barents Sea. Murmansk has around 20 lakes. To fully assess the impact of the urban environment on lake ecosystems, seven lakes located in different parts of Murmansk and having great recreational significance for the city's residents and visitors were selected for the study.

Sediment samples were taken in July 2020 and 2021 from seven lakes located in the city of Murmansk: Severnoe (69°01'58.0"N, 33°07'04.1"E), Semenovskoe (68°59'28.8"N, 33°05'24.5"E), Srednee (68°58'51.7"N, 33°07'13.8"E), Treugolnoe (68°58'05.1"N, 33°00'10.5"E), Okunevoe (68°57'00.8"N, 33°07'37.0"E), Ledovoe (68°55'58.74"N, 33°6'17.72"E) and

Yuzhnoe (68°53'03.2"N, 33°04'31.2"E) (Fig. 1). All these lakes are experiencing anthropogenic impacts to a greater or lesser extent (Slukovskii et al. 2020; Slukovskii et al. 2021).

The morphometric parameters of these lakes were estimated before this study (Slukovskii et al. 2020). The water of lakes Severnoe, Semenovskoe, Treugolnoe, Ledovoe, and Yuzhnoe belongs to the chloride class and the sodium group; the water of lakes Srednee and Okunevoe belongs to the hydrocarbonate class and the calcium group. Moreover, was detected increased (compared to the background level) pH, mineralization, and concentrations of major ions, nutrients, and potentially toxic elements in the water of these lakes (Postevaya et al. 2021; Slukovskii et al. 2020; Slukovskii et al. 2021).

### Sediment sampling

The sediments of the lakes, including the cores of the sediments, were collected at the lakes' points of maximum depth using the Ekman sampling grabber (for all lakes in triplicate in 2020 and 2021) and the Limnos gravity sampler for further layer-by-layer analysis (for all lakes except Treugolnoe and Yuzhnoe in 2021). Immediately after the sampling, all the cores were divided into 5-cm layers. After collection, all the samples were placed into plastic containers, which were labelled and packed in a cooler bag.

### Laboratory analysis

The sediment samples were air-dried and powdered before extraction. A portion of the sample (1–3 grams) was placed in a 100-ml flask with a ground glass stopper. A sample in a flask was poured with 10 ml of carbon tetrachloride and stirred for 1 hour. The extract obtained was filtered through a paper filter "white tape" and poured into a bottle. The extraction was repeated two more times with new portions of carbon tetrachloride, 10 ml each. All the extracts were combined, and the total volume was recorded.

The sediment extracts were cleaned up in a chromatographic column (10 mm i.d. × 10 cm) packed with 7 g of activated aluminium oxide. A blank sample was processed the same way for quality assurance.

The TPH content in the samples was assessed by IR spectrometry based on measuring the integral intensity of absorption of C–H bonds of methyl and methylene groups of various classes of organic compounds in non-polar and low-polar solvents using the analyzer AN-2 (Quantitative chemical analysis of soils 2005).



Fig. 1. Map of the lakes' location in Murmansk. 1 – Severnoe, 2 – Semenovskoe, 3 – Srednee, 4 – Treugolnoe, 5 – Okunevoe, 6 – Ledovoe, 7 – Yuzhnoe

The organic carbon content was determined in air-dry samples using the Nikitin's method with a colorimetric modification. The ashing of organic compounds was carried out with a chromium mixture when heated to 150°C in an oven. The amount of carbon was determined by the amount of green trivalent chromium formed as a result of the reaction using a photocolorimeter (wavelength 540 nm). The conversion factor from organic carbon (OC) content to organic matter (OM) content was taken to be 2 (Agatova et al. 2013).

### Data analytical methods

The results were statistically processed. The arithmetic mean, standard deviation, median, and Spearman correlation coefficients were calculated. Statistical calculations were carried out in Microsoft Excel 2010.

### RESULTS

The amount of TPH in sediment samples from the 0–10 cm layer that were grabbed by the Ekman grabber ranged from 928 to 22,175 mg/kg (Table 1). Lake Ledovoe, situated near a busy highway under significant anthropogenic pressure, had the

highest TPH content. Moreover, Lake Ledovoe is located 3.4 km from the Murmansk thermal power plant, which uses fuel oil. One of the streams flowing along the highway (Kolskiy Avenue), a gas station, several car dealerships, and a large bus transportation company (both on the surface and in the collector under the road) flow into Lake Ledovoe.

In the sediments of Lake Srednee and Okunevov, the TPH content was the lowest and did not exceed 946 and 928 mg/kg, respectively. Due to their forest surrounds and distance from potential pollution sources, these lakes endure less anthropogenic pressure.

In the analyzed cores, the TPH content decreased with depth, especially in Lake Srednee (Fig. 2A). In the sediment samples from this lake, taken from a depth of 30–35 cm, the TPH content was 76 mg/kg.

There was no significant decrease in the TPH content with depth in the sediments of Lake Ledovoe, where the TPH concentrations varied from 14,116 to 25,037 mg/kg. The sediment samples from this lake contained a large amount of TPH, even in the 25–30 cm layer (Fig. 2E). The TPH concentrations in this layer served as background concentrations for the other studied lakes. In the sediments of Lake Semenovskoe, an increase in the hydrocarbon content in the 10–20 cm layer was noted (Fig. 2D).

**Table 1. TPH and organic matter content in sediments (0–10 cm) of urban lakes**

	Severnoe	Semenovskoe	Srednee	Treugolnoe	Okunevov	Ledovoe	Yuzhnoe
TPH content, mg/kg	2735±322*	2610±957	946±305	1706±295	928±70	22175±5023	1862±105
OM content, %	28.7±3.5	32.6±4.1	26.7±3.8	37.6±3.7	30.1±2.5	13.5±4.8	6.9±1.1

\*Here and below the figures show the standard errors of the mean.

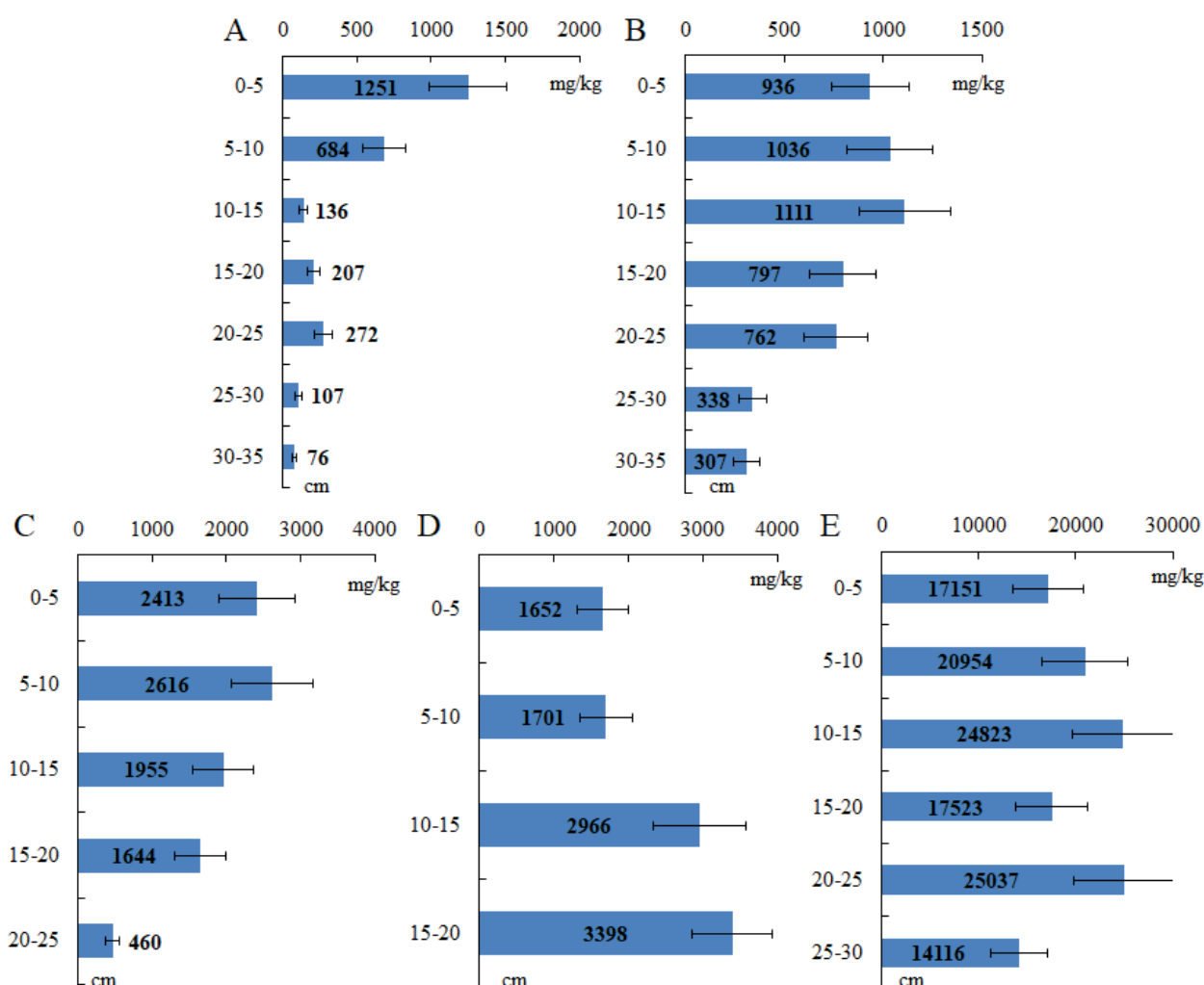


**Fig. 2. The TPH content (mg/kg) in the sediment cores from lakes Srednee (A), Okunevov (B), Severnoe (C), Semenovskoe (D) and Ledovoe (E)**

The lake's current load is shown by the layer of sediment on the surface, and natural background concentrations are shown by the deeper part of the core (usually more than 20–25 cm) (Dauvalter 2012). Thus, the data obtained allowed us to draw a preliminary conclusion that the background content of organic compounds identified as TPH in the sediments of the lakes in Murmansk ranges from 76 to 307 mg/kg. The rate of sedimentation in the lakes of Northern Fennoscandia, including the Murmansk region, is on average 1 mm per year, and the range is from 0.3 to 3 mm/year (Dauvalter and Kashulin 2018). However, with a high anthropogenic load, the rate of sedimentation can increase due to the supply of large amounts of suspended mineral and organic substances. Taking this fact into account, we can say that the accumulation of hydrocarbons in sediments began about 70 years ago and continues today.

The surface layers of the sediments in Kola Bay (Murmansk region), which has the highest concentration in north-western Russia, previously showed similar hydrocarbon content values (average 1615 mg/kg) (Shakhverdov and Shakhverdova 2016). The highest hydrocarbon concentration (up to 2375 mg/kg) was observed in the areas located in the southern knee, as well as in the middle knee in the Severomorsk area. In general, the TPH content in the sediments of Murmansk's urban lakes is comparable to the that in Kola Bay's sediments. This indicates a high total anthropogenic load on the aquatic ecosystems in Murmansk.

To assess the degree of sediment pollution in the urban lakes of Murmansk, the data on the TPH content should be compared with the maximum permissible concentration (MPC) or the background content in the region.

The Murmansk region does not have established TPH content standards. However, there are standards for other regions of Russia and other countries. The sediments with TPH more than 15 mg/kg are considered polluted in the Persian Gulf (Massoud et al. 1996), more than 50 mg/kg in the countries of South Africa (Environmental Guidelines and Standards for The Petroleum Industry in Nigeria 2002), more than 500 mg/kg in Canada (Atlantic Risk-Based Corrective Action for Petroleum Impacted Sites in Atlantic Canada 2015). Regional documents in Russia regulate the hydrocarbon content of sediments. The regional standard «Maximum permissible level of oil and oil products in the

sediments of surface water bodies on the territory of Khanty-Mansiysk Autonomous Okrug – Yugra» (dated 10.11.2004) and the regional standard «Norms and criteria for assessing sediment pollution in water bodies of St. Petersburg» (dated 22.07.1996) are among the examples. The latter document was developed based on the standards and criteria proposed by the Dutch Environmental Protection Agency (DCMR), the Center of Soil Research (TNO), and HASKONING. When assessing sediment contamination, the content of organic matter is taken into account in the regional standard for St. Petersburg.

The highest content of organic matter was observed in the sediments of lakes Triugolnoe (37.6%), Semenovskoe (32.6%), Okunevoe (30.1%), Severnoe (28.7%) and Srednee (26.7%), the lowest – the sediments of lakes Ledovoe (13.5%) and Yuzhnoe (6.9%) (Table 1).

The sediment pollution of the Murmansk urban lakes was assessed following these standards (Table 2).

The sediments of Lake Ledovoe are dangerously polluted and require prompt intervention and remediation. The sediments of Lake Yuzhnoe are moderately polluted and can have a negative impact on the aquatic environment. The sediments of the other studied lakes are slightly polluted and represent the maximum acceptable risk for human health and the ecosystem.

## DISCUSSION

The most polluted lake in Murmansk is Lake Ledovoe, in the catchment area of which there are residential zones, highways, car parking, gas stations, and a bus transportation company. A stream flows into the lake, which is considered one of the most polluted in Murmansk. Lake Yuzhnoe is the second most polluted lake. In the catchment area of the lake Yuzhnoe, there is truck parking and a gas station. There is also a thermal power plant 1.5 km from the lake. The sediments of these lakes contain the least amount of organic matter, which classifies them as dangerously polluted and moderately polluted in accordance with the Regional standard "Norms and criteria for assessing sediment pollution in water bodies of St. Petersburg". In accordance with foreign standards, all studied urban lakes can be classified as polluted.

In the absence of MPC, the level of sediment contamination can be estimated by the background TPH

**Table 2. Degree of sediment pollution in urban lakes of Murmansk**

Regulating document	Degree of sediment pollution of lakes						
	Severnoe	Semenovskoe	Srednee	Okunevoe	Treugolnoe	Yuzhnoe	Ledovoe
Regional standard "Maximum permissible level of oil and oil products in the sediments of surface water bodies on the territory of Khanty-Mansiysk Autonomous Okrug - Yugra"	polluted; depression of the bottom ecosystem						
Regional standard "Norms and criteria for assessing sediment pollution in water bodies of St. Petersburg"	slightly polluted					moderately polluted	dangerously polluted
Atlantic RBCA (Risk-Based Corrective Action) for Petroleum Impacted Sites in Atlantic Canada. Version 3. User Guidance	polluted						
Environmental Guidelines and Standards for the Petroleum Industry in Nigeria, (EGASPIN)	polluted; attention level						polluted; intervention level

content. According to the study of sea silt (Kravchenko and Bibichkov 1988), the background TPH concentrations in the sediments are 10–200 mg/kg. The average TPH content in the sediment core (depth 20–50 cm) from Halifax Bay (Canada) is 18 mg/kg (Gearing et al. 1991). It is close to the TPH concentrations in the surface sediments of the Gulf of Mexico (Gearing et al. 1976; Kennicutt et al. 1987), but higher than the background TPH content in the sediments from the Scottish shelf area and other zones of the open ocean (Farrington and Tripp 1977; Keizer et al. 1978; Boehm 1984). The total TPH concentrations in the sediments of Lake Washington (USA) and Lake Zurich (Switzerland) are 20–40 and 10–25 mg/kg, respectively. These values were calculated for depths ranging from 30 to 100 cm (Wakeham 1980).

The calculated background content of hydrocarbons in the sediments of the Murmansk region is 32 mg/kg (Shakhverdov and Shakhverdova 2016), in Lake Onega it does not exceed 50 mg/kg (Belkina et al. 2008), in the water bodies of the Republic of Tatarstan, it is estimated at 50–80 mg/kg (Ivanov et al. 2011; Ivanov 2012), which is many times lower than our results.

Lake Treugolnoe, which we consider a background water body, is located on the western shore of Kola Bay. It is surrounded by forest, and there is an unused road nearby. Near the lake, there are no direct sources of pollution. At the same time, the sediment of this lake contains the largest amount of organic matter (37.6%), which likely affects the content of compounds identified as hydrocarbons (1706 mg/kg). The content of TPH in the sediments of the other background lakes of the Murmansk region and Karelia, located at a considerable distance from pollution sources, ranged from 123 to 1091 mg/kg.

High background concentrations of hydrocarbons can be associated with a large amount of slightly humified organic matter in lakes' sediments. The study of sediments of Lake Chini (Malaysia) revealed that n-alkanes primarily originate from biogenic sources, which are wax-like compounds of higher plants and microorganisms (Bakhtiari et al. 2011). The source of aliphatic hydrocarbons in the sediments of Lake Chaohu (China) was mainly higher plants (31%), fossil fuel combustion (30%), petroleum products (26%), and phytoplankton (19%) (Wang et al. 2012). Hydrocarbons in Crater Lake sediments are also of both biogenic origin (waxy compounds of terrestrial plants and algae) and anthropogenic origin (petroleum products)

and enter the lake through direct input and atmospheric transport. The amount of naturally occurring n-alkanes is up to 240 mg/kg (Oros et al. 2007).

It should be noted that the lakes located in Murmansk have a high content of organic sediments (20–50%) (Slukovskii et al. 2020). The process of humification in the studied lakes is slowed down due to the climatic conditions and the significant level of anthropogenic pollution of the water bodies. Aliphatic fragments totally prevailed in the molecular structure of all sediments (Guzeva 2022).

The high content of slightly humified organic matter does not allow for accurate determination of the level of hydrocarbon pollution in urban lakes and requires additional research.

## CONCLUSIONS

The urban lakes of Murmansk are subject to the anthropogenic impact of enterprises and transport. In terms of the hydrocarbon content in the sediments, the studied lakes can be classified as slightly polluted, representing the maximum acceptable risk for human health and ecosystems; Lake Yuzhnoe – as moderately polluted; and Lake Ledovoe – as dangerously polluted, posing a threat to human health and requiring urgent intervention and remediation.

The background content of organic compounds identified as TPH in the sediments of the lakes in Murmansk ranges from 76 to 307 mg/kg. High background concentrations of hydrocarbons can be associated with a large amount of organic matter in the sediments of lakes. At the same time, the standards for the content of hydrocarbons in sediments, developed for other regions, give an ambiguous assessment of their content in the sediments of lakes in Murmansk. Also, it's not entirely accurate to judge the level of pollution by the hydrocarbons that are already present in the sediments of lakes in other parts of the world, since these sediments have different amounts of organic matter, particles of different sizes, and chemicals.

For an objective assessment of the level of urban lake pollution in the Arctic, it is necessary to develop a regional standard for the maximum permissible content of hydrocarbons in sediments, taking into account the high content of organic matter of natural origin. ■

## REFERENCES

- Adeniji A.O., Okoh O.O. and Okoh A.I. (2017a). Petroleum Hydrocarbon Profiles of Water and Sediment of Algoa Bay, Eastern Cape, South Africa. *International Journal of Environmental Research and Public Health*, 14, 1263, DOI: 10.3390/ijerph14101263.
- Adeniji A.O., Okoh O.O. and Okoh A.I. (2017b). Petroleum Hydrocarbon Fingerprints of Water and Sediment Samples of Buffalo River Estuary in the Eastern Cape Province, South Africa. *Journal of Analytical Methods in Chemistry*, 2629365, DOI: 10.1155/2017/2629365.
- Agatova A.I., Lapina N.M. and Torgunova N.I. (2013). Biochemical monitoring of the Black Sea Coastal Waters. *Proceedings of VNIRO*, 150, 57–64 (in Russian).
- Bakhtiari A.R., Zakaria M.P., Yaziz M.I., Lajis M.N.H. and Bi X. (2011). Variations and Origins of Aliphatic Hydrocarbons in Sediment Cores from Chini Lake in Peninsular Malaysia. *Environmental Forensics*, 12(1), 79–91, DOI: 10.1080/15275922.2011.547439.
- Belkina N.A., Ryzhakov A.V. and Timakova T.M. (2008). Distribution and transformation of petroleum hydrocarbons in the bottom sediments of Lake Onega. *Water resources*, 35(4), 472–481 (in Russian).
- Boehm P.D. (1984). Aspects of the saturated hydrocarbon geochemistry of recent sediments in the Georges Bank region. *Organic Geochemistry*, 7, 11–23.
- Dauvalter V.A. (2012). *Geoecology of bottom sediments of lakes. Murmansk, Russia: MSTU Publishing* (in Russian).
- Dauvalter V.A. and Kashulin N.A. (2018). Distribution of background contents of elements in sediments of Lake Imandra. *Bulletin of MSTU*, 21(1), 128–138 (in Russian), DOI: 10.21443/1560-9278-2018-21-1-128-138.
- Environmental Guidelines and Standards for the Petroleum Industry in Nigeria. Vol. 2. (2002). Lagos, Nigeria: DPR.
- Farrington J.W. and Tripp B.W. (1977). Hydrocarbons in western North Atlantic surface sediments. *Geochimica et Cosmochimica Acta*, 41, 1627–1641, DOI: 10.1016/0016-7037(77)90173-9.
- Gearing J.N., Buckley D.E. and Smith J. (1991). Hydrocarbon and metal contents in a sediment core from Halifax Harbour: a chronology of contamination. *Canadian Journal of Fisheries and Aquatic Sciences*, 48, 2344–2354.



- Gearing P., Gearing J.N., Lytle T.F. and Lytle J.S. (1976). Hydrocarbons in northeast Gulf of Mexico shelf sediments: a preliminary survey. *Geochimica et Cosmochimica Acta*, 40, 1005-1007, DOI: 10.1016/0016-7037(76)90043-0.
- Giger W., Reinhard M., Schaffner C. and Stumm W. (1974). Petroleum-derived and indigenous hydrocarbons in recent sediments of Lake Zug, Switzerland. *Environmental Science & Technology*, 8(5), 454-455, DOI: 10.1021/es60090a011.
- Guzeva S.A. (2014). Ecological state of surface waters and bottom sediments of Tyumen lakes. *Bulletin of the Krasnoyarsk State Agrarian University*, 8, 134-139 (in Russian).
- Guzeva A. (2022). Geochemical features of humic acids extracted from sediments of urban lakes of the Arctic. *Environmental Monitoring and Assessment*, 194:749, DOI: 10.1007/s10661-022-10419-8.
- Ighariemu V., Donatus C.B. and Matthew O.W. (2019). Level of Petroleum Hydrocarbons in Water and Sediments of Ikoli Creek Bayelsa State Nigeria. *Toxicology and Environmental Health Sciences*, 11(2), 114-119, DOI: 10.1007/s13530-019-0395-3.
- Inyang S.E., Aliyu A.B. and Oyewale A.O. (2018). Total Petroleum Hydrocarbon Content in Surface Water and Sediment of Qua-Iboe River, Ibeno, Akwa-Ibom State, Nigeria. *Journal of Applied Sciences and Environmental Management*, 22(12), 1953-1959, DOI: 10.4314/jasem.v22i12.14
- Ivanov D.V. (2012). Bottom sediments of the Sredny Kaban Lake in Kazan. *Georesources*, 7(49), 19-23 (in Russian).
- Ivanov D.V., Shagidullin R.R., Ziganshin I.I. and Osmelkin E.V. (2011). Bottom sediments of the Zainsk reservoir. *Scientific notes of Kazan University, Ser. Natural Sciences*, 153(1), 190-202 (in Russian).
- Keizer P.D., Dale J. and Gordon D.C. (1978). Hydrocarbons in surficial sediments from the Scotian Shelf. *Geochimica et Cosmochimica Acta*, 42, 165-172, DOI: 10.1016/0016-7037(78)90129-1.
- Kennicutt M.C., Sericano J.L., Wade T.L., Alcazar F. and Brooks J.M. (1987). High molecular weight hydrocarbons in Gulf of Mexico continental slope sediments. *Deep Sea Research*, 34, 403-424, DOI: 10.1016/0198-0149(87)90145-2.
- Kravchenko E.V. and Bibichkov A.G. (1988). Oil products in modern marine sediments as an ecological indicator during dumping. *State Design and Survey*. Moscow, Russia: Morteinform-reklama (In Russian).
- Lukin A.A. and Dauvalter V.A. (1997). Distribution of heavy metals, aluminum and petroleum products in bottom sediments and fish of the Pechora river basin. *Biology of inland waters*, 2, 70-78 (in Russian).
- Lukin A.A., Dauvalter V.A. and Novoselov A.P. (2000). Ecosystem of the Pechora River in modern conditions. *Apatity, Russia: KSC RAS* (in Russian).
- Massoud M.S., Al-Abdali F., Al-Ghadban A.N. and Al-Sarawi M. (1996). Bottom sediments of the Arabian Gulf-II. TPH and TOC contents as indicators of oil pollution and implications for the effect and fate of the Kuwait oil slick. *Environmental Pollution*, 93(3), 271-284, DOI: 10.1016/S0269-7491(96)00042-5.
- Nøst T., Lukin A., Schartau A.K.L., Kashulin N., Berger H.M., Yakovlev V., Sharov A. and Dauvalter V. (1997). Impacts of pollution on freshwater communities in the border region between Russia and Norway. III. Results of the 1990-96 monitoring programme. *NINA Fagrapport: Norway, Trondheim*.
- Oros D.R., Collier R.W. and Simoneit B.R.T. (2007). The extent and significance of petroleum hydrocarbon contamination in Crater Lake, Oregon. *Hydrobiologia*, 574, 85-105, DOI: 10.1007/s10750-006-0347-1.
- Ou Sh., Zheng J., Zheng J., Richardson B.J. and Lam P.K.S. (2004). Petroleum hydrocarbons and polycyclic aromatic hydrocarbons in the surficial sediments of Xiamen Harbour and Yuan Dan Lake, China. *Chemosphere*, 56(2), 107-112, DOI: 10.1016/j.chemosphere.2004.02.022.
- Panicheva L.P., Kremleva T.A. and Volkova S.S. (2013). Accumulation of petroleum products by bottom sediments in background reservoirs of Western Siberia. *Bulletin of Tyumen State University*, 12, 204-211 (in Russian).
- Postevaya M.A., Slukovskii Z.I., Dauvalter V.A. and Bernadskaya D.S. (2021). Estimation of Heavy Metal Concentrations in the Water of Urban Lakes in the Russian Arctic (Murmansk). *Water*, 13, 3267, DOI: 10.3390/w13223267.
- Quantitative chemical analysis of soils. Methodology for measuring the mass fraction of oil products in mineral, organogenic, organomineral soils and sediments by IR spectrometry. (2005). Moscow, Russia: FBU FTsAO (in Russian).
- Risk-Based Corrective Action for Petroleum Impacted Sites in Atlantic Canada. Version 3. User Guidance. (2012). Canada: Atlantic RBCA.
- Shakhverdov V.A. and Shakhverdova M.V. (2016). Assessment of the modern geoecological state of the Kola Bay according to geochemical data. *Arctic: ecology and Economics*, 4(24), 22-31 (in Russian).
- Slukovskii Z., Dauvalter V., Guzeva A., Denisov D., Cherepanov A. and Siroezhko E. (2020). The Hydrochemistry and Recent Sediment Geochemistry of Small Lakes of Murmansk, Arctic Zone of Russia. *Water*, 12, 1130, DOI: 10.3390/w12041130.
- Slukovskii Z., Medvedev M., Mitsukov A., Dauvalter V., Grigoriev V., Kudryavtzeva L. and Elizarova I. (2021). Recent Sediments of Arctic Small Lakes (Russia): Geochemistry Features and Age. *Environmental Earth Sciences*, 80(8), 1-16. DOI: 10.1007/s12665-021-09609-3.
- Tolosa I., Mesa-Albernas M. and Alonso-Hernandez C.M. (2009). Inputs and sources of hydrocarbons in sediments from Cienfuegos bay, Cuba. *Marine Pollution Bulletin*, 58(11), 1624-1634, DOI: 10.1016/j.marpolbul.2009.07.006.
- Uvarova V.I. and Zakharova T.V. (2016). Assessment of the content of petroleum products and heavy metals in the bottom sediments of the Pur and Nadym rivers. *Bulletin of Fisheries Science*, 3(11), 62-72 (in Russian).
- Vane C.H., Chenery S.R., Harrison I., Kim A.W., Moss-Hayes V. and Jones D.G. (2011). Chemical signatures of the Anthropocene in the Clyde estuary, UK: sediment-hosted Pb, 207/206Pb, total petroleum hydrocarbon, polyaromatic hydrocarbon and poly-chlorinated biphenyl pollution records. *Philosophical Transactions of the Royal Society A*, 369, 1085-1111, DOI: 10.1098/rsta.2010.0298.
- Vorobyev D.S. and Popkov V.K. (2005). Oil products in water and bottom sediments of the Vasyugan river basin. *Izvestiya of Tomsk Polytechnic University*, 308(4), 48-50 (in Russian).
- Wakeham S.G. and Farrington J.W. (1980). Hydrocarbons in contemporary aquatic sediments. In: *Contaminants and sediments*. Michigan, USA: Ann Arbor Science, 1, 3-32.
- Wang J., Yang Z. and Chen T. (2012). Source apportionment of sediment-associated aliphatic hydrocarbon in a eutrophicated shallow lake, China. *Environmental Science and Pollution Research*, 19, 4006-4015, DOI: 10.1007/s11356-012-0988-8.
- Zubova E.M., Kashulin N.A., Dauvalter V.A., Denisov D.B., Valkova S.A., Vandysh O.I., Slukovskii Z.I., Terentyev P.M. and Cherepanov A.A. (2020). Long-term environmental monitoring in an arctic lake polluted by heavy metals under climate change. *Environments*, 7(34), DOI: 10.3390/environments7050034

# POTENTIALLY HAZARDOUS ELEMENTS IN ATMOSPHERIC PRECIPITATION DURING THE WARM SEASON (MAY–SEPTEMBER) OF 2019 IN MOSCOW

**Dmitrii Vlasov<sup>1\*</sup>, Irina D. Eremina<sup>2</sup>, Natalia E. Kosheleva<sup>3</sup>, Galina Shinkareva<sup>1,4</sup>,  
Natalia E. Chubarova<sup>2</sup>, Nikolay S. Kasimov<sup>3</sup>**

<sup>1</sup> Department of Geography, Geology, and the Environment, Illinois State University, IL 61790, Normal, USA

<sup>2</sup> Department of Meteorology and Climatology, Faculty of Geography, Lomonosov Moscow State University, 119991, Moscow, Russian Federation

<sup>3</sup> Department of Landscape Geochemistry and Soil Geography, Faculty of Geography, Lomonosov Moscow State University, 119991, Moscow, Russian Federation

<sup>4</sup> Department of Geosciences, Middle Tennessee State University, TN 37132, Murfreesboro, USA

\*Corresponding author: vlasov.msu@gmail.com

Received: May 21<sup>st</sup> 2024 / Accepted: July 25<sup>th</sup> 2024 / Published: October 1<sup>st</sup> 2024

<https://doi.org/10.24057/2071-9388-2024-3408>

**ABSTRACT.** Atmospheric precipitation acts as a significant pathway for pollutants from the atmosphere to the Earth's surface, and analyzing urban precipitation data on intensity, fallout regime, transfer patterns, and solid particle content helps identify pollution sources. For the first time in the Moscow megacity, the levels of soluble forms of potentially hazardous elements (PHEs) in atmospheric precipitation were studied during the whole summer season of May–September 2019. The concentrations of Al, As, B, Ba, Be, Bi, Cd, Ce, Co, Cu, Fe, La, Li, Mn, Ni, P, Pb, Rb, Sb, Sn, Sr, and Zn were determined using inductively coupled plasma mass spectrometry and atomic emission spectroscopy methods. The research underscores the crucial role of atmospheric precipitation in washing PHEs out of the atmosphere. In May and September, concentrations of PHEs surpass the warm-season average. Notable contamination in May stems from elevated traffic during vacations, extensive burning of plant debris and wood, and pollen transport. Summer months are characterized by reduced forest and agricultural fires, traffic, and increased vegetation, leading to lower PHE concentrations, especially in July, with typical amount of precipitation contributing to pollutant dispersion. Elevated PHE levels in September are observed due to increased traffic load, biomass burning, and the expansion of unvegetated soil areas. Rainwater is enriched with Sb, Pb, Cd, Zn, Cu, B, Bi, P, and Sr, sourced from vehicle emissions, soil particles, industry, construction dust, biomass burning, and forest fires. Moderate enrichment with Ba, Mn, Ni, Co, and Sn also occurs episodically. Regression analysis highlights solid particles' role as a major PHE source in rainwater, with the longer antecedent dry periods and the higher acidity level of rain intensifying the accumulation of PHEs. Long-range transport plays a lesser role, with Southern and Northern Europe, Western Siberia, and the central part of European Russia contributing meaningfully.

**KEYWORDS:** rainwater, metals and metalloids, urban environment, sources of contamination, atmospheric pollution, anthropogenic impact

**CITATION:** Vlasov D., Eremina I. D., Kosheleva N. E., Shinkareva G., Chubarova N. E., Kasimov N. S. (2024). Potentially Hazardous Elements In Atmospheric Precipitation During The Warm Season (May–September) of 2019 In Moscow. *Geography, Environment, Sustainability*, 3(17), 70-84  
<https://doi.org/10.24057/2071-9388-2024-3408>

**ACKNOWLEDGEMENTS:** The study was supported by the Russian Science Foundation (grant № 19–77–30004–P).

**Conflict of interests:** The authors reported no potential conflict of interest.

## INTRODUCTION

Atmospheric precipitation plays a crucial role in the global hydrogeochemical cycle (Seinfeld and Pandis 2016; Bezrukova and Chernokulsky 2023), acting as a significant pathway for transporting atmospheric pollutants to the Earth's surface (Zeng et al. 2024a). Observations of atmospheric parameters and the chemical composition of precipitation in urban areas yield valuable insights into both local and remote sources of pollution, which determine the levels of heavy metals, metalloids, and other

toxic elements and compounds present in rainwater. Joint analysis of the data, including factors such as precipitation intensity, duration of preceding dry periods, long-range transport patterns, atmospheric dust levels, etc., facilitates the identification of weather conditions leading to the highest levels of contamination in precipitation with toxic elements and compounds, as well as assessing the frequency of such events (Vlasov et al. 2021a, 2021b; Adhikari et al. 2023; Rathore et al. 2023; Zeng et al. 2024b).

Analyzing the chemical composition of atmospheric precipitation allows for the assessment of the intensity

of washing out and deposition of potentially hazardous elements (PHEs), including carcinogens such as As, Cd, Pb, Be, Ni, and Co, as well as those causing systemic toxicity to the body or specific organs and systems, such as Sb, Zn, Cu, Sn, Ba, Mn, and others (Bayramoğlu Karşı et al. 2018; Orlović-Leko et al. 2020; Tsamos et al. 2022). Therefore, PHE content in atmospheric precipitation has been extensively studied worldwide. In Russia, such studies are often conducted in background areas, while the analysis of PHEs in urban precipitation is less frequent (Chudaeva et al. 2008; Yanchenko and Yaskina 2014; Semenets et al. 2017; Stepanets et al. 2021; Bezrukova and Chernokulsky 2023). In Moscow, the largest megacity in Europe, the content of organic compounds in individual rain samples has been analyzed (Polyakova et al. 2018), the ratio of PHE forms in spring precipitation in 2018 and 2019 has been determined (Chubarova et al. 2020; Vlasov et al. 2021a, 2021b), and the role of precipitation in the purification of the atmosphere from metals and metalloids accumulated in aerosols in April–July 2020 was assessed (Kasimov et al. 2023). However, the content of PHEs in precipitation and its variability throughout the entire warm period (May–September) in Moscow megacity has not been studied in detail.

Therefore, the study aims to examine the distribution of PHEs in atmospheric precipitation in Moscow during the entire warm period, when the influence of heating-related pollution is less pronounced compared to the increased contribution from other sources: vehicular traffic, industrial enterprises of various sectors, soil and road dust particle resuspension, forest and agricultural fires in the Moscow region, controlled burning of biomass and waste, etc. Data from measurements conducted at the Meteorological Observatory of Lomonosov Moscow State University (MO MSU) were used.

We focused on solving the following problems: (1) to determine the content of PHEs and its variability in atmospheric precipitation during the studied period based on observation data; (2) to identify the main sources of PHEs; and (3) to analyze the influence of the precipitation amount and the properties of rainwater, as well as air advection regions, on the content of PHEs in precipitation.

## MATERIALS AND METHODS

The Meteorological Observatory of Lomonosov Moscow State University (55.707° N, 37.522° E) is located in the MSU Botanical Garden, far from local industrial pollution sources and highways; and can be considered a background city site (Chubarova et al. 2024). For characterizing meteorological conditions during the analyzed period, we used standard meteorological measurements and compared them with monthly means over 60 years of observations since 1954 (Chubarova et al. 2014).

Precipitation samples (N=56) were taken at a height of 2 m from the ground surface using a vinyl plastic funnel (80x80 cm) and a white plastic bucket. Each case of rainfall was considered from the beginning to its end on the current or adjacent days separately: there were 11 cases in May (May 2, 3, 5, 8, 9, 10, 13, 15, 16, 23, and 30), 8 cases in June (8, 14, 22, 26, 27, 28, 29, 30), 14 cases in July (2, 3, 6, 11, 12, 13–14, 16, 17, 18, 19, 20, 24, 25, 31), 12 cases in August (2, 3, 4, 5, 7, 9, 10, 15, 16, 17, 18, 19), and 11 cases in September (5, 14, 15, 16, 17, 18, 20, 22, 24, 29, 30).

In precipitation samples, pH and specific conductivity (EC,  $\mu\text{S}/\text{cm}$ ) were determined using potentiometric and conductometric methods, respectively. To isolate soluble forms of PHEs, samples were filtered through Millipore®

filters with pore diameters of 0.45  $\mu\text{m}$ . The filters were weighed on an analytical balance “Discovery DV114C” (Ohaus, Greifensee, Switzerland; repeatability: 0.1 mg) before and after filtration (with preliminary drying) to determine the mass of suspended matter on them and, accordingly, the content of solid particles in precipitation samples.

The concentrations of Al, As, B, Ba, Be, Bi, Cd, Ce, Co, Cu, Fe, La, Li, Mn, Ni, P, Pb, Rb, Sb, Sn, Sr, and Zn in the resulting solution were determined at the N.M. Fedorovsky VIMS laboratory using inductively coupled plasma mass spectrometry (ICP-MS) and inductively coupled plasma atomic emission spectroscopy (ICP-AES) on the “iCAP Qc” mass spectrometer (Thermo Scientific, USA, produced in 2017) and “Optima–4300 DV” atomic emission spectrometer (Perkin Elmer, USA, produced in 2018) according to certified methods (NSAM № 520 AES/MS 2017). The VIMS laboratory is accredited by the Analytics International Accreditation System (AAS.A.00255) and the national accreditation system (RA.RU.21GP11); it meets the requirements of the International Standards ISO Guide 34:2009, ISO/IEC 17025:2017, and ISO/IEC 17043:2010. The VIMS laboratory is also accredited to certificate measurement techniques and provides metrological examinations in the Russian Federation (accreditation certificate No. 01.00115-2013). Standard reference materials “Trace metals in Drinking Water (TMDW)” (High-Purity Standards, USA) and blank samples were utilized. The limit of detection (LOD) for PHEs were as follows ( $\mu\text{g}/\text{L}$ ): Al, 0.78; As, 0.066; B, 0.043; Ba, 0.021; Be, 0.002; Bi, 0.004; Cd, 0.003; Ce, 0.003; Co, 0.009; Cu, 0.16; Fe, 6.6; La, 0.0015; Li, 0.004; Mn, 0.07; Ni, 0.054; P, 10; Pb, 0.038; Rb, 0.011; Sb, 0.04; Sn, 0.012; Sr, 0.027; Zn, 0.32. For low concentrations of PHEs (<5 LOD), the relative standard deviation did not exceed 20%, and for higher concentrations of PHEs (>5 LOD), the relative standard deviation did not exceed 10%.

Due to the substantial variability of soluble PHE concentrations in precipitation from one episode to another, volume-weighted concentrations were calculated to compare individual months and periods (Eq. (1)):

$$C_w = \left( \sum (C_i \times X_i) \right) / X_s \quad (1)$$

where  $C_i$  and  $X_i$  are PHE concentration ( $\mu\text{g}/\text{L}$ ) and the precipitation amount (mm) in the  $i$ -th episode of precipitation,  $X_s$  is the precipitation amount for the averaging period, i.e., for the entire studied warm season or for a separate month (mm).

One of the most common methods, known for its simplicity and efficiency, was chosen to identify sources of PHEs in atmospheric precipitation. It involves calculating the enrichment factors (EF) (Eq. (2)):

$$EF = \left( C_i / C_{Al} \right) / \left( K_i / K_{Al} \right) \quad (2)$$

where  $C_i$  and  $C_{Al}$  are the concentrations of the  $i$ -th and reference (Al) elements in the precipitation sample, and  $K_i$  and  $K_{Al}$  are the abundances of the  $i$ -th and reference elements in the upper continental crust. We used the crustal abundances provided by R.L. Rudnick and S. Gao (2014),  $\mu\text{g}/\text{g}$ : Al, 81,505; As, 4.8; B, 17; Ba, 624; Be, 2.1; Bi, 0.16; Cd, 0.09; Ce, 63; Co, 17.3; Cu, 28; Fe, 39,180; La, 31; Li, 21; Mn, 774; Ni, 47; P, 655; Pb, 17; Rb, 84; Sb, 0.4; Sn, 2.1; Sr, 320; Zn, 67. Aluminum was used as the reference element, as in most other studies of precipitation composition in cities around the world (Özsoy and Örnektekin 2009; Guo et al. 2014; Cable and Deng 2018; Xu et al. 2022; Adhikari et al. 2023). It is considered that  $EF < 10$  for soluble PHEs

indicates their natural sources (predominantly derived from the continental crust). If  $EF$  falls within the range of 10–100, anthropogenic sources are likely present, and when  $EF \geq 100$ , PHEs have anthropogenic sources (Chon et al. 2015).

To assess the difference in PHE content in rainwater from episode to episode, the geochemical range ( $GD$ ) was calculated (Eq. (3)):

$$GD = (C_{max} / C_{min}) \quad (3)$$

where  $C_{max}$  and  $C_{min}$  are the maximum and minimum concentrations of the same PHE in the precipitation sample for the entire study period, respectively.

For comparison of dissolved PHE concentrations across different months, a “growth index”  $Ks$  was calculated (Eq. (4)):

$$Ks = (Cw_m / Cw_{ave}) \quad (4)$$

where  $Cw_m$  and  $Cw_{ave}$  are the volume-weighted concentrations of a chemical element in the respective month and over the entire study period (May–September), respectively.

For a comprehensive assessment of each rainfall episode in terms of the level of all studied PHEs simultaneously, normalization was conducted (Eq. (5)):

$$C' = (C_i - C_{min}) / (C_{max} - C_{min}) \quad (5)$$

where  $C_i$  and  $C'_i$  are the original and normalized concentrations of PHEs in the  $i$ -th rainfall episode, respectively, and  $C_{max}$  and  $C_{min}$  are the maximum and minimum concentrations of PHEs over the entire warm period, respectively. Then, the total normalized concentrations of PHEs ( $NM$ ) in the  $i$ -th rainfall episode can be determined as follows (Eq. (6)):

$$NM = \sum C'_{ij} \quad (6)$$

where  $j$  represents all considered PHEs (in our case,  $j=1, 2, 3, \dots, 20, 21, 22$ ).

Descriptive statistics and correlation analysis were carried out using the Statistica 10 software by routine methods. Multivariate regression analysis was conducted to investigate the factors influencing PHE concentration in atmospheric precipitation using the method of regression (decision) trees with dendrogram construction in the SPLUS software (Kosheleva et al. 2015, 2023).

To identify possible regions of air mass advections for each rain sampling date, backward trajectories were constructed using the HYSPLIT transport-dispersion model

(Stein et al. 2015; Rolph et al. 2017), available on the READY website<sup>1</sup>. The modeling was conducted for heights of 500, 1000, and 1500 m above ground level, with a time interval of 96 hours from 3 pm Moscow time (12 pm UTC) on the precipitation event date.

## RESULTS AND DISCUSSION

### Meteorological conditions during May–September, 2019

May–September 2019 was marked by variable weather conditions, significantly affecting Moscow’s air pollution. Monthly mean values of the main meteorological parameters in comparison with long-term observations are shown in Table 1. One can see specific conditions in May 2019, when air temperature, water vapor pressure, and precipitation were significantly higher due to the prevailing advection of warm, humid air masses. During this month, the mineralization of precipitation was also very high compared to the 1981–2013 means (Table 1). June was characterized by an increase in air temperature by 16% and a decrease in precipitation by 10% compared to the 1954–2013 means. This happened due to the prevalence of anticyclone conditions, which can also be seen in positive atmospheric pressure deviations. The mineralization of precipitation during this month was close to the 1981–2013 mean. The situation changed in July, when due to the high frequency of cyclones over Moscow the air temperature was lower, the precipitation level was close to the norm, and the mineralization of precipitable water decreased by 22% compared to the 1981–2013 mean. In contrast, August and September had less precipitation, which changed the total mineralization of precipitable water. Compared to the averages from 1981 to 2013, mineralization was 14% lower in August and 54% higher in September. On average, the warm period of 2019 was characterized by a higher temperature (5%), lower precipitation (–19%), and higher mineralization of precipitation (16%).

### Levels of PHEs and their variability in the warm season

The series of PHEs in descending order of average concentrations in precipitation at the MO MSU in the warm season is shown in Fig. 1, where the minimum and maximum concentrations of each PHE, the median, and the 25% and 75% quartiles are also indicated. The highest concentrations in precipitation are characteristic of the macroelements Fe, Al, and Pb. In terms of content levels in

**Table 1. Main meteorological parameters during the warm period of 2019 at the Meteorological Observatory of Lomonosov Moscow State University<sup>2</sup> and their deviations from the monthly mean values over the 60-year period of measurements (Chubarova et al. 2014)**

Period	Air temperature, deg, C		Water vapor pressure, hPa		Atmospheric pressure, hPa		Precipitation, mm		Mineralization, mg/L	
	T	deviation, %	e	deviation, %	P	deviation, %	X	deviation, %	M	deviation, %
May	16.4	23%	11.3	23%	990.9	–0.2%	64.0	17%	32.5	51%
June	19.8	16%	13.2	5%	994.6	0.5%	68.7	–10%	17.1	–3%
July	16.6	–13%	13.7	–7%	984.8	–0.5%	79.6	–2%	11.9	–22%
August	16.4	–4%	13.6	–2%	992.2	0.1%	52.9	–32%	14.0	–14%
September	12.5	10%	10.8	4%	992.1	0.0%	22.1	–65%	24.7	54%
May–September	16.3	5%	12.5	3%	990.9	0%	57.5	–19%	20.0	16%

<sup>1</sup> <http://www.arl.noaa.gov/HYSPLIT.php>

<sup>2</sup> [www.momsu.ru](http://www.momsu.ru)



rainwater, other elements form the following descending sequence:  $P > Zn > Ba > Sr > Mn > Cu > Sb > B > Ni > Rb > Co > Li > Cd > Ce > As > La > Sn > Bi$ . Deviation from the order of elements by decreasing concentrations in precipitation compared to the order of elements in the continental crust is typical for Pb, Zn, Cu, Sb, Cd, and As, which is associated with the anthropogenic supply of these PHEs (Vlasov et al. 2023a; Kasimov et al. 2024).

Variations in precipitation amounts, coupled with changes in the intensity of PHE inputs into the atmosphere from natural and anthropogenic sources, result in significant differences in PHE content in rainwater in Moscow from episode to episode, which is generally typical for other cities worldwide. These differences are characterized by the geochemical range ( $GD$ ). In warm-season precipitation in Moscow, the highest  $GD$  is observed for Sb (714), followed by lower values for Sr (320) and P (252).  $GD$  ranges from 107 to 123 for Ba, Al, and Ce, from 80 to 95 for La, Mn, and Co, decreasing to 43–56 for Pb, Rb, Li, Bi, B, and Cd, to 29–36 for Fe, Be, Ni, and Cu, to 20–22 for Sn and Zn, and to 12 for As throughout the study period (Fig. 2).

A high  $GD$  indicates episodes of exceptionally high concentrations of individual PHEs, attributed to various

reasons: intense emissions from local sources, long-range transport of contaminated aerosols (including those from regions experiencing active forest fires), substantial resuspension of soil or road dust particles into the atmosphere, dissolution of solid carbonate particles washed out by acidic rains, etc. For instance, spikes in Sb levels in rainfall on certain days might result from vehicle emissions, the long-range transport of enriched Sb atmospheric aerosols, waste and biomass burning (Gubanov et al. 2021; Ozaki et al. 2021; Serdyukova et al. 2023; Popovicheva et al. 2024). The latter source can also supply P (Meng et al. 2022); and Sr can come from construction sites (Amato et al. 2009). A more detailed analysis of the PHEs' probable sources is given below.

### Relationship between PHE concentrations and precipitation properties

Elevated concentrations of Sr during specific episodes are caused by the dissolution of atmospheric particles of construction carbonate dust that is washed out by rain since Sr is often a geochemical companion of Ca and Mg in carbonates (Borsato et al. 2016). The increase in Al, Ce, La,

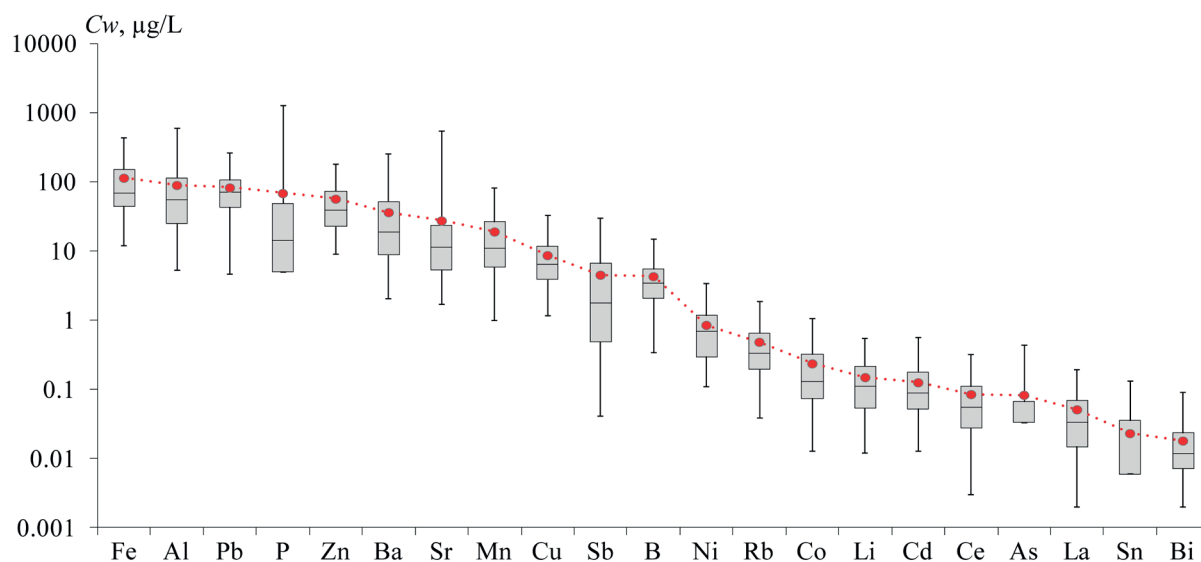


**Fig. 1.** Volume-weighted concentrations of PHEs in rainwater for the warm season (May–September 2019) on the territory of MO MSU. Elements are ordered by decreasing average concentrations (red dots connected by a red dotted line). "Box" shows 25% and 75% quartiles, line in the "box" shows the median, "whiskers" show minimum and maximum values of PHE concentrations

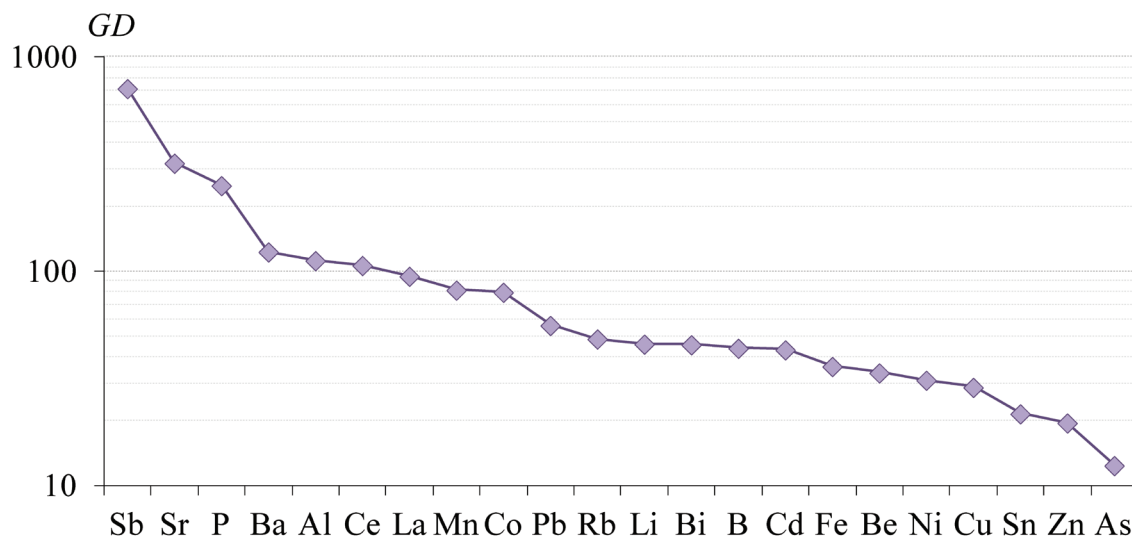


**Fig. 2.** Geochemical range ( $GD$ , the ratio of maximum concentrations to minimum) of PHEs in rainwater precipitation from May to September 2019 on the territory of MO MSU

Li, Co, Fe, and other PHE levels may result from soil particle resuspension and their dissolution in acidic rainwater (Amato et al. 2009; Vlasov et al. 2021b,c). This is accompanied by an increase in the content of solid particles in the rain, likely due to prolonged antecedent dry periods, allowing particle accumulation in the atmosphere. This relationship is supported by high Spearman rank correlation coefficients ( $r_s$ ) between PHE content in solution and solid particles in rain samples (Table 2), ranging from 0.82–0.85 for Co and Mn, 0.74–0.75 for Li, Zn, and Rb, 0.60–0.66 for Be, Ni, Sr, Cd, Bi, La, and Ce, and 0.46–0.59 for other PHEs, except Pb.

Partial dissolution of soil and road dust aerosol components may contribute to an increase in precipitation pH since water extraction from soils and road dust in Moscow has an alkaline reaction (Kosheleva et al. 2018; Kasimov et al. 2019; Vlasov et al. 2022). Under alkaline conditions, anionic elements and some complexing agents can transition from a suspended to a dissolved phase, while cationic PHEs tend to be more soluble in acidic conditions. Thus, significant negative  $r_s$  values are observed between the content of specific cationic elements (Li, Al, Fe, Pb) in rainwater and pH, while  $r_s$  values for other PHEs are insignificant. Low pH can be both a cause of increased PHE solubility and an indicator of PHE input from industrial emissions and thermal power plants supplying

sulfates, as well as transportation sources that release nitrates, leading to atmospheric precipitation acidification to pH 5 and below. Additionally, chlorides from deicing agents also contribute to the acidification of atmospheric precipitation in Moscow (Eremina et al. 2015; Zappi et al. 2023).

One of the main factors leading to the reduction in PHE levels in rainwater as precipitation increases is linked to dilution (Song and Gao 2009; Park et al. 2015; Ma and Kang 2018), which is sometimes also called the “rain-scour effect” (Zeng et al. 2020). During the warm season in Moscow, dilution effects were observed for all PHEs, most notably for Ni ( $r_s = -0.74$ ), Li ( $-0.69$ ), Sr ( $-0.68$ ), Zn ( $-0.67$ ), Mn ( $-0.64$ ), Ba ( $-0.63$ ), Cu ( $-0.62$ ), Co ( $-0.61$ ). Specific conductivity, reflecting the presence of readily soluble compounds in rainwater, also decreases with increasing precipitation amounts but rises with PHE concentration in precipitation (Table 2).

These factors influence the varying levels of PHEs in rainwater across different months. Table 3 presents the monthly concentrations of PHEs in rainwater within the MO MSU area during the 2019 warm season.

For comparison of dissolved PHE concentrations across different months, a “growth index”  $K_s$  was calculated. The  $K_s$  values for May, June, July, August, and September are shown in Fig. 3.

**Table 2. Spearman rank correlation coefficients ( $r_s$ ) between PHE content in rainwater and precipitation amount, pH, specific conductivity (EC), and solid particle content in rainwater (N=56)**

PHE	Precipitation amount	pH	EC	Solid particle content
Mn	<b><i>-0.64</i></b>	0.26	<b><i>0.93</i></b>	<b><i>0.85</i></b>
Co	<b><i>-0.61</i></b>	0.24	<b><i>0.91</i></b>	<b><i>0.82</i></b>
Rb	<b><i>-0.53</i></b>	0.20	<b><i>0.88</i></b>	<b><i>0.75</i></b>
Li	<b><i>-0.69</i></b>	<b><i>0.28</i></b>	<b><i>0.86</i></b>	<b><i>0.74</i></b>
Zn	<b><i>-0.67</i></b>	0.08	<b><i>0.93</i></b>	<b><i>0.74</i></b>
Sr	<b><i>-0.68</i></b>	0.20	<b><i>0.89</i></b>	<b><i>0.66</i></b>
Cd	-0.24	0.01	<b><i>0.70</i></b>	<b><i>0.66</i></b>
Be	<b><i>-0.52</i></b>	-0.06	<b><i>0.78</i></b>	<b><i>0.65</i></b>
Bi	<b><i>-0.41</i></b>	-0.04	<b><i>0.78</i></b>	<b><i>0.65</i></b>
Ni	<b><i>-0.74</i></b>	0.14	<b><i>0.90</i></b>	<b><i>0.64</i></b>
Ce	<b><i>-0.55</i></b>	-0.13	<b><i>0.89</i></b>	<b><i>0.62</i></b>
La	<b><i>-0.57</i></b>	-0.15	<b><i>0.91</i></b>	<b><i>0.60</i></b>
As	-0.24	-0.03	<b><i>0.65</i></b>	<b><i>0.59</i></b>
Cu	<b><i>-0.62</i></b>	-0.10	<b><i>0.88</i></b>	<b><i>0.57</i></b>
B	<b><i>-0.38</i></b>	-0.06	<b><i>0.75</i></b>	<b><i>0.53</i></b>
Al	<b><i>-0.59</i></b>	<b><i>-0.29</i></b>	<b><i>0.81</i></b>	<b><i>0.50</i></b>
Ba	<b><i>-0.63</i></b>	-0.08	<b><i>0.80</i></b>	<b><i>0.46</i></b>
Sb	<b><i>-0.47</i></b>	-0.20	<b><i>0.66</i></b>	<b><i>0.43</i></b>
Fe	<b><i>-0.50</i></b>	<b><i>-0.34</i></b>	<b><i>0.78</i></b>	<b><i>0.41</i></b>
P	-0.14	-0.12	<b><i>0.45</i></b>	<b><i>0.40</i></b>
Sn	<b><i>-0.45</i></b>	-0.08	<b><i>0.66</i></b>	<b><i>0.39</i></b>
Pb	-0.19	<b><i>-0.59</i></b>	<b><i>0.39</i></b>	0.05

Note. Significant  $r_s$  levels at  $p < 0.05$  are highlighted in bold italics. Elements are ranked by  $r_s$  for solid particle content.

**Table 3. Monthly volume-weighted concentrations of dissolved PHEs in rainwater on the territory of MO MSU during the 2019 warm season**

PHE	Concentration in rainwater, µg/L				
	May	June	July	August	September
Li	0.11 (0.045–0.29)	0.085 (0.034–0.52)	0.064 (0.022–0.29)	0.059 (0.012–0.55)	0.16 (0.080–0.32)
Be	0.007 (0.001*–0.018)	0.005 (0.001*–0.032)	0.004 (0.001*–0.014)	0.003 (0.001*–0.019)	0.007 (0.001*–0.037)
B	4.7 (1.9–8.8)	3.5 (1.4–15)	2.4 (0.66–5.4)	2.8 (0.34–13)	3.9 (1.5–13)
Al	90 (37–590)	34 (5.7–265)	26 (12–149)	41 (5.2–239)	86 (23–348)
P	213 (5.0*–1,259)	72 (14–387)	20 (5.0*–204)	9.2 (5.0*–60)	17 (5.0*–123)
Mn	19 (3.8–57)	9.8 (1.9–77)	7.2 (2.1–36)	7.3 (1.0–82)	15 (7.1–40)
Fe	88 (23–348)	66 (26–382)	55 (20–253)	63 (12–429)	110 (34–403)
Co	0.26 (0.022–1.0)	0.15 (0.054–0.81)	0.089 (0.029–0.46)	0.084 (0.013–0.84)	0.16 (0.069–0.44)
Ni	0.52 (0.11–1.7)	0.45 (0.13–2.6)	0.34 (0.12–1.5)	0.37 (0.11–2.5)	1.1 (0.70–3.4)
Cu	6.4 (1.8–19)	6.6 (2.5–33)	4.6 (2.1–16)	4.0 (1.1–23)	9.2 (2.8–20)
Zn	48 (16–157)	34 (12–178)	27 (11–133)	25 (9.1–164)	46 (19–126)
As	0.14 (0.033*–0.36)	0.048 (0.033*–0.41)	0.033* (0.033*–0.033*)	0.047 (0.033*–0.23)	0.046 (0.033*–0.23)
Rb	0.55 (0.19–1.8)	0.36 (0.18–1.8)	0.24 (0.087–0.80)	0.17 (0.038–1.0)	0.38 (0.15–0.75)
Sr	12 (4.1–36)	7.5 (3.7–42)	7.2 (2.2–72)	7.9 (1.7–71)	48 (5.9–535)
Cd	0.16 (0.036–0.35)	0.11 (0.043–0.56)	0.11 (0.019–0.29)	0.047 (0.013–0.22)	0.12 (0.048–0.45)
Sn	0.019 (0.006*–0.089)	0.010 (0.006*–0.13)	0.008 (0.006*–0.056)	0.011 (0.006*–0.043)	0.023 (0.006*–0.081)
Sb	5.5 (2.3–18)	0.20 (0.041–1.6)	0.79 (0.14–13)	3.4 (0.53–29)	2.6 (0.88–11)
Ba	28 (13–92)	6.5 (2.0–42)	10 (5.1–69)	19 (3.2–130)	51 (11–252)
La	0.047 (0.012–0.14)	0.034 (0.006–0.19)	0.018 (0.005–0.091)	0.023 (0.002–0.16)	0.043 (0.010–0.11)
Ce	0.079 (0.019–0.25)	0.057 (0.009–0.32)	0.033 (0.012–0.14)	0.039 (0.003–0.27)	0.065 (0.019–0.17)
Pb	84 (22–258)	99 (53–161)	56 (24–140)	41 (9.0–214)	66 (4.6–225)
Bi	0.019 (0.006–0.091)	0.023 (0.006–0.064)	0.008 (0.002*–0.033)	0.006 (0.002*–0.025)	0.013 (0.007–0.027)

Note: Average monthly concentrations of PHEs are provided, with minimum and maximum concentrations in parentheses.

\*Concentration as half the limit of detection LOD

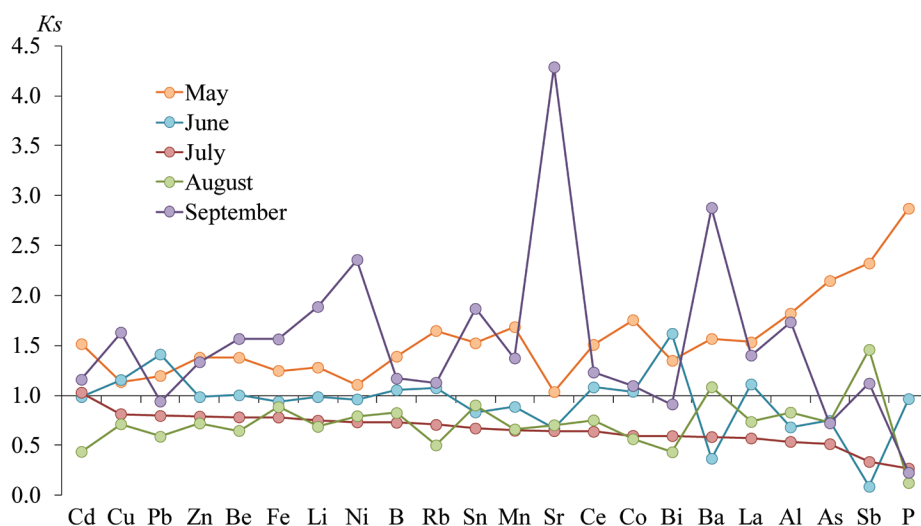


**Fig. 3. The levels of growth index ( $K_s$ ) for PHEs in precipitation on the territory of MO MSU.  $K_s$  shows the ratio between the concentration of PHE in individual months of 2019 relative to the average concentration of the same PHE over the entire study period (May–September 2019)**

In May, concentrations of all PHEs, and in September, concentrations of all PHEs, except Pb, Bi, As, and P, were higher than the average for the entire warm season (Fig. 3). Significant pollution by Sb, Cd, Cu, Pb, Bi, Sn, Zn, and B in May can be attributed to increased transportation activity due to the beginning of the active suburban travel season. Additionally, the burning of large quantities of plant residues in suburban areas and wood coal in forest parks during the May holidays contributed to the release of As, Rb, P, Sb, Sn, and Cd into the atmosphere. Active transport of plant pollen containing P, Mn, Cu, and Zn also played a role. Immature vegetation cover and large open soil areas also impacted the emission of enriched particles (especially Al, Ce, La, Fe, Mn, Rb, Sr, and Ba), increasing PHE levels in precipitation.

During the summer, a reduction in the transport load due to the holiday season and the end of the school year, along with a decrease in the surface area of soils with sparse vegetation cover, caused many of these factors to diminish. This led to lower PHE concentrations in summer rains compared to the warm-season average. July recorded the lowest pollutant concentrations due to relatively high rainfall and prevailing cyclonic circulation with effective dispersion of contaminants (Table 1).

In September, high PHE concentrations in rain were associated with significantly lower precipitation (21.3 mm), which was 65% below the monthly norm and also notably less than in other months (Table 1). This resulted in reduced dilution and, consequently, higher PHE concentrations. Moreover, in September, many residents returned from vacations, transportation loads increased, work on harvesting and preparing for the cold season (including burning of plant residues) was carried out in suburban territories, non-vegetated soil areas increased, and the heating season began at the end of the month, leading to increased emissions of PHEs into the atmosphere and consequently higher concentrations of chemical elements in rainwater. The highest  $K_s$  in September was found for Sr, possibly due to intensified construction and road works near the MO MSU area, which released a large amount of carbonate dust enriched with this metal. The P content in September rains was lower than the warm-season average, as well as the levels in May, June, and July, possibly due to the reduced role of plant pollen in the transport of this element in autumn compared to spring (the highest  $K_s$  for P was noted in May).

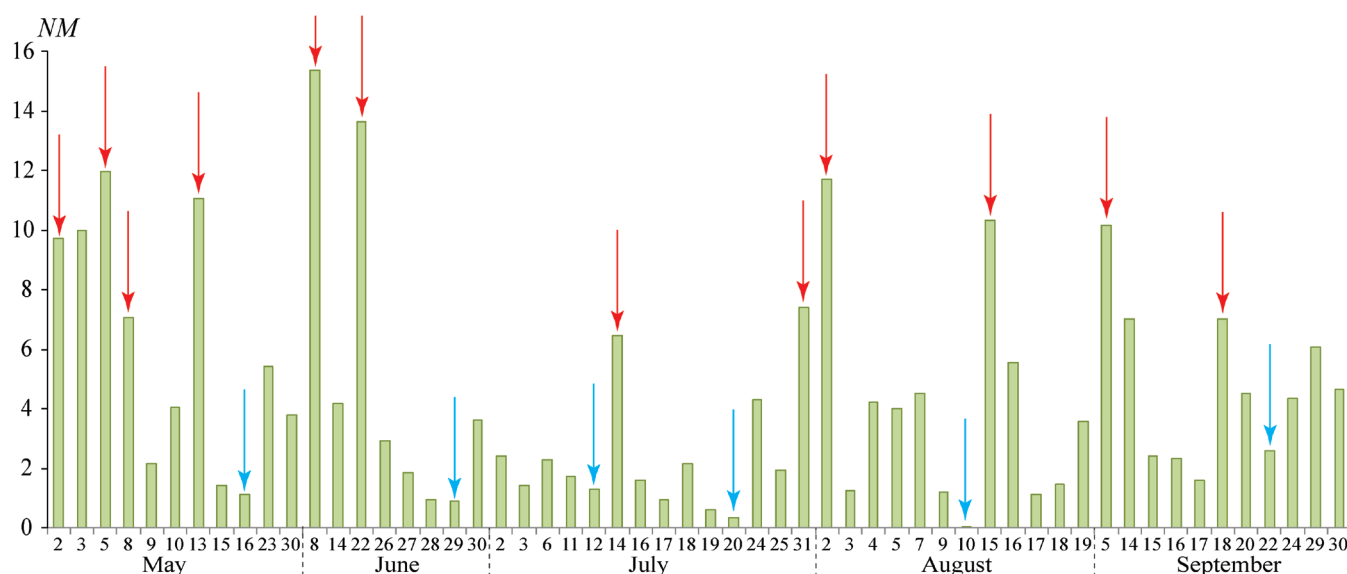
## Regions of air advection and their influence on the content of PHEs in rains

Figure 4 illustrates the variations in total normalized concentrations ( $NM$ ) from May to September 2019. Several episodes exhibited notably high concentrations of PHEs in rainwater: the May holiday period (May 2–8), May 13, June 8 and 22, July 14 and 31, August 2 and 15, September 5 and 18. We previously found that the May holiday period was characterized by active traffic loads and resuspension of soil and road dust particles, leading to a sharp increase in the concentrations of soluble and particulate-bound insoluble PHEs in atmospheric precipitation (Chubarova et al. 2020; Vlasov et al. 2021b, 2023a). Additionally, biomass burning and forest fires contributed substantially to atmospheric aerosol pollution, as indicated by elevated black carbon concentrations (Popovicheva et al. 2020).

Between May 2 and 8, as well as on May 13, Moscow experienced prevailing air advection from Southern Europe and the southern regions of European Russia, where agricultural activities causing soil wind erosion and forest and agricultural fires were intensified (Fig. 5). Emissions from thermal power plants could have also exerted an additional influence on precipitation pollution during this period since the obtained backward trajectories pass over areas with large coal-fired power plants in Southern Europe and European Russia (Global Coal Plant Tracker 2024). In other episodes with high normalized PHE concentrations (June 8 and 22, July 14, and September 5), regional sources significantly influenced air and precipitation pollution (Fig. 5).

At the end of July and the beginning of August, air advection from the north of Western Siberia prevailed, resulting in PHE contamination in precipitation due to forest fires and emissions from oil and gas extraction facilities (Fig. 6), as confirmed by NASA data on fire outbreaks along the path of air masses (FIRMS 2024). During rainfall events on August 15 and September 18, air advection from the northern parts of Europe predominated (Fig. 6).

Episodes of precipitation with low normalized PHE concentrations in rainwater are notably distinct. These include episodes on May 16, June 29, and September 22, when air advection from the North Atlantic prevailed, on July 12 from the Arctic, and on July 20 and August 10 from the Arctic and the northern regions of Northern Europe (Fig. 6).



**Fig. 4. Normalized concentrations of PHEs ( $NM$ ) in atmospheric precipitation on the territory of MO MSU during the warm season of 2019. Red arrows indicate episodes with a significant increase in normalized concentrations relative to other days; blue arrows indicate a significant decrease. For some of these episodes, calculations of backward trajectories are presented in Fig. 5 and Fig. 6**



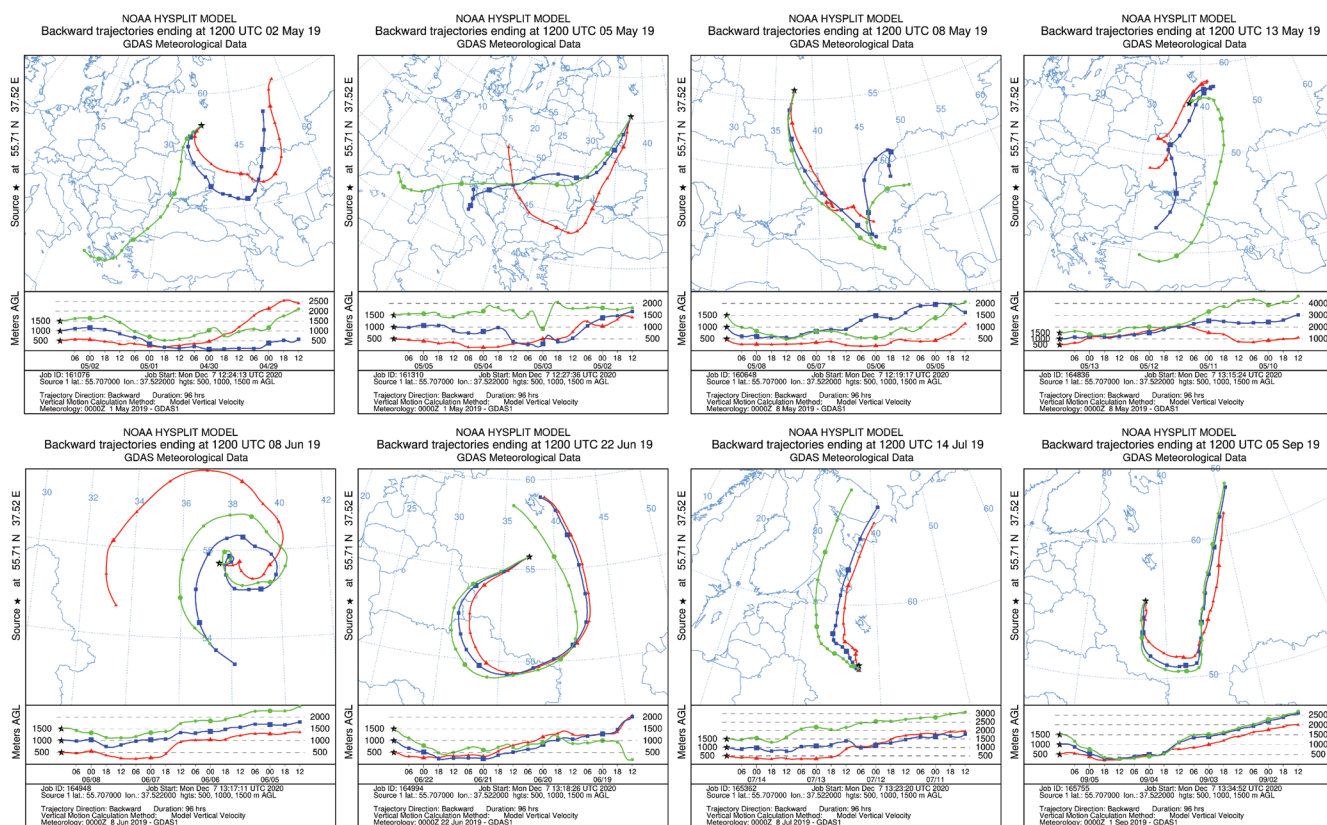


Fig. 5. Backward trajectories (NOAA HYSPLIT) with an endpoint at the MO MSU for dates with a high content of PHEs in precipitation: upper graphs show advection from Southern Europe and southern Russia (May 2, 5, 8, and 13); lower graphs show the impact of regional sources of pollution (June 8 and 19, July 14, and September 19)

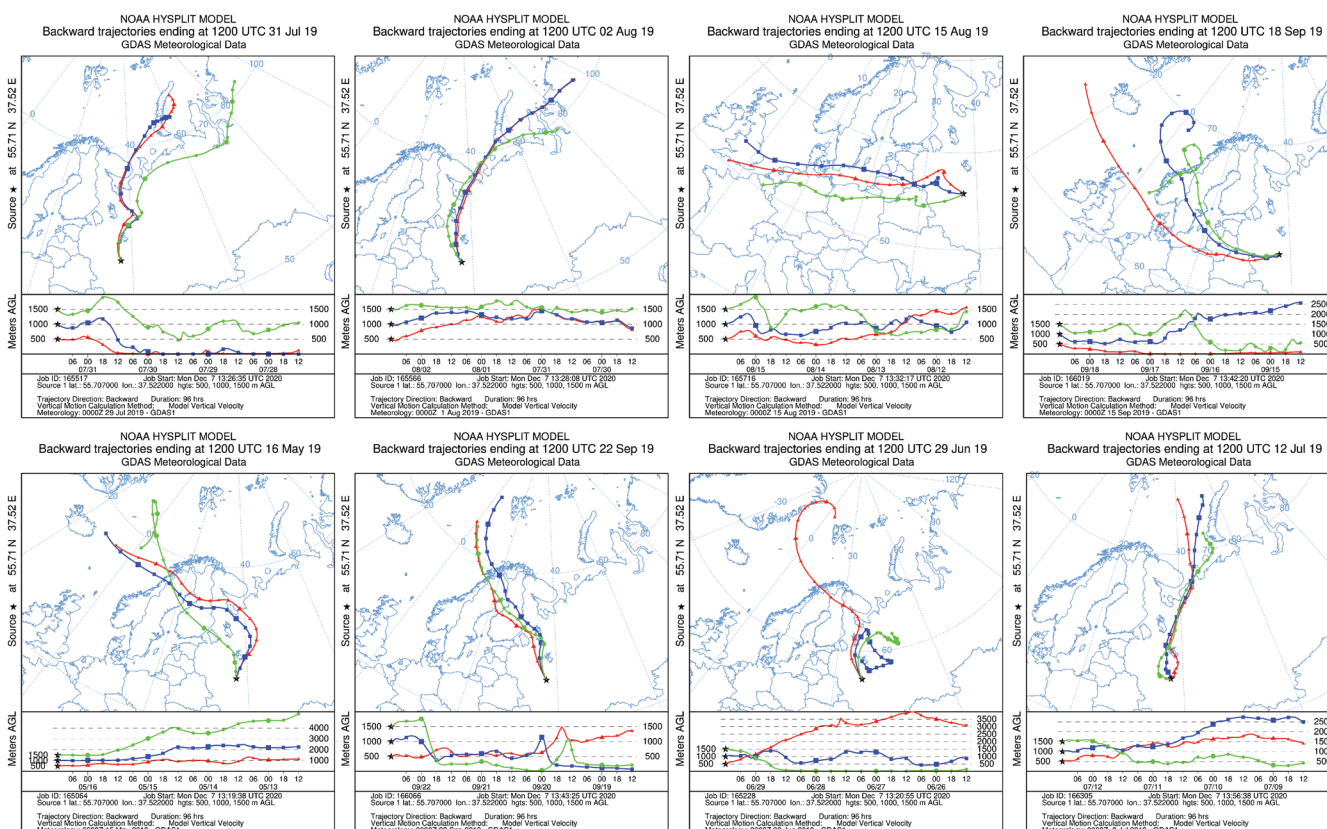


Fig. 6. Backward trajectories (NOAA HYSPLIT) with an endpoint at the MO MSU for dates with the high and low contents of PHEs in precipitation. The upper graphs are made for dates with a high content of PHEs in precipitation during advection from the north of Western Siberia and the Urals (July 31 and August 2), Northern and Western Europe (August 15 and September 18); lower graphs are made for dates with low PHEs content in precipitation during advection from the North Atlantic (May 16, June 29, and September 22) and from the Arctic (July 12)

## Sources of potentially hazardous elements

Figure 7 presents the average, median, minimum, and maximum *EF* values in Moscow rains during the warm season. The highest levels of enrichment, indicating clear anthropogenic sources, are observed for Sb (average *EF* = 10,317), Pb (8,348), Cd (2,233), Zn (1,113), Cu (420), B (365), and Bi (167). P (180) and Sr (131) also belong to this group; however, the influence of anthropogenic sources for these two elements is only evident during specific precipitation episodes, primarily in May and June for P and in September for Sr.

The most probable and active sources of Sb, Cd, Zn, Cu, B, and Bi are non-exhaust vehicle emissions, such as wear and tear of clutch components, brake systems, tires, and road surfaces, along with the resuspension of road dust and soil particles. For instance, brake pads and linings contain Cu, Sb sulfides, Zn borates, and other compounds (European Borates Association 2011, Hulskotte et al. 2014; Grigoratos and Martini 2015; Alves et al. 2018; Budai and Clement 2018; Ramírez et al. 2019). Similarly, tires contain significant amounts of Zn and Cd, making tire abrasion a source of PHEs in the atmosphere (Harrison et al. 2012; Pant and Harrison 2013). In Moscow, the resuspension of road dust can significantly contribute to air and precipitation pollution. It is known that road dust, especially its fine fractions with diameters less than 10  $\mu\text{m}$  ( $\text{PM}_{10}$ ) and less than 1  $\mu\text{m}$  ( $\text{PM}_{1}$ ), is highly enriched with Sb, Zn, Pb, Cd, Bi, Sn, and W (Fedotov et al. 2014; Ermolin et al. 2018; Kasimov et al. 2020, 2024; Ladonin and Mikhaylova 2020; Vlasov et al. 2021c, 2023b; Ivaneev et al. 2023; Kolesnikova et al. 2023; Vetrova et al. 2023).

PHEs can additionally originate from industrial emissions in the city, particularly from metal processing and engineering plants, non-ferrous metal treatment, metallic parts manufacturing, etc. (Demetriades and Birke 2015; Zheng et al. 2018; Serdyukova et al. 2023). Additionally, they can be emitted during the resuspension of contaminated particles from urban soils (Gunawardana et al. 2012; Harrison et al. 2012; Padoan et al. 2016; Morera-Gómez et al. 2020; Konstantinova et al. 2022; Moskovchenko et al. 2022). In Moscow, the top horizons of urban soils are contaminated with Pb, Cu, Cd, Zn, Bi, Sn, W, Cr, Mo, and other PHEs (Kosheleva et al. 2015, 2018; Ermakov et al. 2017; Romzaykina et al. 2021; Vlasov et al. 2022). Soil particles can serve as significant sources of Sr and P, while Sr primarily

originates from carbonate construction dust emissions and dust generated during building demolition (Amato et al. 2009), and P comes from bioaerosols, biomass burning, forest fires, and asphalt wear (Feddes et al. 1992; Yang et al. 2011; von Gunten et al. 2020; Wada et al. 2020; Meng et al. 2022). Fires and controlled biomass and waste burning can also be sources of other PHEs with high *EF*s, such as Sb, Pb, Cd, Bi, Zn, and Cu (Kumar et al. 2015; Jain et al. 2018; Bencharif-Madani et al. 2019).

The factors mentioned above play a lesser role in enriching atmospheric precipitation with the second group of PHEs, characterized by moderate *EF* levels ranging from 10 to 100: Ba (*EF* = 69), Mn (31), As (24), Ni (24), Co (18), and Sn (15). These PHEs are predominantly emitted during biomass and waste burning and the resuspension of soil particles (Christian et al. 2010; Niyobuhungiro and Blottnitz 2013; Konstantinova et al. 2024). The third group mainly comprises PHEs originating from natural (terrigenous) sources such as soils, rocks, and the transport of background aerosols. In Moscow's precipitation, this group includes Li (*EF* = 9), Rb (8), Be (4), Fe (3), rare earths La (1.8) and Ce (1.5), as well as Al. In small quantities, Rb can be emitted during the combustion of plant residues and coal (Grivas et al. 2018), while Fe originates from road dust particles, emissions from metal processing facilities, and mechanical abrasion of metallic vehicle parts (Grigoratos and Martini 2015). Thus, the contribution of the second and third groups of PHEs to atmospheric precipitation is sporadically linked to anthropogenic influence, with the highest contribution often coming from mixed natural-anthropogenic sources (resuspension of contaminated soil and road dust) and natural sources (long-range transport of background aerosols and rock particles).

## Multivariate regression analysis of factors contributing to the accumulation of PHEs in atmospheric precipitation

The collected data were analyzed through multivariate regression to quantitatively assess the role of factors influencing the accumulation of PHEs in rainwater. The regression tree method was used, with dendrograms constructed to illustrate the relationship between the concentrations of individual elements and three groups of factors: (1) meteorological conditions, including the amount of atmospheric precipitation and the duration of the antecedent dry period; (2) below-cloud interactions,

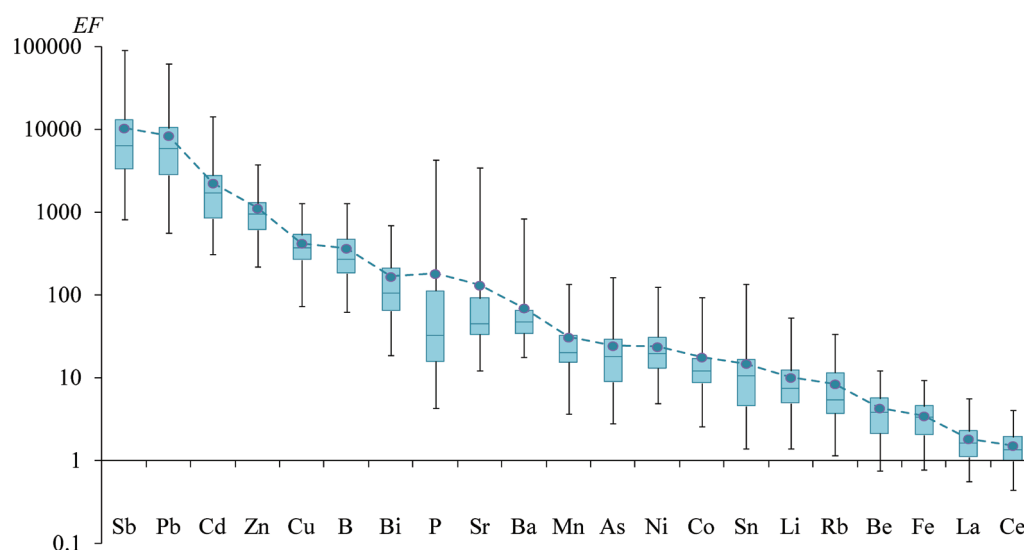


**Fig. 7. Enrichment factors (*EF*) for PHEs in atmospheric precipitation on the territory of MO MSU in May–September 2019. PHEs are ordered by decreasing mean *EF* values (dots connected by a dotted line). “Box” shows 25% and 75% quartiles, the line in the “box” shows the median, “whiskers” show minimum and maximum *EF* values**

characterized by the pH of precipitation and the content of solid particles in rainwater; and (3) long-range transport, which determines the influx of PHEs from various regions identified through backward trajectory analysis.

The calculations revealed that for most PHEs, namely Li, Zn, La, Ce, Mn, Co, Rb, Sb, As, Bi, Cd, Sn, and P, solid particles are the primary factor intensifying their concentration in atmospheric precipitation. The partial dissolution of this material contributes to rainwater pollution (Table 4). In second place in importance, this factor was identified for Ni, Be, and Fe, while in third place, it was found for Li, Cu, Zn, La, Ce, B, Al, Bi, and Cd. For Al and Pb, precipitation acidity emerged as the primary accumulation factor, likely associated with the partial dissolution of solid particles. This is because the solubility of these elements increases significantly with a considerable reduction in the solution's pH, as previously demonstrated in spring precipitation in Moscow (Vlasov et al. 2021b). The pH level is the second most significant accumulation factor for Sb and P, and it is the third for Rb, Be, Fe, Pb, Bi, and Cd.

The length of the antecedent dry period preceding rainfall, an increase of which contributes to the accumulation of pollutants in the atmosphere (which are subsequently washed away by rain), notably impacts the accumulation of Be and B in precipitation. This factor ranks second in importance for Cu, Pb, As, Bi, Sr, and Ba, and third for La, Mn, Pb, and Sn. The primary factor affecting the content of soluble Ni, Fe, Cu, Sr, and Ba in rainwater is the amount of precipitation. An increase in precipitation tends to decrease the level of contamination by these metals due to dilution. This factor ranks second in importance for Li, Zn, Ce, Mn, Co, Rb, Al, Pb, and Sn, and third for Ni, Cu, Be, B, Sb, and Fe.

Long-range transport from other regions significantly contributes to the accumulation of most PHEs, ranking additionally as the second most significant factor for Cu, Mn, Rb, B, Fe, and Cd. Advection from Northern and Northwestern Europe leads to a noticeable increase in La, Ce, Rb, B, Sb, Al, Pb, As, Bi, Cd, and Sn concentrations. Significant rises in the levels of Li, Cu, Zn, La, Ce, Mn, Co, Rb, Be, B, Sb, Al, Fe, As, Bi, Cd, Sn, P, and Ba are observed during advection from the northern European Russia and Western Siberia. Conversely, advection from the southwest of European Russia, Southern Europe, and the Mediterranean typically results in increases in Li, Cu, Be, B, Sb, Al, Fe, Bi, Cd, Sn, and Ba content. Furthermore, regional sources in the central part of European Russia supply Li, Cu, Ce, Mn, Co, Sb, Al, Fe, Sn, and P.

An analysis of dendrograms for Sb, Pb, Cd, and Zn, characterized by the highest *EFs*, is of particular interest. It is essential to identify combinations of influencing factors that lead to their minimum and maximum concentrations (Fig. 8).

The predominant factor influencing the concentration of Sb in atmospheric precipitation in Moscow is the presence of solid particles in rainwater. When their content exceeds 53 mg/L, the Sb concentration increases by 3.3 times, presumably due to the transition of Sb from suspended matter to solution (Fig. 8a). Conversely, when the suspended matter content is < 53 mg/L, Sb concentrations increase by 3.6 times in acidic precipitation with a pH < 4.5 compared to precipitation with a pH > 4.5. In the latter scenario, the reduction in Sb concentration due to dilution is influenced by the amount of precipitation, particularly at levels above 3.4 mm, resulting in a fourfold decrease in the metalloid content. Although atmospheric

**Table 4. Factors of PHEs accumulation in atmospheric precipitation on the territory of MO MSU during the warm season of 2019**

Factors		Li	Ni	Cu	Zn	La	Ce	Mn	Co	Rb	Be	B	Sb	Al	Fe	Pb	As	Bi	Cd	Sn	P	Sr	Ba
Below-cloud interactions	pH	N/A	N/A	N/A	4-	N/A	N/A	N/A	N/A	3-	3-	4-	2-	1-	3-	1-, 3-	N/A	3-	3-	N/A	2-	N/A	N/A
	Solid particle content	1+, 3+	2+, 4+	3+	1+, 3+, 4+	1+, 3+	1+, 3+	1+	1+	1+	2+, 4+	3+	1+, 5+	3+	2+, 4+	4+	1+	1+, 3+	1+, 3+	1+	1+	N/A	N/A
Meteorological conditions	Amount of precipitation	2-	1-, 3-	1-, 3-	2-	2-, 5-	2-	2-	2-	2-	3-	3-	3-	2-	1-, 3-	2-	N/A	5-	N/A	2-	N/A	1-	1-
	Antecedent dry period	N/A	N/A	2+	N/A	3+	N/A	3+	N/A	4+	1+	1+	N/A	N/A	N/A	2+, 3+	2+	2+	N/A	3+	N/A	2+	2+
Long-range transport	A	4+	N/A	2-	3+	4+	3+, 4-	2+	3+	2-	4+	2-	4-	3-	2-, 4+	3-	3-	4-	2-, 4-	4-, 4+	3+	N/A	3-
	B	4+	N/A	2+	3+	4+	3+, 4-	2+	3+	2+	4+	2+	4+, 4-	3+	2+	N/A	3+	4+	2+	4+	3-	N/A	3+
	C	4-	N/A	2-	3-	4-	3-, 4+	2+	3-	2+	4-	2-	4-, 4+	3-	2-, 4-	3-	3-	4+	2-, 4+	4-	3+	N/A	3+
	D	4-	N/A	2-	3-	4+	3-, 4+	2-	3-	2+	4-	2+	4+, 4-	3+	2-, 4-	3+	3+	4+	2+	4+, 4-	3-	N/A	3-
	E	4+	N/A	2+	3-	4-	3-	2-	N/A	2-	4+	2+	4-, 4+	3+	2-, 4+	3-	3-	4+	2+	4+, 4-	3-	N/A	3+
	F	4+	N/A	2-	3-	4-	3-, 4+	2+	3-	2-	4-	2+	4-, 4+	3-	2-, 4-	3+	3-	4-	2-, 4+	4+	3-	N/A	3-
	G	4+	N/A	2+	3-	4-	3+, 4-	2+	3+	2-	N/A	2-	4+	3+	2+	3-	3-	4-	2-, 4-	4-, 4+	3+	N/A	3-

Note: Ranks from 1 to 5 indicate a decrease in the significance of the factor: "+" shows a situation where an increase in the indicator contributes to an increase in the concentration of PHE, "-" shows a situation where an increase in the indicator contributes to a decrease in the concentration of PHE. Regions of advection (long-range transport): A, northern European Russia, Arctic; B, northern European Russia, Arctic, Western Siberia; C, North Atlantic and Scandinavia; D, Northern and Northwestern Europe; E, southwest of European Russia, Ukraine, Southern Europe, Mediterranean; F, the southern part of European Russia and northwestern Kazakhstan; G, the center of European Russia (regional sources). N/A, not available.



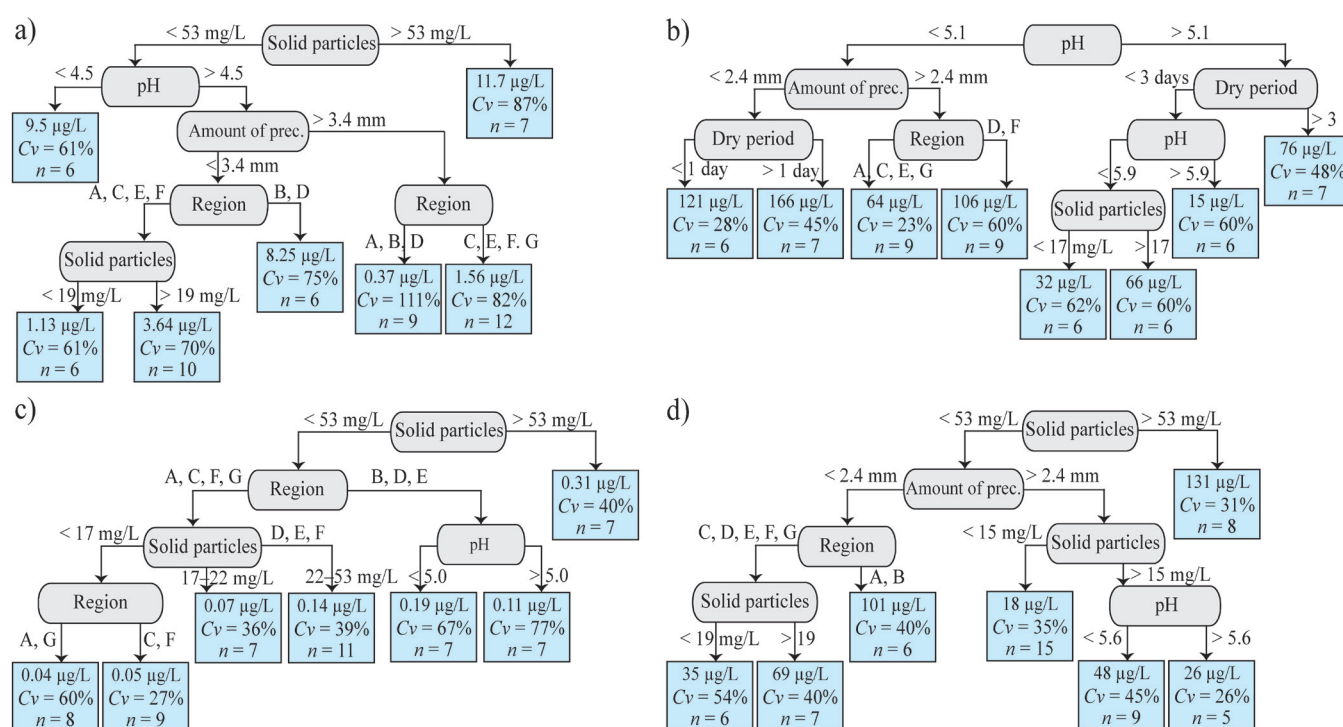


**Fig. 8. Factors of accumulation of Sb (a), Pb (b), Cd (c), Zn (d) in atmospheric precipitation in Moscow. Regions of advection (long-range transport): A, northern European Russia, Arctic; B, northern European Russia, Arctic, Western Siberia; C, North Atlantic and Scandinavia; D, Northern and Northwestern Europe; E, southwest of European Russia, Ukraine, Southern Europe, Mediterranean; F, southern part of European Russia and northwestern Kazakhstan; G, center of European Russia (regional sources)**

advections have minimal impact, elevated Sb levels are attributed to sources in northern European Russia and Western Siberia, as well as during advections from Northern and Northwestern Europe.

The primary accumulation factor for Pb is pH. In acidic rainwater with a pH < 5.1, Pb concentrations tend to double (Fig. 8b), especially with a precipitation amount of less than 2.4 mm. Moreover, rainwater pollution with Pb intensifies with more extended antecedent dry periods. A rise in Pb concentrations in precipitation occurs when air masses originate from regions D and F, namely, during advection from Northern and Northwestern Europe, from the southern part of European Russia, and from the northwest part of Kazakhstan. The alkalization of precipitation with a pH > 5.9 reduces the solubility of Pb, leading to its minimal concentrations.

The main determinant for Cd, similar to Sb, is the content of solid particles in precipitation, with a similar threshold of 53 mg/L delineating sample divisions, above which Cd concentrations in rainwater triple (Fig. 8c). When suspended matter concentrations are below 53 mg/L, the region of advection significantly influences Cd content in rainwater: Cd levels increase during advections from the northern regions of European Russia and Western Siberia, as well as from Northern and Northwestern Europe, the southwest of European Russia, Southern Europe, and the Mediterranean, especially when precipitation pH is below 5.0.

It is noteworthy that Zn follows a similar pattern, with the solid particle content threshold above which metal concentrations increase by 2.9 times also being 53 mg/L (Fig. 8d). When suspended matter concentrations fall below 53 mg/L, Zn content in rainfall is influenced by the amount of precipitation: upon exceeding an amount of 2.4 mm, metal content decreases by 2.4 times due to dilution, and an increase in rainfall acidity is accompanied by a slight rise in Zn concentrations. With amounts less than 2.4 mm, precipitation pollution with Zn intensifies, driven by regional sources situated in the central part of European

Russia as well as during advections from the northern regions of European Russia and Western Siberia.

## CONCLUSIONS

The research has confirmed a significant role of atmospheric precipitation in washing out PHEs from the atmosphere. The concentrations of all PHEs in May, and the content of all PHEs, except Pb, Bi, As, and P, in September, exceeded the warm season's average. Significant contamination of precipitation in May is associated with heavy traffic activity during the vacation season, extensive burning of plant residues and wood during the May holidays, and pollen dispersion. During the summer months, with the reduction of significant forest and agricultural fires, the decrease in vehicular traffic, and the development of grass and deciduous cover, the concentrations of most PHEs decrease. This trend is particularly evident in July, when typical amounts of atmospheric precipitation occur due to active convection in cyclonic conditions, aiding in the dispersion of pollutants. In September, against the backdrop of a small amount of precipitation, there is an increase in PHE concentrations due to increased transportation activity, intense biomass burning during agricultural activities, and the expansion of unvegetated soil areas.

For the first time, data obtained for Moscow on the distribution of PHEs in atmospheric precipitation during the warm season showed significant enrichment of rainwater with Sb ( $EF > 10,000$ ), Pb ( $> 8,000$ ), Cd, Zn (1,000–2,000), Cu, B, Bi, P, and Sr (100–500). The main sources of PHEs are non-exhaust vehicle emissions, resuspension of contaminated soil particles, emissions from industrial facilities, transport of construction dust, biomass and waste burning, and forest fires. Additionally, precipitation shows moderate enrichment with Ba, Mn, Ni, Co, and Sn ( $EF$  15–69), with their input from the mentioned sources occurring episodically. The content of PHEs increases with reduced precipitation amounts and increased levels of solid particles and pH in rainwater.



Multivariate regression analysis identified the leading factors affecting PHE concentrations in Moscow's precipitation. For most elements, solid particles serve as a significant source of PHEs, with their accumulation in the atmosphere increasing with the duration of dry periods and their partial dissolution being particularly pronounced in acidic rainfall. During the warm period of 2019, long-range transport was also a significant factor: episodes with very high concentrations of PHEs in rainwater were identified, during which air advection from Southern Europe and southern regions of European Russia predominated, or the contribution of regional pollution sources dominated, or a significant contribution was made by advection from the north of Western Siberia, where forest fires were observed.

When air advection occurred from the North Atlantic, the Arctic, and the northern part of Northern Europe, PHE concentrations in precipitation generally decreased, but some elements (Rb, Sb, Pb, As, Bi, Cd, P, Ba) increased their content.

A limitation of the obtained results is the analysis of only the dissolved phase of PHEs in rainfall, whereas the insoluble phase can be an essential form for some PHEs in precipitation. Therefore, further research is needed to include the analysis of the insoluble phase of PHEs. Additionally, to assess more accurately the influence of various sources, it is necessary to study the seasonal and interannual variability of atmospheric pollution. ■

## REFERENCES

- Adhikari S., Zeng C., Zhang F., Paudel Adhikari N., Gao J., Ahmed N., Quaiyum Bhuiyan M.A., Ahsan M.A., and Rahaman Khan M.H. (2023). Atmospheric wet deposition of trace elements in Bangladesh: A new insight into spatiotemporal variability and source apportionment. *Environmental Research*, 217, 114729, DOI: 10.1016/j.envres.2022.114729.
- Alves C.A., Evtugina M., Vicente A.M.P., Vicente E.D., Nunes T.V., Silva P.M.A., Duarte M.A.C., Pio C.A., Amato F., and Querol X. (2018). Chemical profiling of PM10 from urban road dust. *Science of The Total Environment*, 634, 41–51, DOI: 10.1016/j.scitotenv.2018.03.338.
- Amato F., Pandolfi M., Viana M., Querol X., Alastuey A., and Moreno T. (2009). Spatial and chemical patterns of PM10 in road dust deposited in urban environment. *Atmospheric Environment*, 43 (9), 1650–1659, DOI: 10.1016/j.atmosenv.2008.12.009.
- Bayramoğlu Karşı M.B., Yenisoý-Karakaş S., and Karakaş D. (2018). Investigation of washout and rainout processes in sequential rain samples. *Atmospheric Environment*, 190, 53–64, DOI: 10.1016/j.atmosenv.2018.07.018.
- Bencharif-Madani F., Ali-Khodja H., Kemmouche A., Terrouche A., Lokorai K., Naidja L., and Bouziane M. (2019). Mass concentrations, seasonal variations, chemical compositions and element sources of PM10 at an urban site in Constantine, northeast Algeria. *Journal of Geochemical Exploration*, 206, 106356, DOI: 10.1016/j.gexplo.2019.106356.
- Bezrukova N.A. and Chernokulsky A.V. (2023). Russian studies on clouds and precipitation in 2019–2022. *Izvestiya, Atmospheric and Oceanic Physics*, 59 (S3), S294–S325, DOI: 10.1134/S0001433823150033.
- Borsato A., Johnston V.E., Frisia S., Miorandi R., and Corradini F. (2016). Temperature and altitudinal influence on karst dripwater chemistry: Implications for regional-scale palaeoclimate reconstructions from speleothems. *Geochimica et Cosmochimica Acta*, 177, 275–297, DOI: 10.1016/j.gca.2015.11.043.
- Budai P. and Clement A. (2018). Spatial distribution patterns of four traffic-emitted heavy metals in urban road dust and the resuspension of brake-emitted particles: Findings of a field study. *Transportation Research Part D: Transport and Environment*, 62, 179–185, DOI: 10.1016/j.trd.2018.02.014.
- Cable E. and Deng Y. (2018). Trace elements in atmospheric wet precipitation in the Detroit metropolitan area: Levels and possible sources. *Chemosphere*, 210, 1091–1098, DOI: 10.1016/j.chemosphere.2018.07.103.
- Chon K., Kim Y., Bae D.H., and Cho J. (2015). Confirming anthropogenic influences on the major organic and inorganic constituents of rainwater in an urban area. *Drinking Water Engineering and Science*, 8 (2), 35–48, DOI: 10.5194/dwes-8-35-2015.
- Christian T.J., Yokelson R.J., Cardenas B., Molina L.T., and Engling G. (2010). Trace gas and particle emissions from domestic and industrial biofuel use and garbage burning in central Mexico. *Atmospheric Chemistry and Physics*, 10, 565–584, DOI: 10.5194/acp-10-565-2010.
- Chubarova N.E., Nezval' E.I., Belikov I.B., Gorbarenko E.V., Eremina I.D., Zhdanova E.Yu., Korneva I.A., Konstantinov P.I., Lokoshchenko M.A., Skorokhod A.I., and Shilovtseva O.A. (2014). Climatic and environmental characteristics of Moscow megalopolis according to the data of the Moscow State University Meteorological Observatory over 60 years. *Russian Meteorology and Hydrology*, 39 (9), 602–613, DOI: 10.3103/S1068373914090052.
- Chubarova N., Zhdanova Y., Androsova Y., Kirsanov A., Shatunova M., Khlestova Y., Volpert Y., Poliukhov A., Eremina I., Vlasov D., Popovicheva O., Ivanov A., Gorbarenko Y., Nezval Y., Blinov D., and Rivin G. (2020). The aerosol urban pollution and its effects on weather, regional climate and geochemical processes. Moscow, Russia: LLC MAKs Press.
- Chubarova N., Androsova E., Kirsanov A., Varentsov M., and Rivin G. (2024). Urban aerosol, its radiative and temperature response in comparison with urban canopy effects in megacity based on COSMO-ART modeling. *Urban Climate*, 53, 101762, DOI: 10.1016/j.uclim.2023.101762.
- Chudaeva V.A., Chudaev O.V., and Yurchenko S.G. (2008). Chemical composition of precipitation in the southern part of the Russian Far East. *Water Resources*, 35 (1), 58–70, DOI: 10.1134/S0097807808010077.
- Demetriades A. and Birke M. (2015). Urban topsoil geochemical mapping manual: URGE II; 2015 International Year of Soils. Brussels: EuroGeoSurveys.
- Eremina I.D., Aloyan A.E., Arutyunyan V.O., Larin I.K., Chubarova N.E., and Yermakov A.N. (2015). Acidity and mineral composition of precipitation in Moscow: Influence of deicing salts. *Izvestiya, Atmospheric and Oceanic Physics*, 51 (6), 624–632, DOI: 10.1134/S0001433815050047.
- Ermakov V., Perelomov L., Khushvakhtova S., Tyutikov S., Danilova V., and Safonov V. (2017). Biogeochemical assessment of the urban area in Moscow. *Environmental Monitoring and Assessment*, 189 (12), 641, DOI: 10.1007/s10661-017-6363-y.
- Ermolin M.S., Fedotov P.S., Ivaneev A.I., Karandashev V.K., Fedyunina N.N., and Burmistrov A.A. (2018). A contribution of nanoscale particles of road-deposited sediments to the pollution of urban runoff by heavy metals. *Chemosphere*, 210, 65–75, DOI: 10.1016/j.chemosphere.2018.06.150.
- European Borates Association (2011). Borates. [online] Available at: [https://www.ima-europe.eu/sites/ima-europe.eu/files/minerals/Borate\\_An-WEB-2011.pdf](https://www.ima-europe.eu/sites/ima-europe.eu/files/minerals/Borate_An-WEB-2011.pdf) [Accessed 28 July 2020].
- Feddes J.J.R., Cook H., and Zuidhof M.J. (1992). Characterization of airborne dust particles in turkey housing. *Canadian Agricultural Engineering*, 34, 273–280, DOI: 10.7939/R3BK1734C.

- Fedotov P.S., Ermolin M.S., Karandashev V.K., and Ladonin D.V. (2014). Characterization of size, morphology and elemental composition of nano-, submicron, and micron particles of street dust separated using field-flow fractionation in a rotating coiled column. *Talanta*, 130, 1–7, DOI: 10.1016/j.talanta.2014.06.040.
- FIRMS (2024). NASA's Fire Information for Resource Management System. [online] Available at: <https://firms.modaps.eosdis.nasa.gov/> [Accessed 2 May 2024].
- Global Coal Plant Tracker (2024). Global Energy Monitor. [online] Available at: <https://globalenergymonitor.org/projects/global-coal-plant-tracker/tracker/> [Accessed 12 July 2024].
- Grigoratos T. and Martini G. (2015). Brake wear particle emissions: a review. *Environmental Science and Pollution Research*, 22 (4), 2491–2504, DOI: 10.1007/s11356-014-3696-8.
- Grivas G., Cheristanidis S., Chaloulakou A., Koutrakis P., and Mihalopoulos N. (2018). Elemental composition and source apportionment of fine and coarse particles at traffic and urban background locations in Athens, Greece. *Aerosol and Air Quality Research*, 18 (7), 1642–1659, DOI: 10.4209/aaqr.2017.12.0567.
- Gubanov D.P., Iordanskii M.A., Kuderina T.M., Skorokhod A.I., Elansky N.F., and Minashkin V.M. (2021). Elemental composition of aerosols in the near-surface air of Moscow: Seasonal changes in 2019 and 2020. *Atmospheric and Oceanic Optics*, 34 (5), 475–482, DOI: 10.1134/S1024856021050122.
- Gunawardana C., Goonetilleke A., Egodawatta P., Dawes L., and Kokot S. (2012). Source characterisation of road dust based on chemical and mineralogical composition. *Chemosphere*, 87 (2), 163–170, DOI: 10.1016/j.chemosphere.2011.12.012.
- Guo J., Kang S., Huang J., Zhang Q., Tripathi L., and Sillanpää M. (2014). Seasonal variations of trace elements in precipitation at the largest city in Tibet, Lhasa. *Atmospheric Research*, 153, 87–97, DOI: 10.1016/j.atmosres.2014.07.030.
- Harrison R.M., Jones A.M., Gietl J., Yin J., and Green D.C. (2012). Estimation of the contributions of brake dust, tire wear, and resuspension to nonexhaust traffic particles derived from atmospheric measurements. *Environmental Science & Technology*, 46 (12), 6523–6529, DOI: 10.1021/es300894r.
- Hulskotte J.H.J., Roskam G.D., and Denier van der Gon H.A.C. (2014). Elemental composition of current automotive braking materials and derived air emission factors. *Atmospheric Environment*, 99, 436–445, DOI: 10.1016/j.atmosenv.2014.10.007.
- Ivanev A.I., Brzhezinskiy A.S., Karandashev V.K., Ermolin M.S., and Fedotov P.S. (2023). Assessment of sources, environmental, ecological, and health risks of potentially toxic elements in urban dust of Moscow megacity, Russia. *Chemosphere*, 321, 138142, DOI: 10.1016/j.chemosphere.2023.138142.
- Jain S., Sharma S.K., Mandal T.K., and Saxena M. (2018). Source apportionment of PM10 in Delhi, India using PCA/APCS, UNMIX and PMF. *Particuology*, 37, 107–118, DOI: 10.1016/j.partic.2017.05.009.
- Kasimov N., Chalov S., Chubarova N., Kosheleva N., Popovicheva O., Shartova N., Stepanenko V., Androsova E., Chichayeva M., Erina O., Kirsanov A., Kovach R., Revich B., Shinkareva G., Tereshina M., Varentsov M., Vasil'chuk J., Vlasov D., Denisova I., and Minkina T. (2024). Urban heat and pollution island in the Moscow megacity: Urban environmental compartments and their interactions. *Urban Climate*, 55, 101972, DOI: 10.1016/j.uclim.2024.101972.
- Kasimov N.S., Kosheleva N.E., Popovicheva O.B., Vlasov D.V., Shinkareva G.L., Erina O.N., Chalov S.R., Chichayeva M.A., Kovach R.G., Zavgorodnyaya Yu.A., and Lychagin M.Yu. (2023). Moscow megacity pollution: Monitoring of chemical composition of microparticles in the Atmosphere–Snow–Road Dust–Soil–Surface Water system. *Russian Meteorology and Hydrology*, 48 (5), 391–401, DOI: 10.3103/S1068373923050011.
- Kasimov N.S., Kosheleva N.E., Vlasov D.V., Nabelkina K.S., and Ryzhov A.V. (2019). Physicochemical properties of road dust in Moscow. *Geography, Environment, Sustainability*, 12 (4), 96–113, DOI: 10.24057/2071-9388-2019-55.
- Kasimov N.S., Vlasov D.V., and Kosheleva N.E. (2020). Enrichment of road dust particles and adjacent environments with metals and metalloids in eastern Moscow. *Urban Climate*, 32, 100638, DOI: 10.1016/j.uclim.2020.100638.
- Kolesnikova V.M., Salimgareeva O.A., Ladonin D.V., Vertyankina V.Y., and Shelegina A.S. (2023). Morphological and mineralogical characteristics of atmospheric microparticles and chemical pollution of street dust in the Moscow Region. *Atmosphere*, 14 (2), 403, DOI: 10.3390/atmos14020403.
- Konstantinova E., Minkina T., Konstantinov A., Sushkova S., Antonenko E., Kurasova A., and Loiko S. (2022). Pollution status and human health risk assessment of potentially toxic elements and polycyclic aromatic hydrocarbons in urban street dust of Tyumen city, Russia. *Environmental Geochemistry and Health*, 44, 409–432, DOI: 10.1007/s10653-020-00692-2.
- Konstantinova E., Minkina T., Nevidomskaya D., Lychagin M., Bezberdaya L., Burachevskaya M., Rajput V.D., Zamulina I., Bauer T., and Mandzhieva S. (2024). Potentially toxic elements in urban soils of the coastal city of the Sea of Azov: Levels, sources, pollution and risk assessment. *Environmental Research*, 252, 119080, DOI: 10.1016/j.envres.2024.119080.
- Kosheleva N.E., Kasimov N.S., and Vlasov D.V. (2015). Factors of the accumulation of heavy metals and metalloids at geochemical barriers in urban soils. *Eurasian Soil Science*, 48 (5), 476–492, DOI: 10.1134/S1064229315050038.
- Kosheleva N.E., Vlasov D.V., Korlyakov I.D., and Kasimov N.S. (2018). Contamination of urban soils with heavy metals in Moscow as affected by building development. *Science of The Total Environment*, 636, 854–863, DOI: 10.1016/j.scitotenv.2018.04.308.
- Kosheleva N.E., Vlasov D.V., Timofeev I.V., Samsonov T.E., and Kasimov N.S. (2023). Benzo[a]pyrene in Moscow road dust: pollution levels and health risks. *Environmental Geochemistry and Health*, 45, 1669–1694, DOI: 10.1007/s10653-022-01287-9.
- Kumar S., Aggarwal S.G., Gupta P.K., and Kawamura K. (2015). Investigation of the tracers for plastic-enriched waste burning aerosols. *Atmospheric Environment*, 108, 49–58, DOI: 10.1016/j.atmosenv.2015.02.066.
- Ladonin D.V. and Mikhaylova A.P. (2020). Heavy metals and arsenic in soils and street dust of the Southeastern Administrative District of Moscow: Long-term data. *Eurasian Soil Science*, 53 (11), 1635–1644, DOI: 10.1134/S1064229320110095.
- Ma C.-J. and Kang G.-U. (2018). Particle scavenging properties of rain clarified by a complementary study with bulk and semi-bulk samples. *Journal of Korean Society for Atmospheric Environment*, 34 (1), 177–186, DOI: 10.5572/KOSAE.2018.34.1.177.
- Meng Y., Li R., Cui L., Wang Z., and Fu H. (2022). Phosphorus emission from open burning of major crop residues in China. *Chemosphere*, 288, 132568, DOI: 10.1016/j.chemosphere.2021.132568.
- Morera-Gómez Y., Alonso-Hernández C.M., Santamaría J.M., Elustondo D., Lasheras E., and Widory D. (2020). Levels, spatial distribution, risk assessment, and sources of environmental contamination vectored by road dust in Cienfuegos (Cuba) revealed by chemical and C and N stable isotope compositions. *Environmental Science and Pollution Research*, 27 (2), 2184–2196, DOI: 10.1007/s11356-019-06783-7.
- Moskovchenko D., Pozhitkov R., and Ukarkhanova D. (2022). Geochemistry of street dust in Tyumen, Russia: influence of traffic load. *Environmental Science and Pollution Research*, 29, 31180–31197, DOI: 10.1007/s11356-021-18013-0.
- Niyobuhungiro R.V. and Blottnitz H. von (2013). Investigation of arsenic airborne in particulate matter around caterers' wood fires in the Cape Town region. *Aerosol and Air Quality Research*, 13 (1), 219–224, DOI: 10.4209/aaqr.2012.06.0148.

- NSAM № 520 AES/MS (2017). Determination of the elemental composition of natural, drinking, sewage and sea waters by atomic emission and mass spectral methods with inductively coupled plasma. Moscow, Russia.
- Orlović-Leko P., Vidović K., Ciglencečki I., Omanović D., Sikirić M.D., and Šimunić I. (2020). Physico-chemical characterization of an urban rainwater (Zagreb, Croatia). *Atmosphere*, 11 (2), 144, DOI: 10.3390/atmos11020144.
- Ozaki H., Yoshimura K., Asaoka Y., and Hayashi S. (2021). Antimony from brake dust to the combined sewer collection system via road effluent under rainy conditions. *Environmental Monitoring and Assessment*, 193 (6), 369, DOI: 10.1007/s10661-021-09152-5.
- Özsoy T. and Örnektekin S. (2009). Trace elements in urban and suburban rainfall, Mersin, Northeastern Mediterranean. *Atmospheric Research*, 94 (2), 203–219, DOI: 10.1016/j.atmosres.2009.05.017.
- Padoan E., Malandrino M., Giacomino A., Grosa M.M., Lollobrigida F., Martini S., and Abollino O. (2016). Spatial distribution and potential sources of trace elements in PM10 monitored in urban and rural sites of Piedmont Region. *Chemosphere*, 145, 495–507, DOI: 10.1016/j.chemosphere.2015.11.094.
- Pant P. and Harrison R.M. (2013). Estimation of the contribution of road traffic emissions to particulate matter concentrations from field measurements: A review. *Atmospheric Environment*, 77, 78–97, DOI: 10.1016/j.atmosenv.2013.04.028.
- Park S.-M., Seo B.-K., Lee G., Kahng S.-H., and Jang Y. (2015). Chemical composition of water soluble inorganic species in precipitation at Shihwa basin, Korea. *Atmosphere*, 6 (6), 732–750, DOI: 10.3390/atmos6060732.
- Polyakova O.V., Artaev V.B., and Lebedev A.T. (2018). Priority and emerging pollutants in the Moscow rain. *Science of The Total Environment*, 645, 1126–1134, DOI: 10.1016/j.scitotenv.2018.07.215.
- Popovicheva O., Diapouli E., Chichaeva M., Kosheleva N., Kovach R., Bitukova V., Eleftheriadis K., and Kasimov N. (2024). Aerosol characterization and peculiarities of source apportionment in Moscow, the largest and northernmost European megacity. *Science of The Total Environment*, 918, 170315, DOI: 10.1016/j.scitotenv.2024.170315.
- Popovicheva O.B., Volpert E., Sitnikov N.M., Chichaeva M.A., and Padoan S. (2020). Black carbon in spring aerosols of Moscow urban background. *Geography, Environment, Sustainability*, 13 (1), 233–243, DOI: 10.24057/2071-9388-2019-90.
- Ramírez O., Sánchez de la Campa A.M., Amato F., Moreno T., Silva L.F., and de la Rosa J.D. (2019). Physicochemical characterization and sources of the thoracic fraction of road dust in a Latin American megacity. *Science of The Total Environment*, 652, 434–446, DOI: 10.1016/j.scitotenv.2018.10.214.
- Rathore D.S., Singh P., Misra C.D., Chandel C.P.S., Bugalia S., and Gupta K.S. (2023). Heavy and less common metals in rainwater and the kinetics of the oxidation of hydrogen sulfide by oxygen in rainwater medium. *Environmental Monitoring and Assessment*, 195 (6), 762, DOI: 10.1007/s10661-023-11374-8.
- Rolph G., Stein A., and Stunder B. (2017). Real-time Environmental Applications and Display sYstem: READY. *Environmental Modelling & Software*, 95, 210–228, DOI: 10.1016/j.envsoft.2017.06.025.
- Romzaykina O.N., Vasenev V.I., Paltseva A., Kuzyakov Y.V., Neaman A., and Dovletyarova E.A. (2021). Assessing and mapping urban soils as geochemical barriers for contamination by heavy metal(loid)s in Moscow megapolis. *Journal of Environmental Quality*, 50, 22–37, DOI: 10.1002/jeq2.20142.
- Rudnick R.L. and Gao S. (2014). Composition of the Continental Crust, in *Treatise on Geochemistry*, Elsevier, pp. 1–51.
- Seinfeld J.H. and Pandis S.N. (2016). *Atmospheric Chemistry and Physics: From Air Pollution to Climate Change*, Third Edition. ed. Hoboken, New Jersey, USA: John Wiley & Sons.
- Semenets E.S., Svistov P.F., and Talash A.S. (2017). Chemical composition of atmospheric precipitation in Russian Subarctic. *Bulletin of the Tomsk Polytechnic University. Geo Assets Engineering*, 328 (3), 27–36.
- Serdyukova A.D., Vlasov D.V., Popovicheva O.B., Kosheleva N.E., Chichaeva M.A., and Kasimov N.S. (2023). Elemental composition of atmospheric PM10 during COVID-19 lockdown and recovery periods in Moscow (April–July 2020). *Environmental Geochemistry and Health*, 45, 7909–7931, DOI: 10.1007/s10653-023-01698-2.
- Song F. and Gao Y. (2009). Chemical characteristics of precipitation at metropolitan Newark in the US East Coast. *Atmospheric Environment*, 43 (32), 4903–4913, DOI: 10.1016/j.atmosenv.2009.07.024.
- Stein A.F., Draxler R.R., Rolph G.D., Stunder B.J.B., Cohen M.D., and Ngan F. (2015). NOAA's HYSPLIT Atmospheric Transport and Dispersion Modeling System. *Bulletin of the American Meteorological Society*, 96 (12), 2059–2077, DOI: 10.1175/BAMS-D-14-00110.1.
- Stepanets V.N., Malygina N.S., Lovtskaya O.V., and Papina T.S. (2021). Regional-scale impacts of the major tin plant on the chemical composition of atmospheric precipitation in the south of Western Siberia (Russia). *Environmental Earth Sciences*, 80 (20), 701, DOI: 10.1007/s12665-021-09970-3.
- Tsamos P., Koliass P., Lambropoulou D., and Noli F. (2022). Distribution and temporal variability of uranium and toxic metal(loid)s in snow and rainwater from an oil industry and urban area in Thessaloniki-Greece. *Science of The Total Environment*, 838, 155604, DOI: 10.1016/j.scitotenv.2022.155604.
- Vetrova A.A., Sazonova O.I., Ivanova A.A., Streletskii R.A., Sarzhanov D.A., Korneykova M.V., Novikov A.I., Vasenev V.I., Ivashchenko K.V., Slukovskaya M.V., and Gavrichkova O. (2023). Diversity of microbial communities, PAHs, and metals in road and leaf dust of functional zones of Moscow and Murmansk. *Microorganisms*, 11 (2), 526, DOI: 10.3390/microorganisms11020526.
- Vlasov D.V., Eremina I.D., Shinkareva G.L., Chubarova N.E., and Kasimov N.S. (2021a). Daily variations in wet deposition and washout rates of potentially toxic elements in Moscow during spring season. *Geography, Environment, Sustainability*, 14 (1), 219–233, DOI: 10.24057/2071-9388-2020-162.
- Vlasov D.V., Kasimov N., Eremina I., Shinkareva G., and Chubarova N. (2021b). Partitioning and solubilities of metals and metalloids in spring rains in Moscow megacity. *Atmospheric Pollution Research*, 12 (1), 255–271, DOI: 10.1016/j.apr.2020.09.012.
- Vlasov D.V., Kosheleva N., and Kasimov N. (2021c). Spatial distribution and sources of potentially toxic elements in road dust and its PM10 fraction of Moscow megacity. *Science of The Total Environment*, 761, 143267, DOI: 10.1016/j.scitotenv.2020.143267.
- Vlasov D.V., Kukushkina O.V., Kosheleva N.E., and Kasimov N.S. (2022). Levels and factors of the accumulation of metals and metalloids in roadside soils, road dust and their PM10 fraction in the Western Okrug of Moscow. *Eurasian Soil Science*, 55 (5), 556–572, DOI: 10.1134/S1064229322050118.
- Vlasov D.V., Kasimov N., Eremina I., Shinkareva G., and Chubarova N. (2023a). Major ions and potentially toxic elements in atmospheric precipitation during the COVID-19 lockdown in Moscow megacity. *Urban Climate*, 48, 101422, DOI: 10.1016/j.uclim.2023.101422.
- Vlasov D.V., Vasil'chuk J.Yu., Kosheleva N.E., and Kasimov N.S. (2023b). Contamination levels and source apportionment of potentially toxic elements in size-fractionated road dust of Moscow. *Environmental Science and Pollution Research*, 30 (13), 38099–38120, DOI: 10.1007/s11356-022-24934-1.
- von Gunten K., Konhauser K.O., and Alessi D.S. (2020). Potential of asphalt concrete as a source of trace metals. *Environmental Geochemistry and Health*, 42 (2), 397–405, DOI: 10.1007/s10653-019-00370-y.

- Wada K., Simpson R., Kishimoto N., and Takei N. (2020). Motor vehicle wash-off water as a source of phosphorus in roadway runoff. *Journal of Water and Environment Technology*, 18 (1), 9–16, DOI: 10.2965/jwet.19-047.
- Xu Y., Li Q., Xie S., Zhang C., Yan F., Liu Y., Kang S., Gao S., and Li C. (2022). Overestimation of anthropogenic contribution of heavy metals in precipitation than those of aerosol samples due to different treatment methods. *Environmental Pollution*, 300, 118956, DOI: 10.1016/j.envpol.2022.118956.
- Yanchenko N.I. and Yaskina O.L. (2014). Features of chemical composition of snow cover and precipitation in Bratsk. *Bulletin of the Tomsk Polytechnic University. Geo Assets Engineering*, 324, 27–35.
- Yang X., Wang X., Zhang Y., Lee J., Su J., and Gates R.S. (2011). Characterization of trace elements and ions in PM10 and PM2.5 emitted from animal confinement buildings. *Atmospheric Environment*, 45 (39), 7096–7104, DOI: 10.1016/j.atmosenv.2011.09.037.
- Zappi A., Popovicheva O., Tositti L., Chichaeva M., Eremina I., Kasper-Giebl A., Tsai Y.I., Vlasov D., and Kasimov N. (2023). Factors influencing aerosol and precipitation ion chemistry in urban background of Moscow megacity. *Atmospheric Environment*, 294, 119458, DOI: 10.1016/j.atmosenv.2022.119458.
- Zeng J., Yue F.-J., Li S.-L., Wang Z.-J., Wu Q., Qin C.-Q., and Yan Z.-L. (2020). Determining rainwater chemistry to reveal alkaline rain trend in Southwest China: Evidence from a frequent-rainy karst area with extensive agricultural production. *Environmental Pollution*, 266, 115166, DOI: 10.1016/j.envpol.2020.115166.
- Zeng J., Han G., Wu Q., Peng M., Ge X., Mao S., Wang Z.-J., and Ma Q. (2024a). Chemical evolution of rainfall in China's first eco-civilization demonstration city: Implication for the provenance identification of pollutants and rainwater acid neutralization. *Science of The Total Environment*, 910, 168567, DOI: 10.1016/j.scitotenv.2023.168567.
- Zeng J., Han G., Zhang S., Zhang Q., and Qu R. (2024b). Potentially toxic elements in rainwater during extreme rainfall period in the megacity Beijing: Variations, sources, and reuse potential. *Atmospheric Environment*, 318, 120242, DOI: 10.1016/j.atmosenv.2023.120242.
- Zheng J., Zhan C., Yao R., Zhang J., Liu H., Liu T., Xiao W., Liu X., and Cao J. (2018). Levels, sources, markers and health risks of heavy metals in PM2.5 over a typical mining and metallurgical city of Central China. *Aerosol Science and Engineering*, 2 (1), 1–10, DOI: 10.1007/s41810-017-0018-9.



# CAPACITY AND CURRENT USE OF THE FORMOSO RIVER WATERSHED, BONITO MUNICIPALITY, MATO GROSSO DO SUL, BRAZIL: CONFLICTS AND LAND USE RECOMMENDATIONS

**Rafael Brugnolli Medeiros<sup>1\*</sup>, Charlei Aparecido da Silva<sup>1</sup>**

<sup>1</sup> Federal University of Grande Dourados/Faculdade de Ciências Humanas, Rodovia Dourados/Itahum, Km 12, Cidade Universitária, Dourados/MS, 79.804-970, Brazil

\*Corresponding author: [rafaelmedeiros@ufgd.edu.br](mailto:rafaelmedeiros@ufgd.edu.br)

Received: December 18<sup>th</sup> 2023 / Accepted: September 1<sup>st</sup> 2024 / Published: October 1<sup>st</sup> 2024

<https://doi.org/10.24057/2071-9388-2024-3159>

**ABSTRACT.** The lack of planning and feasibility of controlling actions over land use and land cover lead to relationship problems between the support capacity that environmental systems present and their current use. The goal of this study is to figure out how much land can be used based on its natural and physical features and to find problems that come up because of the heavy use in the Formoso River watershed. It is one of the most recognized Brazilian watersheds, due to its turistic, karst, and environmental characteristics. The methodology consists in handling and generating data in a GIS environment by performing a synthesis map, as well as adopting geoprocessing criteria and techniques in the field to validate the collected data. The results indicate that the watershed presents large areas without conflicts due to its numerous conservation units. However, major conflicts are identified in other areas, affecting the balance and dynamics of the landscape and its water resources. Such conflicts arise because soybean crops advance in fragile and karst areas. The highest concentration of conflict is only 1.61%, particularly near the Formoso River marsh. Therefore, the present work considers a methodology that assesses the capacity of use through a method that has produced a summary document that is applicable and compatible with the karst system

**KEYWORDS:** karst system, water resources, land use, geoprocessing, environmental fragility

**CITATION:** Brugnolli R. M., Silva C. A. da (2024). Capacity And Current Use Of The Formoso River Watershed, Bonito Municipality, Mato Grosso Do Sul, Brazil: Conflicts And Land Use Recommendations. *Geography, Environment, Sustainability*, 3(17), 85-97

<https://doi.org/10.24057/2071-9388-2024-3159>

**ACKNOWLEDGEMENTS:** This study was conducted thanks to the support of the Coordenação de Aperfeiçoamento de Pessoal de Nível Superior—CAPES and the Fundação de Apoio ao Desenvolvimento do Ensino, Ciência e Tecnologia do Estado de Mato Grosso do Sul—FUNDECT. The project was developed at the Federal University of Grande Dourados, where the Physical Geography Laboratory - LGF ([www.lgf-neef.com](http://www.lgf-neef.com)) provides the physical and software support required to conduct this research.

**Conflict of interests:** The authors reported no potential conflict of interest.

## INTRODUCTION

Karst systems offer considerable potential for various uses and activities, including limestone mining, tourism, and monoculture agriculture. This is due to the presence of carbonate rocks, which create fertile soils and relatively flat landscapes. Karst's potential for such activities is undeniable, but their use can trigger impacts and processes that lead to environmental damage. In short, medium, and long terms, significant damages occur, such as sinkholes and landslides caused by rocks depleted by the karst process, contamination of aquifers (Tavares; Vieira and Uagoda 2023), degradation of speleological assets, and impacts on the quality of surface waters. The karst is affected in a big way when its weaknesses are ignored in order to support the development bias of public and private bodies and

documents (like ecological-economic zoning and master plans). Van Beynen, Brinkmann and Van Beynen (2012) highlight the mining activity as the cause for karst damage, whereas Ford and Williams (2007) and Silva and Moraes (2011) indicate that monoculture is an activity that stands out in terms of causing karst implications, contributing to losses in this type of landscape. In both economic activities, sediments and residues transported by rainwater generate impacts that are often irreversible in a karst system. Parise, De Waele and Gutierrez (2009) and Parise (2012) state that the process of transporting sediments from agriculture and mining causes changes in groundwater flow and the quality of surface waters. Therefore, the environmental impacts arising from anthropic actions occur due to the lack of knowledge and comprehension on the relevance of land use, land cover, and the vegetative canopy that covers

the soil in these environments. We highlight here anthropic actions, such as degradation of slopes and valleys, the obliteration of sinkholes, pollution of reservoirs and karst aquifers, the constant use of aquifers for irrigation, and its consequent loss of natural replenishment capacity (Burri et al. 1999). All forms of occupation in a karst watershed must consider its capacity of use in order to cause minimum conflicts with regard to its current use. Lepsch et al. (1991) define capacity of use as possibilities and limitations of use, suitable or not for certain purposes according to the physical environment conditions. Leal (1995) defines capacity as the type of use exercised in a given landscape unit without causing environmental changes or modifying the intrinsic dynamics of the units.

According to Ochieng Odhiambo (2000), Castro and Nielsen (2001) and Hilson (2002) conflicts over natural resources are concerning and debilitating; environmental degradation affects the entire society. The dynamics of land use and land cover are critical watershed management issues, yet the cumulative impacts of these changes are difficult to discern and manage in the typical practice of land use planning (Erickson 1995). Therefore, evaluating the current use and occupation is essential for the territorial and environmental management of watersheds. In addition to providing subsidies for urban and regional planning, it enables a rational relationship between the anthropic advance of land and natural resources (Wilson 2014). The fact that this relationship may be analyzed on a local and regional scale and on a temporal scale brings up the possibility of becoming an environmental monitoring instrument (Angel et al. 2005; Cohen 2006). Suitable forms of land use and land cover for environmental purposes become effective since the existing interactions between the components of the landscape are evaluated, their weaknesses and potentialities, as well as the internal and external influences that affect the system. Thus, negative impacts of use are minimized.

Identifying such contexts in the region of Bonito is a challenge due to the imminent use of its lands for soybean monoculture, which causes recurrent clouding of scenic rivers (Ribeiro 2018; Brugnolli et al. 2022), and damages to its fragile and still preserved karst features. Boggiani et al. (2002) and Sallun Filho, Karmann and Boggiani (2004) point out that the karst characteristics in Bonito, more precisely on Serra da Bodoquena, bring several environmental concerns due to the rapid occupation of the area. The process increases the removal of forest vegetation to allow monocultures and pastures to enter. The mountain karst and its surroundings are extremely vulnerable, and their use requires restrictions. Therefore, the assessment of the system's capacity for use and actual use contributes to watershed management. The present work adopted the Formoso River Watershed as its study area because it is the largest and most significant watershed in Bonito; it has a municipal dimension but is of global relevance, given its potential and recognition as a tourist destination. Large extensions of native forests (Serra da Bodoquena) and soybean crops can be seen in the upper and mid-course of the river. The way land has been used without adequate management, added to other existing anthropic activities, such as cattle confinement areas, limestone extraction, extensive livestock, and tourism, leads to environmental disturbances. In addition, it generates pressure on surface waters that depend directly on the conservation and maintenance of the watershed balance. Evaluating the support capacity brings a technical document with data to assist in a balanced use that may be a conditioning factor for planning and managing the development

on a sustainable basis (Narendra et al. 2021). Although seeking the balance between anthropic actions and the environment is complex, the performance of documents like the one proposed by this work may guide actions and recommendations to reconcile the needs of society with the territory capacity of support.

In addition, some areas have high erosive potential due to their steep slopes. Brugnolli (2023) describes methodologies that assess this potential by analyzing slope, horizontal, and vertical dissection to gauge the likelihood of morphogenetic processes occurring. This approach generates a document that summarizes the terrain's characteristics. The analysis is based on General Systems Theory, which focuses on understanding the interconnected and systemic relationships between different elements. Recognizing that vegetation is essential for minimizing erosion potential, it is concerning that there is little native vegetation outside conservation units. Much of the land not designated for primary vegetation has already lost its ecological balance and is moving towards critical levels of degradation.

It is relevant to highlight the lack of studies and federal, state, and local laws that take karst and its unique dynamics into account. Thus, such a diagnosis in the municipality of Bonito, precisely in the Formoso River Watershed, was carried out aiming to assess the capacity of use and its real use, identifying land use conflicts by following a congruence between capacity, environmental fragility, and the current intensity of use. The Formoso River Watershed (FRW) is located southwest of the state of Mato Grosso do Sul (Fig. 1), in an area of 1,324.67 km<sup>2</sup>. Its spring is located in the Serra da Bodoquena, while its mouth is located mid-course on the left bank of the Miranda River.

## Materials and Methods

The methodology consists of investigating the components of the landscape, identifying the capacity of use, current use, and the conflicts involved in this relationship. The starting point was the lithology of rocks that was carried out with the support of GIS ArcGis 10® using the geological map provided by the Geological Survey of Brazil (Serviço Geológico do Brasil – SGB). A more detailed study was performed using satellite images and field trips to visualize the outcrops and handle rocks along local highways, banks of water sources, and in the midst of pastures and vegetation throughout the Formoso River Watershed. The rainfall was linked to the mapping carried out by Zavattini (1992), which discusses the distribution of precipitation with a climatic regionalization due to the influences of air masses and rainfall in the state of Mato Grosso do Sul. For the relief, we carried out slope and erosive potential energy analysis of the relief, following the methodologies of Brugnolli (2020) and Brugnolli (2024). For the slope analysis, we imported the Digital Elevation Model (DEM/SRTM) based on the classes of the Brazilian Soil Classification System (Sistema Brasileiro de Classificação de Solos – SIBCS 2018), Lepsch et al. (1991) and Ramalho Filho and Beek (1995) for the relief classifications and their facilities, and land use limitations. The erosive potential energy of the relief is defined as the potential erosion capacity or the amount of soil loss that the watershed is capable of promoting. We identified horizontal and vertical dissections with declivity in agreement with a synthesis product described by Mendes (1993) and Brugnolli, Berezuk and Silva (2019). The procedure consists of data interpolation in GIS ArcGis10®, in the *Spatial Analyst Tools > Overlay > Weighted Overlay module*. The module proposes

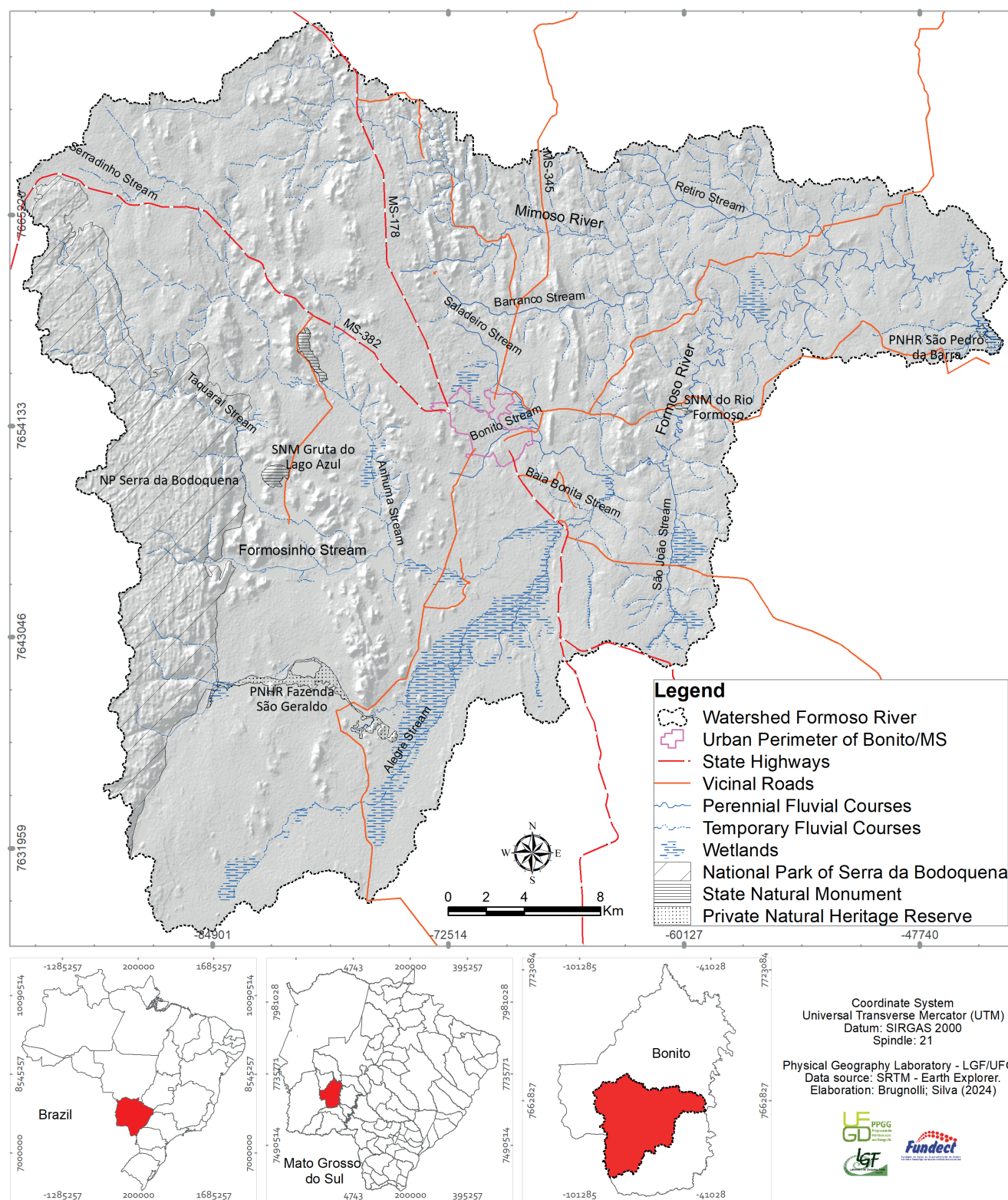


**Fig. 1. Location of the Formoso River Watershed, Bonito/MS**

the interaction of data equally through the weights inserted in each variable. The horizontal and vertical dissections result from the delimitation of all sub-basins and micro-basins supported by the SRTM/DEM (Shuttle Radar Topography Mission/Digital Elevation Model) methodology. The contour lines and the delimitations of the basins of ephemeral, intermittent, and perennial water resources were traced. Thus, a horizontal line was defined in straight lines, which form a 90° angle between the thalweg and the interfluv. The distance corresponds to the terrain slopes in meters (length). In addition, vertical lines are traced for each thalweg until reaching the ridge lines (interfluv), and each of these classes corresponds

to vertical intervals in meters (amplitude). The Brazilian Agricultural Research Corporation (Empresa Brasileira de Pesquisa Agropecuária, EMBRAPA) provided data on the soils, and a pedological detailing with the reality of the land was done. The pedological detailing with the terrestrial reality was required once conflicts in the spatialization of soils in some locations were identified during our field work. Then, some corrections were defined in the initial mapping aided by satellite images. The detailing was supported by the Brazilian System of Soil Classification (Sistema Brasileiro de Classificação de Solos – SIBCS 2018). In mapping land use and land cover, we used GIS Spring 5.2.7 to handle and process CBERS 4A (China–Brazil Earth



Resources Satellite) program satellite images from the year 2023, which underwent supervised classification with 99% accuracy. The method used in this research was unsupervised in GIS Spring 5.2.7, creating a categorization by the histogram classifier. The categorization focuses on differentiating different themes through a region clustering algorithm, which uses a method that computes the distinction between histograms. The method abstracts nearby themes (each theme presents a behavior of targets), according to their spectral signatures. Therefore, we selected fifty themes aiming to provide relevant detailing, reduce conflict between themes, and assist in the final classification and visualization. Eventually, we carried out the reclassification to adjust the classes in each region and change those that presented variations in the spectral signatures, textures, patterns, geometry, and location of the surface targets. The adjustment occurred during field trips to investigate.

Using the data, we investigated the environmental fragility resulting from the interaction of physical environment and anthropic use, providing significant results that pointed out the most fragile locations in the face of erosional processes. The weights were defined according to the degree of environmental fragility represented by the classes, very low (1), low (2), medium (3), high (4), and very high (5). Therefore, when working with the aforementioned components, criteria previously established were adopted to search for a satisfactory index that shows the environmental fragility of the components.

Regarding the rocks, we studied the geological time, fragility, and degree of cohesion of the rocks to morphogenesis and their mineralogical compositions. The precipitation analysis followed the rainfall indices of Zavattini (1992). Although Latin American countries are known for their high spatial variability in rainfall, the unique rainfall values in the Formoso River basin are attributed to its location within the same Zavattini zone. At this scale of analysis, the landscape remains relatively unchanged, and rainfall variations are minimal. In the erosive potential energy of the relief, issues related to the inclination of the slopes (declivity), their length (horizontal dissection), and the amplitude (vertical dissection) were worked. In soils, issues such as porosity, texture, depth, and maturity were observed. In terms of land use and land cover, we evaluated the size of vegetation cover, soil protection, and vegetation density.

The last stage of the methodology focused on providing significant data about existing land use conflicts. Such conflicts were identified in the relationship between the ability to use the land through the physical components, and its current use. Thus, we need to understand whether it may cause environmental impacts and whether it interferes with the resources of the Formoso River Watershed. Therefore, methods and criteria were applied to define the indices and intervals established in each class. Relevant characteristics were identified (Fig. 2) making evident the relationship between the index intervals and the characteristics of the study area.

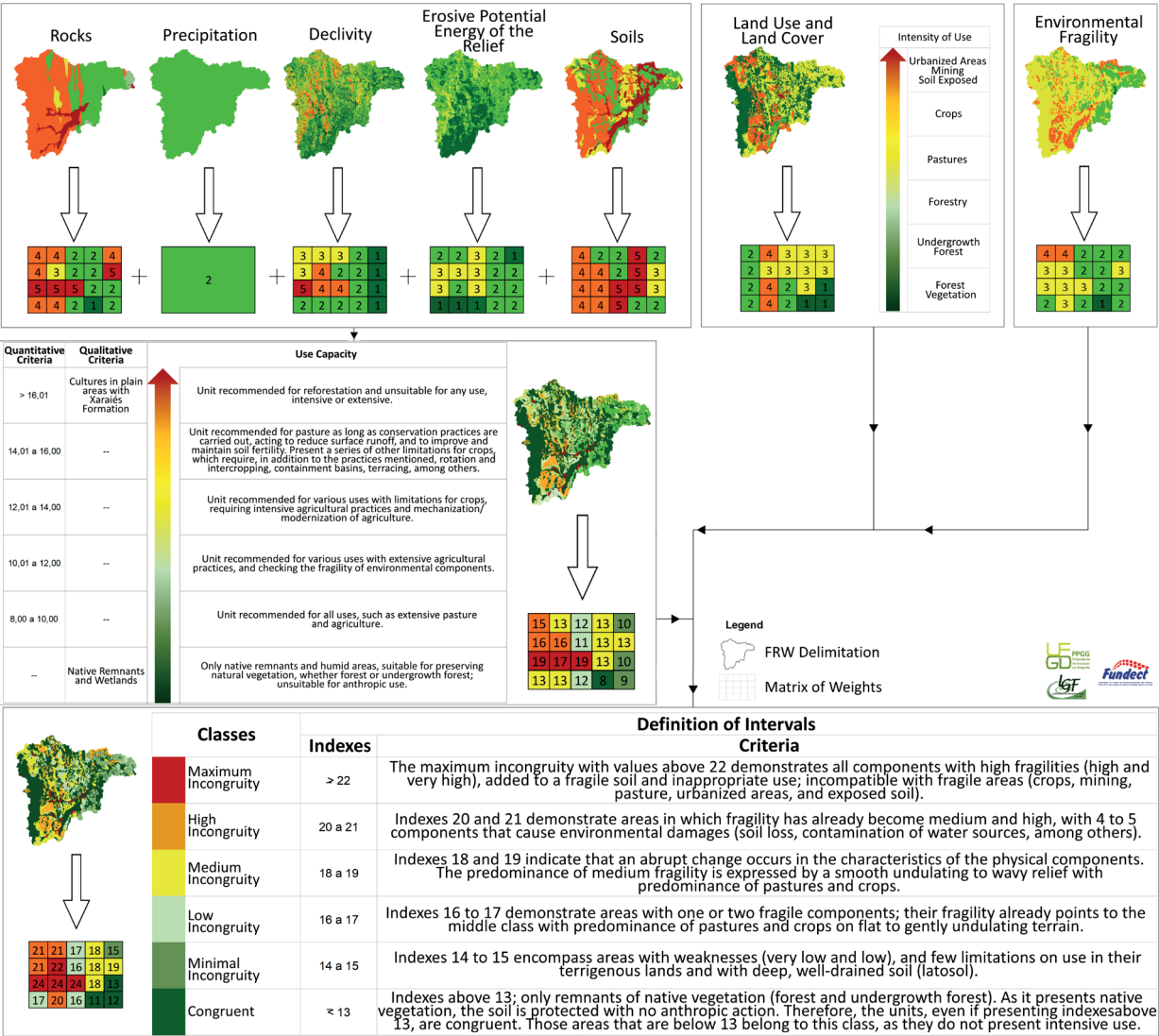


Fig. 2. Methodology for defining classes of land use conflict in the Formoso River Watershed, Bonito/MS



It is important to note that the intervals were established based on terrestrial validation, field visits, and the researchers' expertise in the subject and study area. After defining these intervals, the landscape elements within each were reviewed and adjusted as needed, drawing on the work of Lepsch et al. (1991), Dibieso (2013), Brugnolli (2020), and Brugnolli et al. (2022). The weights used are the same as those established in the analysis of environmental fragility, in which several tests were carried out using the averages. However, the method that brought greater veracity according to the physical components and their relationships with current use and terrestrial reality was the Weighted Sum Module (WSM) inserted in the ArcGis 10® GIS. Thus, the interpretation of these relationships, the empirical knowledge of the research area, and the environmental components addressed congruence classes, highlighting the conflict between capacity and current use. The classes were defined as congruent, minimal incongruity, low incongruity, medium incongruity, high incongruity, and maximum incongruity.

### Results and Discussions: conflicts between land use capacity and the current use of the Formoso River Watershed

Working with the relationship between potential use (Fig. 3), (capacity of use through its physical components) and actual land use (current anthropic use), we present an analysis of existing conflicts and potential adaptation strategies. Several studies identify the capacity of use, such as Lepsch et al. (1991), Fernandes et al. (2010), Silveira et al. (2013), Silva et al. (2013), among others. The preceding authors worked with the determination of land use capacity subclasses, seeking land use planning and practices of soil conservation. According to Dibieso (2013, p. 230), the capacity is expressed by "susceptibility to the development of erosive processes and pollution of waters". The aim is to support decision-making, organize the use of land according to its capacity, and, therefore, reduce the development of erosion, increase productivity, and mitigate environmental damages.

By contextualizing the classes of capacity of use and correlating them with their intensity, Dibieso (2013) highlights that it seeks to draw a parallel between the physical environment and its current use, identify conflicts, and define levels for such conflicts. As a result, the adjustments between the current use and the dynamics of the study unit were characterized as compatible or congruent, as described in this research. They concern a conformity between the weaknesses and potentialities of the components (rock, climate, relief, and soils), and current use. Therefore, an intimate relationship is identified between the incongruities in land use and environmental disturbances in watersheds. Even if not currently visible, in the medium and long term, the susceptibility to the occurrence of environmental damages will be undeniable. Given the incongruities identified in the process of analysis, the conservation practices adopted must be according to the levels of these incongruities. The levels of incongruity were verified based on the specificities of environmental fragility, fragility of rocks, soils, climate, relief, and land use. The methodology applied revealed variations in the levels of incongruity in the relationship between capacity and current use. The levels vary according to their potential and the intensity of current land use. The variation goes from a congruent relationship (when the use is within what is compatible), to the levels of minimal, low, medium, high, and maximum incongruity (Fig. 4).

The existence of few karst areas in Brazil means that these regions host endemic species. As monocultures advance, they fragment habitats, pollute, and contaminate both surface and groundwater. Monocultures typically deplete soil nutrients, increasing dependence on agrochemicals, and often result in the deforestation of forests and other natural habitats. This hinders the survival of many species and reduces regional biodiversity (D'Ettorre, Liso and Parise 2024). Thus, we identified a relationship between conflicts with their (in)congruences and the environmental disturbances that occur in a watershed. However, according to Dibieso (2012), a unit may exhibit high incompatibility, even presenting techniques for mitigating possible disturbances that favor the maintenance of current use. On the other hand, a unit may present low incompatibility, but given specific characteristics and inefficiency of conservation practices, it can lead to serious environmental disturbances (Fig. 5).

Identifying conflicts in the relationship between capacity of use versus current use aims to promote preservation, conservation, and recovery. The focus is on fragile areas, areas of native vegetation still intact, alluvial plains, the Formoso River wetland (refuge of biodiversity, which acts as a sediment filter for the waters of the upper course of the watershed), steep slopes with strong relief energy, among other sectors that require conservation to maintain the ecological balance and water resources, reducing the occurrence of damaging environmental impacts in the Formoso River Watershed. Based on this premise the analysis of conflicts started with the Maximum Incongruence class, characterized by high and very high fragility, mainly formed by carbonate rocks and fragile soils, such as gleisols, chernosols, and neosols. The regions represent 21.39 km<sup>2</sup> or 1.61% of the watershed, which is a relatively small area compared to the overall scope of the watershed. However, the regions require attention due to the inappropriate use associated with high fragility. The use of these lands varies from crops, pastures, and urbanized areas to exposed soil and mining, presenting intensive use capable of causing environmental damages. The regions demand concern due to the rocky substrate formed by limestone tufas and travertines (Xaraiés Formation), as well as carbonate rocks (Cerradinho and Bocaina Formations). In the first case, they present recent river deposits, naturally eroded and extremely fragile. In the second case, the fragility occurs due to the chemical dissolution capacity of limestone in relation to the percolation of water in rock cracks, which may result in disruptions. Moreover, they are located close to native forests in the upper course of the Mimoso River, in the alluvial plain of the upper and middle course of the Formoso River, sub-basin of the Córrego Alegre (upper course), and close to the Formoso River wetland. The Formoso River wetland suffers significant environmental damage from intensive use in karst and fragile alluvial plains. The analysis identified risk areas related to the slope and type of land use. Fig. 6(A) represents an area of exposed soil and the beginning of a steep slope. Additionally, the soils in the location favor their high fragility (shallow and stony). Given the characteristics, we highlight the presence of the Bonito-controlled landfill, which reinforces its classification and incongruity. Fig. 6(B and C) shows the loss of soil due to linear ravinement erosion. It is a fragile area due to its high slope (varies in slopes greater than 45%, which by law are Permanent Preservation Areas - PPAs), and lack of major vegetation to protect the soil. These sectors and their current conditions characterize them as maximum incongruity, due to the residual hills taken over by pastures and the absence of land management to contain or eliminate erosion.

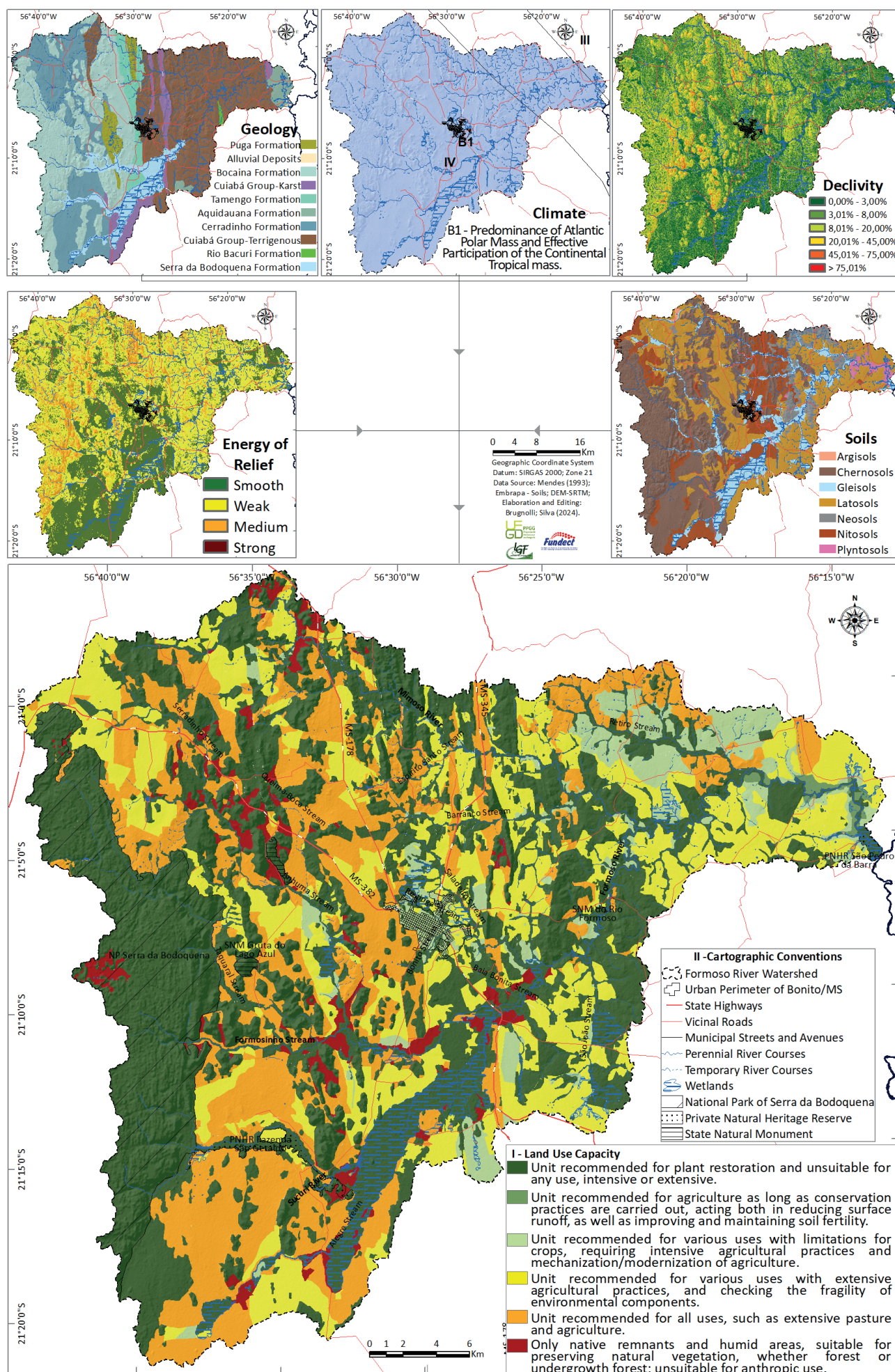


Fig. 3. Land Use Capacity of the Formoso River Watershed, Bonito/MS



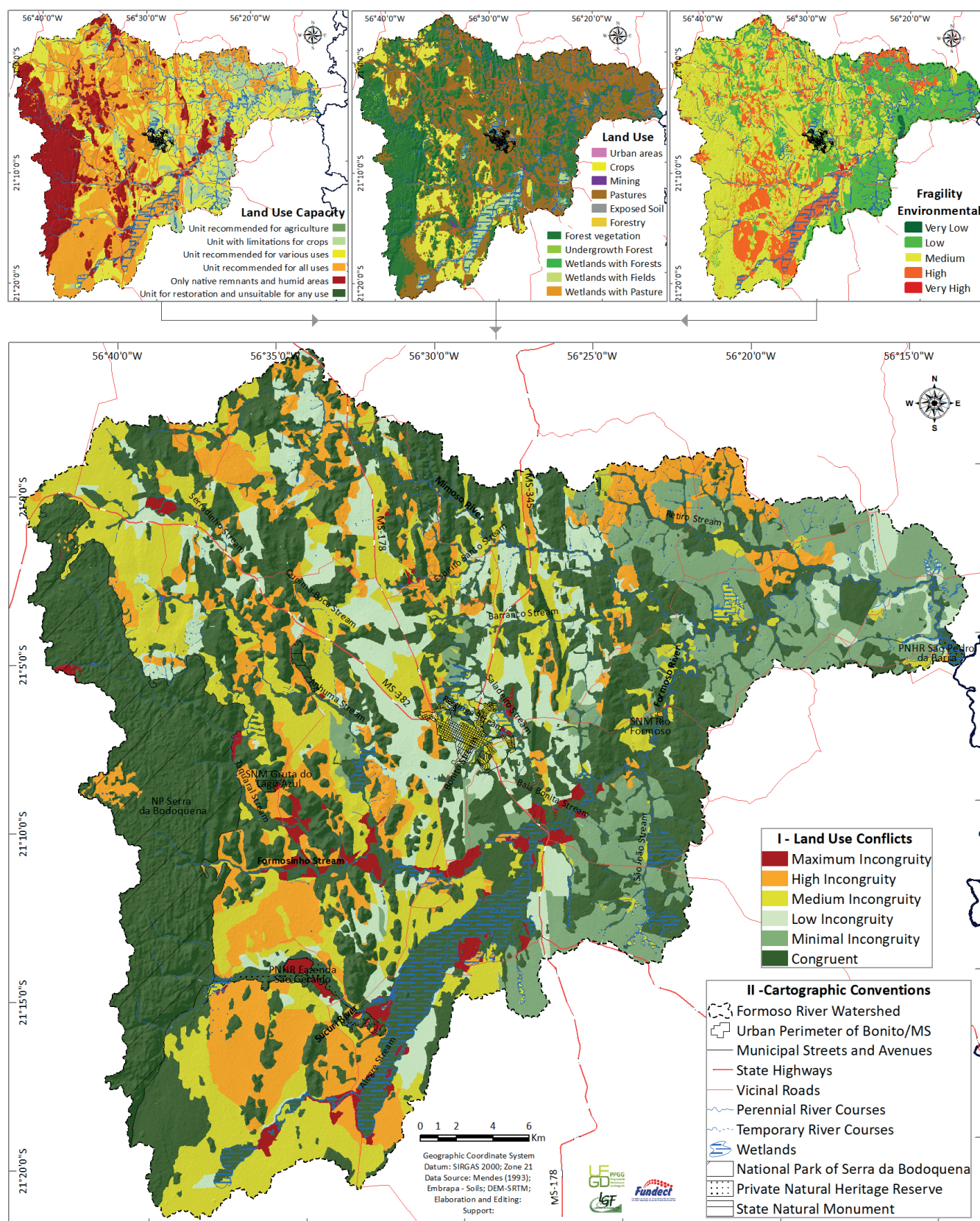








Fig. 4. Land Use Conflicts in the Formoso River Watershed, Bonito/MS

I – Conflicts of Use and Land Cover	Description of Classes	Iconographic points
<div style="display: flex; align-items: center;"> <div style="width: 15px; height: 15px; background-color: red; margin-right: 5px;"></div> <div> <b>Maximum Incongruity</b>             Coverage Area            Km<sup>2</sup>      %            21,39      1,61         </div> </div>	<p>Areas with Maximum Incongruity present high and very high fragility, represented by carbonate rocks, slopes and fragile soils, such as gleisols, chernosols, and neosols. Its use is varied with crops, pastures, urbanized areas, exposed soil, and mining. The class is suitable for reforestation and unsuitable for pastures and crops.</p>	
<div style="display: flex; align-items: center;"> <div style="width: 15px; height: 15px; background-color: orange; margin-right: 5px;"></div> <div> <b>High Incongruity</b>             Coverage Area            Km<sup>2</sup>      %            163,42      12,33         </div> </div>	<p>Areas with High Incongruity present medium and high weaknesses, being the class that present high variety in its characteristics; present flattened or highly undulating relief formed by neosols, chernosols, gleisols, or nitisols, superimposed on terrigenous and karst terrain with pastures, crops, and urbanized areas. The class presents severe restrictions, and the use of pastures is recommended with restrictions, as long as conservation practices are carried out, acting to reduce surface runoff, and to improve and maintain soil fertility. They present a series of limitations for crops, requiring, in addition to the practices mentioned, rotation and</p>	
<div style="display: flex; align-items: center;"> <div style="width: 15px; height: 15px; background-color: yellow; margin-right: 5px;"></div> <div> <b>Medium Incongruity</b>             Coverage Area            Km<sup>2</sup>      %            229,23      17,29         </div> </div>	<p>Areas with Medium Incongruity present medium weaknesses expressed by a smooth undulating to undulating relief, with varied soils and rocks. Pastures and crops predominate the areas. The class is recommended for various uses, however, with limitations for crops, requiring intensive agricultural practices and mechanization/modernization of agriculture.</p>	
<div style="display: flex; align-items: center;"> <div style="width: 15px; height: 15px; background-color: lightgreen; margin-right: 5px;"></div> <div> <b>Low Incongruity</b>             Coverage Area            Km<sup>2</sup>      %            140,20      10,57         </div> </div>	<p>Areas with Low Incongruity present medium fragility, varied rocks and soils, however, pastures and crops predominate the flat to gently undulating terrain. The unit is recommended for various uses, using extensive agricultural practices, checking the fragility of environmental components.</p>	
<div style="display: flex; align-items: center;"> <div style="width: 15px; height: 15px; background-color: darkgreen; margin-right: 5px;"></div> <div> <b>Minimal Incongruity</b>             Coverage Area            Km<sup>2</sup>      %            146,87      11,08         </div> </div>	<p>The class with Minimum Incongruity presents low fragility, and its lands are overlaid on terrigenous rocks with predominance of latosols. Crops (soy, corn, and forestry) and pastures predominate the area. The low fragility favored the high capacity of use of the lands. Recommended for all uses, such as extensive pasture and agriculture.</p>	
<div style="display: flex; align-items: center;"> <div style="width: 15px; height: 15px; background-color: darkgreen; margin-right: 5px;"></div> <div> <b>Congruent</b>             Coverage Area            Km<sup>2</sup>      %            624,63      47,12         </div> </div>	<p>The Congruent class is related to all forest remnants, even if it is highly fragile and, consequently, presents low capacity of use. As long as it presents native vegetation (forest or undergrowth forest), it becomes compatible, as native vegetation protects the soil, leaving it covered against rainfall and anthropic action. The class is suitable only for preservation, being unsuitable for anthropic use.</p>	

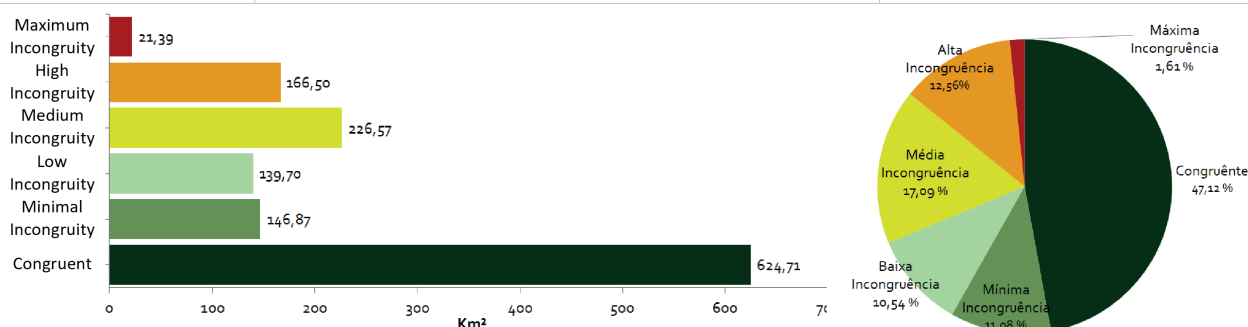
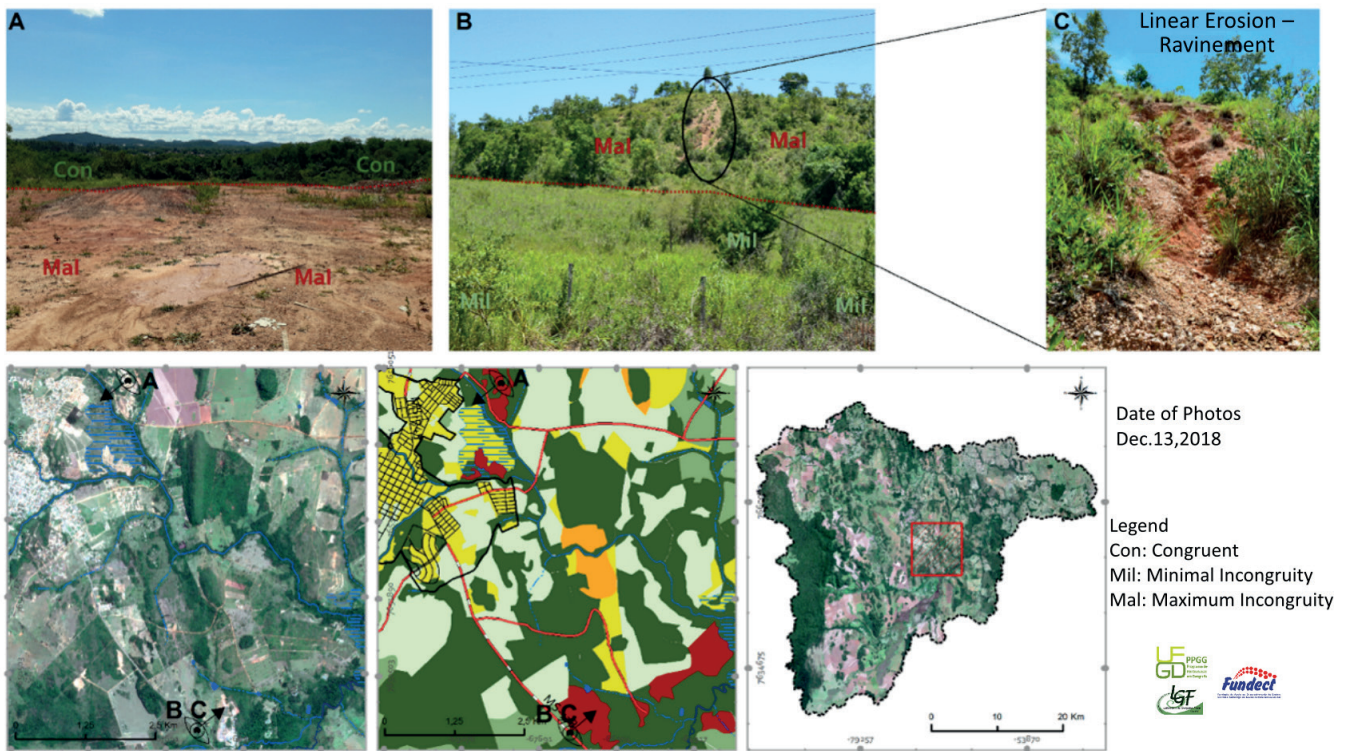


Fig. 5. Land Use Conflicts of the Formoso River Watershed, Bonito/MS, with their respective descriptions and representative points





**Fig. 6. Controlled landfill in areas of maximum incongruity (A), and linear erosion triggered by poor land use (B, C), in the mid-course of the Formoso River Watershed**

Thus, all these regions present themselves suitable for the re-establishment of forest vegetation, as they are not suitable for pasture and/or crops due to their fragility. The inadequate use of soil, added to its greater exposure (exposed soil), makes these places susceptible to erosion, whether due to the dragging of soil particles by rainwater as well as the coarse texture of soils (neosol). Plant restoration is recommended for soil maintenance and protection, benefiting the development of native species of fauna and flora in the vicinity of the Formoso River wetland. In this matter, the aim is to increase the water infiltration capacity in the soil and reduce erosion processes and river damming (an increasingly recurrent problem in the watershed). Lepsch et al. (1991) highlight the issues, stating that the areas are subject to permanent limitations, unsuitable for crops, and restricted to pasture. Plant restoration with appropriate care is required, as it may be susceptible to damage. The definition of the incongruity classes that indicated the limitations determined the frequent environmental changes and how limitations are sustained by the capacity of use. The areas with high incongruity are located throughout the entire Formoso River Watershed, mainly in the upper and middle courses, where carbonate rocks, i.e., karst environments, are prominent. Thus, we studied its characteristics and weaknesses, pastures, and crops as its main uses. The study performed field activities and used satellite images to define the demand for conservation practices. Practices that may aid in reducing sediment carryover and the control of various linear and laminar erosions, adequate management, soil preparation, and planting of forage vegetation in pastures. Yet, a large part of pastures is compacted, due to cattle trampling and the absence of land management. The high incongruity class covers a total area of 163.42 km<sup>2</sup>, or 12.33%. It presents significant extension and denotes reliefs ranging from flat to strongly undulating, formed by neosols, chernosols, gleisols, or nitisols, overlapping in terrigenous and karst terrains. In addition to the exposed weaknesses inherent to the physical components of the watershed, the presence of cattle was identified, making

them prone to the development of erosive processes. Thus, the implementation of fences may prevent animals from entering these regions, as illustrated in Fig. 7.

The slope alone does not determine a legal need for plant restoration or vegetation preservation. However, the other components increase the fragility of the areas, compromising the capacity of use (whether for the rocks of the Tamengo Formation with calcitic limestones, which present high fragility, or due to the average relief energy and its fragile soils, such as chernosol and gleisol). Such factors determine the high fragility in the aforementioned areas of the Formoso River Watershed, where the land used for pasture has brought high incongruity. However, by applying a set of intensive conservation practices that act in reducing surface runoff and improving and maintaining soil fertility, the areas may become suitable for such uses. As for crops, a series of other restrictions are exhibited, requiring the practices mentioned as well as crop rotation, especially in fragile soils and steep relief, terracing, and containment basins with the purpose of dissipating sediment transport. In Fig. 7 (B, C), the slope varies from 0% to 8% (foreground), and may reach up to 45% (background). The sector shows erosion due to rainfall and lack of vegetation. The sector demands actions to recover the local vegetation cover and/or erosion containment. Such actions may occur through the application of techniques, such as the creation of contour lines and/or containment basins to contain the advancement of soil loss, since no type of land management is indicated in the area. The analyses show that areas with maximum incongruity and high incongruity present a high risk of erosion due to the high fragility of the lands, in addition to the steep slope that favors surface runoff. In smaller proportions, the medium incongruity class portrays varied characteristics of the physical environment; however, when unified, it brings certain weaknesses to the system. The areas are spread over 229.23 km<sup>2</sup> or 17.29% of the total area, identified in all regions of the Formoso River Watershed, especially in the upper and middle courses, in gently undulating to undulating locations, and soils that present good drainage, such as latosol and nitisol. The

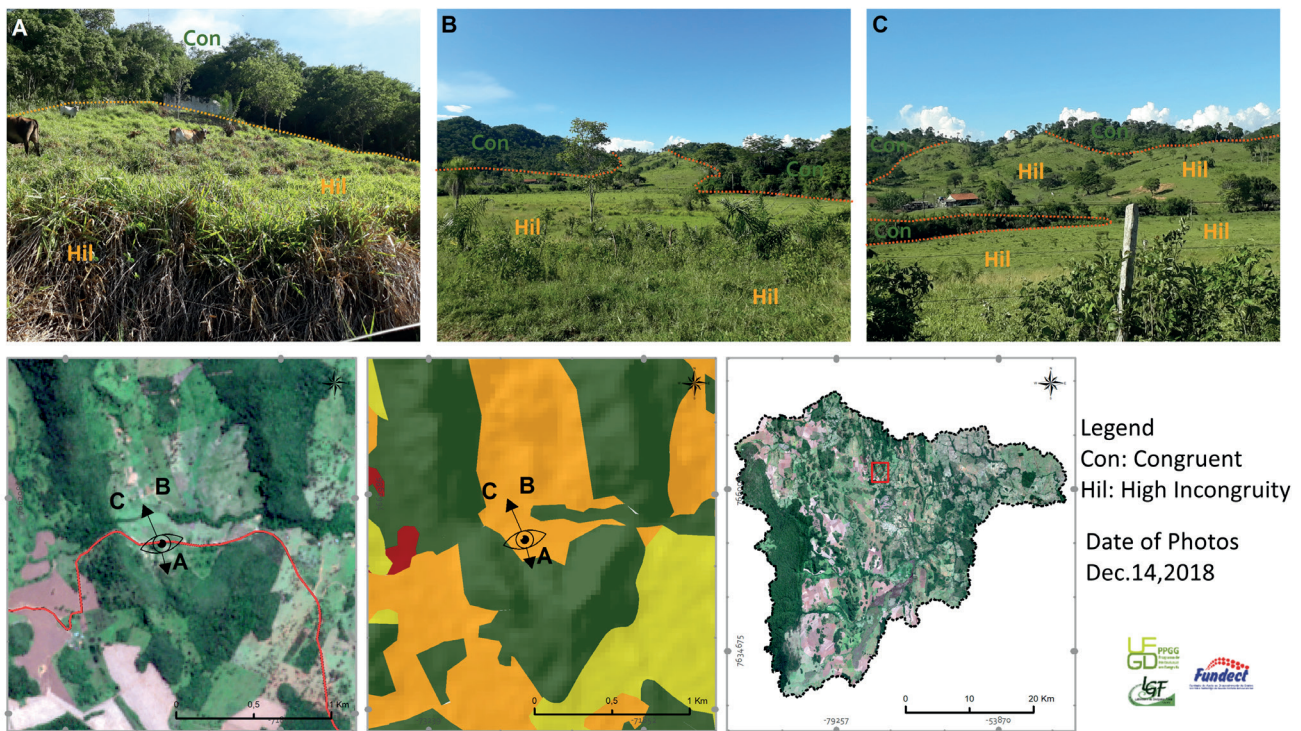


**Fig. 7. Cattle grazing in steep areas (A) with pastures on the hills where erosion processes are observed (B and C), in the middle course of the Formoso River Watershed**

average incongruity reveals factors that make it susceptible to erosion, such as pastures and crops in karst areas. The sector requires significant care and maintenance, due to the high degree of dissolution and risk of disruptions. The units are suitable for various uses, but with limitations for crops, as they require intensive agricultural practices and mechanization/modernization of agriculture. However, as it already represents an intermediate class of incompatibility, conservation practices are required, such as terracing on steep slopes, contour lines in all crops and pastures, and retention boxes on roads. The practice prevents the effect of erosive potential energy of the relief highlighted, in some areas, for medium to mildly strong classes, during soybean harvest. The harvest period leaves the soil exposed to more intense precipitation, the main cause for "river damming". Areas of low incongruity face small conflicts, that is, regions where land uses partially correspond to their capacity of use. The class is spread over 140.20 km<sup>2</sup> or 10.57% of the total watershed, predominantly located in the mid- and lower courses of the watershed. The low incongruity class exhibited a variety of characteristics, always pointing to low and medium weaknesses. The pedogenetic realities aids to reduce erosion, as this class (low incongruity) is located in terrains of latosols, nitosols, and plinthosols that present good to medium drainage, deep/evolved, and medium to sandy texture. Even with improvements in soils capacity, the class deserves concern because pastures and/or crops predominate its lands. Despite being units recommended for various uses, they require extensive agricultural practices to verify the fragility of environmental components. The sectors with minimal incongruity are spread over 146.87 km<sup>2</sup> or 11.08%, and show unique characteristics. One concerning characteristic is that all uses are located on a substrate of terrigenous rocks of the Puga and Cuiabá Group Formations (Psammitic, Pelitic, and Conglomeratic) showing low fragility. Moreover, the soils formed by nitosols, plinthosols, and latosols favor improvement in the land capacity of use as well as reducing surface runoff, as they present good to medium drainage. Thus, these units are suitable for all uses, such as extensive pasture and agriculture, as

long as they meet the capacity/restrictions expressed in the environmental components. The units require simple conservation practices, such as alternation of paddocks for livestock and contour lines. According to Lepsch et al. (1991), areas that present minimal use limitations may be used for annual and perennial crops, pastures, and/or plant restoration, as they pose few environmental disturbs and require common practices to improve and maintain soil fertility and crop rotation. Thus, we highlight that even the sectors with minimal incongruity may present risks for erosive processes, as they depend on the way in which pasture management is carried out (137.87 km<sup>2</sup> or 91.09% of the total for the class), crops (8.93 km<sup>2</sup> or 6.08%), and forestry (0.07 km<sup>2</sup> or 0.05%). As a result, the minimum incongruity class still receives special attention in the Formoso River Watershed, focusing on the management employed rather than the capacity of use. In the sectors of minimum incongruity, a great part of pastures in the lower course of the river present an absence of land management. It becomes a motivating differential for the development of erosion processes, as well as for the development of environmental damages related to poorly planned dams, and the current situation of local roads (extensive erosion) (Fig. 8).

The congruent class does not present conflicts between capacity and current use. It concerns all forest remnants, even if the class presents high fragility and, consequently, low capacity of use. When native vegetation occurs, it becomes congruent/compatible, protecting the soil against rainfall and anthropic actions. The class becomes unsuitable for anthropic use because it is only suitable for preservation, protection of wild fauna and flora, and water storage (dams and dams). According to Lepsch et al. (1991), the class is unsuitable for commercial forests, such as silviculture, or for the production of any other form of permanent vegetation with economic value. Furthermore, the preservation of vegetation maintains the hydrological cycle, thereby reducing erosion processes. It allows water to infiltrate the soil and supplies the Formoso River wetland, being essential during periods of drought.



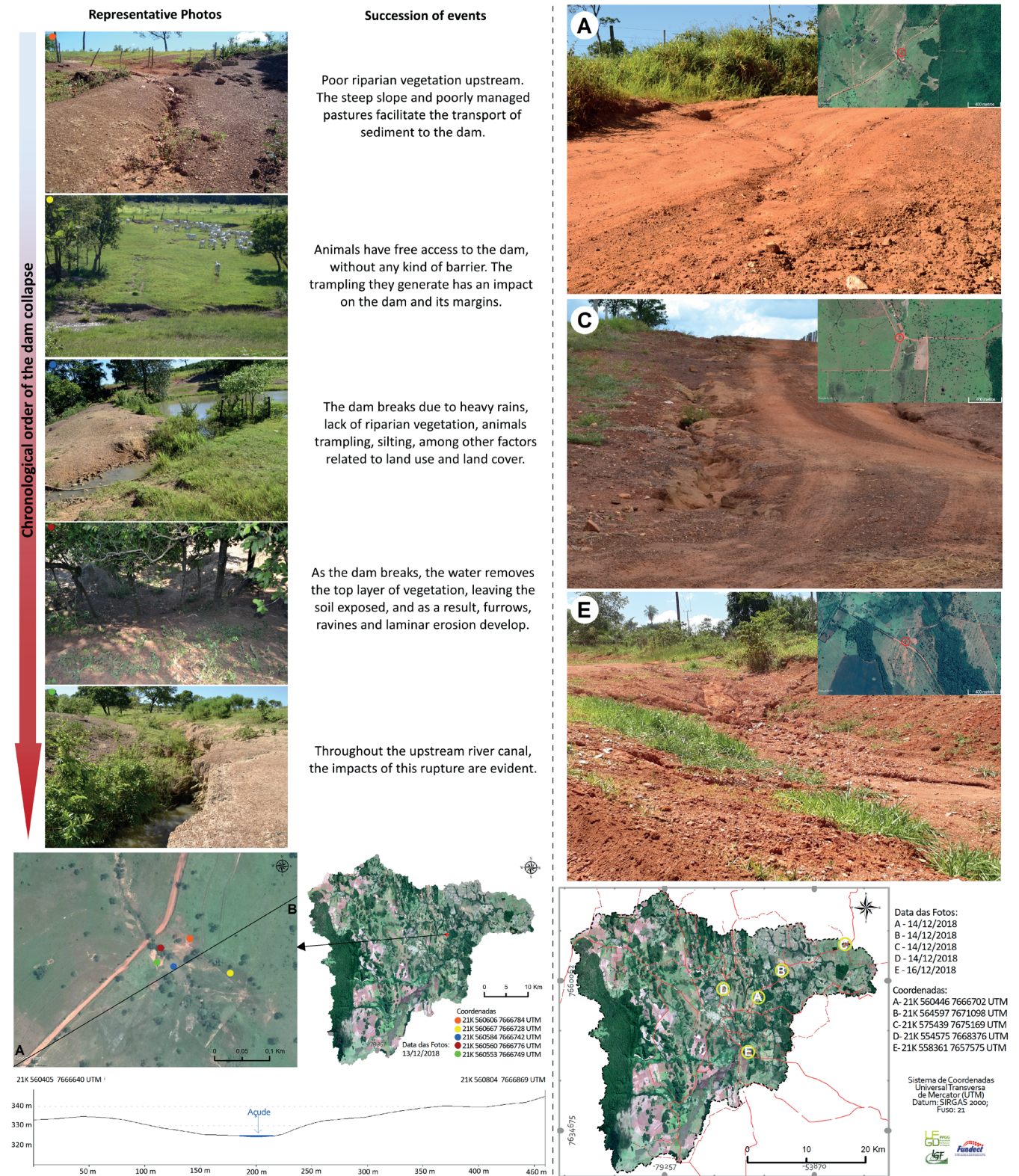


Fig. 8. Examples of the FRW's environmental problems are collapsed dams and erosion on unpaved roads

Thus, the congruent class points to approximately 624.63 km<sup>2</sup> of the total area, or 47.12%. The high values mask some situations. Actually, 152.12 km<sup>2</sup> of the total area (around 25% of remnant native vegetation) is encompassed by Serra da Bodoquena National Park. According to Brazil (2000), it allows for the preservation of natural ecosystems of great ecological relevance and scenic beauty, scientific research and development of environmental education and interpretation activities, recreation with nature, and ecological tourism. The legal aspects protect the area, and its steep slopes pose restrictions on anthropic use. Other areas are worth highlighting, such as the State Natural Monuments and Private Natural Heritage Reserves ( Monumentos Naturais Estaduais - MNEs and Reserva Particular do Patrimônio Natural – RPPNs), which cover 8.57 km<sup>2</sup> (about 1.84% of native vegetation remnants). Thus, 452.06 km<sup>2</sup> of forest remnants remain scattered throughout all regions of the Formoso River Watershed, particularly in steep areas of the upper and mid-course and in the alluvial plains. Yet, residual hills in the Mimoso River sub-basin and the southeastern portion, which present relatively preserved portions, also exist.

It is noteworthy that the Formoso River Watershed, compared to other watersheds in the state of Mato Grosso do Sul, presents significant preserved and conserved areas (Miguel et al. 2013; Braz et al. 2020; Alves, Silva and Brugnolli 2022) due to the fact that a great part of the forest remnants are legally restricted areas and the steep slope does not favor deforestation. Even though deforestation and environmental impacts have occurred in the mid-course of the Mimoso River.

## CONCLUSIONS

The Formoso River Watershed's landscape, with its significant changes, contradicts the municipality of Bonito's commitment to conservation and preservation of natural

resources. The current scenario shows environmental issues and water resources under threat due to clouding and closures of attractions. The economic model acting in Mato Grosso do Sul and throughout the central region of Brazil has contributed to it.

Defining measurements to maintain the use, recovery, conservation and preservation of native vegetation minimizes negative impacts and ensures respect for the environmental legislation as well as the environmental conditions with their strengths and weaknesses. The present research has generated proposals and suggestions to improve environmental quality and increase environmental resilience. Yet, it proposes mitigation actions to handle the conflicts and incongruities identified, as well as the negative environmental disturbances existing in the Formoso River Watershed. The geotechnologies allowed us to provide a synthesis document that coherently portrays the environmental characteristics of the watershed, and its negative aspects. We conclude that:

- the native remnants (Cerrado and Atlantic Forest) in congruent areas demand maintenance to keep the biodiversity and environmental balance, since the sources of Bonito's main springs are located there;
- there is a need to reforest areas with the greatest incongruity, using species native to the Cerrado and the Atlantic Forest. This will help maintain geoeological balance and promote increased biodiversity.
- surface runoff may be reduced by implementing soil, vegetative and mechanical conservation practices in crops and pastures of the watershed;

We emphasize that genuine appreciation of the Formoso River Watershed may address potential environmental issues in the municipality of Bonito. However, the municipality's scientific, geological, hydrological, tourist, speleological, economic, and social potential continues to grow. ■

## REFERENCES

- Alves, L.B., Silva, C.A.da; and Brugnolli, R.M. (2022). Diagnóstico ambiental da bacia hidrográfica do córrego Laranja Doce, Mato Grosso do Sul. *Revista da ANPEGE*, 18(35). DOI: 10.5418/ra2022.v18i35.13822
- Angel, S., Sheppard, D., Civco, R., Buckley, A., Chabaeva, L., Gitlin, A., Kralley, J., Parent, and Perlin M. (2005). *The Dynamics of Global Urban Expansion*. Washington, DC: Department of Transport and Urban Development, World Bank.
- Boggiani, P.C., Coimbra, A.M., Gesicki, A.L., Sial, A.N., Ferreira, V.P., Ribeiro, F.B., and Flexor, J.M. (2002). Tufas Calcárias da Serra da Bodoquena, MS - Cachoeiras petrificadas ao longo dos rios. In: Schobbenhaus, C., Campos, D.A., Queiroz, E.T., Winge, M., Berbert-Born, M.L.C. (Eds.) *Sítios Geológicos e Paleontológicos do Brasil*. 1. ed. Brasília: DNPM/CPRM - Comissão Brasileira de Sítios Geológicos e Paleobiológicos (SIGEP), v.01. p. 249-259.
- Braz, A.M., Mirandola, P.H.G., Pinto, A.L., Chávez, E.S., and Oliveira, I.J.de. (2020). Manejo integrado de cuencas hidrográficas: posibilidades y avances en los análisis de uso y cobertura de la tierra. *Cuad. Geogr. Rev. Colomb. Geogr.*, 29, 69-85. DOI: 10.15446/rcdg.v29n1.76232
- Brugnolli, R.M. A cartografia do relevo como subsídio para a análise de um sistema cárstico Leite, E.F., Silva, C.A. *Cartografia & geotecnologias: conceitos e aplicações*. Porto Alegre: TotalBooks, 2023. DOI: 10.52632/978.65.88393.41.3
- Brugnolli, R.M., Berezuk, A.G., and Silva, C.A.da. (2019). A Morfometria da Bacia Hidrográfica do Rio Mimoso, um Sistema Cárstico do Mato Grosso do Sul/Brasil. *Revista Confins (Paris)*, 40:1-22. DOI: <https://doi.org/10.4000/confins.19845>
- Brugnolli, R.M., Chávez, E.S., Silva, C.A.da; and Berezuk, A.G. (2022). Geoecological diagnosis of landscapes of the Formoso River Watershed, Bonito/MS, Brazil. *Environmental Earth Sciences*, 81, 1-19. DOI: 10.1007/s12665-022-10247-6
- Burri, E., Castiglioni, B., and Sauro, U. (1999). Agriculture, landscape and human impact in some karst areas of Italy. *International Journal of Speleology*, 28, 33-54. DOI: 10.5038/1827-806X.28.1.3
- Castro, A.P., and Nielsen, E., (2001). Indigenous people and co-management: implications for conflict management. *Environmental, Science and Policy*, 4, 229-239. DOI: 10.1016/S1462-9011(01)00022-3
- Cohen, B. (2006). Urbanization in Developing Countries: Current Trends, Future Projections, and Key Challenges for Sustainability. *Technology in Society*, 28, 63-80. DOI: 10.1016/j.techsoc.2005.10.005
- CPRM, Companhia de Pesquisa e Recursos Minerais. (2006). *Geologia e Recursos Minerais do estado de Mato Grosso do Sul*. Brasília, CPRM.
- D'Ettorre, U.S.; Liso, I.S.; and Parise, M. (2024). Desertification in karst areas: A review. *Earth-Sci. Rev.*, 253, 104786. DOI: 10.1016/j.earscirev.2024.104786
- Dibieso, E. P. (2013). *Planejamento ambiental e gestão dos recursos hídricos: estudos aplicados à bacia hidrográfica do manancial do alto curso do rio Santo Anastácio – São Paulo/Brasil*. PhD in Geography.
- Embrapa, Empresa Brasileira de Pesquisa Agropecuária. (2018). *Sistema Brasileiro de Classificação de Solos*. 5.ed. Brasília.



- Erickson, D.L. (1995). Rural land use and land cover change: implications for local planning in the River Raisin watershed. *Land Use Policy*, 12, 223-236. DOI: 10.1016/0264-8377(95)00005-X
- Fernandes, N.B., Moreau, M.S., Moreau, A.M.S.S., and Costa, L.M. (2010). Capacidade de uso das terras na bacia hidrográfica do Jiquiriça, recôncavo sul da Bahia. *Caminhos de Geografia*, 11(34): 105-122. DOI: 10.14393/RCG113416076
- Ford, D.C., and Williams, P. (2007). *Karst Hydrogeology and Geomorphology*. John Wiley, Chichester. DOI: 10.1002/9781118684986
- Hilson, G. (2002). An overview of land use conflicts in mining communities. *Land Use Policy*, 19, 65 - 73. DOI: 10.1016/S0264-8377(01)00043-6
- Lacerda Filho, J.V., Correia de Brito, R.S., Rodrigues, C.V., Cavalcante, C.O., Silva, M.G., Moreton, C.C., Martins, E.G., Lopes, R.C., Muniz Lima, T., Larizzatti, J.H., and Valente, C.R. (2006). *Geologia e recursos minerais do estado de Mato Grosso do Sul*. CPRM/SICME, Campo Grande.
- Leal, A. C. (1995). Meio ambiente e urbanização na microbacia do Areia Branca-Campinas, SP. Master's in Geosciences and Environment.
- Lepsch, I.F., Bellinazi, J.R., Bertolini, D., and Espíndola, C.R. (1991). Manual para levantamento utilitário do meio físico e classificação de terras no sistema de capacidade de uso: 4ª aproximação. Campinas: Sociedade Brasileira de Ciência do Solo.
- Mendes, I. A. (1993). A dinâmica erosiva do escoamento pluvial na bacia do Córrego Lafon – Araçatuba – SP. PhD in Geography.
- Miguel, A.E., Brugnolli, R.M., Oliveira, W. de; and Brugnolli, C.A.C. (2013). Uso e ocupação do solo e análise morfométrica da bacia hidrográfica do córrego Bom Jardim, Brasilândia/MS. *Revista Geonorte*, 4(11):72–84.
- Narendra, B.H.; Siregar, C.A.; Dharmawan, I.W.S.; Sukmana, A.; Pratiwi; Pramono, I.B.; Basuki, T.M.; Nugroho, H.Y.S.H.; Supangat, A.B.; and Purwanto; et al. (2021). A Review on Sustainability of Watershed Management in Indonesia. *Sustainability*, 13, 11125. DOI: 10.3390/su131911125
- Ochieng Odhiambo, M., (2000). *Oxfam Karamoja Conflict Study: a Report*. Oxfam, Kampala.
- Parise, M. (2012). Management of water resources in karst environments, and negative effects of land use changes in the Murge area (Apulia, Italy). *Karst Development: Original Papers*, 2(1): 16-20.
- Parise, M.; de Waele, J., and Gutierrez, F. (2009). Current perspectives on the environmental impacts and hazards in karst. *Environmental Geology*, 58, 235–237. DOI: 10.1007/s00254-008-1608-2
- Ramalho Filho, A., and Beek, K. J. (1995). *Sistema de avaliação da aptidão agrícola das terras*. 3. ed. Rio de Janeiro: EMBRAPA-CNPq.
- Ribeiro, A.F.N. (2018). Que Bonito é esse? Disputas territoriais em terras do agro-eco-turismo. *Revista Entre-Lugar*, 9(18): 37–67. DOI: 10.30612/el.v9i18.8824
- Sallun Filho, W., Karmann, I., and Boggiani, P.C. (2004). Paisagens Cársticas da Serra da Bodoquena (MS). In: *Litologia do continente Sul-americano: evolução da obra de Fernando Flávio Marques de Almeida*, Chapter: XXV, Publisher: Ed. Beca, Editors: Virgínio Mantesso-Neto, Andrea Bartorelli, Celso Dal Ré Carneiro, Benjamin Bley de Brito-Neves, 424-433.
- Silva, F. F. da., and Morais, F. de. (2016). Índice de perturbações ambientais em áreas cársticas do estado do Tocantins – primeira aplicação no Brasil. *Revista Brasileira de Geografia Física*, 09(3), 766–777. DOI: 10.26848/rbgf.v9.3.p766-777
- Silva, M.A., Freitas, D.A.F., Silva, M.L.N., Oliveira, A.H., Lima, G.C., and Curi, N. (2013). Sistema de informações geográficas no planejamento de uso do solo. *Revista Brasileira de Ciências Agrárias*, 8(2), 316-323. DOI: 10.5039/agraria.v8i2a2289
- Silveira, G.R.P., Campos, S., Garcia, Y.M., Silva, H.A.S., Campos, M., Nardini, R.C., and Felipe, A.C. (2013). Geoprocessamento aplicado na determinação das subclasses de capacidade de uso do solo para o planejamento conservacionista. *Comunicata Scienia*, 4(4), 330-336. DOI: 10.14295/cs.v4i4.223
- Spring. (1996). Integrating remote sensing and GIS by object-oriented data modelling. *Camara G, Souza RCM, Freitas UM, Garrido J Computers & Graphics*, 20(3), 395-403.
- Tavares, A.S., Vieira, M.S., and Uagoda, R.E.S. (2023). Desafios e Alternativas na Simulação da Dinâmica Hidrológica e Sedimentológica em Sistemas Cársticos. *Revista Brasileira de Geografia Física*, 16(4), 1714–1731. DOI: 10.26848/rbgf.v16.4.p1714-1731
- Usgs, United States Geological Survey. (2023). Earth Explorer. Available in: <https://earthexplorer.usgs.gov/>. Accessed in: May. 2023.
- Van Beynen, P.E., Brinkmann, R., and Van Beynen, K.M. (2012). A sustainability index for karst environments. *Journal of Cave and Karst Studies*, 74(2), 221–234. DOI: 10.4311/2011SS0217
- Veni, G., Duchene, H., Crawford, N.C., Groves, C.G., Huppert, G.N., Kastning, E.H., Olson, R., and Wheeler, B.J. (2001). Living with karst, a fragile foundation. AGI Environmental Awareness Series. American Geological Institute, 4.
- Wilson, C. (2014). Spectral analysis of civil conflict-induced forced migration on land-use/land-cover change: the case of a primate and lower-ranked cities in Sierra Leone. *International Journal of Remote Sensing*, 35(3), 1094–1125. DOI: 10.1080/01431161.2013.875633
- Wu, Q., and Wang, L. (2024). Farmland hydrological cycle under agroforestry systems and efficient use of water resources in the karst desertification environment. *Heliyon*, 10, e35506. DOI: 10.1016/j.heliyon.2024.e35506
- Zavattini, J. A. (1992). Dinâmica climática no Mato Grosso do Sul. *Geografia*, 17(2), 65-91.

# METROPOLIZATION PROCESS IN THE RURAL SETTLEMENT SYSTEM OF THE CENTRAL CHERNOZEM REGION OF RUSSIA

Nadezhda V. Chugunova<sup>1</sup>, Fedor N. Lisetskii<sup>1\*</sup>, Anastasiya G. Narozhnyaya<sup>1</sup>,  
Tatjana A. Polyakova<sup>1</sup>, Darja N. Morkovskaya<sup>1</sup>

<sup>1</sup> Institute of Earth Sciences, Belgorod State National Research University, Belgorod, 308001, Russia

\*Corresponding author: fnliset@mail.ru

Received: December 22<sup>th</sup> 2023 / Accepted: September 1<sup>st</sup> 2024 / Published: October 1<sup>st</sup> 2024

<https://doi.org/10.24057/2071-9388-2024-3168>

**ABSTRACT.** The Central Chernozem region of Russia has undergone significant changes in socio-demographic processes over the past half-century. The aim of this study was to establish the impact of metropolization on the demographic transformation of sparsely populated rural settlements for the Central Chernozem region and to develop a demographic forecast for 2030. The study's goals were to (1) determine the scale of regional metropolises; (2) identify the impact of metropolization on the quantitative indicators of sparsely populated rural settlements; (3) establish trends in their transformation; and (4) compile a medium-term demographic forecast for the Central Chernozem region. The set objectives were achieved by integrating methods for spatial-temporal and comparative geographical analysis, statistical methods, and a combination of official statistics with sociological methods. Analysis of the level of urbanization of the regions in modern conditions (20<sup>th</sup> and 21<sup>st</sup> centuries) showed that, although this process was and remained below the national average, it did not prevent the formation of regional metropolises (Belgorod, Stary Oskol, Kursk, Voronezh, Lipetsk, Tambov) as an obvious outcome of urbanization processes. A regional pattern of degradation of the network of rural settlements, mainly the smallest and small in terms of population (1-25, 26-50 people), which make up over one third of all settlements in the Central Chernozem region of Russia, was determined. A stable long-term trend of growth in the number of abandoned villages and hamlets was established. Between the last two All-Russian population censuses (11 years), their number increased by 45%. The forecasting results obtained confirm the established patterns in the medium-term trend of "compression" of rural settlement around regional metropolis (with some exceptions). The medium-term demographic forecast showed that population concentration in metropolitan areas and further socio-demographic desertification in peripheral areas will continue with growing territorial differentiation. The obtained results of the study of the transformation of settlement systems of the Central Chernozem region as a result of the metropolization of regional centers can help government institutions in strategic planning of territorial development.

**KEYWORDS:** metropolization processes, rural resettlement, disappearing settlements, socioeconomic development, spatial distribution, geographic information system, demographic forecast

**CITATION:** Chugunova N. V., Lisetskii F. N., Narozhnyaya A. G., Polyakova T. A., Morkovskaya D. N. (2024). Metropolization Process in the Rural Settlement System of the Central Chernozem Region Of Russia. *Geography, Environment, Sustainability*, 3(17), 98-108

<https://doi.org/10.24057/2071-9388-2024-3168>

**Conflict of interests:** The authors reported no potential conflict of interest.

## INTRODUCTION

The historical settlement system in Russia was radically changed during the Soviet era and continues to change due to many factors: urbanization as a global socio-economic process, the demographic crisis, and scientific and technological progress. Ignoring objective changes in society and the population distribution system leads government institutions to make wrong decisions and have negative consequences of a socio-demographic and ekistics nature. The consequence of urbanization as a global socio-economic process are metropolises of various hierarchical levels (from national to regional). It should be clarified that in this article, resettlement refers to a network of populated areas (urban and rural) of a specific territory, and a regional metropolis is the main city

of the territory, the centre of political and economic life with an increased concentration of the urban population, that is, the top in the hierarchy of the regional settlement system. Metropolization is the result of urbanization, when a city (an agglomeration, a region associated with it) has achieved a systemically significant mission, structure, and status but transforms rural areas, leading to stagnation and/or degradation of deep peripheral areas (more often these are rural areas).

Socio-economic processes in rural areas are of interest to researchers (Lynch 2005; Nefedova and Treyvish 2015; Pivovarov and Alekseev 2018; Nefedova 2018; Sokolova and Kuznetsov 2018; Nefedova and Treyvish 2020; Alekseev et al. 2020; Huseynova 2023; Chugunova et al. 2023), who note that agriculture in rural areas is receding into the background, since technical progress and industrial methods

of agricultural production reduce employment, contribute to the migration outflow of "extra" people from the rural community, leading to depopulation in many settlements and the appearance of abandoned (depopulated) villages. The formation of metropolises is the key to the modernization of society (Marshan and Samson 2004), but it is accompanied not only by the concentration of the population and economy in large cities but also by increased segregation of the population in the centre-periphery gradient (Chugunova and Likhnevskaya 2019; Chugunova et al. 2021). In Russian realities, In Russian realities, the deepening of space polarization (Kuzin 2019), the growth of economic and social contrasts, and the emergence of urgent problems in regional development (Yakovenko and Chugunova 2022; Zubarevich 2003) complicate the strengthening of the metropolization process in a market economy. COVID-19 showed that the pandemic damaged the economy and lifestyle of the urban population (Kochurov et al. 2021; Tikunov et al. 2022), but increased the attractiveness of rural settlements, mainly in the first suburban zone, and practically did not affect the periphery of the regions (in the context of the "center-periphery" concept). During the COVID-19 period, the phenomenon of suburban migration (from urban to rural or suburbs) was noted, since in Russian regions many urban families have garden plots with house buildings. Since 2019, under a new law, Russians have received the right to legalize their year-round residence with permanent registration in houses in garden associations suitable for habitation.

Rural settlements are, on the one hand, the result of the development of the country's territory, and, on the other hand, they are the contribution made by many generations of people to territorial development. The population settlement is broadly and socially defined as a spatial form of social organization, and in the second meaning, it is a set of localities within a certain territory. Rural areas also perform some ecological functions: they maintain ecological balance throughout the country, including cities. Agricultural landscapes, like urban lands, require erosion control (Lisetskii et al. 2014; Chizhikova et al. 2022) and control of pollutants in soil and water, as well as the introduction of a more general approach, such as environmental management of key resources (water and land) at the eco-regional level (Yermolaev et al. 2015; Buryak et al. 2019). Solving the water shortage problem, which is receiving much attention (Lisetskii 2021), requires a common basin approach (Buryak et al. 2022), which can replenish underground sources as the main resource for drinking water supply to the population. One distinctive feature of settlement development is its inertia, which, at a certain stage of change, can slow down the structural shifts caused by settlement factors. In particular, the development of geographically dispersed farms (Kaur K. and Kaur G. 2021) can constrain urbanization, which is important for maintaining the socio-economic climate in rural areas.

An analysis of published works revealed that most of the previous publications did not address the impact of metropolises on rural settlements, and did not study the results and development trends of the smallest and small rural settlements of the area, especially with the use of geographic information systems. The demographic approach is the main one in this article. This study, for the first time, uses a scientific and methodological complex for a fundamental study of the region's settlement system, distinguishing it from previous publications' results. It has been shown that there are no works that look at patterns in the growth of a network of disappearing rural settlements and how they are spread out in space in a region of Russia

that is so big in terms of population and land area that we felt the need to fill in the gaps.

This study refers to the important agricultural zone of Russia, where the Belgorod, Kursk, Lipetsk, Tambov, Voronezh Oblasts are located, forming the Central Chernozem region, which is home to 7.2 million people (4.8% of the population of the Russian Federation), and the district area is 1% of the country's territory. In the rural areas of the region, there are 9201 settlements with a population of 2.2 million people<sup>1</sup>.

The subject of the study is regional metropolization processes, which cause transformation of settlement systems. The territorial object of study was the settlement system of the Central Chernozem region.

The study's main objectives, which determine its purpose, include: i) assessing the scale of regional metropolises; ii) identifying the impact of metropolization on the quantitative indicators of sparsely populated rural settlements; iii) establishing the trend of their transformation and developing a medium-term demographic forecast for the Central Chernozem region.

## MATERIALS AND METHODS

The information base included the materials provided by the Federal State Statistics Service (Rosstat) and territorial bodies of the Rosstat (Belgorod, Voronezh, Kursk, Lipetsk, and Tambov regions), multi-year studies by the authors of the Central Chernozem region, and field surveys (materials obtained during expert interviews with rural settlement administrations). Official statistics have been used to compile the tables in this article. The main objectives of the paper have been achieved through the use of spatial-temporal and comparative geographical analysis methods, statistical methods, and a combination of official statistics and sociological methods. The functionality of the Geographical Information System (GIS) allows not only to visualize the territorial features of settlement systems but also to conduct cartographic modelling of demographic characteristics (Igonin and Tikunov 2019; Gaydukov et al. 2022). The study has given significant attention to geoinformation mapping (geoinformation technology – ArcGIS), enabling the visualization of processes and events over time, as well as demonstrating the appeal of regional metropolises to the population. The data of the data.nextgis.com service, tables of attributes, and spatial data served as materials for creating vector maps; the developed scales made it possible to visually reflect the mapped processes.

The quantitative analysis method was used to estimate the number of small settlements in municipalities with a population of 1-25 and 26-50 people. A medium-term demographic forecast was used to establish the expected transformation in the distribution of the population in the Central Chernozem region and the boundaries of areas of increased population concentration and socio-demographic desertification. Using the extrapolation method, the forecast is calculated based on data from the Federal State Statistics Service (01.01.2023).

## RESULTS AND DISCUSSION

### Metropolization processes in the Central Chernozem region of Russia as determinants of settlement changes

In recent decades, the settlement system in all parts of the Central Chernozem region (Oblast) has undergone radical changes. The main ones are the concentration of population in metropolitan areas and their areas

<sup>1</sup> Results of the All-Russian Population Census 2021 (2021) [online] Available at: [https://rosstat.gov.ru/vpn\\_popul](https://rosstat.gov.ru/vpn_popul)



(agglomerations), depopulation of the periphery, degradation of many rural settlements, and the growth of abandoned villages.

As of January 1, 2023, 146,424,729 people lived in Russia, of which 36,789,914 people lived in rural areas. In addition to the fact that the Russian rural area has lost about 30,000 settlements over the past 25-30 years, there are now 75,000 villages in the country with residents from 1 to 25 people<sup>2</sup>. These settlements are clearly doomed. Modern population changes occur at the regional level largely of a “turning point” nature (Kirillov and Makhrova 2019). In rural areas Central Chernozem region of Russia there are some villages 1499 where population is 2.3 million people (Fig. 1). A distinctive feature of the Central Chernozem region urbanization processes was their slow rate up to until the 1970s of the 20<sup>th</sup> century: the city inhabitants made up absolute minority of the region's population – from 33% in Kursk region, up to 46% in Voronezh region<sup>3</sup>. Industrialization of the regions gave rise to the “urban revolution” and caused a drastic increase in migration of rural inhabitants to cities. By the end of the 1970s (1979) Voronezh, Belgorod and Lipetsk regions, and later the Kursk and Tambov regions have overcome the urban transition, which indicates that the society has entered a new phase of evolutionary development.

The high rates of urban resident's growth were accompanied by metropolis formation and population concentration in and around regional centers. Metropolization differed significantly by regions: in 1989 in Lipetsk, the total number 37% including urban population (59%), was concentrated, while in Tambov, 23% and 41% respectively. The metropolization processes in the Belgorod region were more complex: the intensive development

of the Kursk magnetic anomaly of union significance in the region's territory and the development of mining and ferrous metallurgy led to the active development of another metropolis – Stary Oskol; as a result, a polycentric (bipolar) metropolization was established. The presentation of urbanization growth rates of the regions and the dynamics of metropolis share in the regional population the Central Chernozem region of Russia can provide insight into Table 1.

Analysis of statistical data in Table 1 shows that the demographic transition was completed in Soviet time and shows that population tends to be concentrated in metropolitan cities. In the post-Soviet years, the share of urban population continues to increase slightly, which indicates that the urbanization development has completed an extensive stage and reached a qualitatively new level – the stage of “mature urbanization”. This is evidenced by the concentration of population in metropolises from 40% to 49% of the entire and from 59% to 82% urban population, the formation of urban systems (agglomerations). Tambov region is an exception to the general trend of urbanization (and metropolises) development: it has the lowest share of the metropolitan population in the total (23%) and urban population (41%) according to the latest census (2021).

The demographic development of metropolises, the increase in the weight of economic potential, as well as the concentration of administrative and managerial functions, give the capitals advantages in competing for investment and population. However, metropolization also has negative consequences caused by the processes of “compression of space”: the migration of population and productive forces from small and medium-sized cities and rural settlements to metropolises leads to territorial polarization of economic



Fig. 1. Location of the study area (the Central Chernozem region) within Russia

<sup>2</sup> Rural territories of the Russian Federation in 2021 (2021) [online] Available at: <https://rosstat.gov.ru/storage/mediabank/sel-terr.html>

<sup>3</sup> Federal state statistics service (2020) [online] Available at: [http://kurskstat.gks.ru/wps/wcm/connect/rosstat\\_ts/kurskstat/resources](http://kurskstat.gks.ru/wps/wcm/connect/rosstat_ts/kurskstat/resources)



**Table 1. Dynamics of urbanization levels and growth of metropolises in the Central Chernozem region of Russia in 1989-2021, as a percentage**

Population size, %	1	3	5	7	9
	2	4	6	8	10
1989					
Urban population	63	61	58	62	56
Rural population	37	39	42	38	44
Metropolis (s) in the total population	35	36	32	37	23
Metropolis(s) in the composition of the urban population	54	57	55	59	41
2002					
Urban population	65	62	61	64	57
Rural population	35	38	39	36	43
Metropolis (s) in the total population	36	36	33	42	25
Metropolis(s) in the composition of the urban population	57	58	55	65	44
2010					
Urban population	65	64	65	63	58
Rural population	35	36	35	37	42
Metropolis (s) in the total population	38	38	37	44	26
Metropolis(s) in the composition of the urban population	58	60	57	69	45
2021					
Urban population	67	69	69	65	62
Rural population	33	31	31	35	38
Metropolis (s) in the total population	36	46	40	43	27
Metropolis(s) in the composition of the urban population	56	67	59	69	44

Note: According to the All-Union (1989) and All-Russian Population Censuses (2002, 2010, 2021). The materials were provided by the Federal State Statistics Service (Rosstat) and territorial department of the Rosstat.

1 – the Belgorod region, 2 – Belgorod, Stary Oskol, 3 – the Voronezh region, 4 – Voronezh, 5 – the Kursk region, 6 – Kursk, 7 – the Lipetsk region, 8 – Lipetsk, 9 – the Tambov region, 10 – Tambov

and demographic development (Kuzin 2019; Litvinenko et al. 2020; Yakovenko and Chugunova 2022). Population concentration in metropolises and suburban areas is due to a size reduction of the rural settlement network, a growing number of abandoned (depopulated) rural localities, a decline in population, and abandonment of the earlier developed territories. The negative consequences of metropolization are particularly significant for remote and peripheral areas and for the network of small settlements (Aleksiev et al. 2020).

#### **Dynamics of rural settlement under the influence of metropolization processes in the Central Chernozem region**

The development of rural settlement depends on a number of factors: socio-economic, demographic, infrastructural, natural, and institutional. A characteristic feature of the national policy the 1960s and 1970s of the 20<sup>th</sup> century – in the period of rural settlement reconstruction for consolidation of rural localities was treatment of small settlements as “unpromising”. As a result, the rural settlement system underwent a radical change,

and the rural population has sharply declined. In the late Soviet and post-reform eras of Russia, the outflow of rural residents continued, but it was for other reasons. The globalization processes (Giddens 2004), their projection on the countryside, technological transformations in agriculture, and new social realities have set in motion demographic and migration processes. From 1970 to 2021 the number of rural inhabitants in the Central Chernozem region of Russia decreased by two million people, and the largest losses were sustained by the Kursk region (64%) and the Tambov region (56%). Can give an idea of intra-district differences in changing number of the rural population of the district Fig. 2.

The main trends in population changes in the Central Chernozem region of Russia testify to the long-term decline in the number of rural population in the rural-metropolis directions. The decrease in the number of rural residents has largely affected small settlements, leading to the emergence of new deserted (abandoned) villages and hamlets. Table 2 can provide an idea of the number of rurally depopulated localities.

By 2021, the number of abandoned villages in the Kursk region has almost doubled; in the Voronezh region, – one

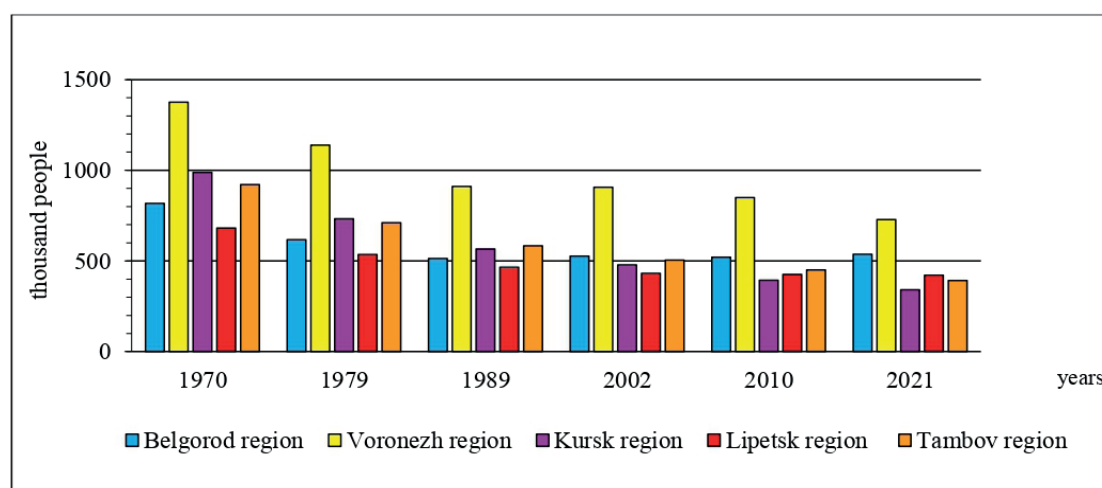


**Fig. 2. Dynamics of the rural population of the regions of the Central Chernozem region of Russia, 1970-2021, thousand people (compiled according to Russian population censuses)**

**Table 2. Rural depopulated settlements of the Central Chernozem region (2010, 2021). Compiled and calculated according to Russian population censuses**

Regions	Total rural settlements		Number of rural depopulated settlements		Share of rural depopulated settlements, %	
	2010	2021	2010	2021	2010	2021
Belgorod	1574	1573	69	104	4.4	6.6
Voronezh	1717	1699	74	118	4.3	6.9
Kursk	2770	2773	172	335	6.2	12.1
Lipetsk	1600	1601	110	135	6.9	8.4
Tambov	1638	1555	122	98	7.5	6.3
Central Chernozem	9299	9201	547	790	5.9	8.5

and a half times; in the Tambov region, it has decreased, which raises doubts among the authors of this article about the quality of statistical data coming from local municipalities (Strakhov 2022). Specifically, in the Petrovsky municipal district of the Tambov region, 15% of the settlements are devoid of population and abandoned. This means that the work of previous generations of people in depopulated villages is irretrievably lost.

In the rural settlement system Central Chernozem region of Russia a significant role is played by differentiation of rural "depopulated" localities. In Kursk, Lipetsk, and Tambov regions, there are more abandoned villages than the average number for the district; in the Tambov region, it is 1.7 times more than in the Voronezh region.

Our previous studies of rural settlement and analysis of statistical materials allowed us to state that the most radical changes have occurred (and will occur) in the growth and status change of the settlements, which we regard as "disappearing" ("smallest" (1-25 people) and "small" (26-50 people)). These conclusions are based on their consistent development trends: stably depressive state, population decrease and transformation of settlements into "depopulated" ones. The number of "smallest" rural settlements is maximum in the Kursk region (31.4%) and the Lipetsk region (29.2%), minimum in the Belgorod region (16.8%) and it is reached throughout the district Central Chernozem region of Russia 2325 or 24.8% network of settlements. To visualize the differences in the spatial distribution of the "smallest" rural settlements, cartograms were built for two different dates (Fig. 3, 4).

A comparative territorial analysis of cartograms of the distribution of the smallest rural settlements (from 1 to 25 people) in the Central Black Earth region between the last two population censuses revealed an increase in their number. In the Kursk region in 2021, they already made up one third of all rural settlements, and even more; for instance, they accounted for 50% in the Khomutovsky district and 42% in the Zheleznogorsk region. In the Tambov region, their share increased to 30%.

In 2021, the "leadership" in terms of the share of the "smallest" was retained and increased by the Kursk region (33%); it is followed by the Tambov region (30%) of all settlements. The number of "small" ones is less significant but it remains very "representative" in particular, it is a tenth of all rural settlements Central Chernozem region of Russia (Fig. 5, 6).

As follows from the cartograms, minimal changes were noted for the Voronezh region; it is the most ekistics "prosperous" both according to the data of 2010 and the 2021 census. In it, the total number of "small" settlements in 2010 was 8.7%, the most "problematic" is the Kursk region – 13.4% (in the Cheremisevsky, Shchigrovsky, Kurchatovsky districts their share reached 23-20%), in the Lipetsk and Tambov regions - the "golden" mean. In 2021, in all regions, there is a persistent trend of fragmentation of the network of settlements, and the type of settlements "26-50 people" accounts for 9% to 10% of the number of all rural settlements (122 in the Central Chernozem region).

The most emissivity "prosperous" both in 2010 and in 2021 remained the Voronezh region: the total number of "small" settlements (2010) was 8.7%, and the "problem" –

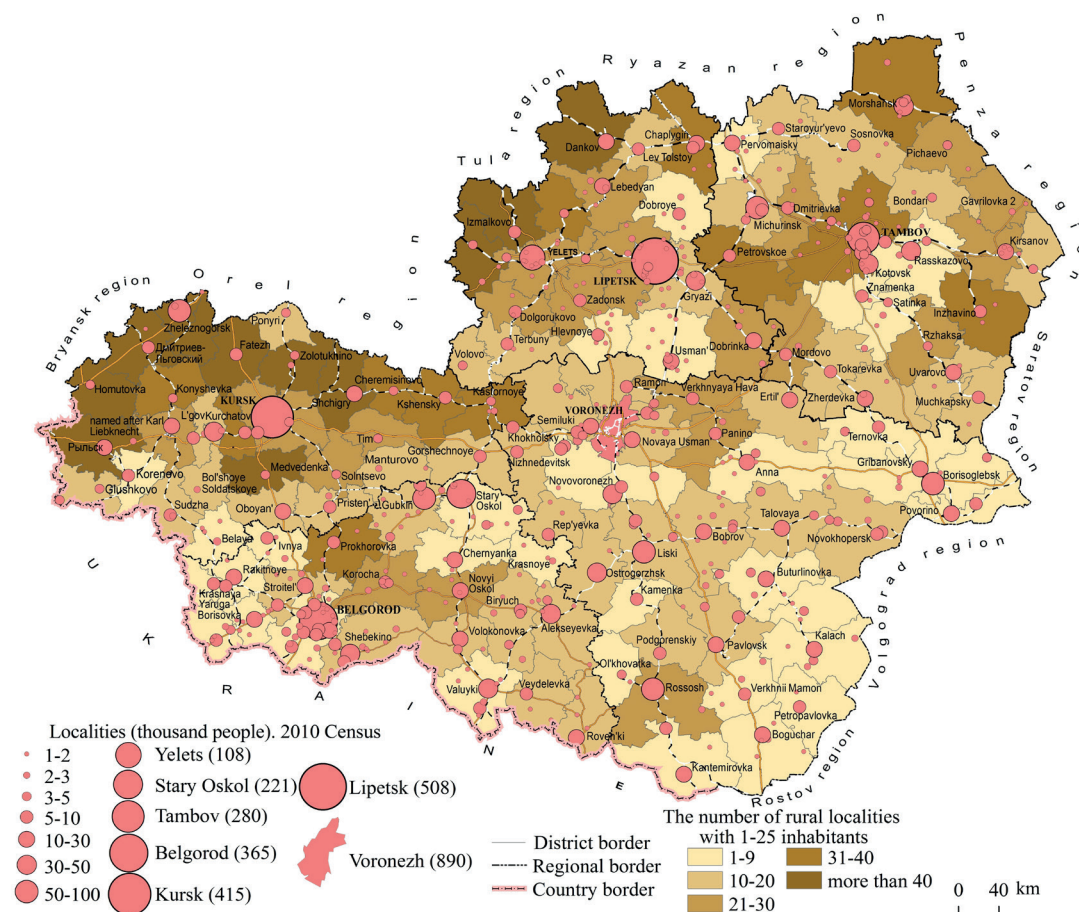


Fig. 3. Distribution of rural localities in the Central Chernozem region of Russia with a population of 1-25 people: 2010 Census

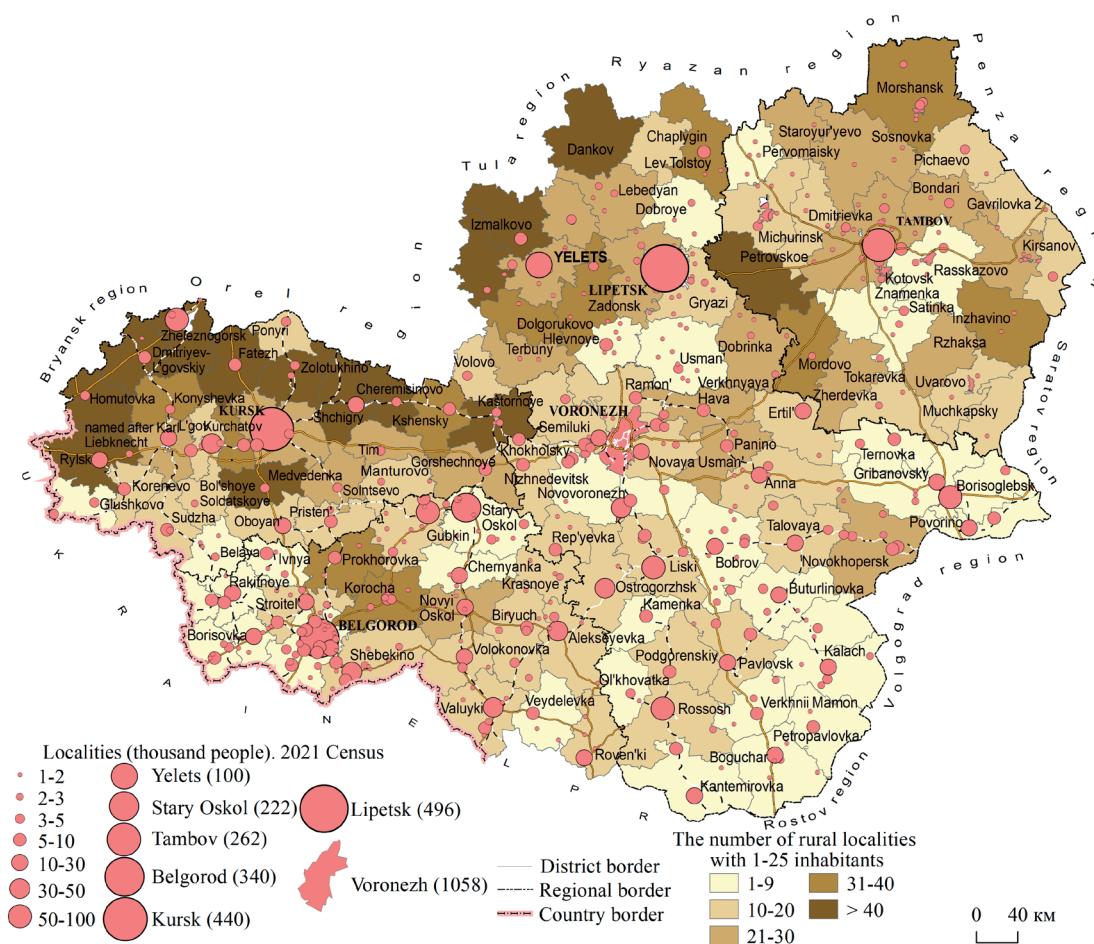


Fig. 4. Distribution of rural localities in the Central Chernozem region of Russia with a population of 1-25 people: 2021 Census



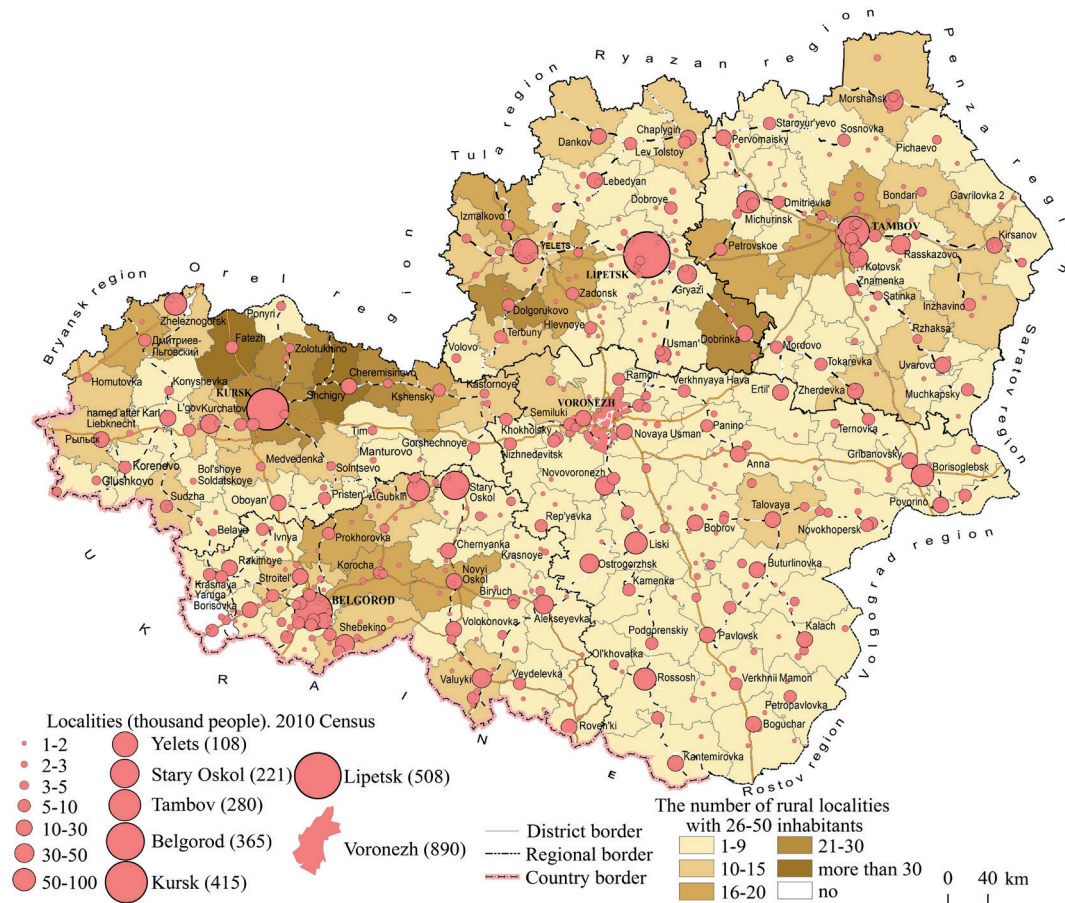


Fig. 5. Distribution of rural settlements in the Central Chernozem region of Russia with a population of 26-50 people: 2010 Census

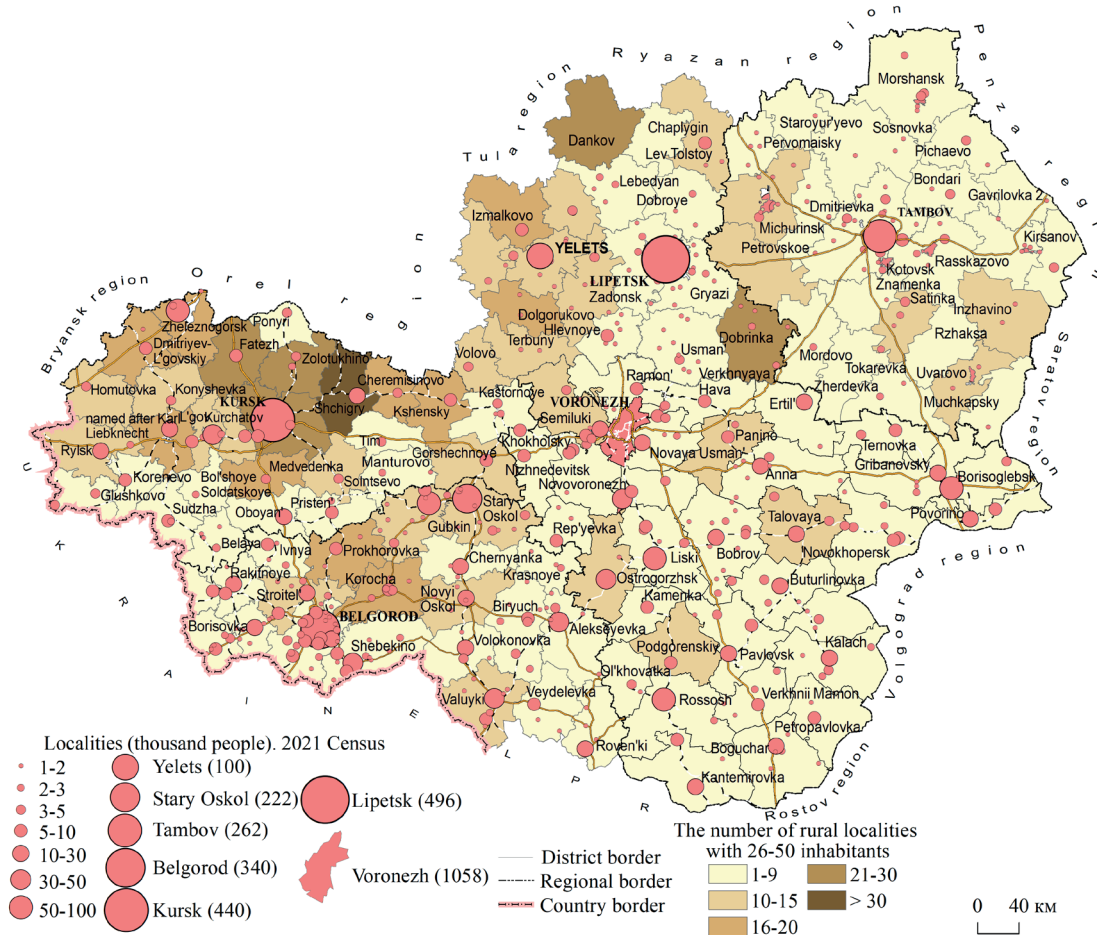


Fig. 6. Distribution of rural settlements in the Central Chernozem region of Russia with a population of 26-50 people: 2021 Census



Kursk region (13.4%), in the Lipetsk and Tambov regions – the “golden” mean; in 2021, in all regions, the trend of shrinking the network of settlements continues and, as a result, the share of the type of settlements “26-50 people” ranges from 9% to 10%. As a result, according to the latest population census, up to 45% (Kursk region) of rural settlements fell into the category of “disappearing” (Results ... 2021). According to our calculations, in the coming years, some of the smallest settlements will move into the category of “depopulated”, field observations in 2018-2022 convince us of the correctness of this conclusion. Their disappearance is natural in the context of the ongoing reforms and the increased demands of the population for the standards of quality of life. The degradation of rural settlements was aggravated by the destruction of social infrastructure of rural areas and the processes of its “optimization” in the country when small schools, kindergartens, and medical and obstetric stations were closed in settlements with up to 100 residents (and even larger ones), which became the determinants of the negative socio-economic conditions of life of rural residents, leading to their outflow to metropolises. The Kursk region, as the most sparsely populated in the rural settlement system of the Central Chernozem region, naturally became the one that suffered the most from the “optimization” reform. Smaller losses were suffered by suburban settlements in the region's metropolises. The prepared demographic forecast for the population system of the Central Chernozem region of Russia confirms our conclusions about further population concentration around metropolises and the socio-demographic desertification of the periphery of the five parts of the region (Oblast).

### Demographic forecast for rural population of the Central Chernozem region of Russia.

The study is based on a medium-term forecast, which is considered optimal for determining the future parameters of territorial differentiation of the population (Vinokurov 2002), as well as allowing to determine the places of population concentration and socio-demographic desertification of the region. The estimated total population and rural population in particular for 2030 was calculated based on data from the Federal State Statistics Service<sup>4</sup> in accordance with the demographic forecast method (Borisov 2001), using the extrapolation method, which is applicable to demographic forecasts for the medium term (Medkov 2006).

The following calculation algorithm was used:

(1) population changes exponentially according to the Eq. (1):

$$P_t = P_0 \times e^{k \times t} \quad (1)$$

where  $P_t$  is the total population at the end of the forecast period;  $P_0$  is the total population at the beginning of the forecast period;  $k$  is the estimated population growth rate in the forecast period;  $t$  is the value of the forecast period;  $e$  is the base of natural logarithms;

(2) according to the results of calculations, the classification of municipalities was carried out;

(3) maps for the entire population and separately for the rural population were constructed based on the obtained data (Fig. 7, 8).

The obtained forecast results indicate a possible trend of a steady decrease in the total population in the study area from 2023 to 2030 by 7.1%. The maximum decrease in

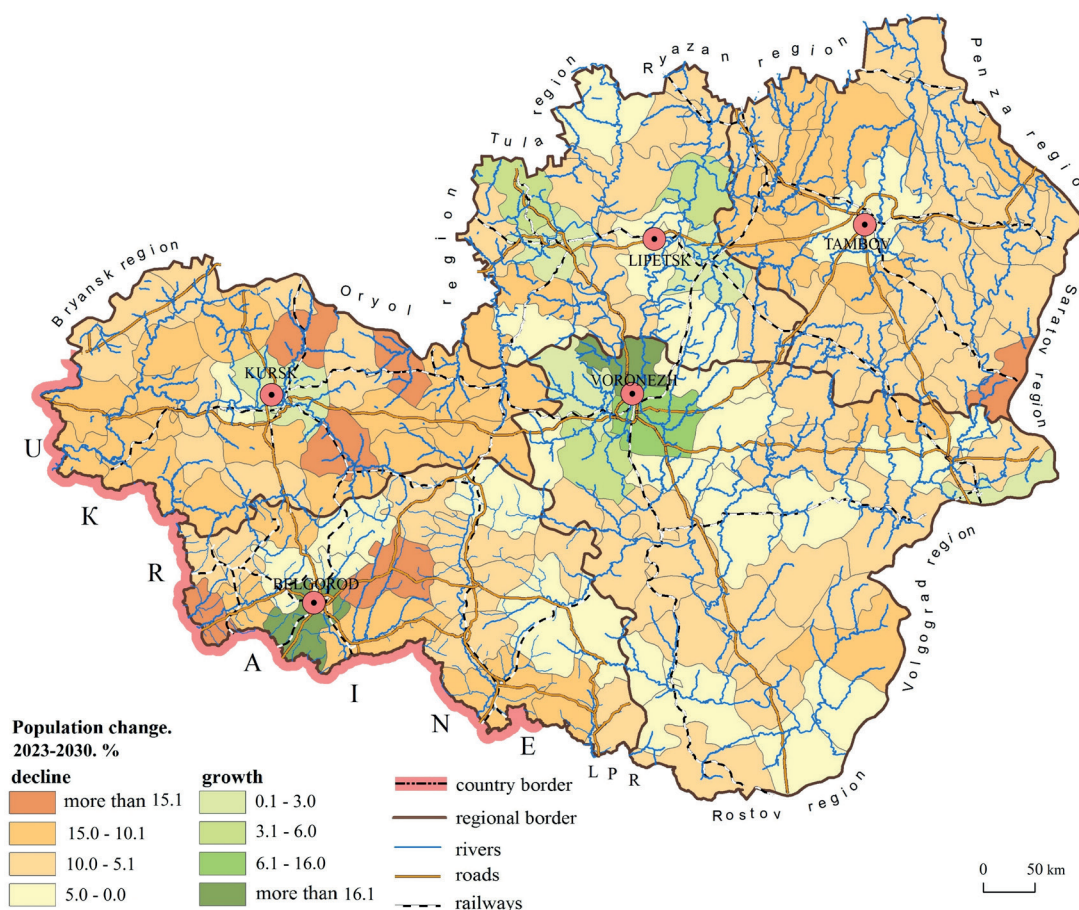


Fig. 7. Forecast of the total population distribution of the Central Chernozem region of Russia for 2030

<sup>4</sup> Regions of Russia. Socio-economic indicators 2022 (2022) Statistical compendium. Moscow: Rosstat (in Russian).

population is expected in the Belgorod region (-12.1%) (as a result of the border location with Ukraine) and, especially, in border municipalities. A new pattern has been identified that reflects the differences in the minimum reduction in the number of residents in all regions (except for the Tambov region) predicted on the periphery of the regions and the maximum reduction on the semi-periphery. According to the forecast for changes in the rural population in the Central Black Earth Region, depopulation will increase by 10.4%. As expected by 2030, the largest losses in the number of rural residents will be suffered by the Kursk (-18.4%) and Belgorod (-17.9%) regions, and the minimum by the Lipetsk region (-3.8%) (Fig. 8).

The forecast suggests that the transformation of the settlement systems of the Central Chernozem region of Russia will continue, which will be reflected in the concentration of rural residents in the suburbs of the capital's metropolises, and the demographic desertification of the semi-periphery and periphery of varying intensity.

## CONCLUSION

The conducted study of the dynamics of demographic processes in the settlement system of the Central Chernozem region showed that regional metropolises acted as loci of post-industrial processes and sources of competitiveness, which was facilitated by the agglomeration effect and economies of scale. A certain role in this was played by the status of regional capitals. Metropolization transformed the regional space, involved territories in the processes of modernization and innovation, but also led to stagnation and/or degradation of peripheral (most often, rural) territories, causing an increase in the number of abandoned villages and hamlets, the number of which increased over the period 2010-2021 (according to the latest population censuses) by 44.7%.

The use of a geographic information system made it possible to identify the spatial distribution of "disappearing" rural settlements and its population in the Central Chernozem region. It has been established that the processes of urbanization of the Central Chernozem region of Russia until the end of the 1970s of the 20<sup>th</sup> century were strongly extensive in nature and caused by regional industrialization. In the region, the urbanization transition ended in the late Soviet period (80-90 years of the 20<sup>th</sup> century) and urbanization reached a qualitatively new level – the stage of "mature urbanization".

The level of urbanization of the regions in the 20<sup>th</sup> and 21<sup>st</sup> centuries was and remained below the national average; however, they did not prevent the formation of regional metropolises (Belgorod, Stary Oskol, Kursk, Voronezh, Lipetsk, Tambov) as a result of urbanization processes. An assessment of the ekistics development of the regional Central Chernozem region of Russia metropolization has shown their significant differentiation. In parallel with the formation of regional metropolises, there has also been phenomena such as a radical transformation of rural settlement systems, a decrease in the rural population and sparse inhabitation of settlements. In the Kursk and Tambov regions, the number of rural residents decreased by half or more. In the structure of rural settlements in the Central Chernozem region of Russia, the number of rural localities with the smallest and small population sizes has increased (3405), which already accounts for 37% of the network of settlements, and most of them will cease to exist and lose their population in the near future. The factors of rural settlement transformation included the impact of globalization processes on rural areas, industrial methods of production in agriculture, an underdeveloped social environment, the attractiveness of large cities for rural inhabitants, and a number of other reasons.

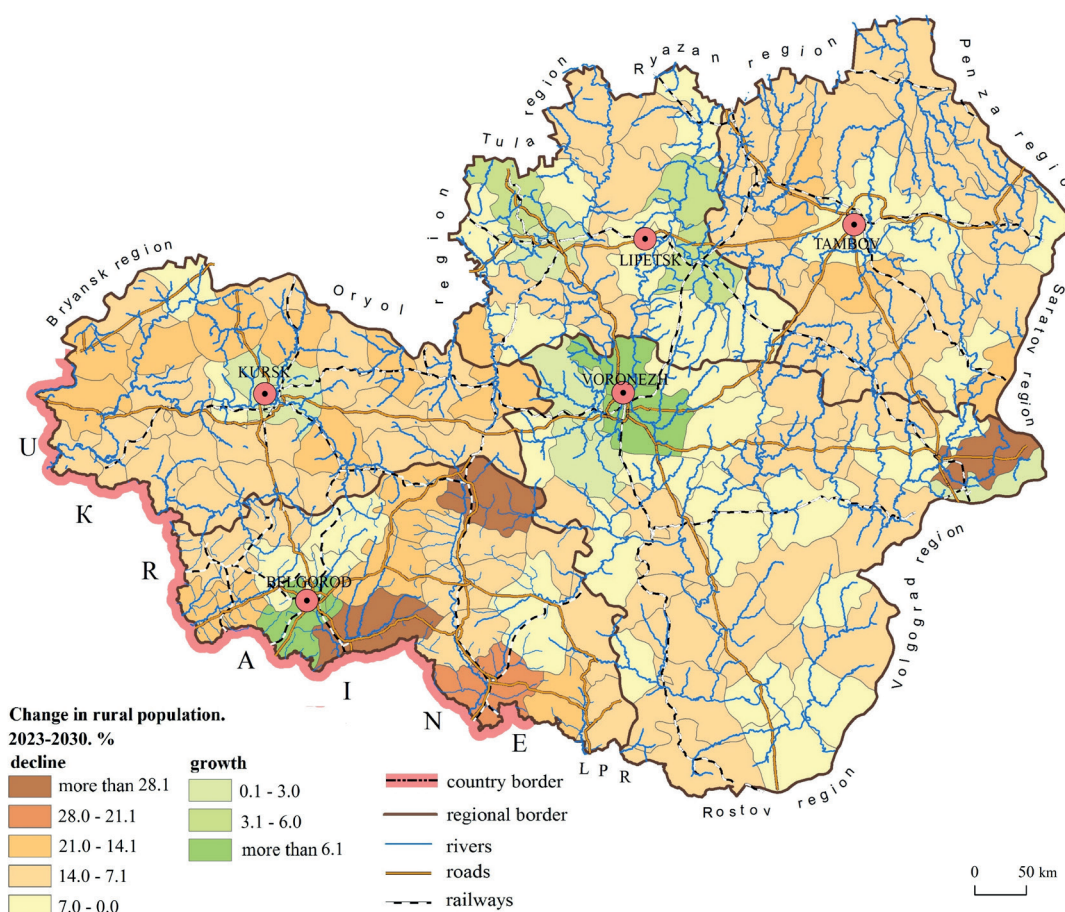


Fig. 8. Forecast of the total population distribution of the Central Chernozem region of Russia for 2030

The calculated medium-term demographic forecast provides a reduction in the total population and, more significantly, in the rural population, for population to be mainly concentrated in and around metropolises, further depopulation of peripheral rural territories, which will lead to increased polarization of the region's settlement system. The results obtained indicate that precisely under the influence of the metropolization process there will be a further consistent "compression" of rural settlement with significant spatial differentiation. The prospect of further developments on this topic may be related to current changes in depopulation of the Russian-Ukrainian border using previously developed methodology and the use of

geoinformation technologies (Igonin, Tikunov 2018). The results of the work confirm the relevance of research into the features of metropolization in the regions of Russia and the need to identify patterns of transformation of rural settlements, and their spatial stratification using a geographic information system.

The study's practical significance lies in providing state institutions with the opportunity to make effective decisions for the timely improvement of the territorial settlement system. State policy should allow for the development of diverse types of settlements, and the quality of the living environment in different settlements should be comparable. ■

## REFERENCES

- Alekseev A.I., Vasilyeva O.E., Udovenko V.S. (2020) Rural way of life: the experience of studying on the example of small villages in the Leningrad region. *Bulletin of St. Petersburg University, Earth Sciences*. 65(3), 468-480, DOI: 10.21638/spbu07.2020.304
- Borisov V.A. (2001) *Demography*. Moscow: Publishing house NOTABENE (in Russian)
- Buryak Z., Lisetskii F., Gusarov A., Narozhnyaya A., Kitov M. (2022) Basin-scale approach to integration of agro- and hydroecological monitoring for sustainable environmental management: a case study of Belgorod Oblast, European Russia. *Sustainability*. 14(2), 927, DOI: 10.3390/su14020927
- Buryak Z.A., Zelenskaya E.Y., Poletaev A.O., Tsybenko V.V. (2019) System approach to soil protection and ecological arrangement of watersheds at the regional level, Belgorod oblast. *Ecology, Environment and Conservation*. 25(1), 219-228.
- Chizhikova N., Yermolaev O., Golosov V., Mukharamova S., Saveliev A. (2022) Changes in the regime of erosive precipitation on the European Part of Russia for the period 1966–2020. *Geosciences*. 12(7), 279, DOI: 10.3390/geosciences12070279
- Chugunova N., Narozhnyaya A., Polyakova T., Kuharuk N., Morkovskaya D. (2021) Spatial differentiation of border areas of the Central Black Earth Region in metropolisation processes. Moscow: Atlantis Press International B.V. 14-19.
- Chugunova N.V., Likhnevskaya N.V. (2019) Spatial differentiation of the standard of living in the population as a representation of disproportions in socioeconomic development: a case study of Belgorod Oblast. *Regional Research of Russia*. 9(3), 267-277.
- Chugunova N., Polyakova T., Narozhnyaya A., Lisetskii F. (2023) Current challenges to the sustainable development of rural communities in Russia's Central Chernozem Region. *Rural and Regional Development*. 1 (1), 10001, DOI: 10.35534/rrd.2023.10001
- Gaydukov V.R., Zheleznyakov A.S., Tikunov V.S., Tikunova I.N. (2022) Creating an index of demographic development of countries and regions on the example of Mongolia and its immediate environment, using GIS technologies. *InterCarto. InterGis*. 28(2), 86-110, DOI: 10.35595/2414-9179-2022-2-28-86-110 (in Russian)
- Giddens E. (2004) *The Elusive world: How globalization changes our life*. Rus. ed., transl. by Jadov, V. Moscow: All the world. (in Russian)
- Huseynova B.A. (2023) Depopulation of the ethnic diverse mountain villages in the northwestern part of Azerbaijan and the development of a sustainable rural development model. *Regional Geosystems*. 47(1), 34-48, DOI: 10.52575/2712-7443-2023-47-1-34-48
- Igonin A.I., Tikunov V.S. (2018) The Russian-Ukrainian border – emergence and sustainability. *Population and Economics*. 2(4), 136-160, DOI: 10.3897/popecon.2.e36062
- Igonin A.I., Tikunov V.S. (2019) Multivariate mathematical and cartographic modeling of demographic characteristics of regions of Russia and Europe. *Geodesy and cartography*. 80(11), 26-36, DOI: 10.22389/0016-7126-2019-953-11-26-36 (in Russian, abs English).
- Kaur K., Kaur G. (2021) Livelihood security of small and marginal farm households in Punjab. *Indian Journal of Economics and Development*. 17(2), 376-382.
- Kirillov P.L., Makhrova A.G. (2019) Shifts in interregional proportions in population settlement over the territory of Russia in 2002–2017. *Population and economics*. 1, 21-37, DOI: 10.3897/popecon.3.e34905
- Kochurov B.I., Blinova E.A., Ivashkina I.V. (2021) Development of Russian cities after the COVID-19 pandemic. *Regional geosystems*. 45(1), 183-193, DOI: 10.52575/2712-7443-2021-45-2-183-193 (in Russian).
- Kuzin V. (2019) Metropolisation process of contemporary Russia in the context of polarization. *Pskov Journal of Regional Studies*. 1(37), 33-45.
- Lisetskii F. (2021) Rivers in the focus of natural-anthropogenic situations at catchments. *Geosciences (Switzerland)*. 11(2), 63, DOI: 10.3390/geosciences11020063
- Lisetskii F.N., Zemlyakova A.V., Terekhin E.A., Narozhnyaya A.G., Pavlyuk Y.V., Ukrainskii P.A., Kirilenko Z.A., Marinina O.A., Samofalova O.M. (2014) New opportunities of geoplanning in the rural area with the implementing of geoinformation technologies and remote sensing. *Adv. Environ. Biol.* 8, 536-539.
- Litvinenko T.V., Kumo K., Savvinova A.N., Filippova V.V. (2020) Rural population dynamics in the Russian extreme North in 1989-2019: a case of Sakha republic (Yakutia). *Geography, Environment, Sustainability*. 13(4), 65-71, DOI: 10.24057/2071-9388-2020-137
- Lynch K. (2005) *Rural-urban interaction in the developing world*. Routledge, London – NewYork.
- Marchand P., Samson I. (2004) Metropolises and Russia's Economic Development. *Voprosy Ekonomiki*. 1, 4-18 (in Russian).
- Medkov V.M. (2006) *Introduction to demography: Textbook for universities* Moscow: Academic Project. ISBN 5-8291-0527-6 (in Russian).
- Nefedova T.G. (2018) Factors and trends of the structure of rural settlements in Russia. *Socio-economic geography. Bulletin of the Association of Russian geographers and social scientists*. 7, 4-21 (in Russian).
- Nefedova T.G., Travish A.I. (2015) *Journey from St. Petersburg to Moscow: 222 years later*. Moscow LENAND (in Russian).
- Nefedova and Treyvish (2020) Polarization and shrinkage of active space in the core of Russia: trends, problems and possible solutions. *Demographic Review*. 7(2), 31-53, DOI: 10.17323/demreview.v7i2.111138
- Pivovarov G.A., Alekseev A.I. (2018) Rural-urban relationships at the border of the Moscow agglomeration. *Vestnik Moskovskogo Universiteta, Seriya Geografiya*. 6, 100-103.
- Sokolova E.V., Kuznetsov D.V. (2018) Main trends in the formation of rural settlements in the territory of Tara (the Irtysh area) between 1920 and 1980. *Scientific papers-series management economic engineering in agriculture and rural development*. 18(3), 429-439.
- Strakhov K.A. (2022) Methods for the reconstruction of municipal statistics data: case study of the intracity municipal district in St. Petersburg. *Izvestiya Rossiiskoi Akademii Nauk, Seriya Geograficheskaya*. 86(4), 503-518.



- Tikunov V.S., Belozarov V.S., Shchitova N.A., Sopnev N.V. (2022) Spatial analysis of the spread of Covid-19 and its demographic consequences in the regions of the South of European Russia. *Population and Economics*. 6(4), 189-208, DOI: 10.3897/popecon.6.e97380
- Vinokurov A.A. (2002) Demographic forecast: formation, methods and results. *Economic analysis: theory and practice*. 3, 30-48 (in Russian).
- Yakovenko N.V., Chugunova N.V. (2022) Multi factor approach to assessing the socio economic and metropolitan environmental development of border areas in the Central Black Soil Region of Russia (Belgorod, Voronezh and Kursk Regions) in order to develop a model concept. *South of Russia: ecology, development*. 17(3), 163-174, DOI: 10.18470/1992-1098-2022-3-163-174
- Yermolaev O.P., Lisetskii F.N., Marinina O.A., Buryak Z.A. (2015). Basin and eco-regional approach to optimize the use of water and land resources. *Biosciences Biotechnology Research Asia*. 12, 145-158, DOI: 10.13005/bbra/2185
- Zubarevich N.V. (2003) Impact of globalization on the development of Russian regions: results and prospects. *Large cities and challenges of globalization*. 37–57.



# INTEGRATION OF GEOSPATIAL TECHNIQUES AND ANALYTICAL HIERARCHY PROCESS (AHP) IN DEMARCATING GROUNDWATER POTENTIAL ZONES IN LAKHIMPUR DISTRICT, ASSAM, INDIA

**Arpana Handique<sup>1</sup>, Pradyut Dey<sup>2\*</sup>, Santanu Kumar Patnaik<sup>2</sup>**

<sup>1</sup> Centre for Studies in Geography, Dibrugarh University, Dibrugarh, India

<sup>2</sup> Department of Geography, Rajiv Gandhi University, Itanagar, Arunachal Pradesh, India

\*Corresponding author: pradyut.dey@rgu.ac.in

Received: January 14<sup>th</sup> 2024 / Accepted: September 1<sup>st</sup> 2024 / Published: October 1<sup>st</sup> 2024

<https://doi.org/10.24057/2071-9388-2024-3208>

**ABSTRACT.** Overexploitation and climate change have threatened the availability and sustenance of groundwater resources. A proper understanding of the regional distribution of groundwater is crucial to ensure long-term water security. The present study aims to identify the groundwater potential zones in the Lakhimpur district of Assam using the Analytical Hierarchy Process (AHP) in combination with geospatial technologies. The occurrence of groundwater in the region was determined by several factors including geomorphology, lithology, slope, distance from the river, drainage density, lineament density, rainfall, curvature, soil, land use, land cover, Normalized difference vegetation index (NDVI), and topographic wetness index (TWI). These factors organized as thematic layers were utilized to generate a groundwater potential zones (GWPZ) map in the GIS environment. The AHP, an effective decision-making technique, was adopted to assign weights to each thematic layer corresponding to their relative importance in influencing groundwater availability. The GWPZ map prepared using the weighted overlay techniques was categorized into three classes: good, moderate, and poor. The result revealed that the good potential zone comprises 1909.41 km<sup>2</sup> (65.12%), moderate 1018.25 km<sup>2</sup> (34.72%) and the poor zone comprises 4.22 km<sup>2</sup> (0.14%) of the total geographical area. The obtained results of 73.33% (Overall accuracy), 0.708 (ROC-AUC), and 0.50 mbgl (groundwater level fluctuation) between pre-monsoon and post-monsoon prove that the model has performed satisfactorily in identifying groundwater potential zones. The findings provide a framework for the effective exploration and management of groundwater resources, ensuring their future availability in the region.

**KEYWORDS:** analytical hierarchical process, groundwater potential zone, remote sensing and GIS

**CITATION:** Handique A., Dey P., Patnaik S. K. (2024). Integration of Geospatial Techniques and Analytical Hierarchy Process (AHP) in demarcating Groundwater Potential Zones in Lakhimpur District, Assam, India. *Geography, Environment, Sustainability*, 3(17), 109-125

<https://doi.org/10.24057/2071-9388-2024-3208>

**Conflict of interests:** The authors reported no potential conflict of interest.

## INTRODUCTION

Groundwater is a crucial natural resource that is extensively used for drinking purposes, agriculture, manufacturing, and ecological sustenance throughout the world. According to Das and Pardeshi (2018), "Groundwater is the second largest important freshwater reservoir and the best alternative for human and economic activities in comparison to surface water". The pattern and availability of groundwater in India are very complex due to a wide range of factors that include, diverse geological settings, differential rock types and formations, climatic variations, diverse hydrological characteristics, and variations in land use and land cover practices. These complexities are intensified by the over-exploitation of groundwater resources in several parts of the country, given that more than 90% of the rural population and nearly 30% of the urban population rely directly on groundwater for drinking and other domestic needs (Parthasarathy and Deka 2019).

Thus, it becomes essential to identify areas that exhibit significant groundwater potential that address growing water demand and ensure sustainability (Saravanan et al. 2021).

The traditional methods of groundwater assessment that involve geophysical surveys are time-consuming and economically less feasible as they require sophisticated instruments, high-tech manpower, and explicit logistic support (Jha et al. 2010; Manap et al. 2014; Vaddiraju and Talari 2023). Moreover, these survey methods may not always take into account numerous factors that influence the groundwater regime (Oh et al. 2011).

In recent times, remote sensing and GIS techniques have proved to be the most cost-effective, and efficient in identifying potential groundwater locations along with field-based data validation (Chakraborty et al. 2018; Arabameri et al. 2020). The widely accessible satellite data providing large spatial and temporal information makes it easier to perform groundwater studies (Shekhar and

Pandey 2014). The ability of GIS to manage a huge amount of spatial data has made it a reliable tool for groundwater exploration and management (Abijith et al. 2020; Ahmad et al. 2020; Arulbalaji et al. 2019). Several studies suggest that the integration of multi-criteria decision-making methods with geospatial technology has been excellent in the assessment of groundwater storage and availability (Qadir et al. 2020; Roy et al. 2020).

The Analytical Hierarchy Process (AHP) is considered to be one of the most user-friendly and reliable MCDM methods which are extensively used in a wide range of fields such as regional planning, natural resource management, and environmental monitoring (Agarwal et al. 2013; Adimalla and Taloor 2020; Dar et al. 2020; Dwivedi et al. 2021). The factors influencing groundwater zonation in the study area namely, geomorphology, lithology, slope, distance from the river, drainage density, lineament density, rainfall, curvature, soil, LULC, NDVI, and TWI were selected based on an extensive review of scholarly literature (Table 1). The prime aim of the research is to identify the groundwater potential zone in the Lakhimpur district, located in Assam which will serve as a repository of information that can

be used by the decision-makers and policy formulators for effective management of groundwater resources, and maintain sustainability.

MATERIALS AND METHODS

Study Area

The study focuses on the Lakhimpur district of Assam which is located on the northern bank of the Brahmaputra River, comprising a geographical area of about 2277 km<sup>2</sup> and situated between 26°48'N and 27°53'N and 93°42' and 94° 20'E longitude (Fig. 1). Its elevation ranges between 56 to 351 meters above sea level. The district is bounded by Arunachal Pradesh to the north, Dhemaji District to the east, Majuli District and the river Brahmaputra to the south, and Biswanath District to the west. The district is well-drained by numerous rivers like Subansiri, Dikrong, Boginadi, and Ranganadi and is known for its fertile alluvial plains and scenic beauty and is relatively flat and is significant for agricultural practices mainly, wet paddy cultivation.

Table 1. Literature review on the control factor selected for the delineation of groundwater potential zone

Authors	Geom	Geol	LD	DD	LULC	SOI	SL	RF	DR	TWI	NDVI	CUR	GWD	Litho
Vaddiraju and Talari 2023		•		•	•	•	•	•	•					
Das et al. 2022	•		•	•	•	•	•	•						•
Hasanuzzaman et al. 2022	•		•	•	•	•	•	•	•	•	•			•
Jari et al. 2022	•	•	•	•			•	•	•					
Mahato et al. 2022	•	•	•	•	•	•	•	•	•	•				
Melese and Belay 2022	•	•	•	•	•	•	•	•		•		•		
Sajil et al. 2022	•		•	•	•	•	•	•					•	•
Deshpande et al. 2021		•	•	•	•	•	•	•			•		•	
Muthu and Sudalaimuthu 2021	•	•	•	•	•	•	•	•						
Saravanan et al. 2021	•	•	•	•	•	•	•	•						

Geom: Geomorphology, Geol: Geology; LD: Lineament Density, DD: Drainage Density, LULC: Land use Landcover, SOI: Soil, SL: Slope, RF: Rainfall, WZT, DR: Distance from the river, TWI: Topographic Wetness Index, NDVI: Normalized Difference Vegetation Index, CUR: Curvature, GWD: Groundwater depth; Litho: Lithology.

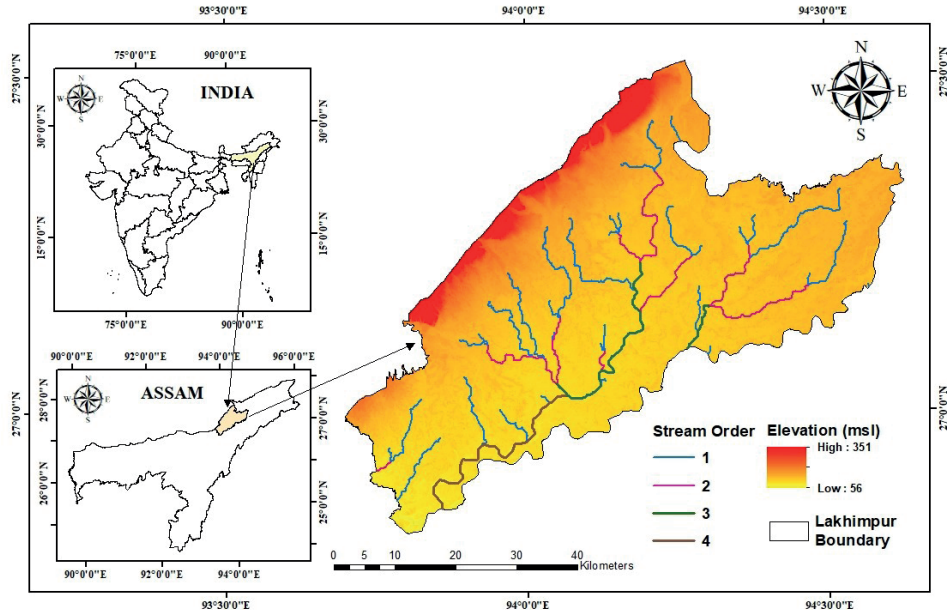


Fig. 1. Location map of the Lakhimpur District, Assam

### Thematic layers preparation

The methodological workflow is depicted in Fig 2. The selection of thematic layers for any scientific study is influenced by the geographical location and the researcher's viewpoint (Machiwal et al. 2011). Delineation of the groundwater availability zones is an intricate process that requires careful selection of the causative factors that influence the groundwater regime of any particular region. The research considered thematic layers including geomorphology, lithology, slope, distance from the river, drainage density, lineament density, rainfall, curvature, soil, LULC, NDVI, and TWI which were acquired from different sources (Table 2). The Geomorphology and Lithological unit maps were collected from the Bhukosh, Geological Survey of India for the entire country which was clipped with the study area shape file using ArcGIS software. The Slope, Lineament Density, Drainage Density, Curvature, distance from the river, and TWI were generated using the SRTM Digital Elevation Model at 30 m resolution in ArcGIS using the Arc toolbox functions. The rainfall data was obtained from the Climate Research Unit (CRU) at 5° resolution in gridded format for the entire world which was clipped with the study area boundary and was interpolated using the Inverse Distance Weighing interpolation technique in ArcGIS 10.4. The soil map was obtained from the International Soil Reference and Information System (ISRIC) in shape file format and was clipped with the study area accordingly. Land use and Land cover map was generated from the Landsat 8 OLI imagery obtained from USGS Earth Explorer using maximum likelihood classification in ArcGIS. Landsat 8 OLI imagery was also utilized to generate NDVI classes.

### Analytical Hierarchy Process and its Application

The Analytical Hierarchy Process (AHP), proposed and popularised by Saaty in the year 1980 was utilized for determining the weights for every thematic layer used in the research (Gautam et al. 2023). AHP is a structural process used in complex decision-making to ascertain the weightage of different factors through a pairwise comparison matrix (Gopinath et al. 2016; Ghosh and Gope 2021). In groundwater and environmental studies, the AHP-based multi-criteria decision-making technique is the most widely recognized and utilized process throughout the world (Shelar et al. 2022).

### Weight assignment and normalization

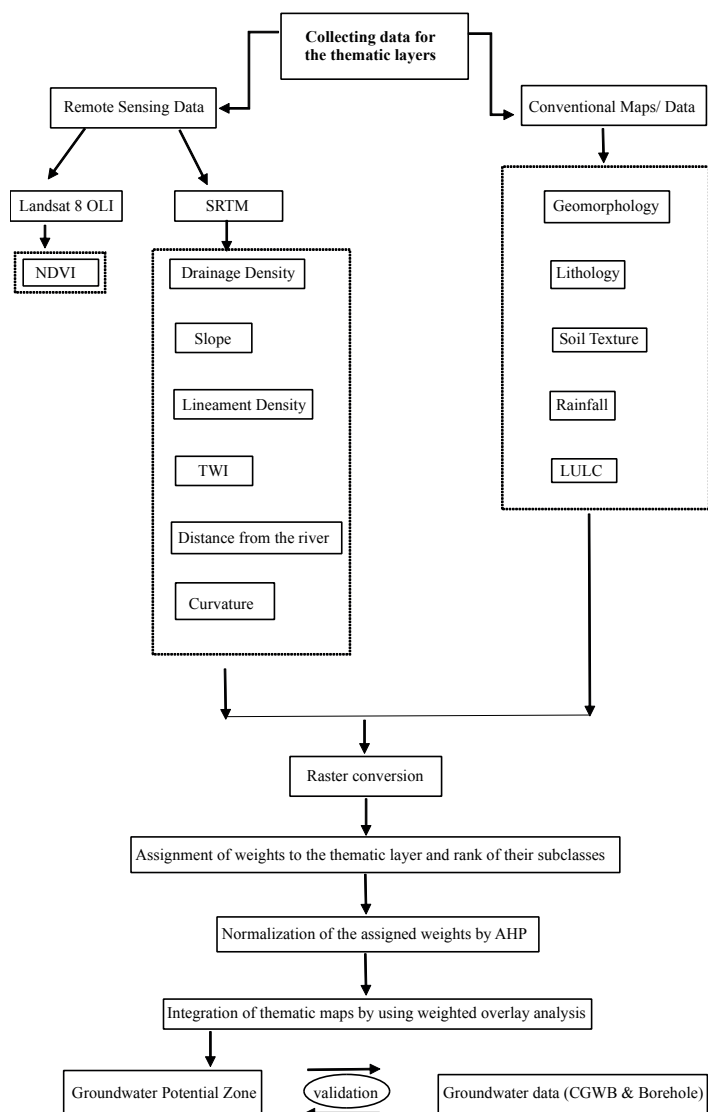
In the process of analysis, the most decisive step is providing weightage to each influencing factor as the outcome is directly dependent on it (Muralitharan and Palanivel 2015). According to Benjmel et al. 2020, "The AHP model has four stages: weight assignment, pairwise comparison matrix, weight normalization, and consistency assessment". To assign a weight, a decision hierarchy was created identifying the importance of different thematic layer and their influence on the groundwater availability of the study area. The pairwise comparison matrix was generated utilizing the causative factors arranged in rows and columns and then ratings were assigned utilizing Saaty's scale which ranges from 1 to 9 (Table 3), where a rating of 1 indicates equal importance and a rating of 9 indicates extreme importance of one criterion over the other (Table 4). Following that the normalized factor weights were derived by normalizing the value of its eigenvector (Table 5). This normalization process is essential to minimize the biases that exist in the weight assignment of the thematic layers (Saravanan et al. 2021). Subsequently, the criterion weights were generated, and the sum of all these weights was found to be 1.

**Table 2. Thematic layers and the data sources**

Causative Factor	Data Source
Geomorphology	Geological Survey of India (1:250,000) <a href="https://bhukosh.gsi.gov.in/">https://bhukosh.gsi.gov.in/</a>
Lithology	Geological Survey of India (scale 1: 2,000,000) <a href="https://bhukosh.gsi.gov.in/">https://bhukosh.gsi.gov.in/</a>
Slope	SRTM- Digital Elevation Model (DEM) 30 × 30 m Resolution <a href="http://earthexplorer.usgs.gov/">http://earthexplorer.usgs.gov/</a>
Lineament Density	SRTM- Digital Elevation Model (DEM) 30 × 30 m Resolution <a href="http://earthexplorer.usgs.gov/">http://earthexplorer.usgs.gov/</a>
Drainage Density	SRTM- Digital Elevation Model (DEM) 30 × 30 m Resolution <a href="http://earthexplorer.usgs.gov/">http://earthexplorer.usgs.gov/</a>
Curvature	SRTM- Digital Elevation Model (DEM) 30 × 30 m Resolution <a href="http://earthexplorer.usgs.gov/">http://earthexplorer.usgs.gov/</a>
Rainfall	Climatic Research Unit (CRU) high-resolution gridded time series dataset at 0.5° resolution (2021-22) <a href="https://data.chc.ucsb.edu/products/CHIRPS-2.0/">https://data.chc.ucsb.edu/products/CHIRPS-2.0/</a>
Soil Texture	International Soil Reference and Information System (ISRIC) <a href="http://soilgrids.org">http://soilgrids.org</a>
LULC	Landsat 8 OLI <a href="http://earthexplorer.usgs.gov/">http://earthexplorer.usgs.gov/</a>
Distance from the river	SRTM- Digital Elevation Model (DEM) 30 × 30 m Resolution <a href="http://earthexplorer.usgs.gov/">http://earthexplorer.usgs.gov/</a>
NDVI	Landsat 8 OLI <a href="http://earthexplorer.usgs.gov/">http://earthexplorer.usgs.gov/</a>
TWI	SRTM- Digital Elevation Model (DEM) 30 × 30 m Resolution <a href="http://earthexplorer.usgs.gov/">http://earthexplorer.usgs.gov/</a>

**Table 3. Pairwise comparison matrix chart for all the factors developed for AHP-based groundwater potential zoning**

Factors	Geomorphology	Lithology	Slope	Lineament Density	Drainage Density	Curvature	Rainfall	Soil	LULC	Distance from the river	NDVI	TWI
Geomorphology	1	1	2	3	4	4	3	4	4	4	5	5
Lithology	1	1	2	2	3	3	5	3	3	4	4	5
Slope	0.5	0.5	1	1	1	3	2	3	3	3	3	4
Lineament Density	0.33	0.5	1	1	1	4	5	3	3	1	4	4
Drainage Density	0.25	0.33	1	1	1	5	5	3	3	3	3	5
Curvature	0.25	0.33	0.33	0.25	0.2	1	3	3	1	3	0.5	1
Rainfall	0.33	0.2	0.5	0.2	0.2	0.33	1	2	0.5	2	2	3
Soil	0.25	0.33	0.33	0.33	0.33	0.33	0.5	1	0.5	3	2	1
LULC	0.25	0.33	0.33	0.33	0.33	1	2	2	1	1	1	2
Distance from the river	0.25	0.25	0.33	1	0.33	0.33	0.5	0.33	1	1	0.5	1
NDVI	0.2	0.25	0.33	0.25	0.33	2	0.5	0.5	1	2	1	2
TWI	0.2	0.2	0.25	0.25	0.2	1	0.33	1	0.5	1	0.5	1

**Fig. 2. Methodological Flowchart**



**Table 4. Description of the Saaty's scales for AHP based pair-wise comparison: (Saaty (1980))**

Ratings	Degree of preferences	Descriptions
1	Equally	Both factors contribute equally
3	Moderately	Experiences and judgment slightly lean towards a specific factor
5	Strongly	Experiences and judgment strongly favor a particular factor over another
7	Very Strongly	One factor is strongly favored over another, and its dominance is shown in practice
9	Extremely	The preference of one factor over another is affirmed to the highest degree possible
2, 4, 6, 8	Intermediate values	Represents compromises between the preferences in ratings 1, 3, 5, 7, and 9

**Table 5. Normalized pairwise comparison matrix and computation of criterion weight**

Factors	Geomorphology	Lithology	Slope	Lineament Density	Drainage Density	Curvature	Rainfall	Soil	LULC	Distance from the river	NDVI	TWI	Criteria Weight
Geomorphology	0.21	0.19	0.21	0.28	0.34	0.16	0.11	0.15	0.19	0.14	0.19	0.15	0.19
Lithology	0.21	0.19	0.21	0.19	0.25	0.12	0.18	0.12	0.14	0.14	0.15	0.15	0.17
Slope	0.10	0.10	0.11	0.09	0.08	0.12	0.07	0.12	0.14	0.11	0.11	0.12	0.11
Lineament Density	0.07	0.10	0.11	0.09	0.08	0.16	0.18	0.12	0.14	0.04	0.15	0.12	0.11
Drainage Density	0.05	0.06	0.11	0.09	0.08	0.20	0.18	0.12	0.14	0.11	0.11	0.15	0.12
Curvature	0.05	0.06	0.04	0.02	0.02	0.04	0.11	0.12	0.05	0.11	0.02	0.03	0.05
Rainfall	0.07	0.04	0.05	0.02	0.02	0.01	0.04	0.08	0.02	0.07	0.08	0.09	0.05
Soil	0.05	0.06	0.04	0.03	0.03	0.01	0.02	0.04	0.02	0.11	0.08	0.03	0.04
LULC	0.05	0.06	0.04	0.03	0.03	0.04	0.07	0.08	0.05	0.04	0.04	0.06	0.05
Distance from the river	0.05	0.05	0.04	0.09	0.03	0.01	0.02	0.01	0.05	0.04	0.02	0.03	0.04
NDVI	0.04	0.05	0.04	0.02	0.03	0.08	0.02	0.02	0.05	0.07	0.04	0.06	0.04
TWI	0.04	0.04	0.03	0.02	0.02	0.04	0.01	0.04	0.02	0.04	0.02	0.03	0.03

**Assessing the Consistency of the AHP model**

$$CR = \frac{CI}{RI} \quad (2)$$

The consistency of the weights assigned through a pairwise comparison matrix was assessed through the Consistency Index ( $CI$ ) and Consistency Ratio ( $CR$ ) following Eq. 1 and Eq. 2 respectively (Saaty 1980). The Consistency Index ( $CI$ ) is dependent on the highest eigenvalue of the comparison matrix and the number of factors under consideration (Ying et al. 2007), while on the other hand Consistency Ratio ( $CR$ ) is dependent on the Consistency Index ( $CI$ ) and Random Index ( $RI$ ) as suggested by Saaty 1980.

$$CI = \frac{\lambda_{max} - n}{n - 1} \quad (1)$$

where,  $\lambda_{max}$  principal eigenvalue and  $n$  is the no. of factors

where  $RI$  is the Random Index value (Table 4) and  $CI$  is the Consistency Index

According to Saaty 1980, "the  $CR$  value should be  $\leq 0.1$  to continue with further analysis. If it is greater than 0.1, then the inconsistency needs to be ascertained and the calculations need to be revised". In the case of the present study,  $CR$  values of  $\leq 0.1$  overall as well as each parameter (Table 7) suggest that there exists a high level of consistency in assigning weight and thus, these assigned weights were further utilized for the identification of the Potential Groundwater Zones in the Lakhimpur District, Assam.

**Table 6. Random index value (Saaty 1980)**

1	2	3	4	5	6	7	8	9	10	11	12
0.00	0.00	0.58	0.90	1.12	1.24	1.32	1.41	1.45	1.49	1.51	1.48

Table 7. Consistency analysis overall and individual parameter

Thematic Layers	$\lambda$ max	N	RI	CI	CR	Consistency Statement
GWPZ	13.09	12	1.48	0.098	0.066	CR < 0.1 (Very Consistent)
Geomorphology	6.08	6	1.24	0.016	0.013	
Lithology	8.24	8	1.41	0.035	0.025	
Slope	5.21	5	1.12	0.054	0.048	
Lineament Density	5.12	5	1.12	0.031	0.028	
Drainage Density	5.07	5	1.12	0.018	0.016	
Curvature	5.23	5	1.12	0.059	0.053	
Rainfall	5.07	5	1.12	0.019	0.017	
Soil	6.22	6	1.24	0.045	0.036	
LULC	7.18	7	1.32	0.046	0.035	
Distance from the river	5.05	5	1.12	0.012	0.011	
NDVI	5.17	5	1.12	0.044	0.039	
TWI	5.21	5	1.12	0.053	0.047	

Where,  $\lambda$  max is the Maximum eigenvalue,  $N$  Number of factors,  $RI$  Random index,  $CI$  Consistency Index,  $CR$  Consistency ratio.

#### Delineation of Potential Groundwater Zones

The groundwater potential regions were identified using weighted overlay analysis methods in the ArcGIS environment (Aykut 2021). The weight assigned to all the causative factors and their sub-classes rated by their level of significance are depicted in Table 6. The groundwater potential index (GWPI) for the Lakhimpur district was calculated as shown in Eq. 3.

$$\begin{aligned}
 GWPI = & GMw \cdot GMr + Lw \cdot LR + SLw \cdot \\
 & SLr + LDw \cdot LDr + DDw \cdot DDr + Cw \cdot \\
 & Cr + Rw \cdot Rr + Sw \cdot Sr + LULCw \cdot \\
 & LULCr + DRw \cdot DRr + NDVIw \cdot \\
 & NDVIr + TWIw \cdot RWIr
 \end{aligned}
 \quad (3)$$

where  $GM$  is geomorphology,  $L$  is lithology,  $SL$  is a slope,  $LD$  denotes lineament density,  $DD$  is drainage density,  $C$  is curvature,  $R$  signifies rainfall,  $S$  represents soil,  $LULC$  indicates land use and land cover,  $DR$  is Distance from the river,  $NDVI$  represents Normalized Difference Vegetation Index and  $TWI$  is topographic wetness index. The suffix  $w$  represents weight, while  $r$  indicates the rank of each layer, respectively.

#### Validation of the groundwater potential zone map (GWPM)

For the validation purpose, 30 sample data from the observation well of the Central Groundwater Board and Borehole were utilized in the accuracy assessment of the groundwater potential map in accordance with the average water level (mbgl). The sample data were overlaid upon the groundwater potential zone map in ArcGIS software to verify the correspondence between them. A remark of 'agree' means that there is consensus between collected value and groundwater potential classes, whereas, a remark of 'partially agree' and 'disagree' means there is a dissonance (Table 9). Thus, the quantification of accuracy was possible following this method using Eq. 4 (Das and Mukhopadhyay 2020; Sajil Kumar et al. 2022)

$$GWPM \text{ Accuracy } (\%) = \frac{\text{Number of Agreement Samples}}{\text{Total Number of Samples}} \times 100 \quad (4)$$

Data from 12 available observation wells of CGWB were also used to show the groundwater level fluctuation during the Pre-monsoon (January to March 2022) and Post-monsoon (October to December 2022) (Table 10). The Receiver Operating characteristics (ROC) curve was used to evaluate the preciseness and reliability of the groundwater potential map by comparing it with the

Table 8. Assigned weights and ranks of all thematic layers through AHP

Causative Factors	Classes	Rank	Weight	Influence (%)
Geomorphology	Flood Plain	5	0.19	19
	Highly Dissected Hills and Valleys	1		
	Alluvial plain	4		
	Piedmont Slope	2		
	Waterbodies-River	5		
	Waterbodies-Other	5		

Lithology	White to greyish sand, silt, pebble and clay	4	0.17	17
	Unstabilised & Unoxidized Sand, Silt and Clay	5		
	Unoxidised Sand, Silt and Clay	5		
	Oxidised to feebly oxidised Sand, Silt and Clay	3		
	Highly Oxidised dark brown to red brown Loamy Sand	2		
	Sandstone, Clay, Comglomerate, Coal & Fossil wood	4		
	Gneiss/ Quartzite Pebbles in oxidised Sand, Silt and Clay	1		
	Cobble Pebble rich dark brown to reddish brown SST	2		
Slope	Very Low (0 - 0.92)	5	0.11	11
	Low (0.92 - 2.99)	4		
	Moderate (2.99 - 6.68)	3		
	High (6.68 - 11.89)	2		
	Very High (11.89 - 29.41)	1		
Lineament Density	Very Low (0 - 3.41)	1	0.11	11
	Low (3.41 - 9.66)	2		
	Moderate (9.66 - 15.20)	3		
	High (15.20 - 22.02)	4		
	Very High (22.02 - 36.23)	5		
Drainage Density	Very Low (0 - 7.31)	5	0.12	12
	Low (7.31 - 19.60)	4		
	Moderate (19.20 - 31.89)	3		
	High (31.89 - 46.23)	2		
	Very High (46.23 - 74.62)	1		
Curvature	-1.27 to - 0.20	5	0.05	5
	-0.20 to - 0.03	4		
	-0.03 to 0.04	3		
	0.04 to 0.24	2		
	0.24 to 1.40	1		
Rainfall	3463.57 to 3691.10	1	0.05	5
	3691.10 to 3870.74	2		
	3870.74 to 4062.34	3		
	4062.34 to 4261.94	4		
	4261.94 to 4481.49	5		
Soil	Waterbodies	5	0.04	4
	Cambisols	4		
	Fluvisols	5		
	Gleysols	2		
	Luvisols	3		
	Vertisols	1		

LULC	Waterbodies	5	0.05	5
	Dense forest	5		
	Shrub land	4		
	Agriculture	3		
	Built-up area	2		
	Sand bar	5		
	Barren land	1		
Distance from the river	Upto 200	5	0.04	4
	200 to 500	4		
	500 to 1000	3		
	1000 to 2000	2		
	Above 2000	1		
NDVI	-0.172 to 0.007	1	0.04	4
	0.007 to 0.106	2		
	0.106 to 0.179	3		
	0.179 to 0.247	4		
	0.247 to 0.447	5		
TWI	5.244 to 9.081	1	0.03	3
	9.081 to 10.747	2		
	10.747 to 12.847	3		
	12.847 to 15.888	4		
	15.888 to 23.708	5		

actual observed data. The ROC analysis is the most popular technique used in the evaluation of the effectiveness of various methods applied for groundwater suitability zone mapping (Pourtaghi and Pourghasemi 2014). The ROC plot is a graphical representation showing the relationship between the true positive (sensitivity) and false positive

(1-specificity) rates (Shelar et al. 2023). The value usually ranges from 0.5 to 1.0 analysed through the Area Under the Curve (AUC), where a value of 0.5 indicates that the model is less significant in assessing groundwater potential whereas, a value near 1 indicates better accuracy (Pande et al. 2021).

**Table 9. Location, groundwater level, and agreement with groundwater potential map**

Sl. No.	Location Name	Longitude	Latitude	Source	Average Water level (mbgl)	Reference Class	Map Class	Agreement
1	Bhogpur charali	93.834	27.030	CGWB	1.77	G	M	Disagree
2	Basudeo than	94.357	27.260	CGWB	3.16	P	G	Disagree
3	Bihpuria	93.911	27.034	CGWB	2.43	M	M	Agree
4	Boginadi (balijan)	94.188	27.391	CGWB	1.44	G	G	Agree
5	Dolanghat chara	94.003	27.167	CGWB	1.54	G	G	Agree
6	Harmoti	93.856	27.126	CGWB	2.28	M	G	Partially Agree
7	Kadam	94.155	27.296	CGWB	1.16	G	G	Agree
8	Laluk	93.908	27.129	CGWB	1.49	G	M	Disagree
9	N. Lakhimpur (old)	94.106	27.218	CGWB	2.43	M	M	Agree
10	Narayanpur	93.858	26.963	CGWB	2.09	M	M	Agree



11	Panigaon	94.113	27.119	CGWB	2.51	M	M	Agree
12	Pathalipam	94.281	27.442	CGWB	2.65	M	G	Partially Agree
13	Dhakuakhana	94.426	27.229	Borehole	2.19	G	G	Agree
14	Gumto Check Gate	93.807	27.136	Borehole	1.65	G	M	Partially Agree
15	Nowboicha	94.014	27.161	Borehole	1.43	G	G	Agree
16	Abeeda Pathar	94.594	27.347	Borehole	1.33	G	G	Agree
17	Ananda Bagan	94.224	27.446	Borehole	2.96	M	M	Agree
18	Surya Tea Estate	94.123	27.391	Borehole	3.62	P	G	Disagree
19	Naharani	93.990	27.000	Borehole	1.87	G	G	Agree
20	Bihpuria 2	93.915	27.018	Borehole	2.76	M	M	Agree
21	Banpurai	93.801	26.850	Borehole	1.42	G	G	Agree
22	Kekuri Bebejia NC	94.305	27.117	Borehole	2.07	M	M	Agree
23	No.2 Koroiguri	94.337	27.132	Borehole	2.2	M	M	Agree
24	Dhalpur	93.803	26.914	Borehole	2.56	M	M	Agree
25	Banderdawa	93.828	27.108	Borehole	2.27	M	G	Partially Agree
26	Simantapur	94.296	27.428	Borehole	2.34	M	M	Agree
27	Khanajan	94.029	27.222	Borehole	2.65	M	M	Agree
28	Chauldhowa	94.246	27.449	Borehole	2.19	M	M	Agree
29	Tarioni	94.161	27.404	Borehole	2.22	M	M	Agree
30	Borchapori	94.208	27.190	Borehole	1.65	G	G	Agree

**Table 10. Groundwater level fluctuation for existing CGWB sites (pre-monsoon and post-monsoon)**

Sl. No.	Location Name	Longitude	Latitude	Source	Average Water level (mbgl)	Pre-monsoon (mbgl) (Jan-March, 2022)	Post-monsoon (mbgl) (Oct-Dec, 2022)	Variation in water-level	Rise/Fall
1	Bhogpur charali	93.834	27.030	CGWB	1.77	2.14	1.59	0.55	Rise
2	Basudeothan	94.357	27.260	CGWB	3.16	4.15	3.13	1.02	Rise
3	Bihpuria	93.911	27.034	CGWB	2.43	2.85	1.3	1.55	Rise
4	Boginadi (balijan)	94.188	27.391	CGWB	1.44	1.89	2.02	-0.13	Fall
5	Dolanghat chara	94.003	27.167	CGWB	1.54	1.32	1.47	-0.15	Fall
6	Harmoti	93.856	27.126	CGWB	2.28	3.03	1.55	1.48	Rise
7	Kadam	94.155	27.296	CGWB	1.16	1.51	0.99	0.52	Rise
8	Laluk	93.908	27.129	CGWB	1.49	1.92	1.01	0.91	Rise
9	N. Lakhimpur (old)	94.106	27.218	CGWB	2.43	3.23	3.17	0.06	Rise
10	Narayanpur	93.858	26.963	CGWB	2.09	2.52	1.4	1.12	Rise
11	Panigaon	94.113	27.119	CGWB	2.51	2.46	3.64	-1.18	Fall
12	Pathalipam	94.281	27.442	CGWB	2.65	2.83	2.54	0.29	Rise

## RESULTS AND DISCUSSION

### Geomorphology

Geomorphology is considered the most significant determining factor in the recharge and storage of groundwater (Ghosh and Sahu 2023). It significantly influences various hydrological and hydrogeological processes, namely runoff, water infiltration, and the aquifer recharge process (Abijith et al. 2020). The Lakhimpur District is characterized by different geomorphological landform units namely, alluvial plains (1454.01 km<sup>2</sup>), flood plains (1211.44 km<sup>2</sup>), highly dissected hills and valleys (83.97 km<sup>2</sup>), piedmont slopes (30.73 km<sup>2</sup>), rivers (213.97 km<sup>2</sup>), and other water bodies (0.51 km<sup>2</sup>) (Fig. 3a). The dominance of alluvial plains, flood plains, and waterbodies which is roughly 96% of the total geographical area signifies that the area has a high potential for groundwater storage and recharge and thus, was given higher weights whereas, the highly dissected hills and valleys and Piedmont slope which constitute roughly 3.84% area are considered least significant due to high surface runoff and lower recharge area and were therefore given lower weights (Table 8).

### Lithology

Lithological characterization is vital in identifying groundwater potential zones as it regulates percolation (Muralitharan and Palanivel 2015; Murmu et al. 2018; Shaban et al. 2006). The lithological settings of the Lakhimpur District are divided into eight sub-classes based on their physical and chemical properties including, the Barpeta I formation consists of white to greyish sand, silt, pebble, and clay from the late Holocene period covering 881.34 km<sup>2</sup> (roughly 29%), the Barpeta II formation consists of unstabilized & unoxidized sand, silt and clay from the late Holocene period covers 1198.79 km<sup>2</sup> (around 40 %), the Hauli formation having unoxidized Sand, Silt, and Clay of the Holocene epoch spread across 77.03 km<sup>2</sup> (2.57%), the Sorbhog formation consisting of oxidised to feebly oxidised sand, silt and clay of Pleistocene to Holocene period covers 558.97 km<sup>2</sup> (18.67%), the Chapar formation with highly oxidised dark brown to red-brown loamy sand of Middle to Late Pleistocene period covers 7.11 km<sup>2</sup> (0.23%), the Kimin formation consists of sandstone, clay, conglomerate, coal, and fossil wood from the Pliocene to Pleistocene covers 97.47 km<sup>2</sup> (3.25%), the Corramore formation having gneiss/ quartzite pebbles in oxidized sand of Early Pleistocene spread across 35.49 km<sup>2</sup> (1.18%) and the Chapar formation consist of silt and clay and cobble pebble rich dark brown to reddish brown SST of Middle to Late Pleistocene covers the remaining 136.83 km<sup>2</sup> (4.57%) of the total area (Fig 3b.). The newer alluvium namely, the Barpeta and Hauli formations and the Kimin formation (part of Siwalik Himalayas) were given higher weight as the lithology provides ample opportunity for water to percolate and recharge the groundwater. The Corramore, Chapar, and Sorbhog formations dominated by older alluvium were given lower weight due to the compactness and consolidated properties obstructing the percolation of water and reducing the porosity (Table 8).

### Slope

The topographical effect on the infiltration of surface water and the infiltration rate is directly related to the slope characteristics of the region (Abijith et al. 2020). The low slope angle represents a flat surface and is considered suitable for groundwater recharge as the water gets more

time to percolate in the sub-surface region whereas, steep slopes are not considered suitable as water drains fast down the slope affecting percolation time (Ghosh and Sahu 2023). The Lakhimpur District is divided into five slope categories (Fig. 3c), namely, very low (0–0.92°), low (0.92–2.99°), moderate (2.99–6.68°), high (6.68–11.89°), and very high (11.89–29.41°). The flat and gentle slopes were assigned higher weights and the steep and very steep slopes were assigned lower weights (Table 8).

### Lineament Density

Lineaments are linear features that provide an idea about the underlying fault and fracture zones which are essential for groundwater movement and storage. The region with high lineament density signifies high porosity and permeability resulting in higher groundwater potential and vice-versa (Tolche 2021). The Lineaments were digitized manually from SRTM DEM images and were used to generate the final lineament density map in the ArcGIS environment. The obtained lineament density map was divided into five classes (Fig. 3d), namely, very low (0–3.41 km/km<sup>2</sup>), low (3.41–9.66 km/km<sup>2</sup>), moderate (9.66–15.20 km/km<sup>2</sup>), high (15.20–22.02 km/km<sup>2</sup>), and very high (22.02–36.23 km/km<sup>2</sup>). The regions with high lineament density have a positive relationship with the recharge of groundwater and thus, were given higher weights and vice-versa. Table 8 shows the assigned weights and ranks.

### Drainage Density

Drainage Density is defined as the ratio between the basin area and the sum of the length of all the streams in that particular river basin (Horton 1945). It is inversely related to permeability, making it a key parameter in groundwater potential assessment (Rizeei et al. 2019). Higher drainage density indicates insignificant groundwater recharge due to greater surface runoff and less infiltration and lower drainage density means more infiltration contributing to greater groundwater potential (Chenini and Ben Mammou 2010). Five drainage density classes were recognized (Fig. 3e), namely, very low (0–7.31 km/km<sup>2</sup>), low (7.31–19.60 km/km<sup>2</sup>), moderate (19.60–31.89 km/km<sup>2</sup>), high (31.89–46.23 km/km<sup>2</sup>), and very high (46.23–74.62 km/km<sup>2</sup>). Higher weights were assigned to the areas with low drainage density and lower weights were assigned to the areas with high density in the zonation of groundwater potential of Lakhimpur District (Table 8)

### Curvature

Curvature describes the nature of earth's surface profile namely, concave and convex (Arunbalaji et al. 2019). According to Khoshtinat et al. 2019, "The curvature of a slope provides a better understanding of the subsurface hydrology dynamics, soil formation, and accumulation". The deceleration and accumulation of groundwater depend upon the curvature of that particular area (Nair et al. 2017). The derived curvature values of the Lakhimpur District range between – 1.27 to 1.40 (Fig 3.f). Flat surface (–0.03 to 0.04) covering 1482.51 km<sup>2</sup> (49.50%) dominates the region which is the result of denudational activity of the rivers flowing in this region. The concave slope (–1.27 to – 0.03) occupies nearly 863.45 km<sup>2</sup> (28.83 %) and the convex slope (0.04 to 1.40) occupies 648.69 km<sup>2</sup> (21.65%). High weights were provided to the concave slopes where water can accumulate and higher infiltration occurs, whereas, the low weights were given to the convex slopes due to their poor water retention capacity (Table 8).

## Rainfall

The intensity and spatiotemporal distribution of the precipitation directly influence the quantity of groundwater recharge and thus, influence the groundwater potential (Şen 2015). Rainfall with low intensity and of longer duration enables higher infiltration whereas, high-intensity rainfall for short duration increases surface runoff and reduces infiltration (Das et al. 2022). Although the Lakhimpur district region receives a very high amount of annual rainfall, the rainfall map was categorized into five classes based on the intensity of rainfall (Fig. 3g), namely, very low (3463.57 – 3691.10 mm/yr), low (3691.10 to 3870.74 mm/yr), moderate (3870.74 to 4062.34 mm/yr), high (4062.34 to 4261.94 mm/yr), and very high (4261.94 to 4481.49 mm/yr). The highest rainfall areas have the highest groundwater potentiality and thereby, were provided with the highest weight and vice-versa. Table 8 shows the assigned ranks and weights for the rainfall map and its sub-categories.

## Soil

Soil physical properties namely, texture, depth, and composition play a pivotal role in determining groundwater recharge which makes it a crucial component in identifying groundwater potential (Arulbalaji et al. 2019; Saade et al. 2021). According to Tesfaye 2010, "The degree of permeability, which is established by the interaction between infiltration rates, and runoff and the properties of the soil, defines the groundwater potential". Fig 3 h. depicts the soil types of the Lakhimpur District. The region contains five different types of soil such as Cambisols (2812.57 km<sup>2</sup>), Fluvisols (89.54 km<sup>2</sup>), Gleysols (11.31 km<sup>2</sup>), Luvisols (1.21 km<sup>2</sup>) and Vertisols (2 km<sup>2</sup>). Out of these, Cambisols was found to be the most dominant type of soil covering almost 94 percent of the study area. Higher weightages were provided to the soil types with coarse to fine materials and a good drainage while lower weightages were provided to the soil types with more clay content and water saturation capacity leading to poor drainage (Table 8).

## Land use and Land cover

Land use and Landcover are crucial determinants of the groundwater availability and its storage in any region. It provides various details on soil moisture, infiltration, surface drainage, and other available water resources that are required to identify groundwater zones (Kom et al. 2022). Forest areas have high groundwater potential whereas, built-up and bare soil have less groundwater potential (Sajil et al. 2022). The LULC map was prepared from Landsat 8 OLI image in ArcGIS 10.4 using a supervised image classification algorithm. The accuracy of the LULC map was accessed by computing a confusion matrix in spatial analyst tools using seventy (70) randomly generated points in the ArcGIS environment. The overall accuracy and kappa values stood at 88.57% and 0.86 respectively. Seven Land use/cover were categorized (Fig. 3 i) namely, waterbodies (192.22 km<sup>2</sup>), dense forest (346.05 km<sup>2</sup>), shrublands (4.54 km<sup>2</sup>), agriculture (1708.62 km<sup>2</sup>), built-up areas (563.07 km<sup>2</sup>), sand bars (105.57 km<sup>2</sup>), and barren land (74.54 km<sup>2</sup>). Waterbodies, dense forests, and sand bars were provided the highest weight due to their greater role in groundwater recharge, whereas, the barren land was provided the lowest weight due to their poor water retention capacity (Table 8)

## Distance from the river

River waters are the prime source of groundwater within a river basin aquifer, thus, the areas nearby to that of a river have a good probability of groundwater potential (Vrzel et al. 2018; Halder et al. 2020). The distance from the river map was derived by creating buffers of up to 200 m, 500 m, 1000 m, 2000 m, and above 2000 m using Analysis tools in ArcGIS 10.4. The map was classified into five categories namely, < 200m (171.63 km<sup>2</sup>), 200 – 500 m (266.62 km<sup>2</sup>), 500 – 1000 m (377.44 km<sup>2</sup>), 1000 – 2000 m (773.57 km<sup>2</sup>), and > 2000 m (1405.89 km<sup>2</sup>). Fig. 3j displays the distance from the river map for the Lakhimpur District. The area nearby to the major waterbodies was provided higher weight and vice-versa (Table 8).

## Normalized Difference Vegetation Index (NDVI)

NDVI helps in estimating the amount of vegetation present and the groundwater potential zones over any area (Parizi et al. 2020). NDVI values range from -1 to +1, with values close to 1 indicating dense and healthy vegetation, values close to 0 indicating sparse vegetation, and values close to -1 indicating an absence of vegetation (Hasanuzzaman et al. 2022). The NDVI map was prepared from Landsat 8 bands 4 and 5 using a raster calculator in ArcGIS 10.4. The range of NDVI values carries from - 0.17 to 0.44. The NDVI map was classified into five categories (Fig 3 k) namely, -0.172 to 0.007 (71.77 km<sup>2</sup>), 0.007 to 0.106 (231.39 km<sup>2</sup>), 0.106 to 0.179 (1226.15 km<sup>2</sup>), 0.179 to 0.247 (974.47 km<sup>2</sup>), and 0.247 to 0.447 (490.55 km<sup>2</sup>). The findings suggest the vegetation cover of the region falls under the moderate category (Swarnim et al. 2023). The areas with higher NDVI values were provided higher weight and those areas which have lower NDVI values were given lower weightage (Table 8).

## Topographic wetness index (TWI)

TWI is a commonly used technique to estimate the topographic control over hydrological processes, including the infiltration of groundwater (Sørensen et al. 2006). Generally, higher TWI values indicate a higher probability of groundwater potential (Nampak et al. 2014). According to Shekar and Mathew 2023, "Areas with low TWI are more prone to generating overland flow than facilitating groundwater recharge, owing to the hillslope effect". The TWI map was classified into five categories (Fig. 3l) namely, very low (5.244 to 9.081), low (9.081 to 10.747), moderate (10.747 to 12.847), high (12.847 to 15.888), and very high (15.888 to 23.708). The lower TWI values were provided with low weights and the higher TWI values were provided with comparatively higher weights. (Table 8).

## Groundwater Potential Zone (GWPZ)

A groundwater potential zone map was prepared using the Analytical Hierarchy Process (AHP) considering twelve parameters providing relative weights to each factor for their influence in the groundwater prospect of the region. The estimated Groundwater Potential Zones map of the Lakhimpur District, Assam was divided into three classes (Fig. 4) namely, Poor, Moderate, and Good. The areas within different groundwater potential zones are depicted in Table. 11. The findings illustrate that moderate and good potential zones are mostly found in the region with more than 99% of area coverage. The good groundwater potential zones (covering 65.12% area) are mostly found in the northeast, east,



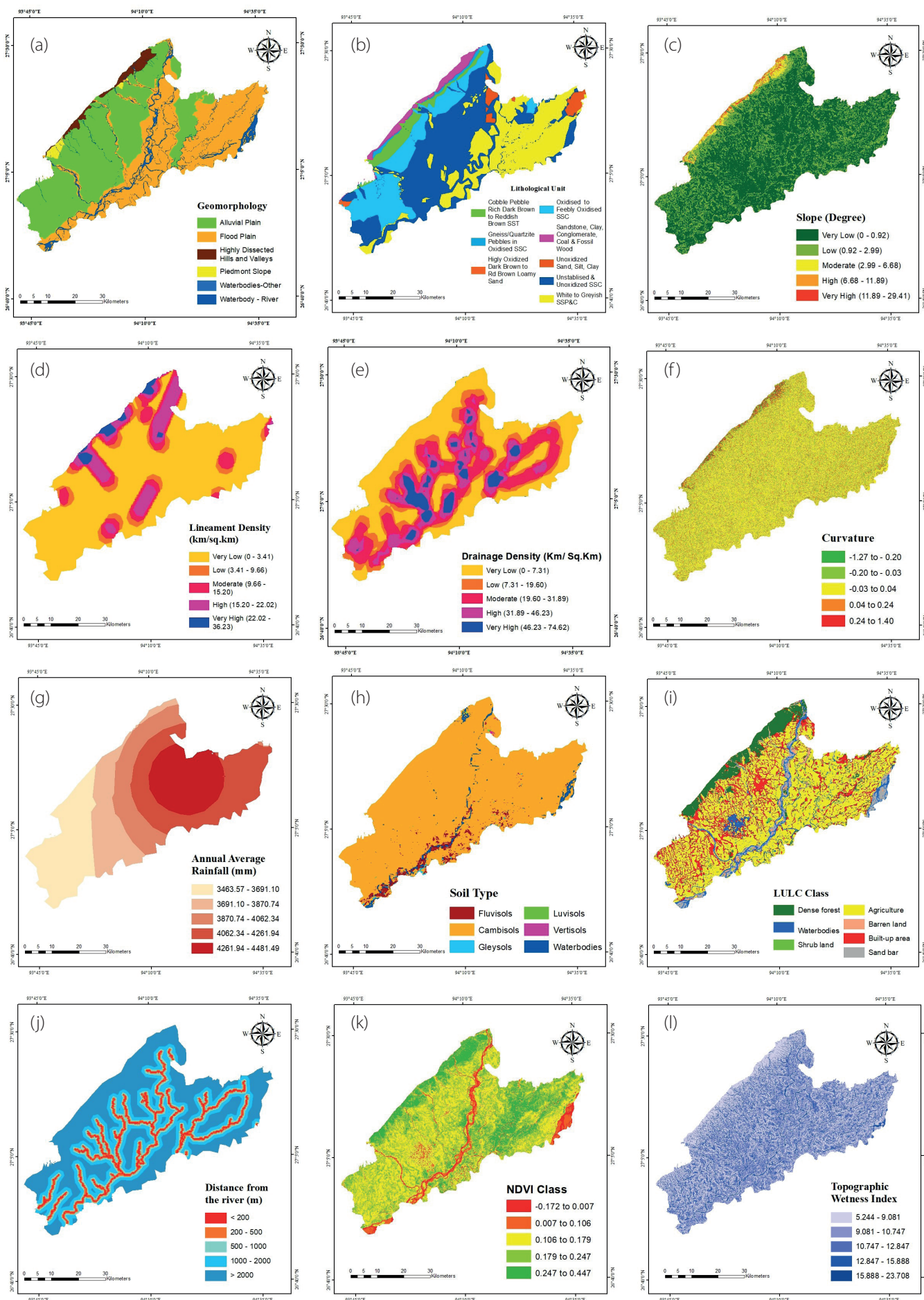


**Fig. 3. (a) Geomorphological map; (b) Lithological map; (c) Slope map; (d) Lineament Density Map; (e) Drainage Density map; (f) Curvature map; (g) Average Annual Rainfall map; (h) Soil Type Map; (i) Land use and Landcover map; (j) Distance from the river map; (k) NDVI map; (l) TWI Map**



southeast, and south corresponding to alluvial and floodplains, permeable materials, and lower slopes. There are some isolated pockets in the northern region where good groundwater potential was found because of the favourable geological structures, the existence of fault corridors, good drainage sources, and a high rate of infiltration. The zone of moderate groundwater potential covering 34.72% of the Lakhimpur District was found in the north, northwest, and western parts corresponding to the areas of moderately permeable rocks, moderate to low slope angle, presence of dense vegetation, and moderate drainage. Moreover, some isolated pockets of moderate potential zones were seen in the southeastern part of the region mainly covered with shrubs and permeable sediments. Poor groundwater potential zones were distributed in a small area (0.14%) in the northern portion mostly in the outer boundary of the Lakhimpur District where the highly dissected hills and valleys with high slope angles are present which favours more surface runoff and restrict infiltration.

### Validation of the Outcome Map

The authentication and verification of the outcome are essential steps in evaluating the accuracy and credibility of any model. Without proper validation, models lack scientific significance (Das 2019; Chung et al. 2003). For validation of the groundwater potential map prepared using the Analytical Hierarchy Process (AHP) Model, this study used 30 ground truth data from twelve (12) observation wells of Central Groundwater Commission and eighteen (18) boreholes from various locations. The model validation process includes comparing the specific groundwater depth values with the groundwater potential map prepared using geospatial techniques. Table 9.

shows the location of all the ground truth data points and the agreement status. The calculation process is stated as follows:

Number of ground sample data = 30

Number of ground sample data that agreed with the result of the mapping = 22

Number of ground sample data that disagreed with the result of the mapping = 08

Overall accuracy of the GWP map =  $22/30 \times 100 = 73.33\%$

The Receiver Operating Characteristics (ROC) curve was used to analyse the performance of the model. The model accuracy, as determined by the AUC – area under the curve, was ascertained to be 0.708. This analysis establishes that the global success rate of the groundwater map is 70.8% (Fig. 5). Therefore, it is affirmed that the approach employed in the present research exhibited favourable accuracy in mapping groundwater potential, exceeding the threshold of 70%.

Pre-monsoon and post-monsoon groundwater level data from twelve (12) observation wells of the Central Groundwater Board for the year 2022 were also used for validation of the GWP map (Table 10). The groundwater level in these stations during the pre-monsoon period ranges from 1.32 to 4.15 mbgl, while the groundwater level in the post-monsoon period ranges between 0.99 to 3.64 mbgl. The region with higher groundwater potential experiences minimal water level fluctuation and vice-versa (Bera et al. 2020). The region shows an average water level fluctuation of 0.50 mbgl between the pre-monsoon and post-monsoon periods (Fig. 6), indicating a reliable prediction of the moderate to good groundwater potential zones of the Lakhimpur District.

**Table 11. Classification of Groundwater Potential Zones**

GWP Classes	Area (km <sup>2</sup> )	Area (%)
Poor	4.22	0.14
Moderate	1018.25	34.72
Good	1909.41	65.12

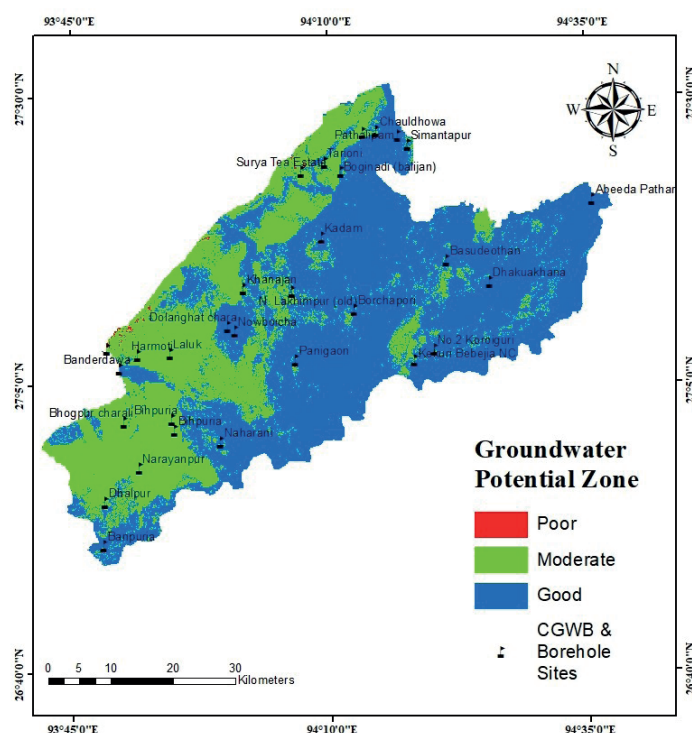


**Fig. 4. Groundwater Potential Zone Map**

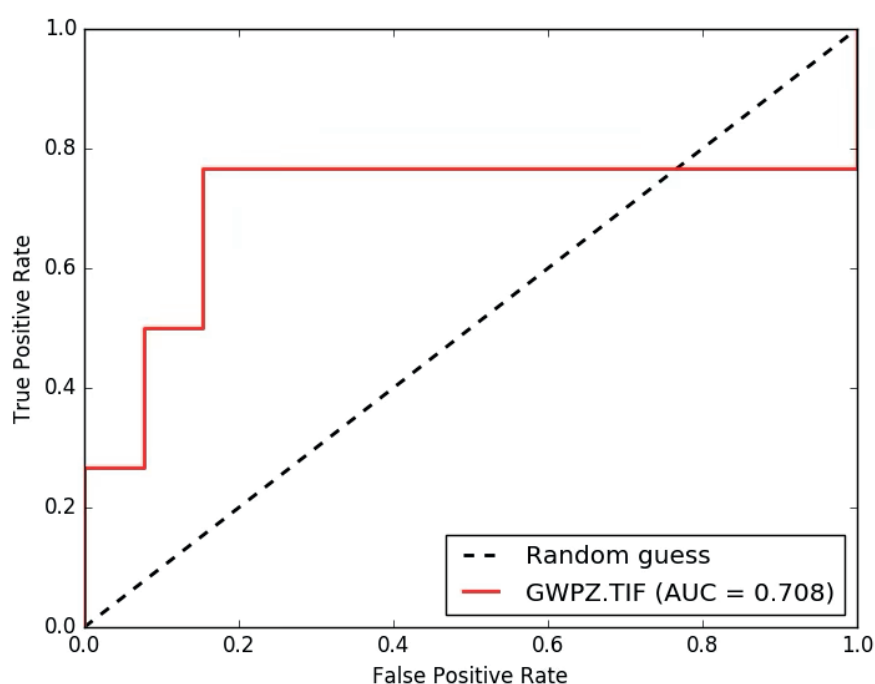


Fig. 5. ROC plot for the validation of groundwater potential zone map

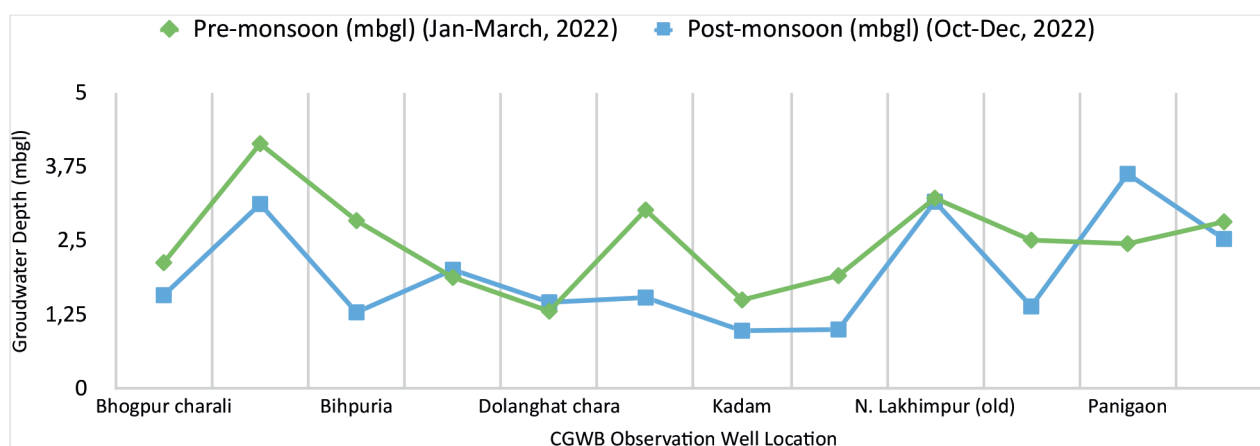


Fig. 6. Groundwater Level Fluctuation in various locations within the Lakhimpur District

## CONCLUSIONS

This study attempted to assess the groundwater potential zones in Lakhimpur district, Assam, through the integration of remote sensing, GIS, and the Analytical Hierarchy Process (AHP) based multi-criteria decision-making techniques. The AHP technique was used to assign weights to the twelve factors considered for the research. The weights provided are based on the relative importance of each causative factor, determined using pair-wise comparison which were integrated into the GIS framework to produce the groundwater potential zone map. Among the factors, geomorphology and lithology were given higher weights compared to the others due to their significant roles in a fluvially originated landform, affecting infiltration rates, recharge processes, groundwater storage, and sedimentation. The resultant GWPZ map was classified into three categories: good, moderate, and poor zones, covering 1909.41 km<sup>2</sup> (65.12%), 1018.25 km<sup>2</sup> (34.72%), and 4.22 km<sup>2</sup> (0.14%), respectively. The findings revealed that the majority of the good potential zones are concentrated in the north, northeast, east, southeast, and southern directions, characterized by alluvial and floodplains, permeable and lower slope angles, and favourable geological conditions. The occurrence of moderate potential zones mainly in

the west, northwest, and northern directions correspond with moderate permeability, moderate slope angles, and less dense vegetation cover. The areas with poor potential were found to be minimal, mostly located in the northern boundary marked by steep slopes and high surface runoff, which limits infiltration. The findings of the research were authenticated using groundwater level data derived from CGWB, field surveys, and the ROC method. The overall accuracy of 73.33%, ROC-AUC value of 0.708, and minimal water level fluctuation between pre-monsoon and post-monsoon periods suggest that the model performed well in identifying groundwater potential zones in the Lakhimpur District of Assam. The present study suggests that the use of geospatial techniques and AHP in groundwater potential zone identification is very effective and saves time and cost. Since the study area has a huge area under agriculture, the result will help in developing irrigation facilities and agricultural productivity. Lakhimpur District, Assam is experiencing a rapid rate of urbanization with a growing demand for freshwater for domestic and industrial purposes, the outcome of the research can be used by planners and policymakers for the identification of suitable groundwater sites and effective management of groundwater resources in the region. ■

## REFERENCES

- Abijith D., Saravanan S., Singh L., Jennifer J.J., Saranya T., and Parthasarathy K.S. (2020). GIS-based multi-criteria analysis for identification of potential groundwater recharge zones: a case study from Ponnaniyar watershed, Tamil Nadu, India. *HydroResearch*, 3, 1–14. <https://doi.org/10.1016/j.hydres.2020.02.002>
- Adimalla N. and Taloor A.K. (2020). Hydrogeochemical investigation of groundwater quality in the hard rock terrain of South India using Geographic Information System (GIS) and groundwater quality index (GWQI) techniques. *Groundwater for Sustainable Development*, 10:100288. <https://doi.org/10.1016/j.gsd.2019.100288>
- Agarwal E., Agarwal R., Garg R.D., and Garg P.K. (2013). Delineation of groundwater potential zone: an AHP/ANP approach. *Journal of Earth System Science*, 122 (3), 887–898. <https://doi.org/10.1007/s12040-013-0309-8>
- Ahmad I., Dar M.A., Andualem T.G., and Tekla A.H. (2020). GIS-based multi-criteria evaluation of groundwater potential of the Beshilo River basin. Ethiopia. *Journal of African Earth Science*, 164:103747. <https://doi.org/10.1016/j.jafrearsci.2019.103747>
- Arabameri A., Lee S., Tiefenbacher J.P., and Ngo P.T.T. (2020). Novel ensemble of MCDM-artificial intelligence techniques for groundwater potential mapping in arid and semi-arid regions (Iran). *Remote Sensing*, 12, (3), 490. <https://doi.org/10.3390/rs12030490>
- Arulbalaji P., Padmalal D., and Sreelash K. (2019). GIS and AHP techniques based delineation of groundwater potential zones: a case study from Southern Western Ghats, India. *Scientific Report*, 9:1–17. <https://doi.org/10.1038/s41598-019-38567-x>
- Aykut, T. (2021). Determination of groundwater potential zones using geographical information systems (GIS) and analytic hierarchy process (AHP) between Edirne-Kalkansogut (northwestern Turkey). *Groundwater for Sustainable Development*, 12, 100545. <https://doi.org/10.1016/j.gsd.2021.100545>
- Benjmel K., Amraoui F., Boutaleb S., Ouchchen M., Tahiri A., and Touab A. (2020). Mapping of groundwater potential zones in crystalline terrain using remote sensing, GIS techniques, and multicriteria data analysis (Case of the Ighrem Region, Western Anti-Atlas, Morocco). *Water*, 12, (2), 471. <https://doi.org/10.3390/w12020471>
- Bera A., Mukhopadhyay B. P., and Barua S. (2020). Delineation of groundwater potential zones in Karha river basin, Maharashtra, India, using AHP and geospatial techniques. *Arabian Journal of Geosciences*, 1315 (13), 1–21. <http://dx.doi.org/10.1007/s12517-020-05702-2>
- Chakraborty R., Pal S.C., Malik S., and Das B. (2018). Modeling and mapping of groundwater potentiality zones using AHP and GIS technique: a case study of Raniganj Block, Paschim Bardhaman, West Bengal. *Modelling Earth System and Environment*, 4 (3): 1085–1110. <https://doi.org/10.1007/s40808-018-0471-8>
- Chenini I. and Mammou A.B. (2010). Groundwater recharge study in arid region: an approach using GIS techniques and numerical modeling. *Computers and Geosciences*, 36, (6) : 801–817. <https://doi.org/10.1016/j.cageo.2009.06.014>
- Chung C. J. F. and Fabbri A. G. (2003). Validation of spatial prediction models for landslide hazard mapping. *Natural Hazards*, 30, 451–472. <http://dx.doi.org/10.1023/B:NHAZ.00000007>
- Dar T., Rai N., and Bhat A. (2020). Delineation of potential groundwater recharge zones using analytical hierarchy process (AHP). *Geology, Ecology and Landscape*, 5: 292–307. <https://doi.org/10.1080/24749508.2020.1726562>
- Das N., and Mukhopadhyay S. (2020). Application of multi-criteria decision making technique for the assessment of groundwater potential zones: a study on Birbhum district, West Bengal, India. *Environment Development and Sustainability*, 22 (2), 931–955. <https://doi.org/10.1007/S10668-018-0227-7>
- Das S., and Pardeshi S.D. (2018). Integration of different influencing factors in GIS to delineate groundwater potential areas using IF and FR techniques: a study of Pravara basin, Maharashtra, India. *Applied Water Science*, 87, (8): 1–16. <https://doi.org/10.1007/s13201-018-0848-x>
- Das, S. (2019). Comparison among influencing factor, frequency ratio, and analytical hierarchy process techniques for groundwater potential zonation in Vaitarna basin, Maharashtra, India. *Groundwater for Sustainable Development*, 8, 617–629. <https://doi.org/10.1016/j.gsd.2019.03.003>
- Das, S., Mukherjee, J., Bhattacharyya, S. et al. (2022). Detection of groundwater potential zones using analytical hierarchical process (AHP) for a tropical river basin in the Western Ghats of India. *Environmental Earth Science*, 81, 416. <https://doi.org/10.1007/s12665-022-10543-1>
- Deshpande, V. P., Sinha, M. K., and Shende, A. (2021). Identification of Critical Ground Water Potential Zones Using AHP & Geospatial Techniques. *Design Engineering*, 1774–1786.
- Dwivedi C., Raza R., Mitra D., Pandey A., Jhariya D. (2021). Groundwater Potential Zone Delineation in Hard Rock Terrain for Sustainable Groundwater Development and Management in South Madhya Pradesh, India. *Geography, Environment, Sustainability*, 14 (1), 106–121. <https://doi.org/10.24057/2071-9388-2020-195>
- Gautam V.K., Pande C.B., Kothari M., Singh P.K., and Agrawal A. (2023). Exploration of groundwater potential zones mapping for hard rock region in the Jakham river basin using geospatial techniques and aquifer parameters. *Advances in Space Research*, 71, (6): 2892–2908. <https://doi.org/10.1016/j.asr.2022.11.022>
- Ghosh M., and Gope D. (2021). Hydro-morphometric characterization and prioritization of sub-watersheds for land and water resource management using fuzzy analytical hierarchical process (FAHP): a case study of upper Rihand watershed of Chhattisgarh State India. *Applied Water Science*, 11(2): 17. <https://doi.org/10.1007/s13201-020-01340-x>
- Ghosh M., and Sahu A.S. (2023). Delineation of groundwater potential zones using AHP and GIS techniques: a case study in Barakar river basin, India. *Arabian Journal of Geosciences*, 16, 157. <https://doi.org/10.1007/s12517-023-11253-z>
- Gopinath G., Nair A.G., Ambili G.K., and Swetha T.V. (2016). Watershed prioritization based on morphometric analysis coupled with multi criteria decision making. *Arabian Journal of Geoscience*, 9 (2): 129. <http://dx.doi.org/10.1007/s12517-015-2238-0>
- Halder, S., Roy, M.B., and Roy, P.K. (2020). Fuzzy logic algorithm based analytic hierarchy process for delineation of groundwater potential zones in complex topography. *Arabian Journal of Geoscience*, 13 (13), 1–22. <https://doi.org/10.1007/s12517-020-05525-1>
- Hasanuzzaman, M., Mandal, M.H., Hasnine, M. et al. (2022). Groundwater potential mapping using multi-criteria decision, bivariate statistic and machine learning algorithms: evidence from Chota Nagpur Plateau, India. *Applied Water Science*, 12, 58. <https://doi.org/10.1007/s13201-022-01584-9>
- Horton R.E. (1945). Erosional development of streams and their drainage basins; hydrophysical approach to quantitative morphology. *Geol Soc Am Bull* 56 (3): 275–370 <https://doi.org/10.1177/030913339501900406>
- Jari A., Bachaoui E. M., Jellouli A., Harti, A. E., Khaddari A., and Jazouli A. E. (2022). Use of GIS, Remote Sensing and Analytical Hierarchy Process for Groundwater Potential Assessment in an Arid Region – A Case Study. *Ecological Engineering Environmental Technology*, 23 (5), 234–255. <https://doi.org/10.12912/27197050/152141>
- Jha M.K., Chowdary V.M., and Chowdhury A. (2010). Groundwater assessment in Salboni Block, West Bengal (India) using remote sensing, geographical information system, and multi-criteria decision analysis techniques. *Hydrogeology Journal*, 18, 1713–1728. <https://doi.org/10.1007/s10040-010-0631-z>

- Khoshtinat S., Aminnejad B., Hassanzadeh Y., and Ahmadi H. (2019). Groundwater potential assessment of the Sero plain using bivariate models of the frequency ratio, Shannon entropy, and evidential belief function. *Journal of Earth System Science*, 128 (6), 152. <https://doi.org/10.1007/s12040-019-1155-0>
- Kom, K.P., Gurugnanam, B. & Sunitha, V. (2022). Delineation of groundwater potential zones using GIS and AHP techniques in Coimbatore district, South India. *International Journal of Energy and Water Resources*. 1, 25. <https://doi.org/10.1007/s42108-022-00188-y>
- Machiwal, D., Jha, M.K. and Mal, B.C. (2011). GIS-based assessment and characterization of groundwater quality in a hard-rock hilly terrain of Western India. *Environmental Monitoring and Assessment*. 174, 645–663. <https://doi.org/10.1007/s10661-010-1485-5>
- Mahato, R., Bushi, D., Nimasow, G. et al. (2022). AHP and GIS-based Delineation of Groundwater Potential of Papum Pare District of Arunachal Pradesh, India. *Journal of Geological Society of India*. 98, 102–112. <https://doi.org/10.1007/s12594-022-1936-y>
- Manap, M. A., Nampak, H., Pradhan, B., Lee, S., Sulaiman, W. N. A., and Ramli, M. F. (2014). Application of probabilistic-based frequency ratio model in groundwater potential mapping using remote sensing data and GIS. *Arabian Journal of Geosciences*, 7, 711–724. <http://dx.doi.org/10.1007/s12517-012-0795-z>
- Melese T., and Belay T. (2022) Groundwater potential zone mapping using analytical hierarchy process and GIS in Muga Watershed, Abay Basin, Ethiopia. *Global Challenges*, 6: 2100068. <https://doi.org/10.1002/gch2.202100068>
- Muralitharan J., and Palanivel K. (2015). Groundwater targeting using remote sensing, geographical information system and analytical hierarchy process method in hard rock aquifer system, Karur district, Tamil Nadu, India. *Earth Science Informatics*. 8, (4): 827–842. <http://dx.doi.org/10.1007/s12145-015-0213-7>
- Murmu P., Kumar M., Lal D., and Sonker I. (2018). Singh SK (2019) Delineation of groundwater potential zones using geospatial techniques and analytical hierarchy process in Dumka district, Jharkhand, India. *Groundwater for Sustainable Development*. 9 :100239. <https://doi.org/10.1016/j.gsd.2019.100239>
- Muth, K., and Sudalaimuthu K. (2021). Integration of Remote sensing, GIS, and AHP in demarcating groundwater potential zones in Pattukottai Taluk, Tamilnadu, India. *Arabian Journal of Geosciences*. 14, 1748 <https://doi.org/10.1007/s12517-021-08110-2>
- Nair H. C., Padmalal D., Joseph A. and Vinod P. G. (2017). Delineation of groundwater potential zones in river basins using geospatial tools – an example from Southern Western Ghats, Kerala, India. *J. Geo visualization Spatial Analysis*. 1, 5. <https://doi.org/10.1007/s41651-017-0003-5>
- Nampak H., Pradhan B., and Abd Manap M. (2014). Application of GIS based data driven evidential belief function model to predict groundwater potential zonation. *Journal of Hydrology*. 513, 283–300. <https://doi.org/10.1016/j.jhydrol.2014.02.053>
- Oh H. J., Kim Y. S., Choi J. K., Park E., and Lee S. (2011). GIS mapping of regional probabilistic groundwater potential in the area of Pohang City, Korea. *Journal of Hydrology*. 399, 158–172. <https://doi.org/10.1016/j.jhydrol.2010.12.027>
- Pande C.B., Moharir K.N., and Khadri S. (2021). Watershed planning and development based on morphometric analysis and remote sensing and GIS Techniques: A case study of semi-arid watershed in Maharashtra, India. In *Groundwater resources development and planning in the semi-arid region*. Cham: Springer. [https://doi.org/10.1007/978-3-030-68124-1\\_11](https://doi.org/10.1007/978-3-030-68124-1_11)
- Parizi E., Hosseini S. M., Ataie-Ashtiani B., and Simmons C. T. (2020). Normalized difference vegetation index as the dominant predicting factor of groundwater recharge in phreatic aquifers: case studies across Iran. *Scientific Reports*, 10, 17473. <https://doi.org/10.1038/s41598-020-74561-4>
- Parthasarathy K. S. S., and Deka P.C. (2019). Remote sensing and GIS application in assessment of coastal vulnerability and shoreline changes: a review. *ISH Journal of Hydraulic Engineering*. 27, 588–600. <https://doi.org/10.1080/09715010.2019.1603086>
- Pourtaghi Z.S., Pourghasemi H.R., (2014). GIS-based groundwater spring potential assessment and mapping in the Birjand Township, southern Khorasan Province. Iran. *Hydrogeology Journal*. 22, (3): 643–662. <http://dx.doi.org/10.1007/s10040-013-1089-6>
- Qadir J., Bhat M.S., Alam A, and Rashid I. (2020). Mapping groundwater potential zones using remote sensing and GIS approach in Jammu Himalaya, Jammu and Kashmir. *Geojournal* 85, (2): 487–504. <https://doi.org/10.1007/s10708-019-09981-5>
- Rizeei H.M., Pradhan B., Saharkhiz M.A., and Lee S. (2019). Groundwater aquifer potential modeling using an ensemble multi-adoptive boosting logistic regression technique. *Journal of Hydrology*. 579: 124172. <https://doi.org/10.1016/j.jhydrol.2019.124172>
- Roy S., Hazra S., Chanda A., and Das S. (2020). Assessment of groundwater potential zones using multi-criteria decision-making technique: a micro-level case study from red and lateritic zone (RLZ) of West Bengal, India. *Sustainable Water Resource Management*. 6, (1), 1–14. <https://doi.org/10.1007/s40899-020-00373-z>
- Saade J., Atieh M., Ghanimeh S. and Golmohammadi G. (2021). Modeling impact of climate change on surface water availability using SWAT model in a semi-arid basin: case of El Kalb River, Lebanon. *Hydrology* 8 (3), 134. <https://doi.org/10.3390/hydrology8030134>
- Saaty T. L. (1980). *The Analytic Hierarchy Process*. McGrawhill, Juc. New York.
- Sajil Kumar P.J., Elango L., and Schneider M. (2022). GIS and AHP Based Groundwater Potential Zones Delineation in Chennai River Basin (CRB), India. *Sustainability*, 14 (3), 1830. <http://dx.doi.org/10.3390/su14031830>
- Saravanan S., Saranya T., Abijith D., Jacinth J. J., and Singh L. (2021). Delineation of groundwater potential zones for Arkavathi sub-watershed, Karnataka, India using remote sensing and GIS. *Environmental Challenges*, 5, 100380. <https://doi.org/10.1016/j.envc.2021.100380>
- Şen Z. (2015). *Applied drought modelling, prediction, and mitigation*. Elsevier. <https://doi.org/10.1016/C2014-0-01944-2>
- Shaban A., Khawlie M., and Abdallah C. (2006) Use of remote sensing and GIS to determine recharge potential zones: the case of Occidental Lebanon. *Hydrogeology Journal*. 14 (4): 433–443. <http://dx.doi.org/10.1007/s10040-005-0437-6>
- Shekar P.R., and Mathew A. (2023). Integrated assessment of groundwater potential zones and artificial recharge sites using GIS and Fuzzy-AHP: a case study in Peddavagu watershed, India. *Environmental Monitoring and Assessment*. 195, 906. <https://doi.org/10.1007/s10661-023-11474-5>
- Shekhar S., and Pandey A.P. (2014). Delineation of groundwater potential zone in hard rock terrain of India using remote sensing, geographical information system (GIS) and analytic hierarchy process (AHP) techniques. 30 (4), 402–421. *Geocarto International*. <https://doi.org/10.1080/10106049.2014.894584>
- Shelar R. S., Nandgude S. B., Pande C. B., Costache R., El-Hiti G. A., Tolche A. D., ... and Yadav K. K. (2023). Unlocking the hidden potential: groundwater zone mapping using AHP, remote sensing and GIS techniques. *Geomatics, Natural Hazards and Risk*, 14 (1), 2264458. <https://doi.org/10.1080/19475705.2023.2264458>
- Sorensen R., Zinko, U., and Seibert, J. (2006). On the calculation of the topographic wetness index: Evaluation of different methods based on field observations. *Hydrology and Earth System Sciences*, 10, 101–112. <https://doi.org/10.5194/hess-10-101-2006>
- Swarnim, Tripathi J.N., Sonker I. et al. (2023). Groundwater potential mapping in Trans Yamuna Region, Prayagraj, using combination of geospatial technologies and AHP method. *Environmental Monitoring and Assessment*. 195, 1375. <https://doi.org/10.1007/s10661-023-11934-y>
- Tesfaye T. (2010). Ground water potential evaluation based on integrated GIS and RS techniques in Bilate river catchment, South rift valley of Ethiopia. *American Scientific Research Journal for Engineering, Technology, and Sciences*, 2313–4402. *Global Society of Scientific Research and Researchers*. Available from: <http://asrjetsjournal.org>



- Tolche A. D. (2021). Groundwater potential mapping using geospatial techniques: A case study of Dhungeta-Ramis sub-basin, Ethiopia. *Geology, Ecology, and Landscapes*, 5 (1), 65–80. <https://doi.org/10.1080/24749508.2020.1728882>
- Vaddiraju S.C., and Talari R. (2023). Assessment of groundwater potential zones in Saroor Nagar watershed, Telangana, India, using geospatial techniques and analytical hierarchy process. *Environment Science and Pollution Research*. 30, 79758–79773. <https://doi.org/10.1007/s11356-023-26185-0>
- Vrzel J., Solomon D. K., Blažeka Ž., and Ogrinc N. (2018). The study of the interactions between groundwater and Sava River water in the Ljubljansko polje aquifer system (Slovenia). *Journal of Hydrology*, 556, 384–396. <https://doi.org/10.1016/j.jhydrol.2017.11.022>
- Ying X., Zeng G. M., Chen G. Q., Tang L., Wang K. L., and Huang D. Y. (2007). Combining AHP with GIS in synthetic evaluation of eco-environment quality—A case study of Hunan Province, China. *Ecological modelling*, 209, Issue 2-4, 97–109. <https://doi.org/10.1016/j.ecolmodel.2007.06.007>







[ges.rgo.ru/jour/](http://ges.rgo.ru/jour/)

ISSN 2542-1565 (Online)